University of Reading

Synthesis, Characterisation and Physical Properties of Gallium and Germanium Sulphides

A Thesis Submitted for the Degree of Doctor of Philosophy

School of Chemistry, Food and Pharmacy

Department of Chemistry

Sarah Makin

May 2018

Abstract

Different synthetic-methods were explored to pursue novel gallium and germanium sulphides. Materials were characterised using single-crystal and powder X-ray diffraction. Elemental analysis, thermogravimetric analysis, Fourier-transform infrared spectroscopy and diffuse reflectance spectroscopy were used to analyse materials further. Energy-dispersive X-ray analysis was performed when the metal-content was ambiguous.

Hybrid T3 supertetrahedra $[Ga_{10}S_{16}(L)_4]^{2-}$ were formed, where T3 denotes a tetrahedron with three $[GaS_4]^{5-}$ tetrahedra along each edge and L is a pyridine-based ligand. Discrete-cluster based $[C_{12}H_{13}N_2]_{0.5}[C_6H_8N]_{1.5}[Ga_{10}S_{16}(NC_6H_7)_4](C_6H_7N)_{0.5}$ was synthesised, using an ionic liquid as a structure-directing agent, in 4-methylpyridine (4-MPy). $[C_6H_8N]_2[C_{12}H_{14}N_2][Ga_{10}S_{16}(NC_6H_7)_4]_2(C_{12}H_{12}N_2)(C_6H_7N)_2$, consisting of discrete T3 units and $[C_3H_3N_2C_4H_9CH_3][C_6H_8N][Ga_{10}S_{16}(NC_6H_7)_2(NC_6H_6)_2](C_6H_7N)_{0.5}$, containing chains of clusters linked *via* ethylenedipyridine (EDPy), were also synthesised using this method.

Materials containing T3-supertetrahedra were also synthesised solvothermally in 4-MPy. $[NC_6H_8]_{2.5}[N_2C_4H_6][C_3H_5N_2]_{0.5}[Ga_{20}S_{32}(N_2C_{12}H_{12})_2(NC_6H_7)_5]$ consisted of dimers of T3 clusters linked *via* EDPy, whereas $[C_6H_8N]_4[Ga_{10}S_{16}(NC_6H_7)_3(NC_6H_6)]$ - $[Ga_{10}S_{16}(NC_6H_7)_4](C_6H_7N)_2$ contained a 1:2 ratio of dimers to discrete clusters. $[C_6H_8N]_6[Ga_{20}S_{32}(NC_6H_7)_6(N_2C_{12}H_{12})][Ga_{10}S_{16}(NC_6H_7)_3(C_6H_6N)](C_6H_7N)_6$ contained both dimers and chains. The synthesis of a tetrahedron of supertetrahedra $[C_6H_8N]_{14}[Ga_{10}S_{20}]_7(NC_2H_7)_4(NC_6H_7)_8(N_2C_{12}H_{12})_8$ was also optimised throughout this work. Some materials showed photoluminescence, as measured by collaborators; materials absorbed in the UV-region and emitted in the visible region.

T2 germanium-sulphides were also synthesised in 4-MPy, including a novel trimer of T2 units $[NC_6H_8]_8[Ge_{12}S_{28}]$ and a polymeric T2-based structure $[NC_6H_8]_2[Ge_4S_9](C_6H_7N)_{0.5}$. Germanium-gallium sulphide frameworks were also produced. $[C_6H_8N]_2[Ga_2Ge_2S_8]$ had the double-diamond structure, whereas $[NC_6H_8][GaGe_3S_8](NC_6H_7)(H_2O)_5$ was constructed from single tetrahedra, with a structure which has not been observed before.

$[(CH_3(CH_2)_5)_3P(CH_2)_{13}CH_3]_{0.25}[NH_4]_{5.75}[Ga_{10}S_{18}](NH_3)$ is the first example of a double diamond net of $[Ga_{10}S_{18}]^{6-}$ clusters, synthesised using an ionic liquid with no

amine. The first non-hybrid discrete T3 cluster $[Ga_{10}S_{16}(SH)_4]^{6-}$ was synthesised in polyethylene glycol-400, to give $[C_9H_{18}N_2]_6[Ga_{10}S_{16}(SH)_4]$. $[C_7H_{13}N_2][GaS_2]$, containing chains of $[GaS_4]^{5-}$ tetrahedra, with different packing to those previously observed, was synthesised in 1,5-Diazabicyclo[4.3.0]non-5-ene .

Single-crystals of $[NH_4][Ga_3(SO_4)_2(OH)_6]$ were obtained, where the sulphate was unusually formed from gallium nitrate and sulphur.

Declaration: I confirm that this is my own work and the use of all material from other sources has been properly and fully acknowledged.

Sarah Makin

Acknowledgements

I would like to acknowledge my supervisor Dr Paz Vaqueiro, firstly for offering me this PhD studentship and the chance to carry out this research. Her expertise, ideas, knowledge and support has been invaluable to me throughout the course of my doctorate. There are many people I would like to thank in the Department of Chemistry at the University of Reading. I would like to thank Dr Ann Chippindale and Professor Anthony Powell for providing additional support and inspiration in many aspects of my research and PhD journey. I would like to thank Nick Spencer for providing support, training and advice in all areas of the XRD measurements that were carried out in the department and Amanpreet Kaur for training me on and helping me with the SEM instrument and EDX software. I would also like to thank the University of Reading for providing me with my PhD studentship.

I would like to thank John Lampkin and Jesús Prado for providing me with unlimited support and advice throughout my PhD, it truly would not have been the same experience without them. I would also like to thank Radek Kowalczyk, Gabin Guélou, Sebastian Long and Jethro Beamish-Cook.

I would like to thank The University of Edinburgh for giving me a solid grounding in chemistry and providing me with the knowledge and enthusiasm to pursue a PhD in the field. This is especially true of my Masters Project supervisor Dr Stephen Moggach and my crystallography lecturer Professor Simon Parsons, who inspired me to pursue crystallography further.

I must also thank my incredible housemates Adam Bourke and Charlotte Marriot who provided me with a happy and relaxing environment to go home to every night and will be friends for life. I would also like to thank my friend Sarah Karodia for always being there for me.

Finally I would like to thank my family and my partner Graeme Lynch for doing all that they could to support me throughout my PhD. I could definitely not have done it without them.

Abbreviations

ACN	Acetonitrile
BenzIm-	Benzimidazole
bipy	4,4′-Bipyridine
$[BMMIm]^+$	1-Butyl-2,3-dimethyl-imidazolium
CTAB	Cetyltrimethylammonium bromide
DABCO	1,4-Diazabicyclo[2.2.2]octane
DBN	1,5-Diazabicyclo(4.3.0)non-5-ene
DBU	1,8-Diazabicyclo(5.4.0)-undec-7-ene
DMA	Dimethylamine
DMF	*N,N'*-Dimethylformamide
DMM	2,6-Dimethylmorpholine
DMMP	2,6- Dimethlymorpholine
EDPy	Ethylenedipyridine
EDX	Energy-dispersive X-ray
en	Ethylenediamine
FTIR	Fourier-Transform Infrared
IL	Ionic Liquid
Im	Imidazole
ISC	Isolated Hybrid Supertetrahedral Cluster
3,5-Lut	3,5-Dimethylpyridine
4-MPy	4-Methylpyridine
MOF	Metal-Organic Framework
NCS	National Crystallography Service
PEG-400	Polyethylene glycol-400
ppz	Piperazine
PVP	Polyvinylpyrrolidone
PXRD	Powder X-ray Diffraction
SBU	Structural Building-Unit
SCIF	Supertetrahedral chalcogenide imizadolate framework
SCXRD	Single Crystal X-ray Diffraction
SDA	Structure-Directing Agent
TAA	Thioacetamide
TBD	Triazabicyclodecene
TGA	Thermogravimetric Analysis
[THTDP]Cl	Trihexyltetradecylphosphonium Chloride
TMA	Tetramethylammonium
TMDPy	4,4′-Trimethylenedipyridine
tren	Tris(2-aminoethyl)amine
ZIF	Zeolitic imidazolate framework

Table of Contents

1 Introduction

1.1 Background

The area of solid-state chemistry is currently of great importance in chemical research; new materials are constantly being developed for many given applications. Some of these lie in the area of renewable and sustainable energy, such as efficient materials for power generation like thermoelectric materials,[1, 2] solid-state fuel cells and solar cells or materials for hydrogen storage such as metal-organic frameworks (MOFs).[3-7] The development of materials for renewable and sustainable energy can be associated with creating efficient materials for applications such as catalysis and electronics for novel devices.[8-10] It is within this area that materials with semiconducting and optical properties are of vital importance.[11-13]

There is ongoing research into producing these with improved or novel properties, such as higher efficiencies, lower band-gaps in semiconductors or integration of porosity.[14] Many known semiconductors are based on elemental Si and Ge or metal oxides such as ZnO and TiO_2, but recently there has been growing interest in the use of chalcogenide-based materials like sulphides, selenides and tellurides, such as CdE (E = S, Se, Te),[15, 16] as highly efficient materials for both semiconductors and thermoelectric materials along with their catalytic and optical applications.

In 1995, Hoffmann *et al.* described how semiconductors can be used for photocatalysis,[16] with an in-depth discussion of the mechanistic and physical aspects of the processes; focusing mainly on the oxide TiO_2. In 2001, O'Brien *et al.* then compared the properties of bulk material semiconductors with those that are nanocrystalline. In a recent review, Kanatzidis *et al* explore how chalcogenides are currently used and how they may develop within the field of non-linear optic materials.[11, 12]

The main focus of this project has been on combining the properties of condensed phase solid state and nanocrystalline chalcogenides with the properties of porous materials to create novel compounds that could have potential as semiconducting and optically-active porous materials. The literature described throughout this work will focus on existing porous materials and how they have been expanded into the field of chalcogenides, along with examples of their applications. There will be many examples of existing porous chalcogenide materials and related compounds, in order to highlight

areas where further research is needed and how these have been addressed throughout the course of this project.

1.2 Introduction to Porous Materials

The field of porous materials, which includes those such as zeolites and metal-organic frameworks,[4] is a rapidly growing field of research in which materials are constantly being discovered for applications in areas such as hydrogen storage,[3, 17] catalysis,[18] molecular sieving,[19-21] ion exchange and even medicine.[22-25] Porous materials are those which contain nanometre-sized (or sometimes larger) voids in the structure and as a result can host different chemical species within their structure.

1.2.1 **Zeolites**

The area of porous materials is largely developed from the naturally occurring minerals zeolites, which are aluminosilicate materials with porous structures, based on a number of different structural types. Currently there are many known zeolite structures, some occur naturally and some are synthetic but all are aluminosilicates.

The structural building units (SBUs) of zeolites are corner sharing $[AlO_4]^{5-}$ and $[SiO_4]^{4-}$ tetrahedra. Pure silicate materials are not charged, due to corner sharing of the tetrahedra; adding aluminium into these structures gives a negatively-charged framework, with an overall charge of -1 for each Al^{3+} atom.[26] The ratio of Si:Al varies between different zeolites, however this cannot be lower than 1:1. This is because there can be only Si-O-Si or Al-O-Si bonds present; Al-O-Al bonding would cause an accumulation of negative charge that would destabilise these sites. Frameworks are also often hydrated, contain water in the pores, or both.

Due to the frameworks of zeolitic materials being negatively charged, cations must be present in the pores to balance this charge. In naturally-occurring zeolites these will be small metal-cations; either singly charged such as Na^+ and K^+, or doubly charged, such as Ca^{2+}. Through the development of synthetic zeolites, organic cations can also be present in the pores when they are used as reagents in their syntheses.

Zeolites are traditionally synthesised using high temperatures and pressures.[27] This can be achieved via hydrothermal methods where reactants are heated together in water at approximately 140 – 270 ^oC;[28] this is carried out in an autoclave that maintains autogenous pressure of *ca.* 10-50 atm throughout the reaction. This synthesis method was

developed to include the use of templates (or structure directing agents "SDA"s) to aid formation of the pores. This was initially introduced by Barrer *et al.* who used the alkyl ammonium cation TMA (tetramethylammonium) in their zeolite syntheses and found that a sodalite cage would form around these cations.[27] This allows the incorporation of a positively-charged organic species into the pores.

Zeolites can be used as ion-exchange materials.[29, 30] On interaction with a solution containing an alternative ionic substance, cations can leave the pores and be replaced with the cations from the given substance. This can allow for the removal of metal cations from water,[31] e.g. the softening of water by adding zeolites to detergents. It can also allow the post-synthetic removal of organic templating-agents from the pores of zeolitic materials.

The properties of zeolites can change greatly depending on their structure. Varying pore sizes can allow zeolites to be used as molecular sieves, where channels throughout the structure can be selective towards a certain size or shape of molecule.[32] This can be built upon by tuning other properties to combine shape selectivity with other types of selectivity, such as charge, polarity and acidity/basicity.[18] One of the fields that these can then be applied is in catalysis. The main benefit of using porous materials as catalysts is that the internal surface area of the pores contributes largely to the total surface area and is often larger than the external surface area; this greatly enhances their ability to adsorb reactants.

There are numerous frameworks that zeolites can have and the field is abundant in different structure-types, such as the sodalite cage (SOD) in structure $Na_8Al_6Si_6O_{24}(OH)_2.2H_2O$, which has a 1:1 Si:Al ratio.[33] Examples of other zeolites include the synthetic zeolite ZSM-5 (Zeolite Socony Mobil 5) with the formula $Na_{1.1}(Al_{1.1}Si_{94.9}O_{192})(H_2O)_{2.36}$ (Figure 1.1),[34,35] first synthesised by Kokotailo *et al.* in 1978 in the Mobil Research and Development Corporation Research Department. The age of this publication reflects how zeolite chemistry is a long established field which is still of major importance today.

One way to further tune the properties of zeolites is to substitute Si^{4+} and Al^{3+} with different metal ions. Zeolitic materials with substituted elements include compounds such as aluminophosphates and gallium phosphates.[36, 37] However, both ions can be substituted by a wide range of different elements. These are most commonly Ga^{3+},[37, 38] Fe^{3+},[39, 40] Ti^{4+},[41-43] P^{5+} or B^{3+} but substitution of other elements is known.[44-48]

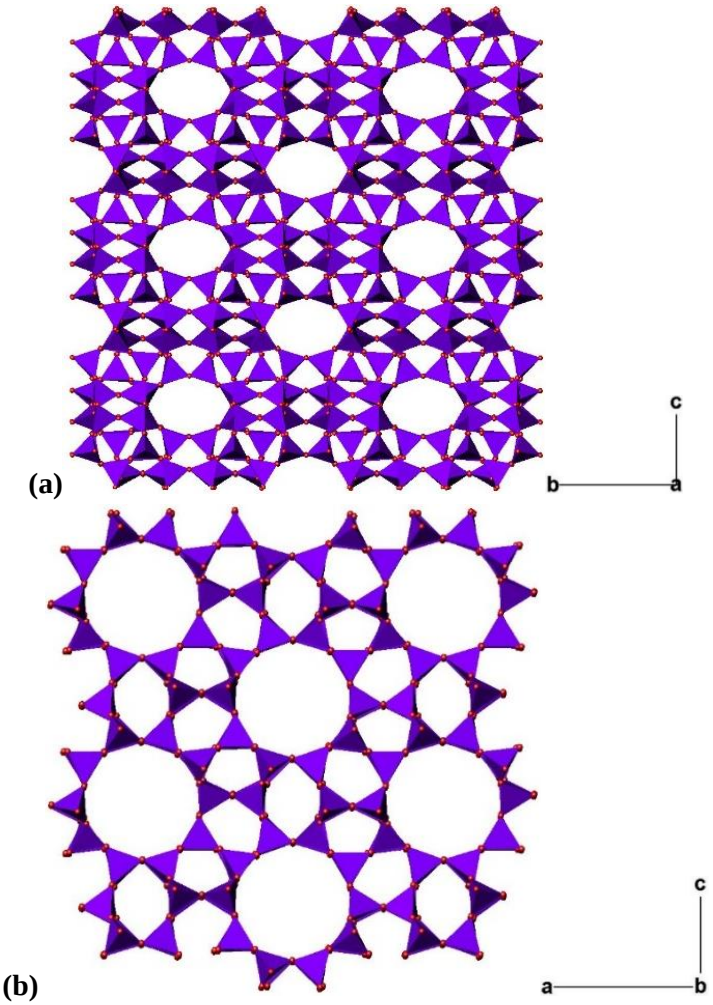

Figure 1.1 ZSM-5 viewed down **(a)** the *a*-axis and **(b)** the *b*-axis. SiO_4 or AlO_4 = purple, O = red. Water and Na have been omitted for clarity.

ZSM-5 has the MFI framework-type and it can be observed from the formula that this material has an extremely high Si:Al ratio. The structure (Figure 1.1) displays 10-membered rings (Figure 1.1 **(b)**) running along the *b*-axis with a diameter of *ca.* 5.5 Å. ZSM-5 (Figure 1.1) was heavily investigated between the 1980s and 1990s as a potential catalyst for the decomposition of nitrogen monoxide when functionalised with copper.[49, 50]

There is also a large amount of literature on the conversion of alkanes into aromatic species using ZSM-5 and many publications discuss the effect that substituting Ga^{3+} onto Al^{3+} sites has on the conversions.[51, 52] Many conclude that Ga^{3+} substitution increases the selectivity of aromatic products but slows down the rate of reaction. B^{3+} and Fe^{3+} substitution have also been discussed;[53, 54] substitution at this site mainly affects the acidity of the framework -OH groups, where the acidities are ranked as Si-(OH) < B-(OH)-Si , Fe-(OH)-Si < Ga(OH)-Si < Al-(OH)-Si.[55]

1.3 Metal-Organic Frameworks

Recently, the area of zeolite chemistry has developed towards other framework materials, such as metal-organic frameworks (MOFs), which are a rapidly growing new trend in research and examples of MOFs are abundant. There are also a significant number of reviews on the subject including those by Ferey, Cheetham and O'Keefe.[56-58] The metals used currently vary substantially; however many consist of transition metals such as zinc,[59, 60] copper,[61] iron,[62] and cobalt.[6, 44] Not only do the metals vary greatly but so does the choice of organic linker, although there are some features that are important for this application. The linkers should generally have two or more groups capable of binding to the given metal (ditopic or greater ligands), such as amine, nitrile, cyanide or carboxylate groups so they can link the metal centres throughout the structure.

A significant benefit of incorporating organic linkers into these materials is to further increase the pore sizes and create different functionalities in the structures. The applications of MOFs therefore mainly lie in catalysis and separations but there is also potential for use in hydrogen storage,[3] CO_2 adsorption and medicine.[24, 63]

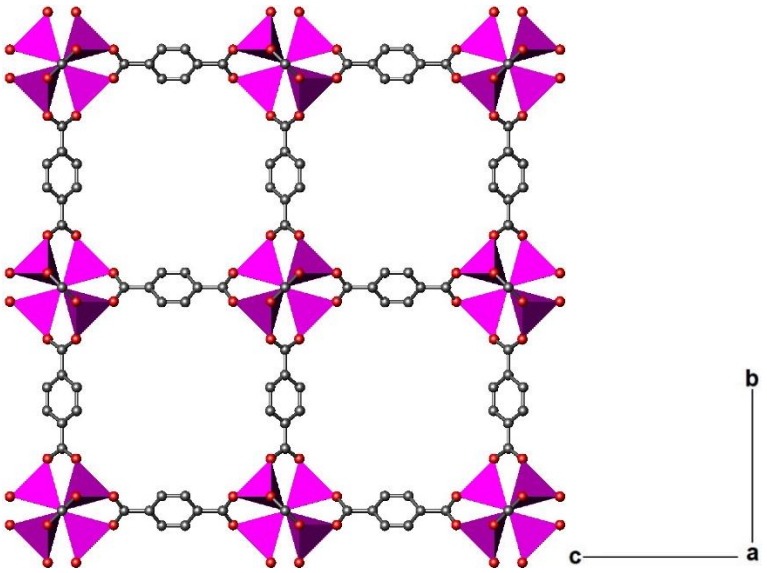

Figure 1.2 Structure of MOF- 5 viewed along the *a*-axis, pink = ZnO_4 tetrahedra, red = O and grey = C. H atoms have been omitted for clarity.[59]

One example of a MOF with large pores is MOF-5, synthesised by Yaghi *et al.* (Figure 1.2**)**.[59] The framework has the formula $Zn_4O(BDC)_3.(DMF)_8(C_6H_5Cl)$ and consists of Zn_4O tetrahedra linked by 1,4-benzenedicarboxylate (BDC) moieties. Guest

molecules of *N,N'*-dimethylformamide (DMF) and chlorobenzene (C_6H_5Cl) from the reaction mixture are present in the pores and the final structure has a large pore volume of 54-61 % and substantial surface area of 2900 m^2g^{-1}.

Examples of frameworks linked through nitrogen sites include the zeolitic imidazolate-frameworks (ZIFs);[64] a number of these materials are known and are described by Huang *et al.*[60] These frameworks contain Zn^{2+}, Co^{2+} or Fe^{2+} metal centres and the singly-deprotonated imidazolate moieties (Figure 1.3) link the metal cations to give an M-Im-M angle of 145°; close to that of the Si-O-Si angle found in zeolites.

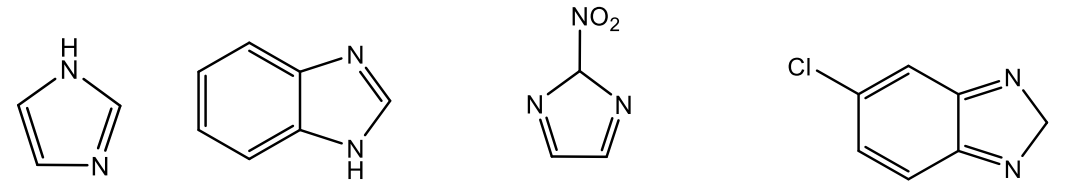

Figure 1.3 Linkers used in ZIFs described in this section.

These materials have been synthesised using a range of different heating-methods and amine SDAs. It was demonstrated by Park *et al.* that two of these ZIFs (ZIF-8 (Figure 1.4 **(a)**) and ZIF-1) have extremely high thermal stabilities,[65] up to 550°C in N_2, even with the pores fully evacuated. ZIF-8 and -11 utilise 2-methylimidazole and benzimidazole linkers respectively.

ZIFs can be used for the capture of CO_2 and there are a number of examples where they have been tested. One example includes a high-throughput method of synthesis where a large number of small samples can be synthesised at once.[66] Banerjee *et al.* describe how 25 different ZIF structures were synthesised using this technique, of which 16 were novel materials. Three of the ZIFs (68 - (Figure 1.4 **(b)**), 69- and 70-) showed exceptional and reversible adsorption of CO_2, they are also selective of CO_2 over CO. In these materials, Zn metal centres are linked *via* two linkers in each case; these are BenzIm and NIm, NIm and ClBIm, along with Im and NIm (Figure 1.3) respectively. ZIF-69 was observed to store 82.6 litres of CO_2 per kg of framework. There are also a number of frameworks known to have magnetic, conducting or optical properties, many of which are described in a detailed review by Maspoch *et al.* [62, 67]

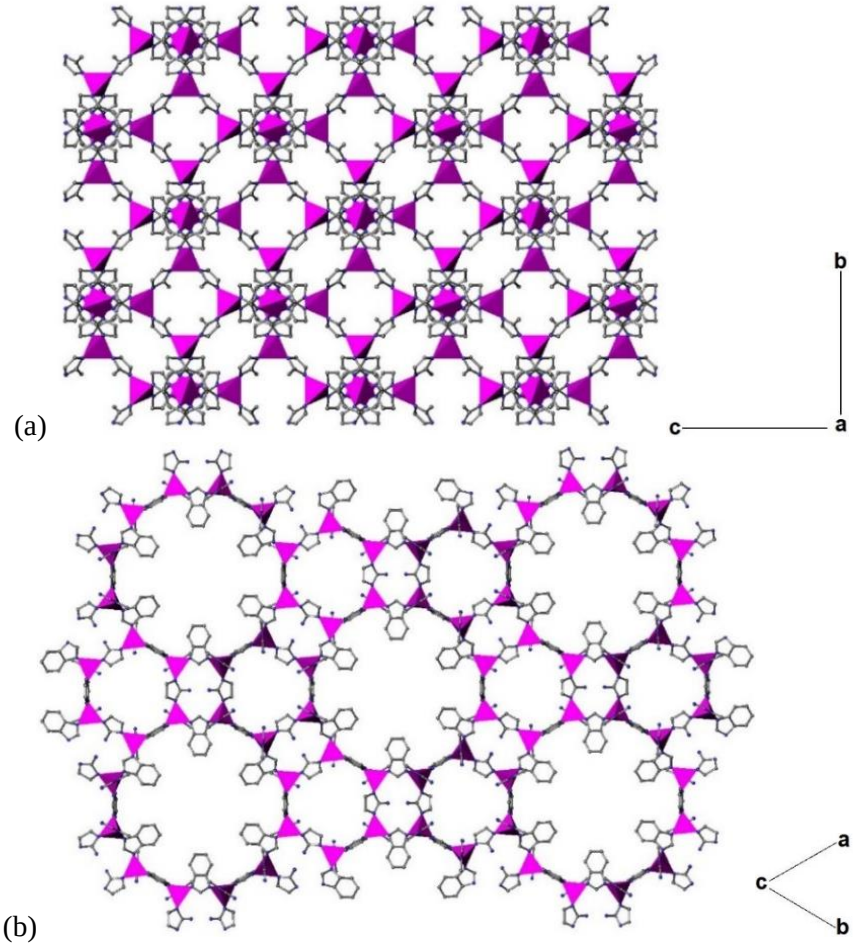

Figure 1.4 (a) Structure of ZIF-8 viewed along the *a*-axis **(b)** Structure of ZIF-68 viewed along the *c*-axis. Pink= ZnN_4 tetrahedra, blue = N and grey = C. H-atoms and water have been omitted for clarity.[65 66]

1.4 Supertetrahedral Chalcogenide Clusters

1.4.1 **Introduction to Chalcogenides**

Chalcogenide materials are widely used in solid-state chemistry due to a number of superior properties that sulphur, selenium and tellurium have in comparison to oxygen for a number of applications. Many of the applications of chalcogenide materials utilise their semiconducting properties, such as photovoltaics,[68, 69] data storage,[70-72] energy conversion and storage and electronics.[73-76] However, chalcogenides can also possess interesting optical properties, which allow them to be used in lasers and in devices requiring non-linear optical properties.[11, 77-79] Along with these applications; there is also evidence that metal chalcogenides can be used in catalysis,[80, 81] as described in Section 1.7

1.4.2 **Introduction to Supertetrahedral Clusters**

Supertetrahedral clusters are tetrahedra-based clusters varying in size, denoted T*n*; this notation was first used by Yaghi *et.al* to express the different cluster sizes.[82] The *n* stands for the number of tetrahedral units along the edges (or layers of metal atoms M), therefore T1 units have the simple formula MX_4, where M is a metal atom and X is another atom such as a chalcogenide. T2 units have the formula M_4X_{10} and T3 and T4 units have the formulae $M_{10}X_{20}$ and $M_{20}X_{36}$ respectively (Figure 1.5).

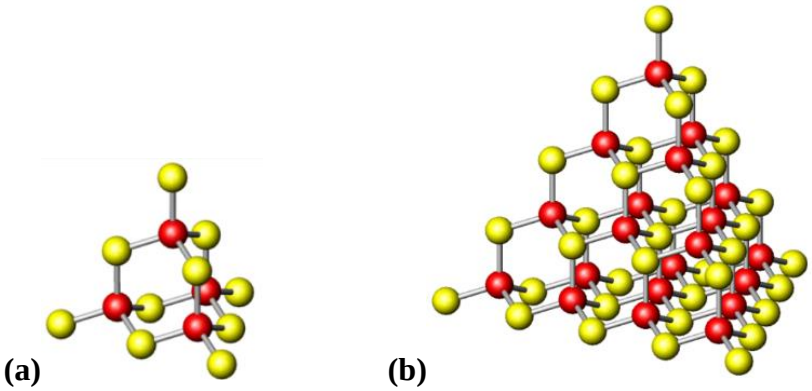

Figure 1.5 (a) T2 (M_4X_{10}) and **(b)** T4 ($M_{20}X_{36}$) supertetrahedra. M = red and X = yellow.

There are many examples of these throughout the literature, but the first example was created by Dance *et al.*,[83, 84] who describe the chemistry of chalcogenide clusters in a 1994 review.[85] This type of supertetrahedron is mainly based on the chalcogenides sulphur and selenium combined with group 13 or 14 metals. Cluster sizes vary based on the charge of the metal atoms in the supertetrahedron. This is due to Pauling's electrostatic valence rule.[86] Coordination number is proportional to the cation charge, therefore metal ions with a smaller positive charge will create a larger cluster in order to preserve electroneutrality. In general, T2 clusters are formed by M^{4+} (Figure 1.5 **(a)**) and T3 by M^{3+}. T4 (Figure 1.5 **(b)**) and T5 clusters are less common and normally require a transition metal, or another metal with a lower oxidation-state, to be included in the cluster; such as Cu^{2+} or Cd^{2+}.[87-89]

Although many compounds are known to utilise the tetrahedral coordination of oxygen, there are few examples of oxygen-based supertetrahedra.[90] This is due to the different angles of the tetrahedral bonds; the T-O-T angle is 140-150° in zeolites, whereas a typical T-S-T angle is 105-115° and lies around the ideal tetrahedral bond angle of 109°. This difference means that the formation of extended tetrahedra is greatly favoured by sulphur compared to oxygen; the resulting structures described above resemble the

ZnS lattice sphalerite.[91] The greater size of sulphur also makes tetrahedral coordination more favourable than for oxygen.

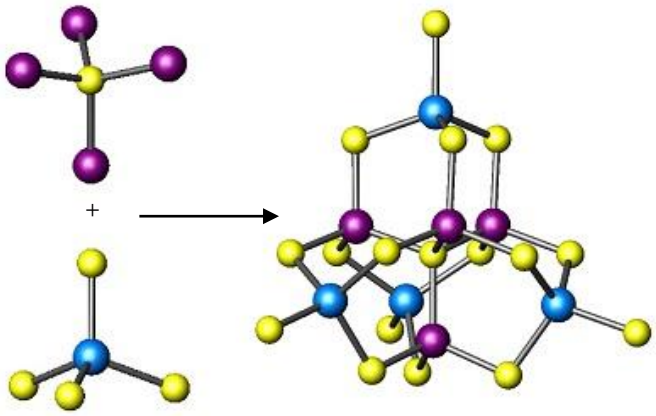

Figure 1.6 A P1cluster formed built from an inverted XM_4 tetrahedron (M=purple, X=yellow) and three MX_4 tetrahedra (M=blue, X=yellow).

The majority of existing supertetrahedra are of the regular T*n* type as described, but there are also variations of these known as pentasupertetrahedra (Figure 1.6). Pentasupertetrahedra differ from regular supertetrahedra and are denoted P*n*;[92, 93] they consist of an inverted tetrahedron/supertetrahedron (e.g. XM_4, X_4M_{10},...) with a corresponding regular tetrahedron/supertetrahedron on each edge to form the rest of the pentasupertetrahedral unit.[94,91]

A P1 cobalt tin selenide cluster was reported by Dehnen *et al.*[95, 96] It exists as a discrete cluster of formula $[Co_4(\mu_4\text{-}Se)(SnSe_4)_4]^{10-}$, in this case the central inverted-tetrahedron $[Co_4Se]^{6+}$ has its faces capped by $[SnSe_4]^{4-}$ tetrahedra. The structure also contains discrete $[SnSe_4]^{4-}$ tetrahedra between the P1 units and the negative charge is balanced by K^+, complexed by either methanol or water

Pentasupertetrahedral clusters are also observed in UCR-26 by Feng *et al.*,[92] where the P2 cluster $[Li_4In_{22}S_{44}]^{18-}$ is linked by its corner into an interpenetrating-framework. This material showed high ionic-conductivity of the Li^+ ions, this value was *ca.* 0.15 $\Omega^{-1}cm^{-1}$, with typical crystalline lithium conductors described as having ionic conductivities of *ca.* 10^{-3} $\Omega^{-1}cm^{-1}$. The material was also found to have an optical band-gap of 3.51 eV.

Other distinctive clusters are of the T*p,q* type and have the normal MX_4 unit replaced with a larger supertetrahedral-unit in the overall composition, i.e. a T2,2 unit will consist of a T2 unit, but rather than two T1 units along each edge there are two T2

units (Figure 1.7). The resulting supertetrahedron contains voids between the T2 building blocks, also described as a "missing core", whereas regular T*n* tetrahedra are uniform.

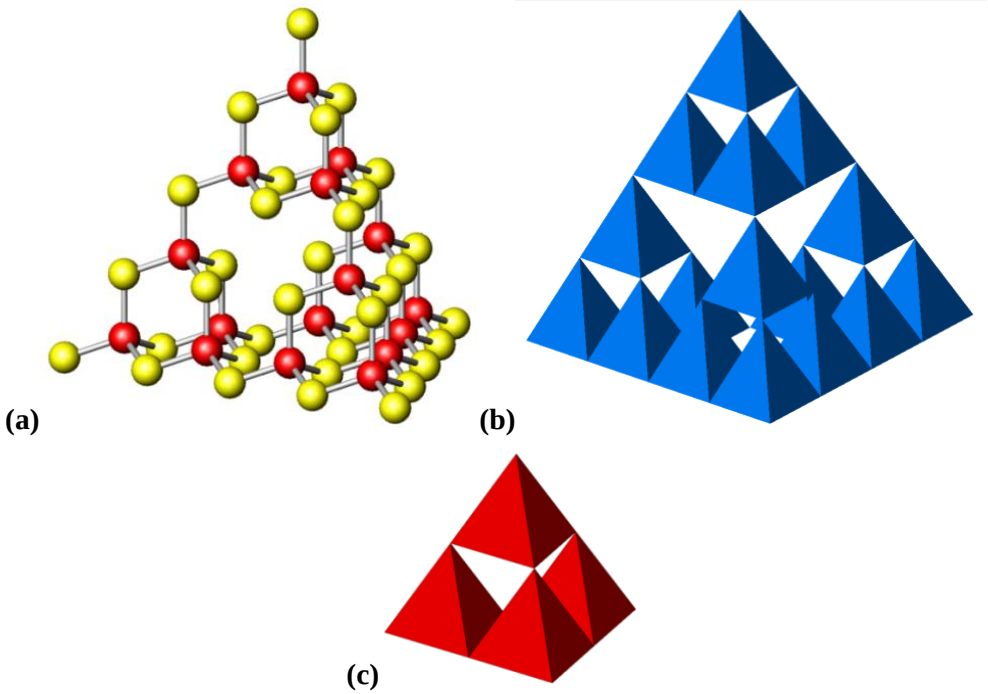

Figure 1.7 Representations of the **(a)** T2,2 **(b)** polyhedral T2,2 and **(c)** polyhedral T2 supertetrahedra.

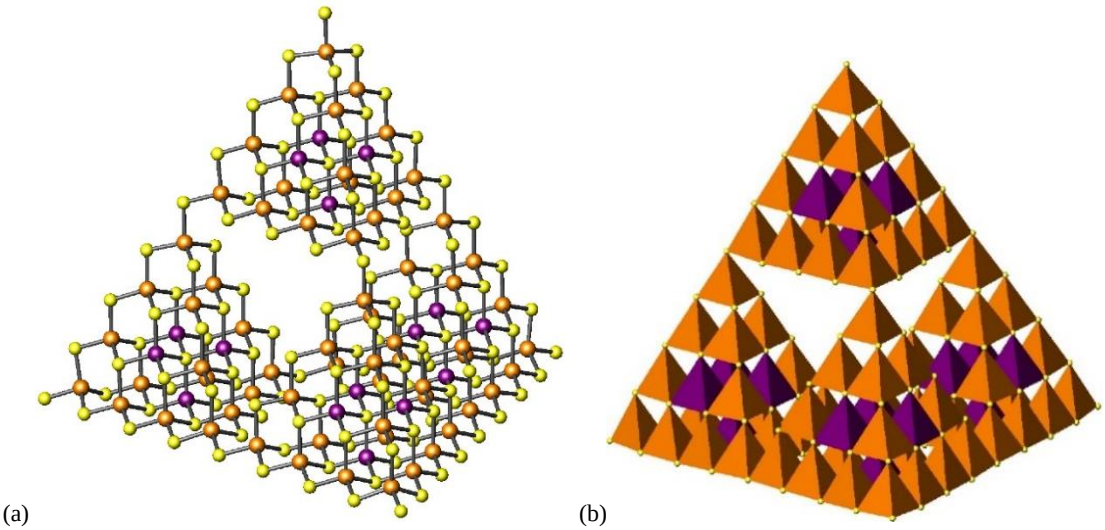

Figure 1.8 (a) Perspective and **(b)** polyhedral representations of the T2,4 cluster in CdInS-420.[97] Orange = In, orange tetrahedra = InS_4, purple = Cd, purple tetrahedra = CdS_4, yellow = S.

Yaghi *et al.* reported a material containing a T2,4 supertetrahedral cluster $[Cd_6In_{64}S_{134}]^{44-}$ (Figure 1.8).[97] The cluster can be described as a T2 cluster, with each tetrahedron replaced by a T4 $[Cd_4In_{16}S_{36}]^{8-}$ cluster. Synthesis of the material, with an

overall formula of $[C_7H_{14}N_2]_{11}[C_8H_{20}N_2O]_{11}[Cd_{16}In_{64}S_{134}](H_2O)_{50}$, utilised the bases DBN and DEAEM.

The final distinct class of supertetrahedral clusters are the capped clusters denoted C*n*. These clusters have a central regular T*n* cluster; capped by barrelenoid cages; which resemble the hexagonal wurtzite ZnS-lattice, rather than the cubic sphalerite ZnS lattice that the regular clusters resemble (Figure 1.9).

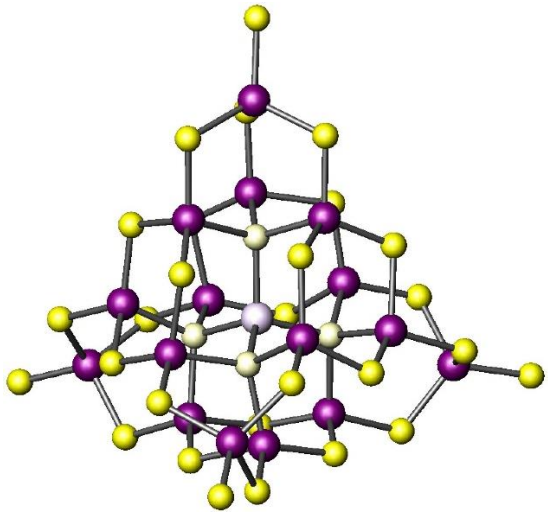

Figure 1.9 Perspective view of a C1 cluster. Purple = M, yellow = X; the central T1 cluster is highlighted.

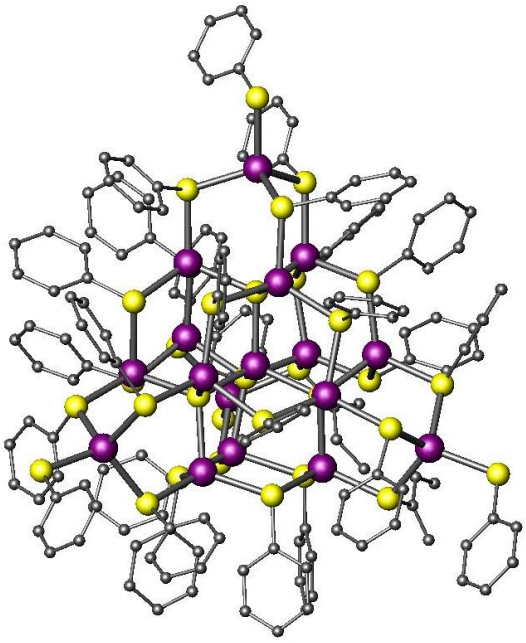

Figure 1.10 Perspective view of the C1 cluster $[S_4Cd_{17}(SPh)_{28}]^{2-}$. Purple = Cd, yellow = S, grey = C. H-atoms are omitted for clarity.

The first example of a C1 cluster was reported in 1988 by Lee *et al.*[98] The cluster (Figure 1.10) has the formula $[S_4Cd_{17}(SPh)_{28}]^{2-}$ and is charge-balanced by TMA^+ cations.

In this case, edge and corner S-atoms are replaced by SPh^{2-} moieties; this reduces the negative charge of the cluster from -30 to -2. Therefore, the organic components are essential to fulfilling the electrostatic valence rule in this case. Clusters containing organic components are known as hybrid clusters and are described in more detail in Section 1.4.5.

It can be observed in both Figure 1.9 and Figure 1.10 that, although these clusters are denoted C1 due to the core T1 cluster, they are much larger than a typical T1 cluster. Therefore, all examples of capped clusters so far have the X^{2-} atoms replaced by XR^{-}, where R is an organic group. This is in order to reduce the resulting negative-charge and stabilise the cluster.

1.4.3 **Gallium-Sulphide and Germanium-Sulphide Supertetrahedra**

In general, germanium-sulphide supertetrahedra exist as T2 clusters $[Ge_4S_{10}]^{4-}$, which can also be described as adamantane units. Gallium sulphide T2 clusters $[Ga_4S_{10}]^{8-}$ are also known and were among those first synthesised by Krebs *et al.* in 1982 and reported by Eisenmann *et al.* in 1983.[99, 100] The $[Ge_4S_{10}]^{4-}$ cluster was known prior to the synthesis of the gallium-sulphide analogues and was reported by Krebs *et al.* in 1971.[5]

Ga^{3+} often forms T3 clusters rather than T2, occurring either in corner-sharing networks of supertetrahedra (Section 1.4.4) or as hybrid supertetrahedral-clusters (Section 1.4.5).

The different metals and chalcogenides that can form these supertetrahedra have been previously mentioned in Section 1.4.2. When it comes to examples of materials based on these types of tetrahedra the field is rich in literature, however there are some which appear to have been more widely investigated than others. There are many examples of indium sulphide and germanium/gallium selenide-based materials, compared to a limited number of examples of gallium sulphides. It is also evident from the literature that T3 gallium-sulphide supertetrahedral clusters do not currently exist as discrete clusters but are generally found in framework structures or hybrid clusters (described in Sections 1.4.4 and 1.4.5 respectively). In many of these structures there is another metal present such as germanium, antimony or tin and these structures will be described.

1.4.4 Gallium-Sulphide and Germanium-Sulphide Zeolite Analogues

MacLachlan *et al.* reported a germanium-sulphide zeolite analogue, which they named δ-GeS_2.[101] In this case, T2 $[Ge_4S_{10}]^{4-}$ clusters are linked *via* corner sharing into a framework (Figure 1.11). The charge of the framework is balanced by TMA^+ cations that reside in the pores.

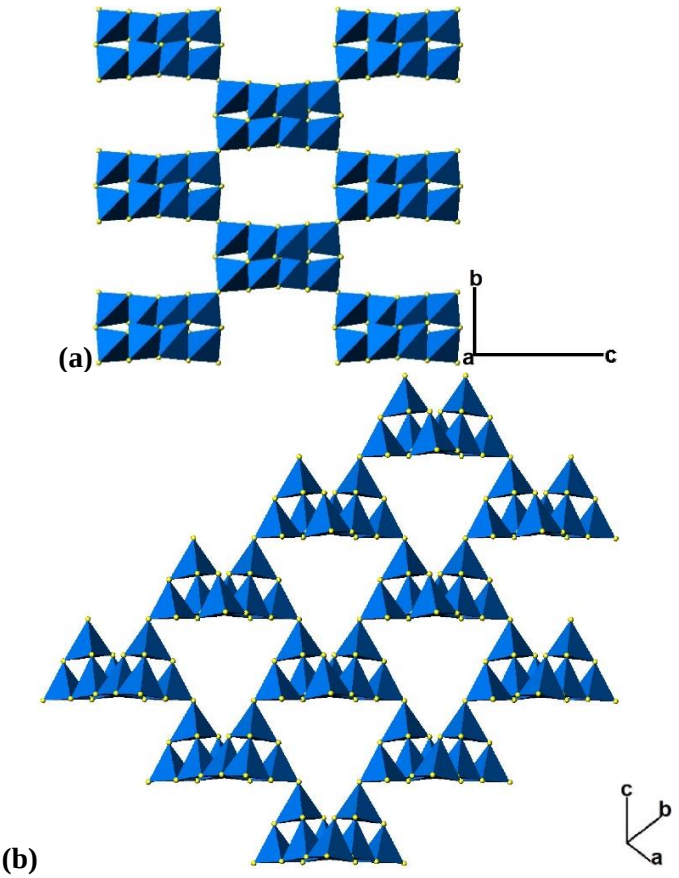

Figure 1.11 Structure of $[C(NH_3)_4]_4[Ge_4S_{10}]$ framework,[101] showing one of the interpenetrating nets **(a)** along the *a*-axis and **(b)** along [111].

This framework was formed by adding HCl to a sample of $[C(NH_3)_4]_4[Ge_4S_{10}]$ with discrete clusters and heating. Therefore this material was produced by post-synthetic linkage of the discrete clusters. This product consisted of white powder and the structure was solved from PXRD data. The structure can be described as the diamond-structure where each C-atom is replaced by $[Ge_4S_{10}]^{4-}$ (Figure 1.11). The material displays interpenetration of two frameworks, giving a double-diamond structure; there are therefore no accessible channels.

Another 3-dimensional structure based on T2 germanium-sulphide clusters was $[C_6H_{14}N_2][MnGe_4S_{10}].3H_2O$ (Figure 1.12); where the T2 clusters are linked *via* Mn^{2+}

into a framework.[102] The material was synthesised in an aqueous solution of 1,4-diazabicyclo[2.2.2]octane (DABCO), which resides in the pores of the framework.

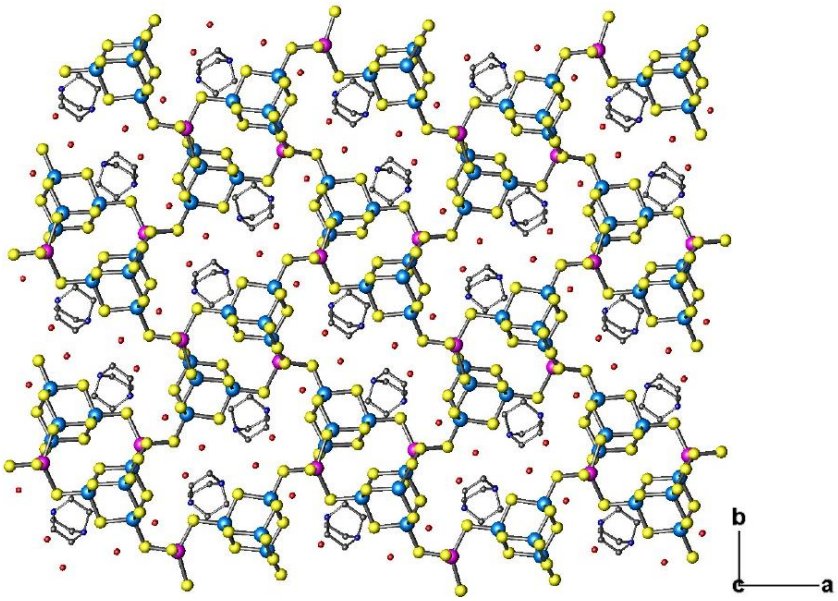

Figure 1.12 $[MnGe_4S_{10}].[C_6H_{14}N_2].3H_2O$ viewed along the *c*-axis.[102] Blue = Ge, yellow = S, magenta = Mn, red = O, dark blue = N, grey = C. H –atoms are omitted for clarity.

Another material based on linked $[Ge_4S_{10}]^{4-}$ clusters consists of chains of T2 units linked together *via* Ag^+ ions; this was also synthesised by Parise *et al.* (Figure 1.13).[103] In this case, the Ag^+ bonds to sulphur trigonally rather than tetrahedrally as in the structure linked *via* Mn^{2+}. The material has the formula of $[H_3O][C_6H_{13}N_2]_2[AgGe_4S_{10}].H_2O$, with the negatively-charged clusters balanced by singly-protonated DABCO moieties and water.

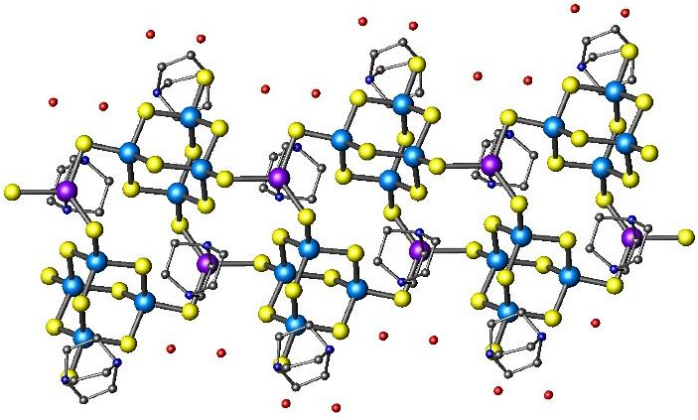

Figure 1.13 Perspective view of a section of a chain in dabco-AgGeS-SB2.[103] Blue = Ge, yellow = S, purple = Ag, red = O, dark blue = N, grey = C. H –atoms are omitted for clarity.

In 2002, Feng *et al.* reported a number of framework materials from a range of group 13 and 14 metals with sulphur or selenium and seventeen new framework materials

are described in detail, of which four were gallium and germanium-sulphides.[104] These materials are listed in Table 1.1, where UCR = University of California Riverside and the final-term denotes the amine used to make the material.

Table 1.1 Gallium and germanium-sulphide zeolite-analogues reported by Zheng et al.[104]

Compound Name	Cluster Formula
UCR-20GaGeS-TAEA	$[Ga_{2.67}Ge_{1.33}S_8]^{2.67-}$
UCR-21GaGeS-APO	$[Ga_{3.30}Ge_{0.70}S_8]^{3.3-}$
UCR-22GaGeS-AEP	$[Ga_{3.33}Ge_{0.67}S_8]^{3.33-}$
UCR-23GaGeS-AEM	$[Ga_{2.67}Ge_{1.33}S_8]^{2.67-}$

TAEA = Tris(2-aminoethyl)amine (also known as tren), APO = 1-amino-2-propanol, AEP = 1-(2-aminoethyl)piperazine, AEM = (2-aminoethyl)morpholine.

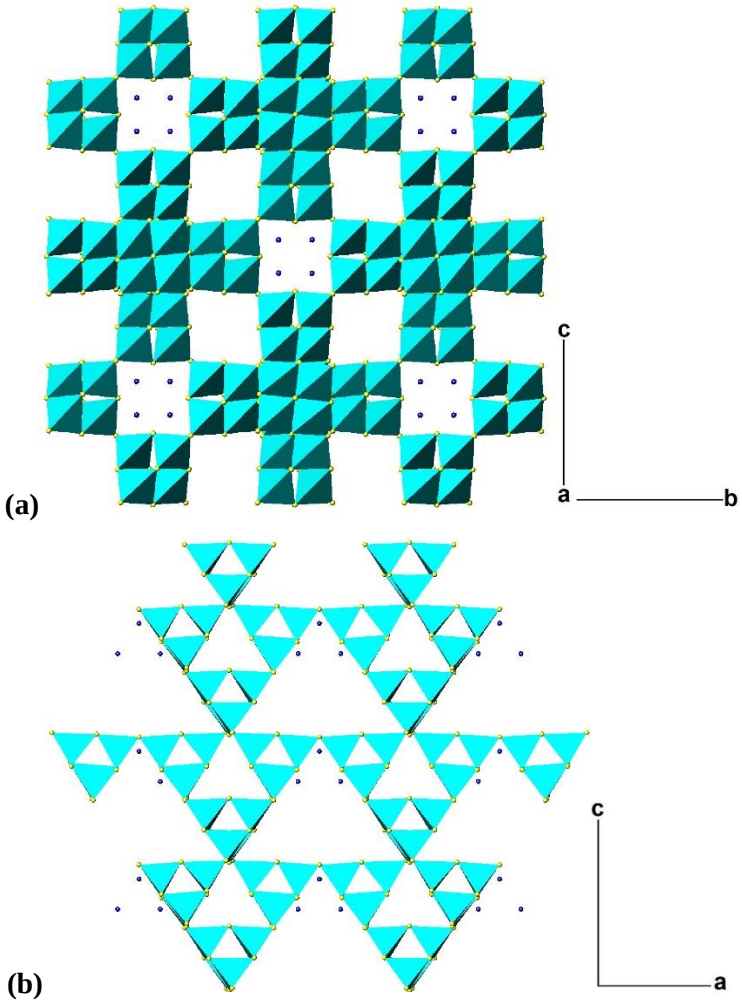

Figure 1.14 The UCR-20GaGeS-TAEA framework viewed **(a)** along the *a*-axis and. **(b)** along [110].[104] Teal tetrahedra = GeS_4 or GaS_4, yellow = S and blue = N.

In these materials, UCR-20 (Figure 1.14), -21 and -23 contain T2 clusters, whereas UCR-22 contains a coreless T4 cluster, which can also be described as T2,2. These resulting products are purely-inorganic porous materials and have an overall negative-charge resulting from the high proportion of chalcogenide anions, this allows for cation exchange, analogous to that which can take place in zeolites.

UCR-20 (Figure 1.14 **(b)**) displays how the structure can be described as a sodalite net, with each $[SiO_4]^{4-}$ or $[AlO_4]^{5-}$ replaced by a T2 cluster; giving a combination of 4-membered and 6-membered rings. UCR-21 has the diamond net as shown in δ-GeS_2 (Figure 1.11) but some germanium-sites are replaced by gallium.

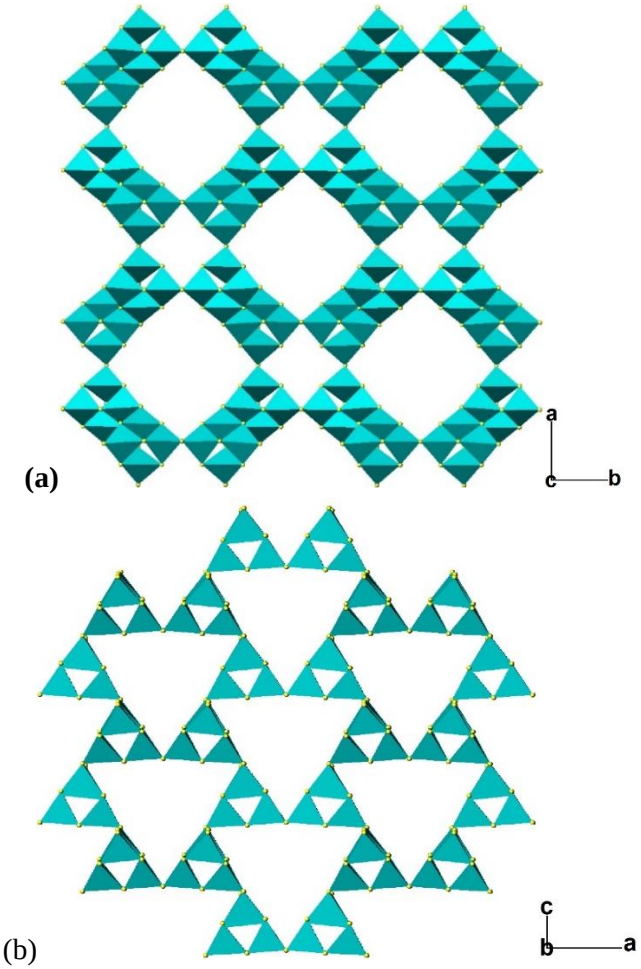

Figure 1.15 The UCR-23GaGeS-AEM framework viewed along the **(a)** the *c*-axis and **(b)** the *b*-axis.[104] Teal tetrahedra = GeS_4 or GaS_4 and yellow = S.

UCR-22 also has a structure based on the ZnS lattice, as seen in UCR-21 and δ-GeS_2. In this case, $[ZnS_4]^{2-}$ tetrahedra are replaced with the T2,2 cluster $M_{16}S_{34}$, where M = Ga or Ge in a Ga:Ge ratio of 5:1.

UCR-23 crystallises with a crystobalite structure (Figure 1.15), consisting of 6-membered and 4-membered rings of T2 clusters. All of these materials showed ion exchange with NH_4^+ and mono- and divalent metal-cations.[104] They also showed photoluminescence, with longer excitation and emission wavelengths for materials containing heavier elements.

The same group later reported a number of corner-sharing frameworks containing gallium-sulphide clusters,[105] some of which also contain Zn^{2+}. This was the first instance in which a T3 gallium-sulphide cluster was observed. The materials formed are listed in Table 1.2. These materials are also described in a review by Bu *et al*.[91]

Table 1.2 Further gallium -sulphide zeolite-analogues reported by Zheng *et al*.[105]

Compound Name	Cluster Formula
UCR-5ZnGaS-BAPP	$[Zn_4Ga_{16}S_{33}]^{10-}$
UCR-7GaS-TETA	$[Ga_{10}S_{18}]^{6-}$
UCR7GaS-TAEA	$[Ga_{10}S_{18}]^{6-}$
UCR-7GaS-DBA	$[Ga_{10}S_{18}]^{6-}$
UCR-18GaS-AEP	$[Ga_{10}S_{17.5}(S_3)_{0.5}]^{6-}$
UCR-19ZnGaS-TETA	$[Ga_{10}S_{18}Zn_4Ga_{16}S_{33}]^{16-}$

The UCR-7 and UCR-18 (Figure 1.16 **(a)**) structures are built from purely T3 clusters and UCR-5 from purely T4 clusters. UCR-19 alternates between T3 and T4 clusters (Figure 1.16 **(b)**); displaying the first occurrence of a material containing two different sizes of supertetrahedra. They also state that the gallium-sulphide analogues of these materials have higher thermal stabilities than the corresponding indium-sulphides and some show strong photoluminescence.

UCR-7 contains two interpenetrating-frameworks based on the ZnS structure; with each tetrahedron replaced with a T3 unit. All of these materials contain a diamond lattice substituted with different supertetrahedra; UCR-5 with T4 supertetrahedra on each site.

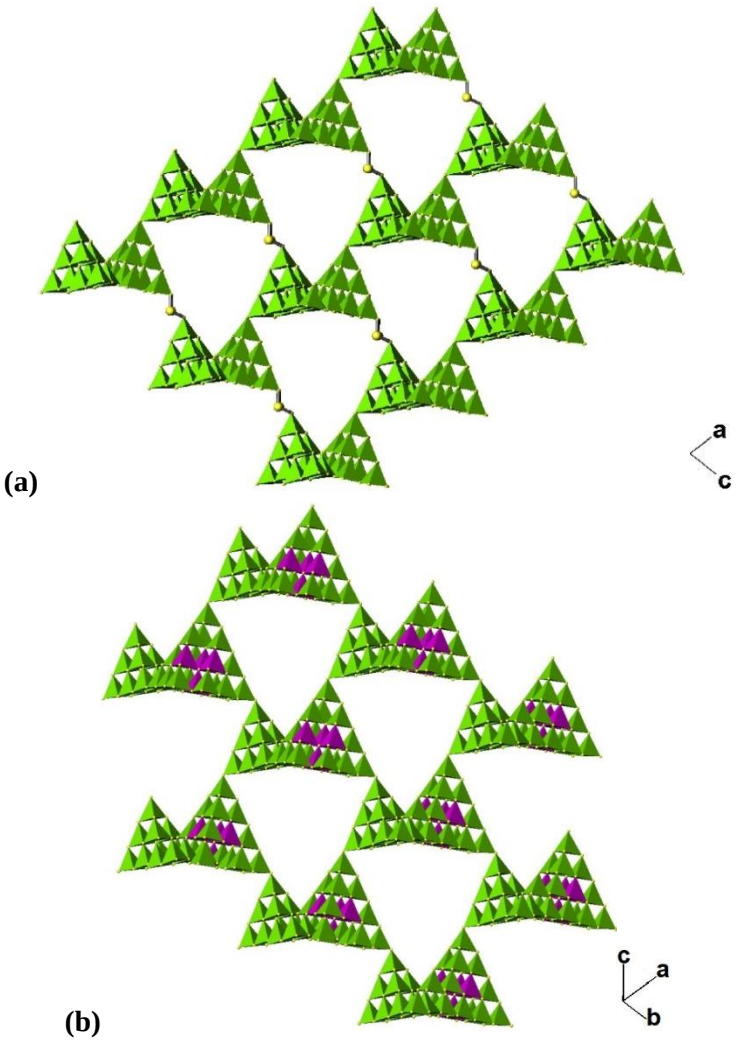

Figure 1.16 (a) The UCR-18GaS-AEP framework viewed along [110] and **(b)** the UCR-19ZnGaS-TETA framework viewed along [111].[105] Green tetrahedra = GaS_4, magenta tetrahedra = ZnS_4 and yellow = S.

In the case of the T3 clusters in UCR-18, one of the corners links to another cluster *via* an -S-S-S- bridge; rather than directly through corner sharing (Figure 1.16 **(a)**). This material also consists of two interpenetrating-frameworks; if there was no interpenetration then the S-S bond would provide larger pore-sizes in the material.

UCR-19 alternates between substituting T3 and T4 supertetrahedra onto the ZnS_4 sites (Figure 1.16 **(b)**). T4 supertetrahedra are formed in cases where zinc is included in the reaction mixture; due to the reduction in the average charge of the cations, which causes an increase in cluster size (Section 1.4.2).

1.4.5 **Hybrid Supertetrahedral Clusters**

It can be observed in UCR-18 that linking *via* –S-S-S- bridges would produce an increase in pore size in a supertetrahedra-based framework. Linking *via* longer units would therefore increase the pore size by a greater amount. This has been investigated by forming supertetrahedral clusters with different ligands co-ordinating to the corner metal-atoms. Hybrid supertetrahedral-clusters can therefore be described as being functionalised by an organic group or ligand.

In the past, hybrid materials have been described where the edge and corner atoms on a cluster have been substituted by organically-functionalised sulphur or selenium atoms; as described for the capped cluster $[S_4Cd_{17}(SPh)_{28}]^{2-}$ by Lee *et al.* in Section 1.4.1.[98] These also include materials reported by Behren *et al.* where Se-atoms are replaced with $[SePh]^-$ ions (Figure 1.18).[106, 107]

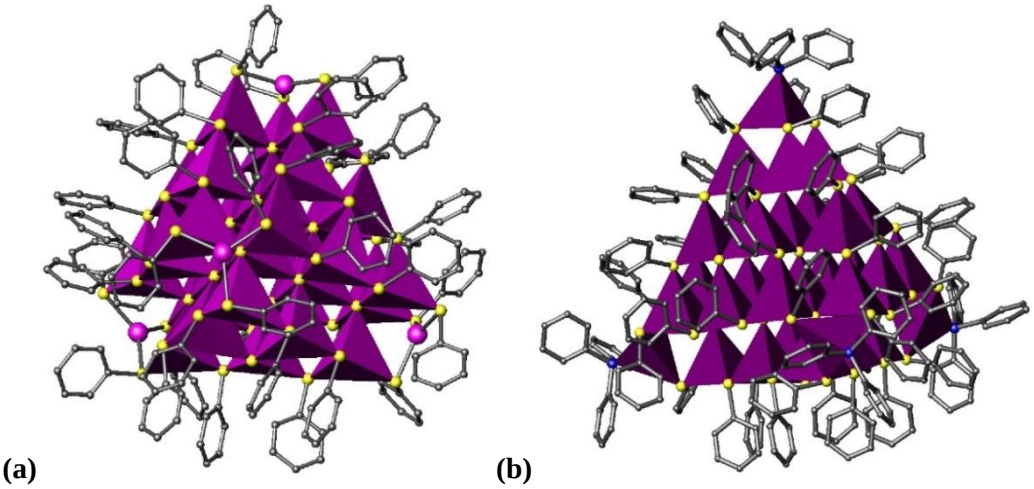

(a) **(b)**

Figure 1.17 (a) Perspective view of $[Hg_{32}Se_{14}(SePh)_{36}]$; magenta tetrahedra = $HgSe_4$ and magenta = Hg.**(b)** Perspective view of $[Cd_{32}Se_{14}(SePh)_{36}\text{-}(PPh_3)_4]$.[106] Purple tetrahedra = $CdSe_4$ or $CdSe_3P$, grey = C and yellow = Se. H-atoms are omitted for clarity

It can be observed that the T4-based $[Hg_{32}Se_{14}(SePh)_{36}]$ cluster (Figure 1.17 **(a)**) does not contain tetrahedra on the corners, but trigonal-planar $[Hg(SePh)_3]^-$ units; resulting in a neutral cluster. Terminating corners with $[Hg(SePh)_4]^{2-}$ would result in an overall charge of -4; this explains the formation of trigonal units. The T4 cluster $[Cd_{32}Se_{14}(SePh)_{36}\text{-}(PPh_3)_4]$ is also neutral (Figure 1.17 **(b)**); this is due to the replacement of the corner Se-atom with neutral PPh_3. There are many materials containing clusters based on the functionalisation of these clusters *via* incorporation of SePh, SPh and also TePh;[108, 109] metals used include Hg,[110] Zn,[111] and Cd.[112]

More recently, hybrid clusters have been formed *via* co-ordination of an amine nitrogen-site to the corner metal of the cluster. This concept has previously been demonstrated by Vaqueiro through the synthesis of the hybrid gallium-sulphide cluster $[Ga_{10}S_{16}(NC_7H_9)_4]^{2-}$ (Figure 1.18).[113] The corner S-atoms of the T3 gallium-sulphide cluster are replaced with 3,5-dimethylpyridine (3,5-Lut) units by using the amine as the solvent. The negative charge on the cluster is stabilised by protonated DMP counter-cations disordered throughout the structure.

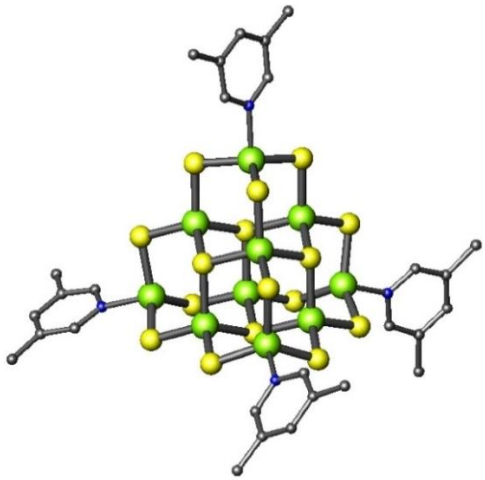

Figure 1.18 Perspective view of the cluster $[Ga_{10}S_{16}(NC_7H_9)_4]^{2-}$.[113] Green = Ga, yellow = S, blue = N, grey = C. H-atoms are omitted for clarity.

Vaqueiro has also reported the synthesis of discrete dimeric units of T3 gallium sulphide clusters, where the clusters are bridged by bidentate ligands (Figure 1.19).[114] The compounds contain anionic clusters; the first a dimer $[Ga_{20}S_{34}H_2(NC_7H_9)_4$ - $(N_2C_{12}H_{10})]^{6-}$, in which the two clusters are linked through one corner *via* by EDPy (4,4'-Ethylenedipyridine) ligands. Two of the other corners are terminated by 3,5-Lut ligands, with an –SH on the final corner.

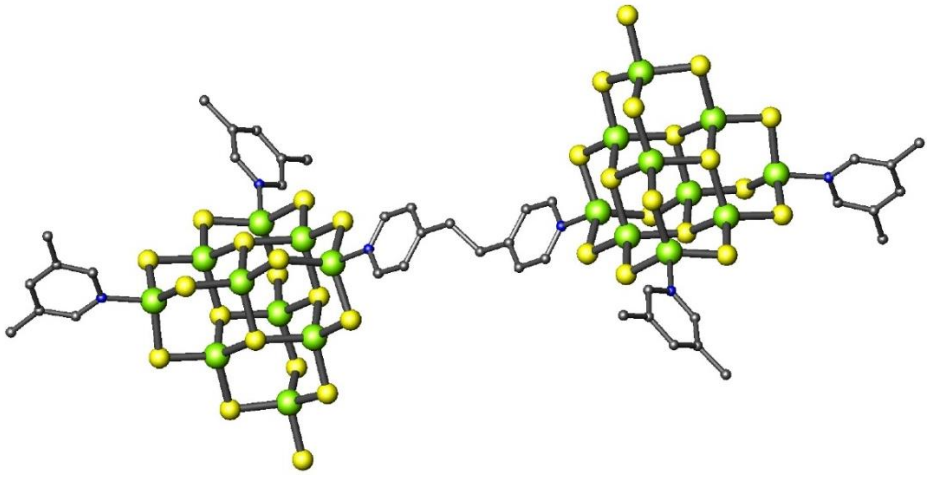

Figure 1.19 Perspective view of the bridged-clusters $[Ga_{20}S_{34}H_2(NC_7H_9)_4(N_2C_{12}H_{10})]^{6-}$.[114] Green = Ga, yellow = S, blue = N, grey = C. H-atoms are omitted for clarity.

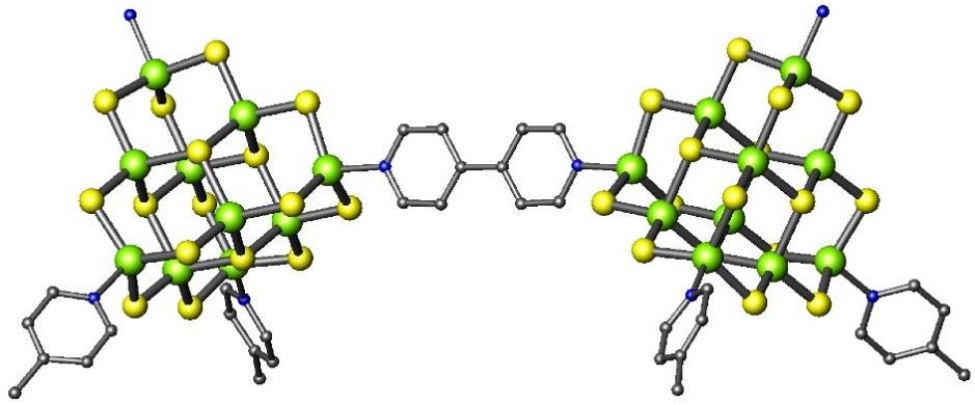

(a)

Figure 1.20 Perspective view of **(a)** bridged-clusters $[Ga_{20}S_{32}(NH_3)_2(NC_6H_7)_4(N_2C_{10}H_8)]$ and **(b)** discrete cluster $[Ga_{10}S_{16}(NC_7H_9)(N_2C_{10}H_8)_3]^{2-}$.[114] Green = Ga, yellow = S, blue = N, grey = C. H-atoms are omitted for clarity.

The second material consisted of a combination of dimers $[Ga_{20}S_{32}(NH_3)_2$ - $(NC_6H_7)_4N_2C_{10}H_8)]^{4-}$ (Figure 1.20) with discrete T3 units $[Ga_{10}S_{16}(NC_7H_9)$ - $(N_2C_{10}H_8)_3]^{2-}$.

Table 1.3 Hybrid supertetrahedra, synthesised in bicyclic amines, reported by Zheng *et al.*[115]

Compound Name	Cluster Formula	Cluster Size
ISC-1	$[Ga_{10}S_{16}(SH)(3,5\text{-Lut})_3]^{3-}$-	T3
ISC-2	$[Ga_{10}S_{16}(SH)(3,4\text{-Lut})_3]^{3-}$	T3
ISC-3	$[In_{10}S_{16}(DBN)_4]^{2-}$	T3
ISC-4	$*[In_{16}Cd_4S_{31}(DBN)_4]^{6-}$	T4
ISC-5	$*[In_{16}Cd_4S_{31}(DBN)_4]^{6-}$	T4
ISC-9	$[In_{22}Cd_{13}S_{52}(1\text{-MIm})_4]^{12-}$	T5
SCIF-10	$[In_{16}Cd_4S_{31}(DMBIM)(DBN)_2]^{7-}$	T4

*Polymorphs heated for 8 and 12-days respectively. DMBIM = 5,6-dimethylbenzimidazolate

Discrete hybrid gallium sulphide clusters have also been reported by Feng *et al.*,[115] who have synthesised a number of these clusters for a range of different metals with sulphur. Of these different structures, ISC-1 and ISC-2 (where ISC= Isolated Hybrid Supertetrahedral Cluster) are gallium sulphides, which have been synthesised using the templates 3,5-Lut and 3,4-Lut respectively. These materials consist of T3 clusters $[Ga_{10}S_{16}(SH)(NC_7H_9)_3]^{3-}$, where three of the corners are coordinated by the given ligand and the other by an SH^- moiety. The negative charge of each cluster is balanced by three

equivalents of the protonated ligand, which are ordered in ISC-1 but in ISC-2 are highly disordered.

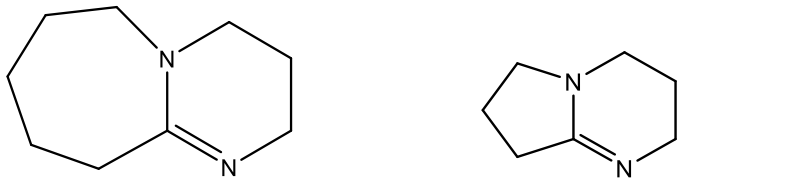

1,8-Diazabicyclo(5.4.0)undec-7-ene (DBU) 1,5-Diazabicyclo(4.3.0)non-5-ene (DBN)

Figure 1.21 Superbases used by Feng *et al.* in the synthesis of hybrid supertetrahedra.

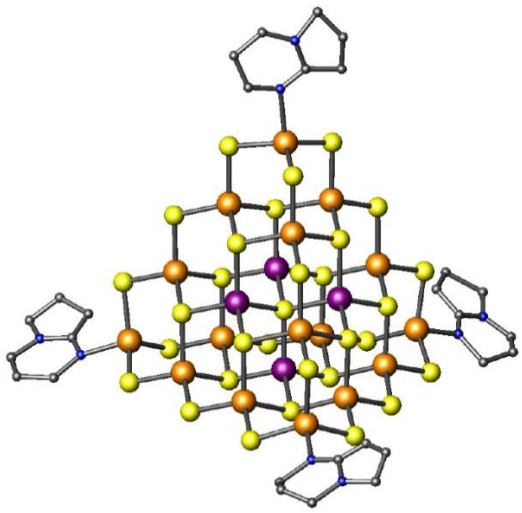

Figure 1.22 Perspective view of the cluster $[In_{16}Cd_4S_{31}(DBN)_4]^{6-}$.[115] Orange= In, purple = Cd, yellow = S, blue = N, grey = C. H-atoms are omitted for clarity.

Although the gallium sulphides reported here are both based on T3 clusters, T4 and T5 indium-sulphide analogues have also been reported, all containing a second divalent metal (Cd, Mn, Co or Fe, Figure 1.22). In this case, the templates used were the bicylcic amines DBN (1,5-Diazabicyclo(4.3.0)non-5-ene) and DBU (1,8-Diazabicyclo(5.4.0)-undec-7-ene, Figure 1.21); also known as "superbases" due to the higher pKa values of their conjugate acids (Section 2.1.1). Li^+ ions were also present in the reaction mixture; from the sulphur-source of Li_2S.

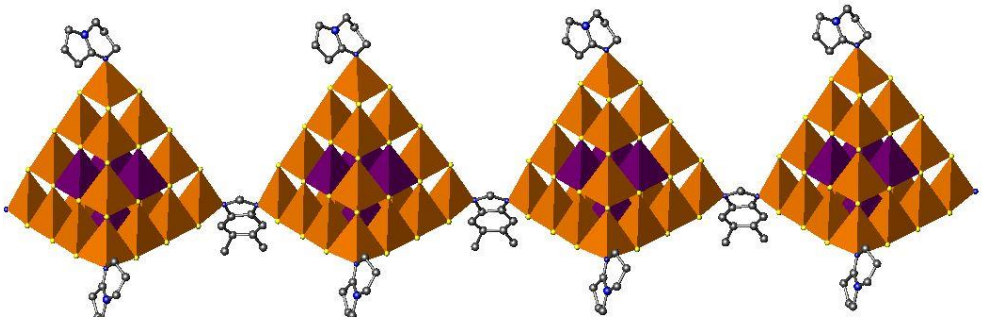

Figure 1.23 Perspective view of a chain in SCIF-10 $[In_{16}Cd_4S_{31}(DMBIM)(DBN)_2]^{7-}$.[115] Orange tetrahedra = InS_4 or InS_3N, purple tetrahedra = CdS_4, yellow = S, blue = N, grey = C. H-atoms are omitted for clarity.

SCIF-10 (Table 1.3) consists of T4 $[In_{16}Cd_4S_{31}(DMBIM)(DBN)_2]^{7-}$ clusters linked into chains *via* the 5,6-dimethylbenzimidazolate ligands (Figure 1.23). Further materials in this series (SCIF-1 – SCIF-9) are described in a separate publication and consist of different indium-sulphide clusters linked *via* imidazole-based ligands (SCIF = supertetrahedral chalcogenide imizadolate framework).[116] The materials were all synthesised using DBU as a template and contain doubly or triply-interpenetrating frameworks with the diamond-topology (Figure 1.24).

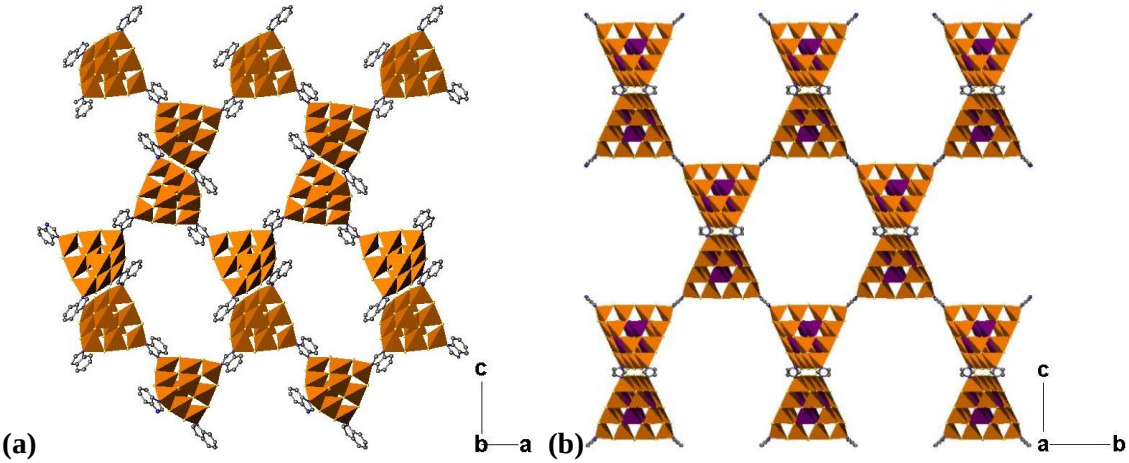

Figure 1.24 One interpenetrating network in **(a)** SCIF-5 $[In_{10}S_{16}(BenzIm)_2]^{4-}$, viewed along the *b*-axis and **(b)** SCIF-8 $[In_{16}Cd_4S_3(2\text{-}EIm)_2]^{8-}$ viewed along the *a*-axis. [115] Orange tetrahedra = InS_4 or InS_3N, purple tetrahedra = CdS_4, yellow = S, blue = N, grey = C. BenzIm = benzimidazole, 2-EIm = 2-ethylimidazole. H-atoms are omitted for clarity.

In 2005, Zheng *et al.* reported the linking of the SPh-functionalised cadmium-sulphide supertetrahedral clusters *via* pyridyl ligands (Figure 1.25).[117] In a separate publication they also reported the linking of P1 zinc-sulphide clusters, also *via* pyridyl ligands. In both of these cases the clusters have been linked into 1-dimensional chains.

Capped clusters are reported to link into chains *via* either bipy or TMDPy. In this case, materials were labelled COV, due to the fact the clusters are linked *via* covalent ligands. In total, five different materials were described; all based on capped supertetrahedral-clusters. COV-3CdS-Bpy (Figure 1.25) consists of C1 clusters $Cd_{17}S_4(SPh)_{26}(C_{10}H_8N_2)_2$ linked into a zigzag chain *via* bipy ligands.

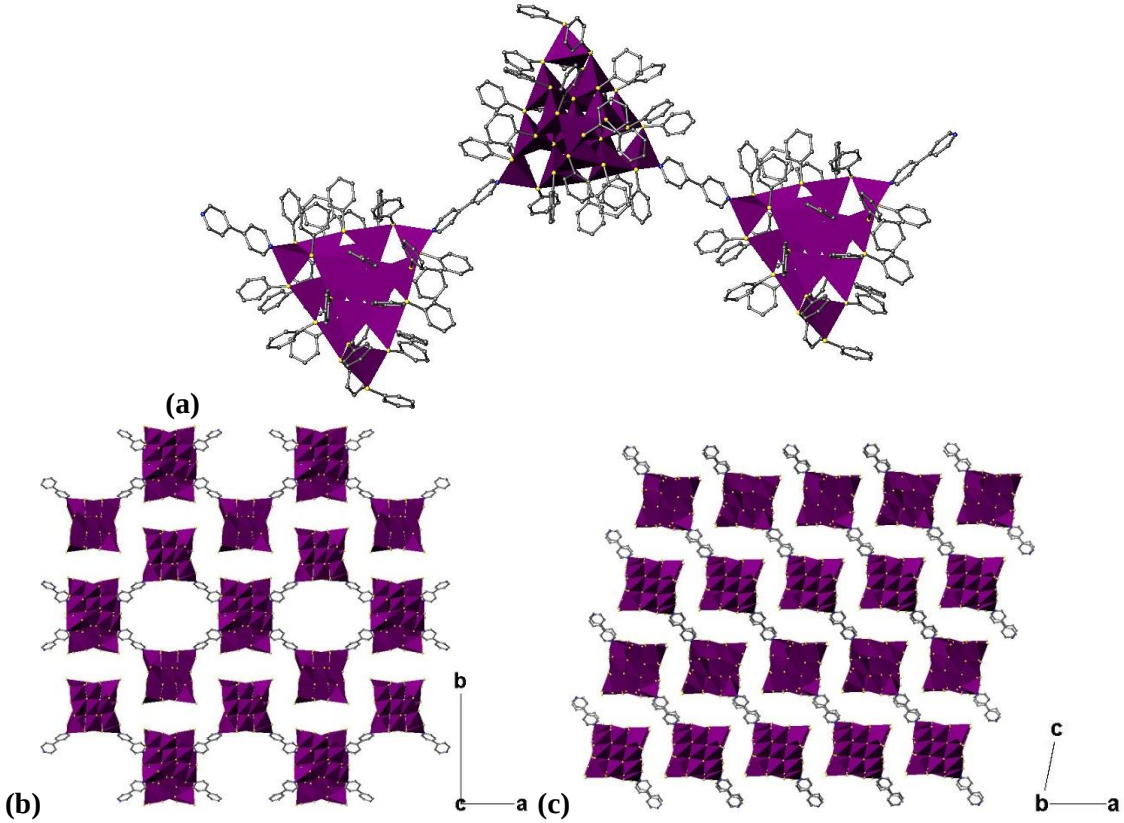

Figure 1.25 Chains of $Cd_{17}S_4(SPh)_{26}(C_{10}H_8N_2)_2$. **(a)** Perspective view, **(b)** viewed along the *c*-axis and **(c)** along the *b*-axis.[115] Purple = Cd, yellow = S, blue = N, grey = C. Edge -Ph groups and H-atoms are omitted for clarity.[117]

In the same publication, four more materials are described, one of which is named COV-3CdSSe-Bpy and is therefore isostructural with COV-3CdS-Bpy but S-atoms on the central T1 unit are replaced with Se. They also report a new type of capped supertetrahedral-cluster; which they denote C*n,m*. In this case, *n* denotes the class of capped cluster, but *m* denotes the number of corners that are rotated by 60° and therefore *m* = 1-4. Another type of capped cluster is labelled C0, however this can be considered to be a P1 cluster, as described in Section 1.4.2. The material containing these clusters is labelled COV-4CdS-TMDPy, where TMDPy links $Cd_8S(SPh)_{14}(C_{12}H_{12}N_2)_2$ clusters into linear chains.

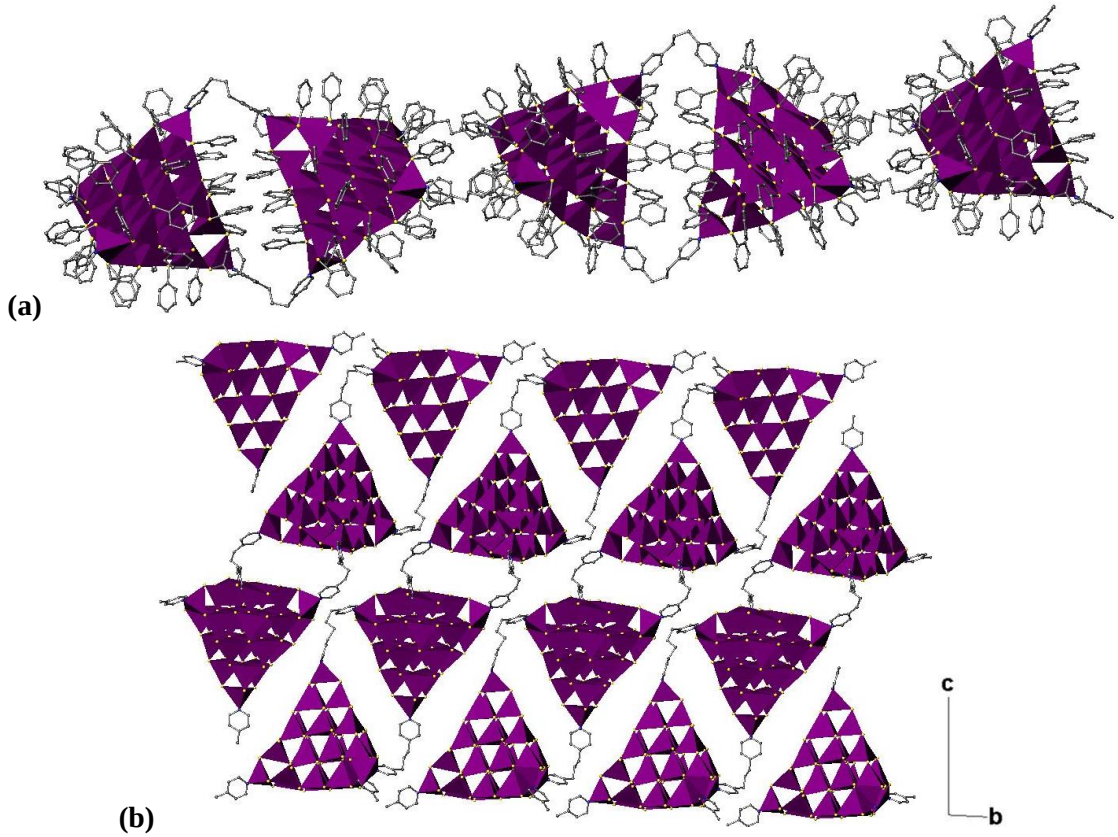

Figure 1.26 Chains of $Cd_{32}S_{14}(SPh)_{36}(C_{12}H_{12}N_2)_4$. **(a)** Perspective view, H-atoms are omitted for clarity. **(b)** viewed along [100], edge -Ph groups and H-atoms are omitted for clarity. Purple = Cd, yellow = S, blue = N, grey = C.[117]

COV-1CdS-TMDPy (Figure 1.26) consists of C2,1 clusters, which are C2 clusters with one corner rotated by 60°. In this case, clusters are linked *via* two of their corners into 1-dimensional chains through TMDPy ligands. Here, the chains propagate a straight line; rather than in a zigzag fashion. It is unusual for clusters to create doubly-bridged chains as observed here, whereas singly-bridged chains, as described for other structures in this publication, are often observed.[94, 117, 118] The remaining structure is denoted COV-2CdS-TMDPy-TPhP, containing negatively-charged C2,2 clusters linked *via* TMDPy. Tetraphenylphosphonium cations in the void space balance the charge of the chains. This is the only material reported here to contain void space; as the other materials all contain neutral chains.

Zheng *et al.* report, in a separate publication,[118] the linking of –SPh functionalised P1 zinc-sulphide clusters *via* either EDPy in $Zn_8S(SC_6H_5)_{14}(C_{12}H_{10}N_2)$ or 4,4'-propyldipyridine (PDPy) in $Zn_8S(SC_6H_5)_{14}$-$(C_{13}H_{14}N_2)$ into 1-dimensional chains. In $Zn_7CoS(SC_6H_5)_{14}(C_{13}H_{14}N_2)$, the PDPy-linked clusters are heterometallic, with one Zn atom replaced with Cd.

Vaqueiro *et al.* later reported a material containing 1-dimensional chains of T3 gallium-sulphide clusters linked *via* EDPy;[119] this is described in further detail in Section 3.3. In the same publication, a material containing T3 gallium-sulphide clusters linked into 2-dimensional layers *via* EDPy was described.

Dehnen *et al.* reported the synthesis of organically-functionalised germanium-chalcogenide clusters (Figure 1.27).[120] The germanium sulphide reported consists of the T2 cluster $[(NC(CH_2)_2Ge)_4S_6]$ (Figure 1.27 **(a)**), which is unusual due to coordination by ethyl cyanide (ECN) *via* the terminal carbon and not *via* the nitrogen-site. The synthesis of this material involves a multistep process, where $Cl_3Ge(CH_2)_2CN$ is firstly produced. This compound then reacts with sodium sulphide to give the final product of $[(NC(CH_2)_2Ge)_4S_6]$. The Ge-Cl bonds are therefore more susceptible to attack from the Na_2S, rather than the Ge-C bond.

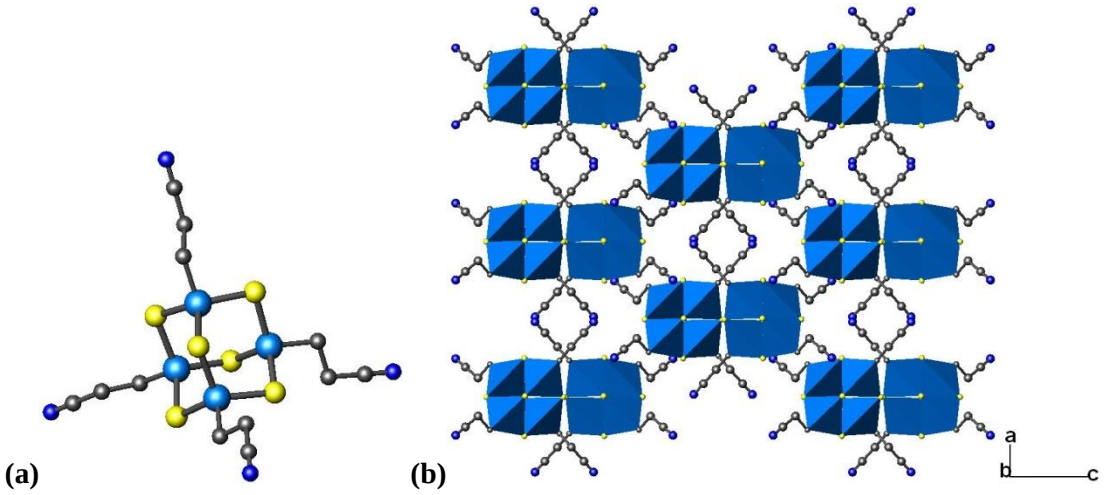

Figure 1.27 (a) Perspective view of the cluster $[(NC(CH_2)_2Ge)_4S_6]$.[120]
(b) $[(NC(CH_2)_2Ge)_4S_6]$.viewed along the b-axis. Blue = Ge, yellow = S, dark blue = N, grey = C. H-atoms are omitted for clarity.

They also built on this method to produce a 3-dimensional structure from propanoic-acid substituted units; linked *via* manganese, methanol and DMF into a framework material (Figure 1.28).[121]

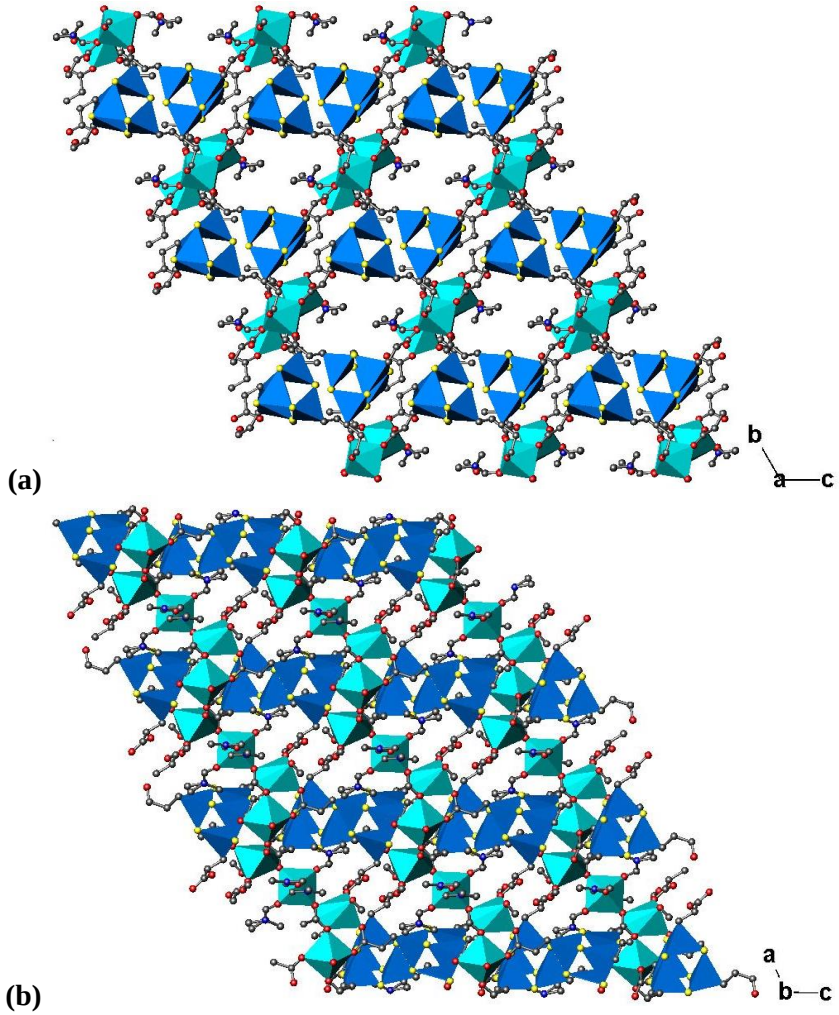

Figure 1.28 $[Mn_2((OOCC_2H_4Ge)_4S_6)(MeOH)(DMF)_2]$ viewed along **(a)** along the *a*-axis and **(b)** along the *b*-axis. Blue tetrahedra = GeS_4 or GeS_3C, teal octahedra = MnO_6, yellow = S, dark blue = N, grey = C and red = O. H-atoms are omitted for clarity.

1.4.6 Other Gallium and Germanium Sulphides Containing Organic Components

Gallium and germanium sulphides have been reported to exist in forms other than those consisting of supertetrahedra. These range from 1-dimensional chains to 3-dimensional frameworks; of which a number will be discussed here. Organic moieties are present in all cases, either linked to the inorganic component or as charge-balancing species in the voids of the material. Zhou *et al.* have reviewed a number of different

chalcogenide-compounds of group 13-15 metals, containing those containing discrete complexes and also those covalently linked by organic or organometallic moieties.[122]

1.4.6.1 *Gallium-Sulphides*

Vaqueiro reported a number of structures synthesised using ethylenediamine as a template.[123] Three of the five reported structures with formula $[M(en)_3]_{0.5}[GaS_2]$ (M=Mn, Co, Ni) had a similar one-dimensional chain structure, consisting of $[GaS_2]^-$ building units with metal complexes $[M(en)_3]^{2+}$ as counter ions to the chains (Figure 1.29).

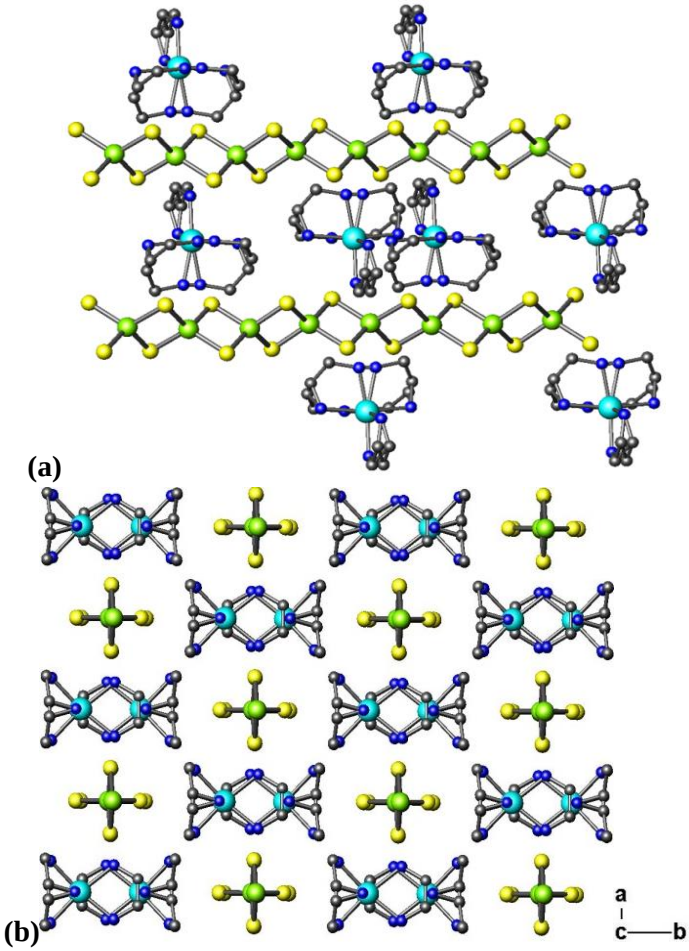

Figure 1.29 $[Mn(en)_3]_{0.5}[GaS_2]$ **(a)** perspective view **(b)** viewed along the *c*-axis. Green =Ga, cyan = Mn, grey = C, blue = N, yellow = S. H-atoms have been omitted for clarity

Another reported material reported by Vaqueiro synthesised in en had the formula $Mn(en)_2Ga_2S_4$, in which it was found that the $[GaS_2]^-$ chains were linked via $[Mn(en)_2]^{2+}$ complexes into a 3-dimensional framework. The only difference in the reaction conditions here was the quantity of ethylenediamine added to the mixture.[123]

The final compound described in this work was the framework material $[enH_2][Ga_4S_7(en)_2]$ (Figure 1.30) which contains negatively-charged layers of

$[Ga_4S_7(en)_2]^{2-}$ and enH^+ moieties residing between to maintain charge neutrality. In this structure these $[Ga_4S_7(en)_2]^{2-}$ units link through the corner sulphur-atoms to form a continuous layer

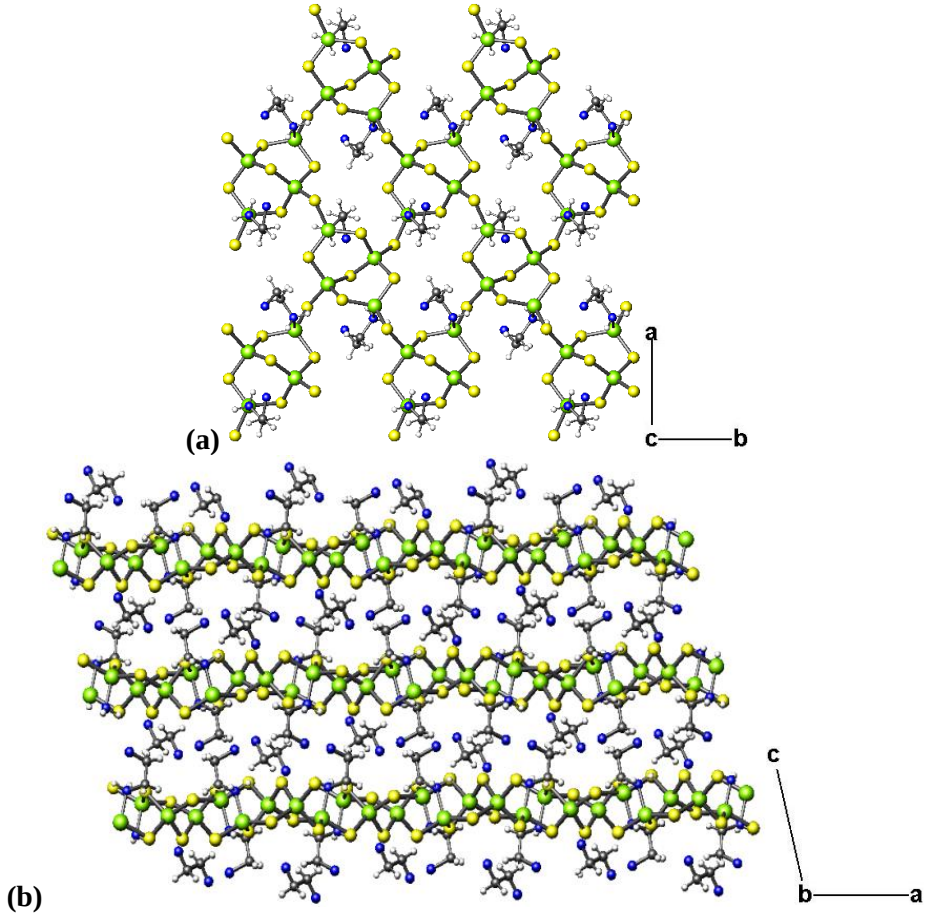

Figure 1.30 The structure of$[enH_2][Ga_4S_7(en)_2]$ **(a)** a single layer viewed along the *c*-axis, **(b)** viewed along the *b*-axis.. Green =Ga, grey = C, blue = N, yellow = S and white = H.

The chains described above (Figure 1.29) are generated from regular T1 tetrahedra alternating in orientation, while sharing two of their corner atoms with the next tetrahedron. These types of chains are observed often in main-group chalcogenides and Ewing *et al.* reported an indium-selenide analogue $[NH_4][InSe_2]$, containing chains of this nature, balanced by ammonium ions.[124-128] In a separate paper by Ewing *et al.* gallium-sulphide chains $[C_6H_{16}N_2][GaS_2]_2$ are reported;[129] the negative charge of the chains is balanced by protonated DACH cations.

These one-dimensional chains are also present in both indium and gallium-sulphide structures,[125] reported by Vaqueiro, which have the formulae

$[C_{10}N_4H_{26}]_{0.5}[InS_2]$ and $[C_{10}N_4H_{26}]_{0.5}[GaS_2]$. Both were synthesised using a template of BAPP, as the first examples of 1-dimensional indium and gallium sulphides.

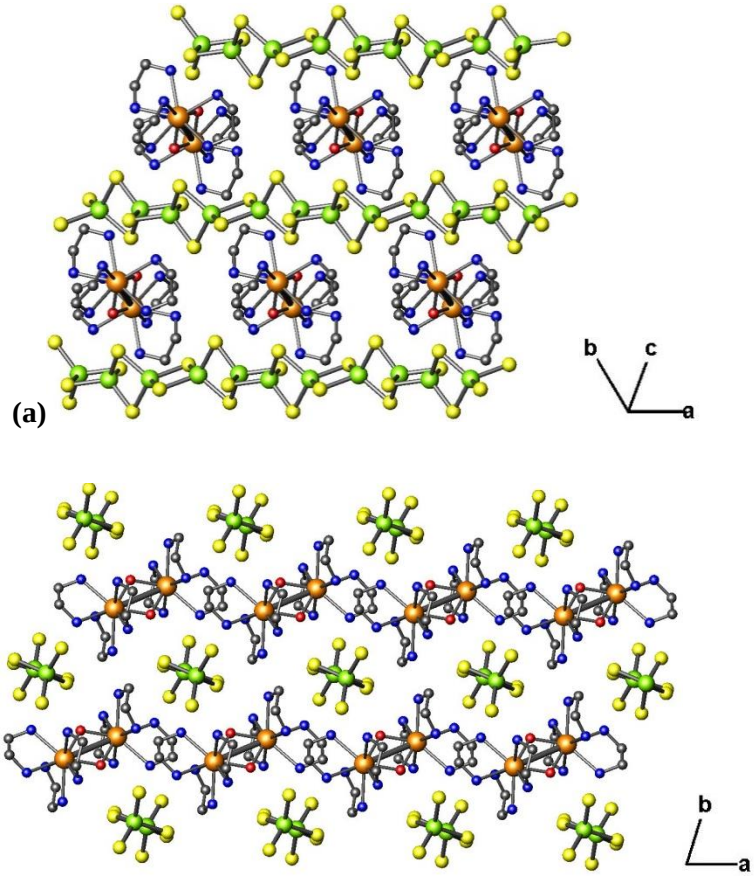

Figure 1.31 $[Dy_2(en)_6(\mu_2\text{-}OH)_2]Ga_4S_8$ **(a)** viewed along [111] and **(b)** perspective view. Green =Ga, orange = Dy, grey = C, blue = N, red = O and yellow = S. H-atoms have been omitted for clarity

In general, the -Ga-S-Ga- linkages in these chains are rotated 180° at every alternate Ga atom (Figure 1.29), this is the favoured orientation for these chains to possess.[129] However, $[Dy_2(en)_6(\mu_2\text{-}OH)_2]Ga_4S_8$ reported by Zhou *et al.* contains chains where this angle deviates to between 164.16(5) and 166.94(5)° (Figure 1.31).[128]

1.4.6.2 *Germanium-Sulphides*

Jia *et al.* reported materials $(enH)_4Ge_2S_6$ and $[M(en)_3]_2Ge_2S_6$,[130] where M = Mn or Ni, synthesised in en. These materials consist of discrete $[Ge_2S_6]^{4-}$ units (Figure 1.32), with either protonated en or $[M(en)_3]^{2+}$ in the voids to balance the charge. The $[Ge_2S_6]^{4-}$ units can be considered dimers of corner sharing GeS_4 tetrahedra.

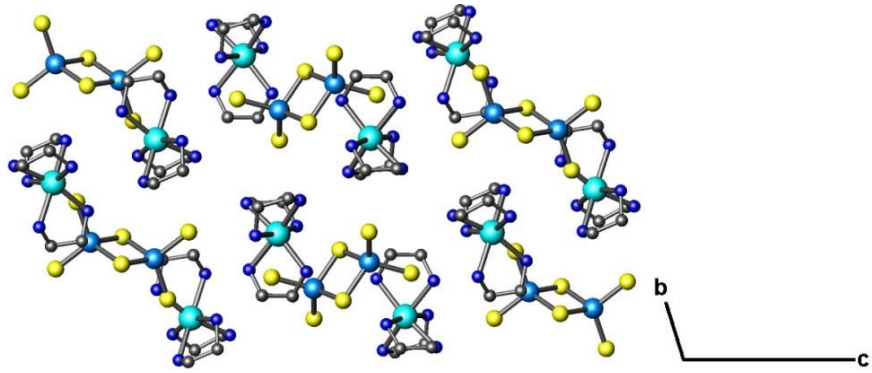

Figure 1.32 Perspective view of $[Mn(en)_3]_2Ge_2S_6$.[130] Blue =Ge, teal = Mn, grey = C, dark blue = N, yellow = S. H-atoms have been omitted for clarity.

Liu *et al.* also describe dimers of this nature,[131] two in which the dimeric units $[Ge_4S_6]^{4-}$ are charge balanced by either $2[Ni(dien)_2]^{2+}$ (dien = diethylenetriamine) or one $[Ni(dien)_2]^{2+}$ complex, along with a protonated piperazine (ppz) moiety. They also describe coordination of manganese and nickel complexes to the dimeric units (Figure 1.33), where two sulphur-atoms on each cluster bridge one Ge^{4+} with one Mn^{2+} or $Ni.^{2+}$.This occurs with the amines tris(2-aminoethyl)amine (tren) in $[Mn(tren)](\mu_2\text{-}Ge_2S_6)$ (Figure 1.33) and tetraethylenepentamine (tepa) in $[Mn(tepa)]_2(\mu_2\text{-}Ge_2S_6)$ and $[Ni(tepa)]_2(\mu_2\text{-}Ge_2S_6)$. Antiferromagnetic interactions were observed between the transition metals in all samples, which also displayed photoluminescence. There are also a number of further reports of materials containing these dimeric units linked to organometallic transition-metal or lanthanide complexes.[132, 133]

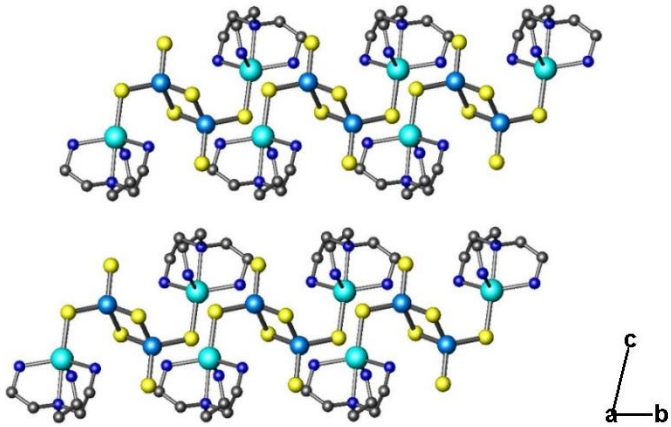

Figure 1.33 $[Mn(tren)](\mu_2\text{-}Ge_2S_6)$ viewed along the *a*-axis.[131] Blue =Ge, teal = Mn, grey = C, dark blue = N, yellow = S. H-atoms have been omitted for clarity.

Yue *et al.* described chains of tetrahedra,[134] resembling those formed by gallium and indium sulphides (Section 1.4.6.1).[123, 125, 126, 128, 129] In this case, germanium possessed both Ge^{2+} and Ge^{4+} oxidation states to give an average oxidation state of Ge^{3+},

as observed for gallium in these chains. Due to the variation in oxidation-state, Ge-S bonds vary in length; Ge(IV)-S bonds have an average length of *ca.* 2.23 Å, whereas Ge(II)-S bonds average at *ca.* 2.48 Å. There is also a distortion of the Ge(II) tetrahedron.

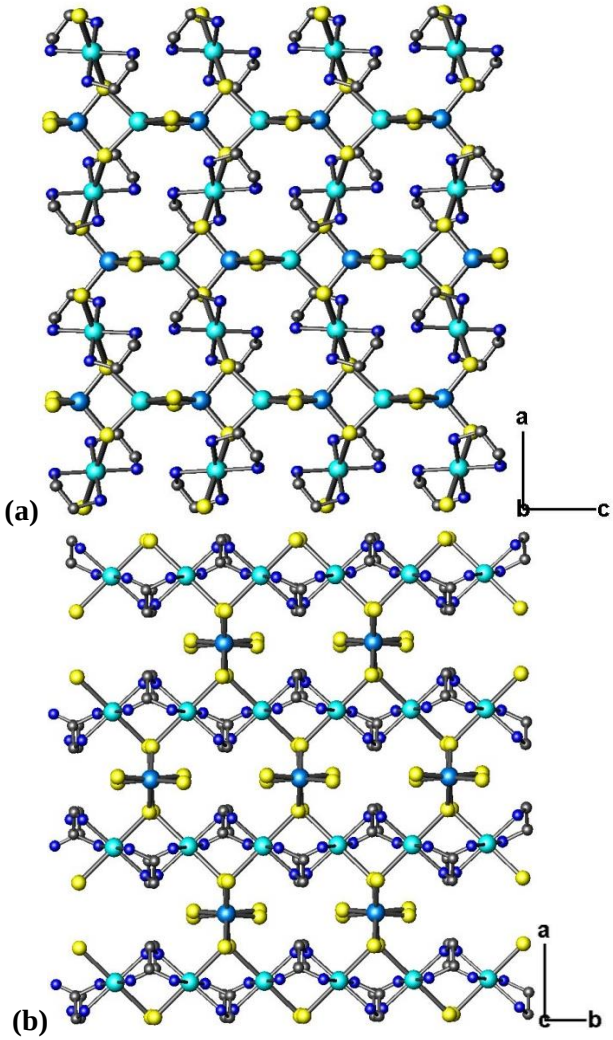

Figure 1.34 $[Mn(en)_2]MnGeS_4]$ viewed along **(a)** the *b*-axis and **(b)** the *c*-axis.[131] Blue =Ge, teal = Mn, grey = C, dark blue = N, yellow = S. H-atoms have been omitted for clarity.

They also reported the synthesis of these chains, where the metal-centres alternate between Ge^{4+} and Mn^{2+}.[135] However, here the chains are linked into a 3-dimensional network *via* $[Mn(en)_2]^{2+}$. This is achieved through distorted trigonal sulphur-sites (Figure 1.34).

1.5 Materials Synthesised *via* Ionothermal Synthesis

As mentioned in Section 1.2.1, the hydrothermal method was first used for synthesising zeolite materials.[28, 136] The first metal-organic frameworks were also synthesised using this method, but as the materials became more advanced different solvents were required, along with their use in synthesising zeolitic materials.[137] The method was therefore adapted for other solvents and termed solvothermal,[138, 139] as described further in Section 2.1.1.

A relatively recent method for zeolite and MOF synthesis is the ionothermal method developed by Morris *et.al.*[140, 141] It differs from solvothermal synthesis as the solvent is replaced with an ionic liquid. Although often performed in an autoclave, it is not essential in this case, as reactions take place at ambient pressures and there are examples of cases where the reactions have been carried out in a round-bottomed flask.[140] The great difference in ionic liquids compared to other regular solvents is that they have an almost negligible vapour-pressure; therefore autogenous pressure is not created in the system.

This type of synthesis has been developed so that the ionic liquid acts as the solvent and structure-directing agent (SDA). It is beneficial in the synthesis of charged frameworks as the charge can be balanced by the ionic liquid without protonation or deprotonation of the solvent molecules. There are numerous examples published by Morris *et.al* and it is also summarised in 2007 and 2009 reviews.[140-144]

There is so far a relatively limited amount of literature on porous materials synthesised in ionic liquids but the field is growing rapidly and many of the known structures are based on zeolitic materials. The first of these syntheses was carried out by Cooper *et al.* where they produced the aluminophosphate $Al_8(PO_4)_{10}H_{3.3}C_6H_{11}N_2$ SIZ-1, (SIZ = St Andrews Ionothermal Zeotype) in 1-Methyl 3-ethyl imidazolium bromide ([MEIm]Br).[140, 145] They also describe the formation of aluminophosphates SIZ-3 – SIZ-5, also synthesised in [MEIm]Br, where SIZ-3 and SIZ-4 are synthesised in the presence of fluoride. Parnham *et al.* also describe cobalt aluminophosphates and further examples of aluminophosphates, all synthesised in ionic liquids.[143, 145-148]

After the establishment of this method it has been used by numerous others such as Xu *et al* for the synthesis of cadmium metal-organic frameworks and Dehnen *et.al* in their research on chalcogenide materials.[141, 143, 149, 150]

1.5.1 Chalcogenide Materials Synthesised in Ionic Liquids

So far literature for chalcogenide materials synthesised in ionic liquids is relatively limited, especially for those containing supertetrahedra. A number of materials are reviewed by Xiong *et al* in a recent publication, which describes products synthesised in ionic liquids, surfactants and hydrazine media.[151] Various ionothermally-synthesised germanium and tin-selenide materials are described by Dehnen *et al.*.[150, 152]

The first of these synthesised has the formula $[BMIm]_4[Sn_9S_{20}]$ (Figure 1.35, BMIm = 1-butyl-3-methyl-imidazolium, Figure 1.36) and has a three-dimensional open framework structure.[152] Synthesis was carried out in the ionic liquid $[BMIm][BF_4]$, with a starting reagent of $[K_4(H_2O)_4][SnSe_4]$. This structure consists of semicubes (Figure 1.35 **(b)**) linked into a zigzag chain by $[SnSe_4]^{4-}$ tetrahedra and then further linked into an open framework by $[Sn_2Se_6]^{2-}$ units (Figure 1.35 **(c)**). This anionic framework is charge-balanced by $[BMIm]^+$ cations, reflecting how these act as both the structure-directing agent and cation due to the lack of auxiliary amine. Further tin - selenide frameworks synthesised in imidazolium-based ionic liquids were also reported by Li *et al.*.[153]

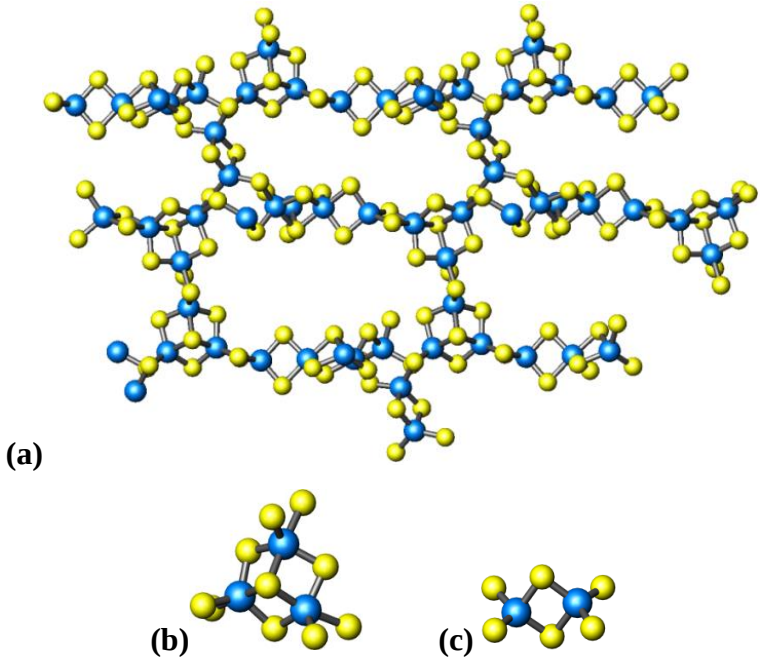

Figure 1.35 (a) Perspective view of $[Sn_9Se_{20}]^{4-}$, **(b)** a semi cube unit, **(c)** a $[Sn_2Se_6]$ unit. Blue =Sn, yellow = Se. Solvent molecules have been omitted for clarity.

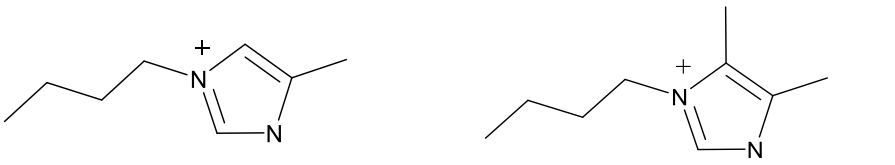

1-Butyl-3-Methyl Imidazolium
$[BMIm]^+$

1-Butyl-2,3-Dimethyl Imidazolium
$[BMMIm]^+$

Figure 1.36 Ionic-liquid cations abbreviated in this section

Materials by Dehnen *et al.* were also created containing 1-dimensional chains of T2 clusters . One of these materials was a germanium selenide (Figure 1.37), whereas the second was a germanium tin selenide. These were synthesised from a starting reagent of $[K_4(H_2O)_3][Ge_4Se_{10}]$ in $[BMIm]BF_4$ and $[BMMIm]BF_4$ (BMMIm = (BMMIm=1-butyl-2,3-dimethylimidazolium, Figure 1.36) respectively. 1-dimensional chains of $([C_8H_{15}N_2]_2[Ge_4Se_9])_n$ are displayed in Figure 1.37 and propagate along the *b*-axis; the negative charge is balanced by $[BMIm]^+$ cations.

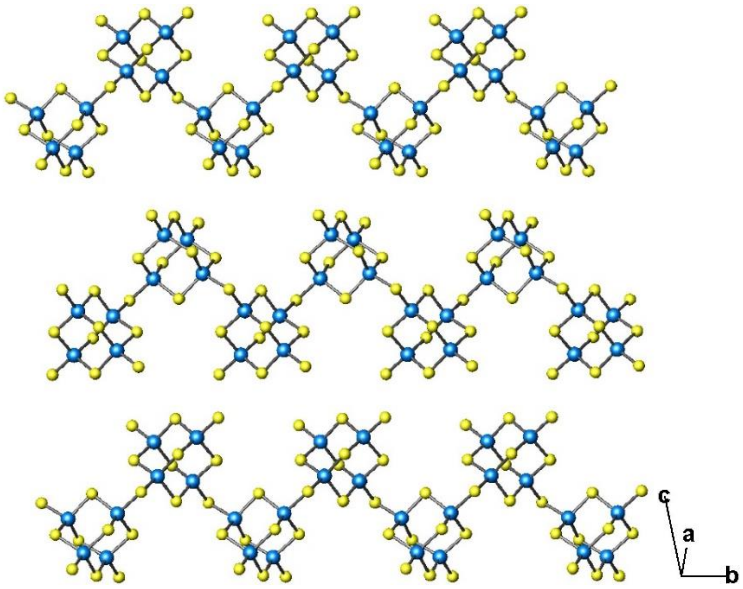

Figure 1.37 Perspective view of $[Ge_4Se_9]^{2-}{}_n$. Blue = Ge, yellow = Se. Counter-cations have been omitted for clarity.

The same group later reported the synthesis of "zeoball" clusters ZBT-1 ($[BMMIm]_{24}[Sn_{36}Ge_{24}Se_{132}]$) and ZBT-2 ($[BMIm]_{24}[Sn_{32.5}Ge_{27.5}Se_{132}]$) (Figure 1.38), where ZBT = zeoball tetrelate).[154] Each "zeoball" was also formed from $[K_4(H_2O)_3][Ge_4Se_{10}]$, with $SnCl_4.H_2O$ and a small amount of DMMP (DMMP = 2,6-dimethlymorpholine). The ionic liquid $[BMMIm]BF_4$ was used to synthesise ZBT-1 and

[BMIm]BF_4 for ZBT-2; all other reagents were unchanged. Here reactions were carried out in sealed Pyrex tubes rather than autoclaves.

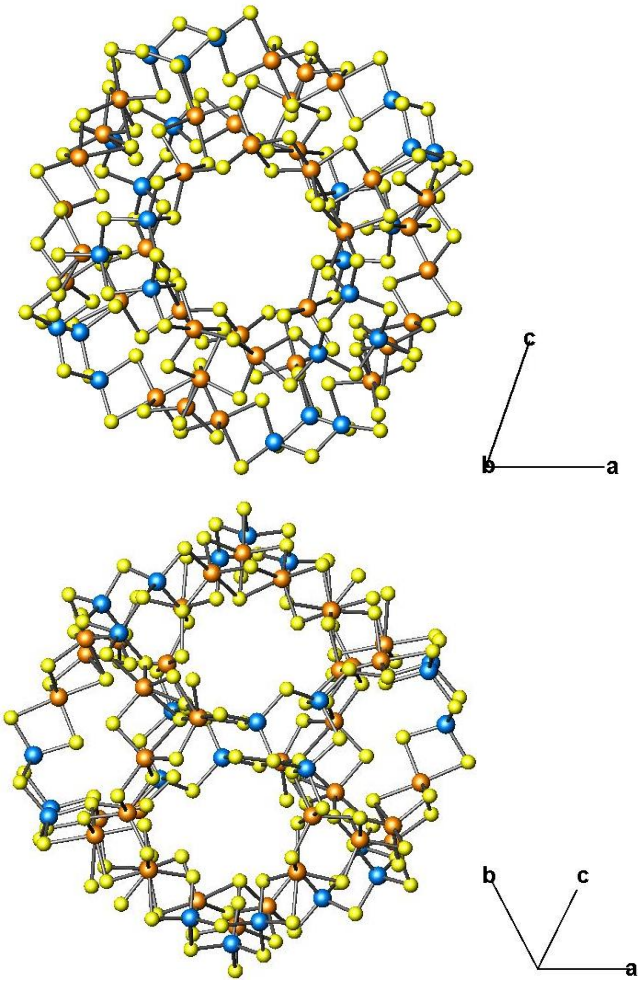

Figure 1.38 ZBT-2 **(a)** viewed along the *b*-axis, **(b)** viewed along [111].
Blue =Ge, orange = Sn, yellow = Se. Cations have been omitted for clarity.

Isolated gallium-sulphide T5 supertetrahedra containing copper have been synthesised ionothermally by Xiong *et.al*; these were prepared from a precursor which had earlier been synthesised solvothermally by Vaqueiro.[123, 155] The further syntheses were carried out in the ionic liquid [BMMIm]Cl, which is reported to act as the solvent, structure-directing agent and counter ion. The resulting structures had formulae $[BMMIm]_{10}[NH_4]_3$-$[Cu_5Ga_{30}S_{52}(SH)_4]$ (Figure 1.39), $[BMMIm]_8[NH_4]_3[Cu_5Ga_{30}S_{52}$-$(SH)_2(BMIm)_2]$ and $[BMMIm]_{9.5}[NH_4]_2[Cu_5Ga_{30}S_{52}(SH)_{1.5}Cl(BIm)_{1.5}]$. These were the first gallium-based T5 clusters described.

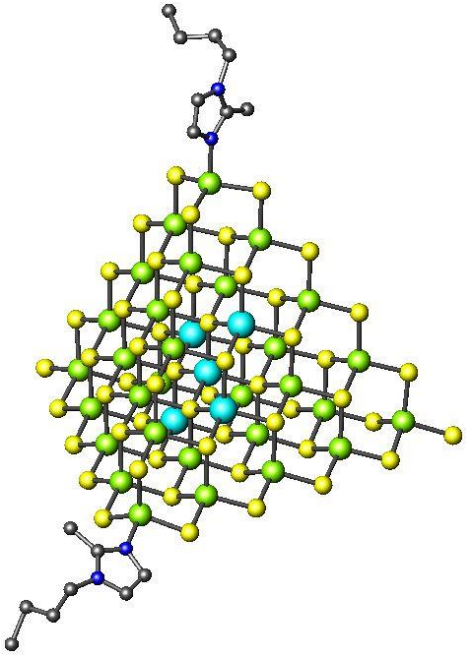

Figure 1.39 The discrete cluster $[Cu_5Ga_{30}S_{52}(SH)_2(BMIm)_2]^{11-}$. Green =Ga, teal = Cu, yellow = S. Cations and H-atoms have been omitted for clarity.

$[BMMIm]_8[NH_4]_3[Cu_5Ga_{30}S_{52}(SH)_4(BMIm)_2]$ and $[BMMIm]_{9.5}[NH_4]_2$-$[Cu_5Ga_{30}S_{52}(SH)_{1.5}Cl(BMIm)_{1.5}]$ are considered to be hybrid clusters due to the coordination of the 1-butyl-2-methyl-imidazole (BMIm) groups, which have been formed *in situ*. These discrete clusters had their corners terminated by SH^-, BMIm or Cl^- moieties, rather than bridging S^{2-}, allowing these clusters to exist as discrete units due to the lower negative-charge and coordinative saturation of the corner sites. These anionic clusters have their charge balanced by $[BMMIm]^+$and $[NH_4]^+$ cations.

As described previously, supertetrahedral clusters larger than T3 are rare; due to the accumulating negative-charge at the corners and edges. Before the synthesis of these clusters; the largest observed were also mixed-metal T5 units, linked into 2-dimensional or 3-dimensional networks *via* the corner sulphur-atoms.[87, 156, 157]

Shen *et al.* produced indium chalcogenide T3 clusters of a similar nature to this T5 cluster.[158] These indium chalcogenides had the formula $[BMMIm]_5$-$[In_{10}Q_{16}Cl_3(BMIm)]$ and could be formed with different chalcogenides. Compounds were denoted IL-InS-1 (Q=S), IL-InSSe-2 ($Q = S_{7.12}Se_{8.88}$), IL-InSe-3 (Q=Se) and (IL-InSeTe-4 ($Q = Se_{13.80}Te_{2.20}$). In this case, materials were synthesised from elemental reagents in [BMMIm]Cl and methylamine.

There are a number of examples of other similar materials to those described in this section in a review by Xiong *et al.*.[151] Ionothermal methods are described along with

surfactant thermal, which will be discussed in more detail in the following section. Ionothermal synthesis for the formation of metal chalcogenides is still a relatively unexplored field, although examples of new materials created in this way have begun to increase. Most examples are of tin selenides or indium selenides and sulphides.[151, 158-163] Research on gallium and germanium sulphides in this area is currently limited.

1.6 Materials Synthesised *via* Surfactant-Thermal Synthesis

Surfactant-thermal synthesis involves replacing the solvent of a solvothermal reaction with a surfactant. Surfactants are long-chain molecules consisting of a hydrophobic "tail" and a hydrophilic "head" (Figure 1.40 **(a)**). They are used to decrease the surface tension at interfaces between immiscible fluids e.g. water and oil or water and air. In many cases, surfactant-thermal synthesis utilises the formation of micelles, where surfactant molecules create a sphere around which the final product is templated (Figure 1.40 **(b)**).

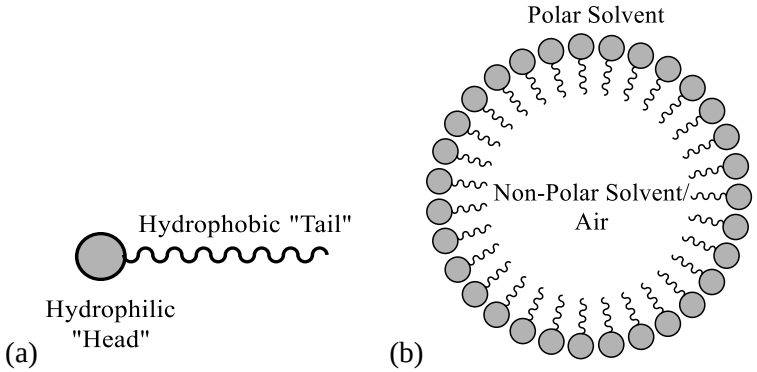

Figure 1.40 Representations of **(a)** a surfactant molecule and **(b)** a micelle.

In cases where micelles are used as templates; materials generally have larger pores and fall into the mesoporous range (pore size 2 – 50 nm), rather than microporous (pore size < 2 nm). Mesoporous silicates synthesised in surfactants are very well established and numerous examples of these, along with functionalised analogues are well known. [25, 164-167]

Some solvents can be considered to be both ionic liquids and surfactants as they contain long alkyl-chains with a polar end-group but are also charged, usually with an inorganic counter-ion. These include the alkyltrimethylammonium surfactants such as cetyltrimethylammonium bromide (CTAB) and are also known to create mesoporous materials.[168, 169] Phosphonium-based surfactants have also been used to create these

phases, but this is rarely reported compared to synthesis with the ammonium analogues.[169, 170]

Beck *et al.* explored the synthesis of molecular sieves using different alkyltrimethylammonium surfactants with formulae $C_nH_{2n+1}(CH_3)_3NBr$.[171] They found that at values of n=6 or lower, either amorphous or microporous materials were formed. Above this value, at n = 8, 10, 12, 14 and 16, materials were found to be mesoporous, suggesting that above this chain length micelles were formed in the reaction mixture.

1.6.1 Chalcogenides Synthesised with Surfactants

Surfactants have previously been used as templates by Kanatzidis *et al.* to produce mesostructures from the $[Ge_4S_{10}]^{4-}$ clusters described in Section 1.4.1.[172] The surfactants used were tetradecyltrimethylammonium, hexadecyltrimethylammonium, octadecyltrimethylammonium and dodecyltrimethylammonium bromides. Although the length of the alkyl chain was increased in each case, all of the materials crystallised in the same manner (Figure 1.41). The surfactant chains align throughout the structure with the hydrophilic ends directed towards the $[Ge_4S_{10}]^{4-}$ units. Figure 1.41 shows the structure of the octadecyltrimethylammonium analogue. They also later described using these surfactants to create mesoporous materials akin to the mesoporous silicates from the same $[Ge_4S_{10}]^{4-}$ clusters.[173, 174] They describe coordination of these clusters by corner-sharing sulphur atoms. A similar material was reported by MacLachlan *et al.* synthesised in a mixture of DMF and CTAB.[175]

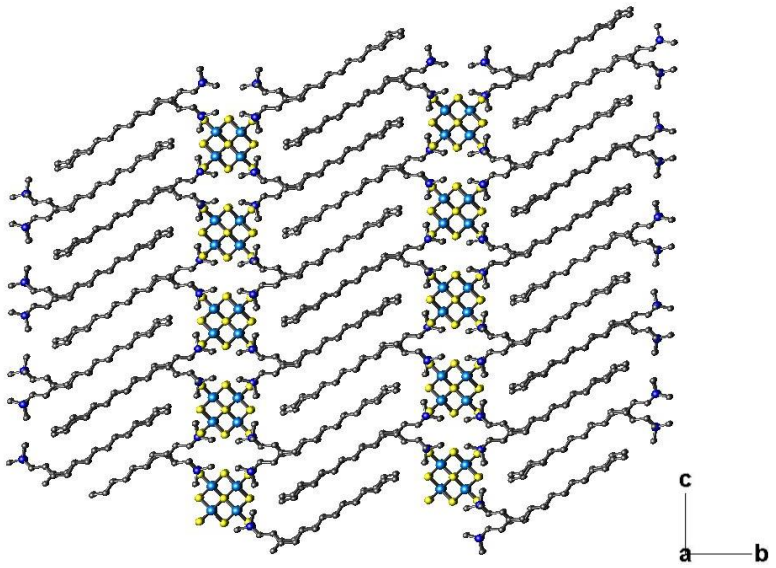

Figure 1.41 $[C_{17}H_{38}N]_4[Ge_4S_{10}]$ viewed along the *a*-axis. Blue = Ge, yellow = S, grey = C and dark blue = N. H-atoms are omitted for clarity.

Surfactant-thermal synthesis has also been investigated for the production of microporous metal-chalcogenides, as described in the review by Xiong *et al.*[151] Although a number of examples will be discussed here, the area of surfactant-thermal synthesis for microporous chalcogenides is new and relatively unexplored but has been growing since 2013.

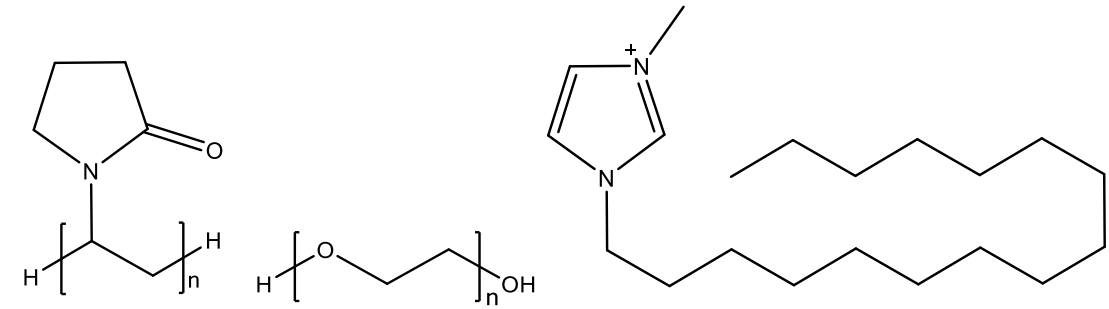

Figure 1.42 Surfactants used by Xiong *et al.*[176]

Xiong *et al.* first reported using surfactant-thermal synthesis to create chalcogenidoarsenates.[176] One of the positive reasons for using surfactants here was that they possess some of the same properties of ILs, such as negligible vapour-pressure and in some cases charged species, but they are cheaper. Surfactants used in this work were polyvinylpyrrolidone (PVP), polyethylene glycol-400 (PEG-400) and 1-hexadecyl-3-methylimidazolium chloride ([HMIm]Cl, Figure 1.42). This gives variety between a long-chain neutral surfactant (PEG-400), a neutral surfactant with a bulkier group (PVP) and a charged surfactant ([HMIm]Cl) (Figure 1.42). They reported materials containing materials of different dimensionalities; starting from 0-dimensional clusters (Figure 1.44) and ranging to a 3-dimensional framework.

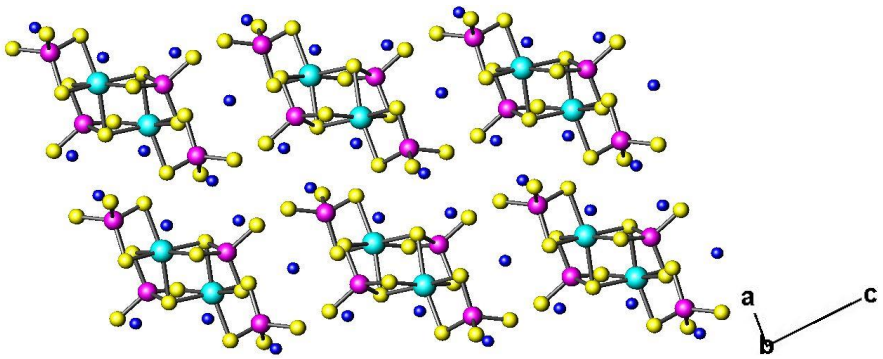

Figure 1.43 Discrete clusters $[Mn_2As_4S_{16}]^{8-}$ viewed along the *b*-axis. Magenta = As, teal = Mn, yellow = S, blue = N. Counter-cations and H-atoms are omitted for clarity.

The 0-dimensional clusters (Figure 1.44 **(a)**) have the formula $[Mn_2As_4S_{16}]^{8-}$.

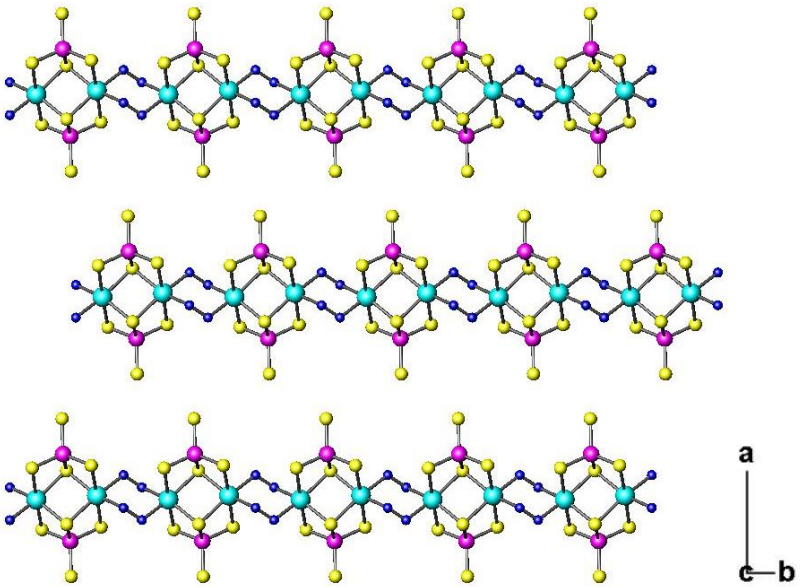

Figure 1.44. 1-dimensional chains of $[Mn_2As_2S_8(N_2H_4)_2]_n^{2n-}$ viewed along the *c*-axis. Magenta = As, teal = Mn, yellow = S, blue = N. Counter-cations and H-atoms are omitted for clarity.

A copper arsenidosulphide layered-material was also described in this publication, along with the 3-dimensional framework built from $[MnAs_3S_6]^-$ semicube units (Figure 1.45). In this case, the surfactant used was [HMIm]Cl, hydrazine was also used in the reaction and decomposed to form the $[NH_4]^+$ cations. Xiong *et al.* also reported 1-dimensional mercury selenidostannates synthesised in PEG-400 with superbase DBU as an auxiliary amine and a 1-dimensional thioantimonate in octylamine and DMF with hydrazine .[177, 178] The use of surfactants for synthesising crystalline inorganic-materials was described in a 2015 review.[179]

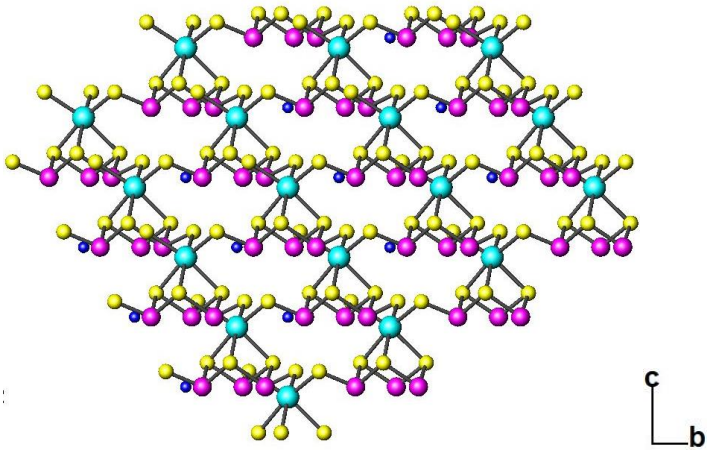

Figure 1.45 $[MnAs_3S_6]_n^{n-}$ viewed along [110]. Magenta = As, teal = Mn, yellow = S, blue = N. H-atoms are omitted for clarity.

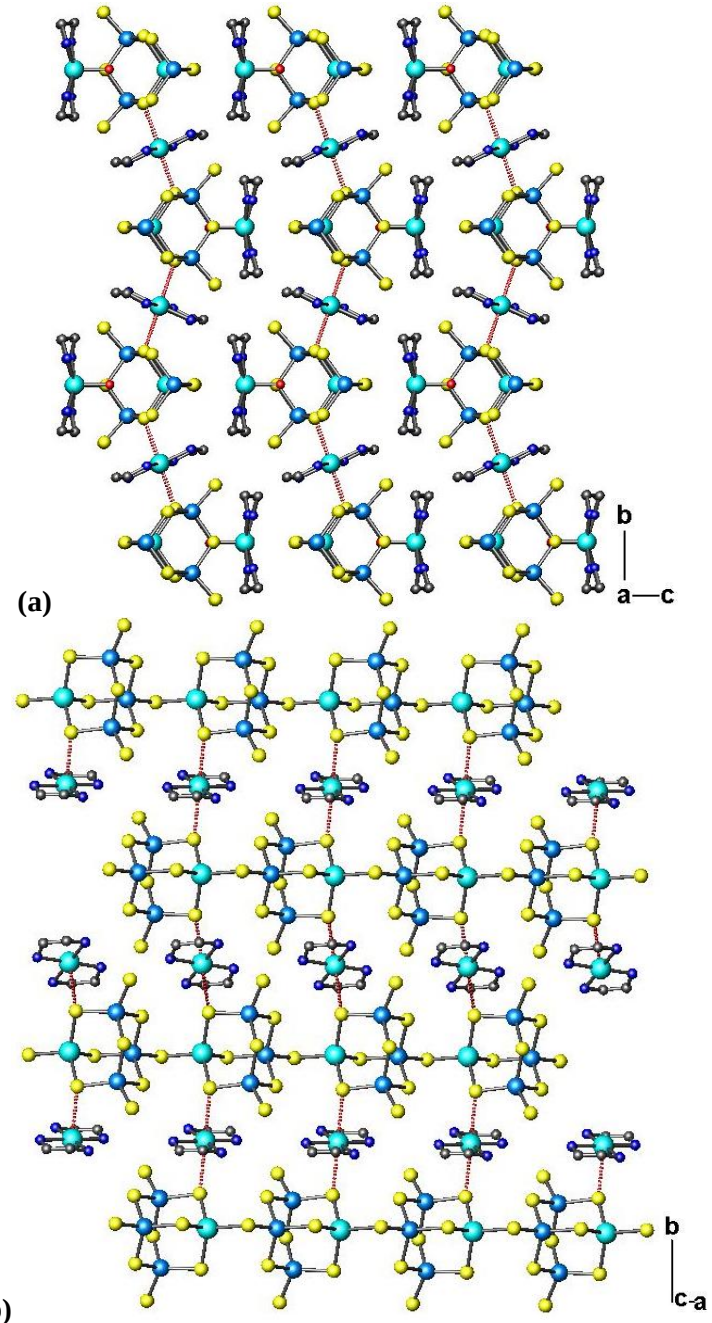

Figure 1.46 $[Mn(en)_2(H_2O)][Mn(en)_2MnGe_3Se_9]$ viewed along **(a)** the *a*-axis and **(b)** perspective view Magenta = As, teal = Mn, yellow = S, blue = N. H-atoms are omitted for clarity.

Zhang *et al.* used surfactant-thermal synthesis with auxiliary amines in PEG-400 to create a number of manganese germanium sulphides and selenides.[180] Here they reported a discrete dimer of $[C_3H_{11}N_2]_2[Mn(C_3H_{10}N_2)_2]Ge_2Se_7$ ($C_3H_{10}N_2$ = 1,2-diaminopropane = 1,2-DAP) 1-dimensional chain compound $[C_3H_{11}N_2][C_4H_9N_2O]$-$[MnGeSe_4]$ ($C_3H_{10}N_2$ = 1,3-diaminopropane = 1,3-DAP, $C_4H_8N_2O$ = *N*,*N*′-trimethyleneurea = TMU), along with a 2-dimensional manganese germanium sulphide $Mn_3Ge_2S_7(NH_3)_4$, synthesised in the presence of hydrazine.

They also described the synthesis of 1-dimensional chains of T2 clusters $[Mn(en)_2(H_2O)][Mn(en)_2MnGe_3Se_9]$, linked into a pseudo 2-dimensional layer *via* intermolecular Mn-S bonding between the T2 clusters and $Mn(en)_2$ complexes (Figure 1.46). They also reported 2-dimensional manganese antimony-sulphides in a separate publication.[181]

As described for ionothermal synthesis, surfactant-thermal synthesis is a very new area in the creation of crystalline chalcogenides. There are a limited number of examples where surfactant-thermal synthesis has been used and so far no examples of T3 or larger supertetrahedral compounds. This is therefore an excellent area to pursue for the formation of novel gallium and germanium-sulphide phases.

1.7 Applications of Porous Main-Group Metal Chalcogenides

The main attractive properties of these materials are the large surface-areas that microporous chalcogenides offer, along with their semiconducting nature and also the similarities between supertetrahedral clusters and quantum dots.[156, 182-185] Quantum dots possess quantum-confinement effects that make them attractive for applications in electronics. Combining these clusters with aromatic amines can also lead to electron transfer within the materials, as discussed further in Section 3.6 and photoluminescence is also a common property of these compounds.[87, 104, 105] The majority of materials based on supertetrahedral clusters have had their band-gaps determined *via* UV-Vis spectroscopy, as described in Section 2.2.7.

There are a number of examples of these materials showing ion exchange; a key ability that these materials must have for application in photocatalysis. Manos *et al.* reported $A_{5-x}K_{1+x}Sn[Zn_4Sn_4S_{17}](A = K^+, Rb^+, Cs^+; x = 0,4,5)$;[186] a framework built from P1 clusters $[Zn_4Sn_4S_{17}]^{10-}$ clusters; linked *via* Sn^{4+} (Figure 1.47). The anionic framework contained alkali metal cations A^+ or K^+ to balance the charge. These cations showed were shown to exchange with one another and the material also showed a band-gap of 2.87 eV.

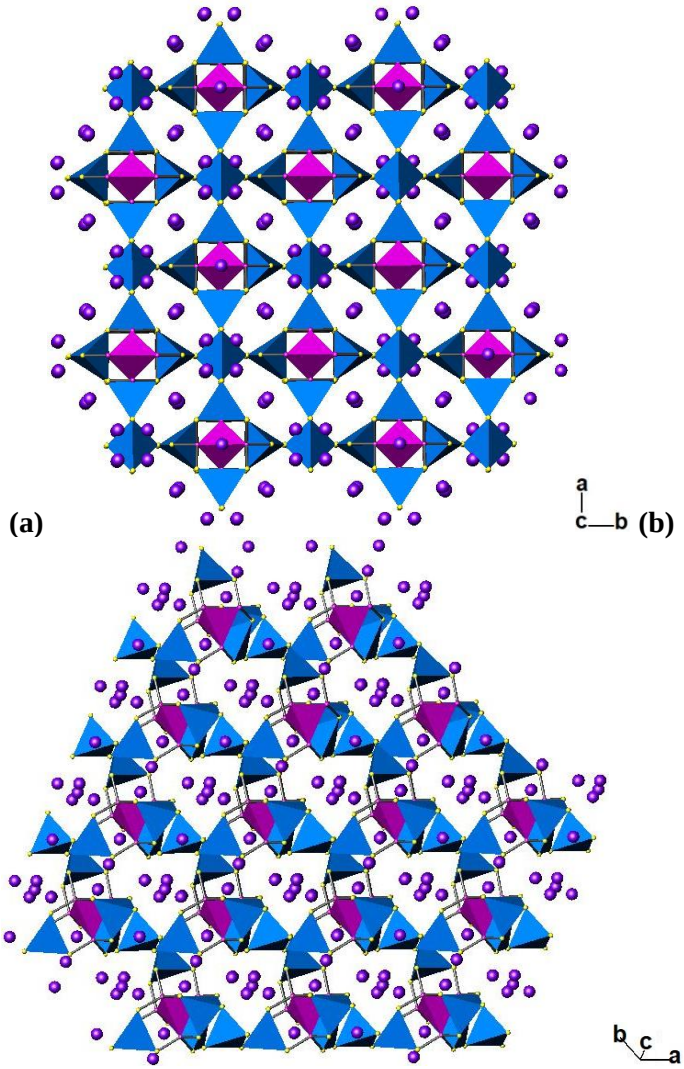

Figure 1.47. $K_6Sn[Zn_4Sn_4S_{17}]$ viewed along **(a)** the *c*-axis and **(b)** [111]. Magenta tetrahedra= SZn_4, blue tetrahedra = SnS_4, yellow = S and purple = K.

In 2003, Feng *et al.* investigated the fast-ion conductivity of their ICF family of materials (ICF = inorganic chalcogenide framework) but found that applications in batteries would not be feasible, due to the fact that the relative humidity must be high to obtain the high fast-ion conductivities measured.[187] They suggest that a better use for these materials would be in photocatalysis, to combine the porosity with the semiconductivity.

Feng *et al.* also show the doping of Mn^{2+} or Cu^{2+} ions into the cores of T2,2 indium cadmium clusters and measured the effect on the electronic properties.[188, 189] Copper doping showed an increase in the conductivity of the material. [189]Mn^{2+} doping was shown to cause a large red-shift in photoemission from weak green-emission at *ca.* 490 nm to strong red-emission at *ca.* 654 nm with an increased lifetime.[188] Aside from this, they showed that their ICF-materials could be used for the generation of hydrogen

from water, in the presence of Na_2S; however the efficiency of the reaction was *ca.* 3.7 % and suspected degradation of the catalysts was observed.[190]

Recently, Shen *et al.* have begun to explore the potential application of these materials as photocatalysts.[158] The investigations were carried out on the indium-chalcogenide T3 clusters $[BMMIm]_5[In_{10}Q_{16}Cl_3(BMIm)]$ (Q = S, Se or Te) synthesised in imidazolium based ILs (Section 1.5.1). Band gaps were found from UV-Vis spectroscopy to be 3.31 eV for IL-InS-1, 3.00 eV for IL-InSSe-2, 2.89 eV for IL-InSe-3, and 2.65 eV for IL-InSeTe-4. They tested these materials as catalysts for the degradation of methyl orange under both UV and visible light. It was discovered that the sulphur derivative had the best activity, causing 95.4 % degradation of methyl orange in 80 minutes, under UV-light. The opposite was shown under visible light, with the telluride derivative showing the highest activity, taking 3 hours to cause 94.1 % degradation of methyl orange; these trends will originate from the different band-gaps of the materials. Experiments in the absence of the clusters showed insignificant degradation of the sample. This is encouraging research in this field and also shows that framework materials are not essential for these compounds to be used in photocatalysis.

1.8 Aims of this Work

The aim of this work was to synthesise novel gallium-sulphides *via* different methods. Efforts were made to explore further the linkage of T3 gallium-sulphide supertetrahedra *via* ditopic amines by using combinations of solvothermal, ionothermal and surfactant-thermal synthesis methods. As explained in Sections 1.5 and 1.6, ionothermal and surfactant-thermal synthesis methods have not been explored in depth for the synthesis of gallium sulphides and there are limited examples of supertetrahedral clusters synthesised using these methods. It was therefore desired to explore these methods to identify whether novel gallium-sulphides could be obtained.

Along with the synthesis of novel hybrid gallium-sulphides, the production of mixed-metal phases was explored. Therefore, reactions were also carried out using a mixture of gallium with sources of germanium or copper. These were also attempted with solvothermal, ionothermal and surfactant-thermal synthesis methods.

Although initial aims were to create novel framework-materials, a number of novel materials of varying dimensionalities are described, along with previously-known materials that have been synthesis using novel methods.

2 Preparation and Characterisation

2.1 Synthesis

2.1.1 **Solvothermal Synthesis**

Synthesis methods were varied throughout the course of the project, all of which utilised autoclaves as the reaction vessels. The most frequently used reaction method was solvothermal synthesis, which involved mixing reactants together in a given solvent. The reaction mixture was then sealed into an autoclave, in this case 23 ml Parr acid digestion bombs were used (Figure 2.1). Acid digestion bombs have components as follows: 23 ml stainless steel acid digestion vessel, PTFE (Teflon™) cup with cover, corrosion disc, rupture disc and spring. These components when assembled create a sealed system, which allows the reactants to be heated while preventing the loss of produced gas.

When autoclaves are heated in an oven, at temperatures of between 140 ^{o}C and 200 ^{o}C in the case of the reactions reported here, the action of the produced gas molecules colliding with the internal surface of a PTFE liner creates an autogenous pressure of *ca.* 10-50 atm. These unique reaction conditions allow the formation of metastable phases, which may not be isolated from other synthetic methods, such as solid-state or standard solution-based methods.

(a)  **(b)** 

Figure 2.1 (a) 23 ml PTFE liner, (b) 23 ml Parr Acid Digestion Bomb 4749

Although this synthesis method has the benefit of creating these metastable phases; when products are created in this way it is difficult to deduce the reaction mechanism as the system is completely closed. However the redox reactions that take place between the amine and the other reactants have been suggested. In the case of

chalcogenide compounds, basic solvents are required in order to produce the S^{2-} ions needed to react with the metal.

Li *et al.* suggest that there are two different mechanisms through which solvothermal reactions can take place.[191] Either direct reduction of the chalcogenide source (X) through bonding to the metal source (M), which is oxidised in the process, or disproportionation of X in a basic solvent, with no change in the oxidation state of the metal. More recently, Dorhout *et al.* have carried out *in situ* measurements on both aqueous and non-aqueous formation of sulphides in solution.[192] Zhou *et al.* also proposed full mechanisms for the synthesis of chalcogenides in the presence of amines, in a 2009 review.[122] The proposed mechanisms can be summarised as follows.

In the case of the disproportionation route, the amine reduces the chalcogenide (X) to create X^{2-} ions (Equation 2.1).[122]

$$X + \text{Amine} \rightarrow X^{2-} (\text{or } X_m)^{2-} + [\text{H(Amine)}]^{+} + \text{Oxidised By-Product} \qquad \textbf{Equation 2.1}$$

The metal coordinates to an amine as follows (Equation 2.2), mainly occurring in cases where organometallic countercations are present (Section1.4.6).

$$M^{n+} + \text{Amine} \rightarrow [M(\text{Amine})_z]^{n+} \qquad \textbf{Equation 2.2}$$

The route through which the chalcogenide coordinates directly to the metal and amine is suggested to occur as follows (Equation 2.3).

$$M + X + \text{Amine} \rightarrow [M(\text{Amine})_z]^{n+} + X^{2-} (\text{or } M_yX_w)^{m-} \qquad \textbf{Equation 2.3}$$

Demazeau *et al.* suggest that there are five different types in which the reactions taking place in solvothermal synthesis can be categorised.[139] These are oxidation-reduction (Equations 2.1 and 2.3), hydrolysis, thermolysis, complex formation (Equation 2.2) and metathesis.

The relatively high number of different processes that can possibly occur in a solvothermal reaction affects the predictability of the outcome and the reproducibility of the products. There are a number of important factors that are known to influence the outcome of the reaction: pH, solubility of reactants, temperature, stoichiometry, reaction time and structure-directing agent (SDA). The solvent should be selected based on the

requirements of the reaction. How the solvent will dissolve the reactants and products should also be considered. It is beneficial for the reactants to be readily dissolved, as this will encourage their reactivity and potentially speed up the reaction. However, if the product is also extremely soluble, then crystals cannot be formed and no product will be obtained. In some cases, solvent can be incorporated into the crystal structure, reiterating the importance of this selection.

The reactions presented here involve reacting gallium (Ga metal, $Ga(NO_3)_3$ or Ga_2O_3) or germanium (GeO_2) precursors with sulphur sources (S or thioacetamide) in a given solvent. As described above, basic conditions are required to produce S^{2-} (Equation 2.1). Gallium metal must also be oxidised to Ga(III) (Equation 2.3). In order to produce the basic conditions, amine-based solvents are used (Figure 2.2). In this case, aromatic amines have been chosen for the majority of reactions; in many 4-methylpyridine (4-MPy) is used, whose N atom is susceptible to protonation (Figure 2.2). The N in 4-MPy is also able to bond directly to Ga(III) through its lone pair (Section 1.4.5). Other solvents have also been explored, as explained further in Sections 2.1.2 and 2.1.3.

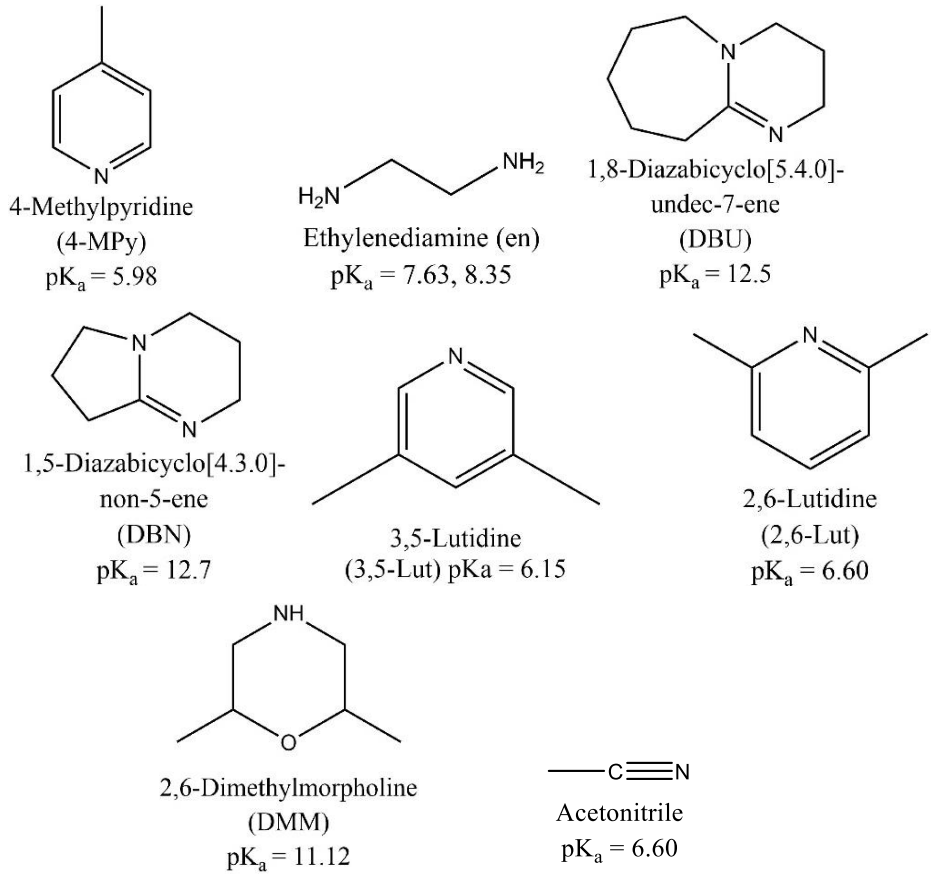

Figure 2.2 Structures of basic solvents used throughout this work.

Temperature also has a strong influence on the outcome of the reaction. It is important that the temperature is high enough to reach the boiling point of any solvents but not high enough to cause decomposition of the starting materials or products. It should also not exceed 250 ^{o}C, as this will cause the PTFE liner to deform. Changing the temperature will normally change the resulting product, even if the starting materials and solvent are unchanged. Stoichiometry does not always affect the reaction as would be expected, often resulting products require a specific balance of all factors and only a small change in stoichiometry can create an entirely different product. This means that when the initial reaction-mixture is stirred in the PTFE liner, the magnetic stirrer remains in the vessel for the full reaction, to prevent loss of starting material on removal of the stirrer.

Along with temperature, length of reaction time has a great effect on the outcome. Reaction times for solvothermal synthesis are usually measured by number of days; in this case, reactions were carried out varying from 4-13 days in length. As a general rule, crystals formed will be larger from a longer reaction if the same reaction is carried out for a longer amount of time. Changing the reaction time can also result in a different product being formed, or no product at all. Cooling rate can also have an effect on the crystallisation, as slower cooling general results in larger crystals.

A structure-directing agent (SDA) is a reagent added to the reaction mixture whose shape directly affects the resulting structure of the product. SDAs used throughout this work are illustrated in Figure 2.3.

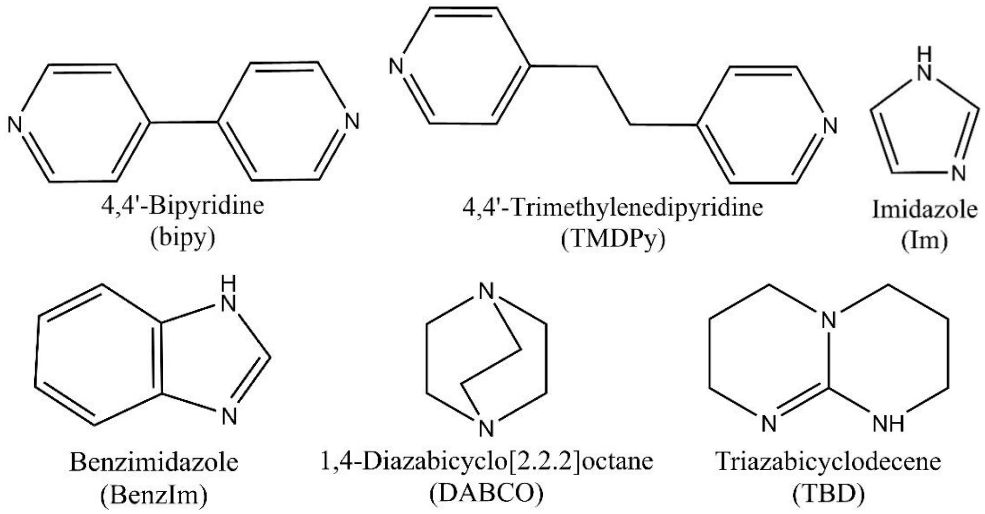

Figure 2.3 Structures of SDAs used throughout this work.

Frameworks are known to form around different organic-species or transition-metal complexes in a number of zeolitic structures and metal-organic frameworks.[136, 193] It is not just the shape of the SDA that has a templating effect, but other interactions with the structure, such as H-bonding and electrostatic interactions. All reactions carried out are described in Appendix 1.

Using this method, reactants (metal source(s), sulphur source, (SDA) and solvent) were added into the PTFE liner of an acid-digestion bomb. The mixture was then stirred magnetically for *ca.* 10 minutes before sealing the liner into the autoclave. Autoclaves were heated in a Memmert© oven with a ramp rate of 1 ^{o}C/min for both heating and cooling. The resulting product was filtered using vacuum filtration and solid products were washed with ethanol, water and acetone respectively.

2.1.2 **Ionothermal Synthesis**

The ionothermal synthesis technique was developed by Morris and Parnham at the University of St Andrews for the synthesis of zeolitic materials and has since been used for synthesising MOFs and chalcogenide materials (Section 1.5).[137, 140, 141, 143, 147, 151, 158, 162, 163] This method involves replacing the standard solvents used in solvothermal synthesis with ionic liquids (ILs). ILs are salts with low melting-points (below 100 ^{o}C). Ionic liquids are different to conventional solvents as they have negligible vapour-pressure, which would not produce the autogenous pressure created by typical solvents. This of course means that the use of autoclaves for these reactions is not essential and they can be carried out in vessels such as round-bottomed flasks. However, the use of autoclaves allows reaction mixtures to be heated consistently for long lengths of time.

Ionothermal synthesis is extremely useful for reactions where a charged structure will be created, where the ionic liquid acts as the solvent, structure-directing agent and charge-balancing species, eliminating the need for a protonation step. ILs also usually consist of an organic cation with an inorganic anion.

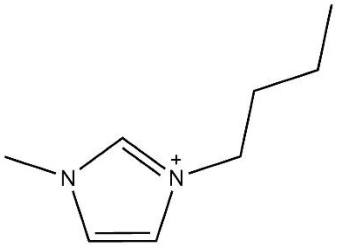

1-Butyl-3-methylimidazolium
([BMMIm]$^{+}$)

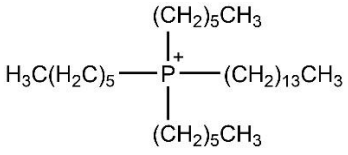

Trihexyltetradecylphosphonium
[THTDP]+

Figure 2.4 Structures of the cations of ionic liquids used throughout this work.

Reactions have been carried out using the ILs [BMMIm]Cl, [BMMIm]BF_4 and [THTDP]Cl (Figure 2.4); they were initially used as solvents in reactions (Section 6.2). Metal sources used in this case were Ga metal, $Ga(NO_3)_3$ and $Cu(NO_3)_2$. The sulphur source consisted of either S, thioacetamide or a combination of both. In some cases previously-synthesised precursors were used as starting materials; as described further in Section 1.5. In some cases SDAs or auxiliary solvents were used alongside the ILs. The SDAs for these syntheses were Im and TMDPy (Figure 2.3), with auxiliary solvents of dimethylamine (DMA, 40 % solution in water), 4-MPy, en or DMM (Figure 2.2). Reaction temperatures used for this method ranged from 160 – 200 ^oC, with reaction times of either 6 or 13 days.

ILs were also used as SDAs in solvothermal reactions to exploit the cationic nature of the organic species, while also having a solvent present that is previously known to effectively facilitate reactions between elemental Ga and S. (Sections 0, 3.3 and 6.2.4). Reactions here took place with metal sources Ga or GeO_2, with S in either 4-MPy or water (hydrothermal). Reactions were carried out using much smaller amounts (*ca.* 1:40) of [BMMIm]Cl, [BMMIm]BF_4 or [THTDP]Cl as SDAs (Figure 2.4). The temperature of these reactions ranged from 170 – 200 ^oC, with times from 5 or 7 days. Syntheses were performed as described for the solvothermal reactions (Section 2.1.1).

2.1.3 **Surfactant-Thermal Synthesis**

Surfactant-thermal synthesis has also developed from solvothermal and involves replacing the solvent with a given surfactant. This can lead to the production of mesoporous materials created due to the formation of micelles in the reaction mixture (Section 1.6); especially when using surfactants with very long alkyl chain lengths (*ca.* eight and or longer).[171] Chains shorter than this are known to template microporous materials such as zeolites and MOFs.[164, 194, 195] There are examples where a small amount of surfactant can be used with another solvent in order to create the micelles and create large pores. [165, 173, 196] There are also a small number of examples of chalcogenide materials synthesised using surfactant-thermal synthesis (Section 1.6.1).[178, 197, 198] Examples of materials synthesised using this method are described further in Section 1.6.

Surfactants share the negligible vapour-pressure of ILs but are cheaper and can have different properties.[151] Surfactants can be either neutral or charged, giving a greater potential for the formation of different phases, along with having different shapes of

either long-chain or branched-chains, while sometimes incorporating bulky groups onto their length, in order to explore different templating-effects.

When using elemental starting materials; a redox reaction must occur. Neutral surfactants such as PEG (polyethylene glycol) and PVP (Polyvinyl pyrrolidone) do not have the ability to support the formation of ions within solution, like ionic liquids and basic solvents. To overcome this, auxiliary solvents or amines can be added. The sulphur source can also be changed from elemental sulphur to thioacetamide, which decomposes to produce S^{2-} ions in solution and also reduces the pH of the reaction. Along with changing the sulphur source, a strong base can also be added in order to promote the formation of Ga^{3+} ions. In this case, the use of bicyclic amines or "superbases" has been explored. These are stronger bases than 4-MPy, which has been described frequently throughout this work (Figure 2.2, Table 2.1). This makes them perfect candidates to be used as auxiliary amines in the surfactant-thermal reactions described.

Table 2.1 Amines used as solvents throughout this work and the pKa values of their conjugate acids.

Base	pKa
4-Methylpyridine	5.98
Imidazole	6.95
DBU	12.5
DBN	12.7
TBD	15.2

There are a number of reactions describing surfactant-thermal synthesis of chalcogenide structures that include hydrazine in the reaction.[151, 199, 200] This is because it is a strong reducing-agent that can produce hydrazinium cations *in situ*, along with reducing the elemental sulphur to S^{2-}. Hydrazine was not used in this work due to its explosive and toxic nature; it was therefore desirable to find a hydrazine-free synthesis method for these structures.

2.2 Characterisation

On obtaining solid products from reactions, as described in Section 2.1, those containing single crystals, as observed using a microscope (Section 2.2.1), had crystals selected and mounted for single-crystal X-ray diffraction (SCXRD, Section 2.2.2). In

most cases, powder X-ray diffraction was performed (PXRD), however not all samples could be measured due to time constraints and limited availability of the high-throughput instrument (Section 2.2.3).

Once materials of interest had been characterised using X-ray diffraction (XRD), the chemical compositions were confirmed using a combination of elemental analysis (Section 2.2.4), Fourier-transform infrared (FTIR) spectroscopy (Section 2.2.5), thermogravimetric analysis (TGA, Section 2.2.6) and in some cases energy-dispersive X-ray (EDX) spectroscopy (Section 2.2.8).

On complete characterisation of the materials, UV-Vis diffuse reflectance spectroscopy (Section 2.2.7) was used to measure the absorption edges of the materials. The absorption edge was then used to estimate the optical band-gap for the material.

2.2.1 Examination with Microscope

All solid products from the described reactions were observed on glass slides with an optical Meiji microscope to determine whether crystals were present. After selecting samples for SCXRD, crystals were picked for mounting using a Nikon zoom stereomicroscope SMZ1000.

2.2.2 Single-Crystal X-Ray Diffraction

Single-crystal X-ray diffraction allows structure determination by irradiating a single crystal with a monochromatic X-ray beam. The X-ray beam is created by bombarding a metal target with an electron beam, which is produced by heating a metal filament. The most common metal-targets used are copper and molybdenum, which when bombarded emit different wavelengths of X-rays. When the electron beam collides with the metal, an electron is removed from one of the inner shells of the atom; this causes an outer electron to drop into its place and the difference in energy is emitted in the form of X-rays. If the electron is ejected from the 1s shell, these transitions are referred to as K-transitions; corresponding to the quantum number (1) for this shell. If an electron drops from the 2p (L) shell, the transition is described as a Kα transition. If it drops from the 3p (M) shell then it is referred to as a Kβ transition. As the 2p shell contains two electrons with different spins (s=1/2 and s=3/2) these two transitions will have slightly different energies, referred to as $K\alpha_1$ (s=3/2) and $K\alpha_2$ (s=1/2). Therefore, a monochromator is required in order to select only one specific wavelength; in this case

$K\alpha_1$ is desired. The characteristic $K\alpha_1$ wavelengths for molybdenum and copper are λ=0.70926 Å and λ=1.54056 Å respectively.

As the incident X-ray can be described as both a wave and a beam of electrons, the electron density within the structure scatters the incident radiation. As the wavelength of X-rays is of the same magnitude as the atomic spacing in a crystal lattice, it can act as a diffraction grating and the resulting diffraction pattern can be used to determine the atom positions within that lattice. Diffraction peaks are created when the resulting reflections from the lattice planes interfere constructively and obey Bragg's law (Equation 2.4).

$$n\lambda=2d\sin\theta \qquad \textbf{Equation 2.4}$$

where n = an integer, λ = wavelength of incident X-ray, d = lattice spacing, θ = Bragg angle.

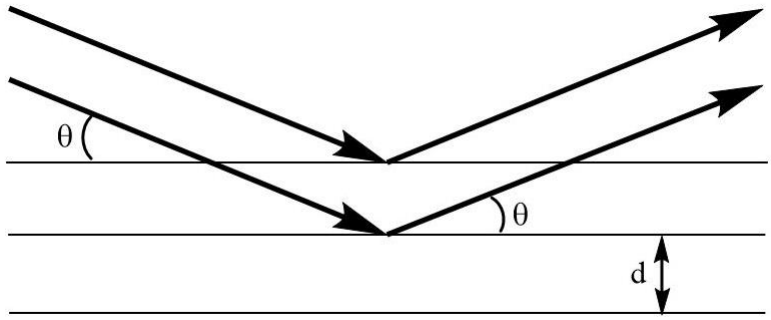

Figure 2.5 Representation of Bragg reflection from lattice planes with d-spacing.

A single-crystal X-ray diffraction pattern appears as a series of spots, this array has symmetry related to the symmetry of the crystal structure. The diffraction pattern changes depending on the orientation of the crystal, which is rotated throughout data collection. On varying the 2θ angle, all d-spacings that satisfy Bragg's law can be determined. These d-spacings occur between lattice planes with Miller indices (*hkl*), which describe how the plane "slices" through the unit cell of the crystal. Each spot in the diffraction pattern can therefore be related to a reflection from a specific hkl plane, which allows determination of the unit cell, with lengths a, b and c and angles α, β and γ, known as lattice parameters. The following relationship (Equation 2.5) relates the Miller indices to unit cell parameters for crystal systems with symmetries of orthorhombic or higher ($\alpha=\beta=\gamma=90^{o}$).

$$\frac{1}{d_{hkl}^2} = \frac{h^2}{a^2} + \frac{k^2}{b^2} + \frac{l^2}{c^2} \qquad \textbf{Equation 2.5}$$

Each j^{th} atom in the structure, with fractional coordinates (x_j,y_j,z_j) contributes to the overall diffraction-pattern and has an atomic scattering factor, f_j based on its electron-density distribution. The sum of the atomic scattering factors of N atoms in the unit cell gives the overall scattering factor, F_{hkl} for the reflection from a given plane with Miller indices (hkl). Equation 2.6 describes the forward Fourier-transform to give the structure factor F_{hkl}. This can be carried out for all reflections in the diffraction pattern using Equation 2.6.

$$F(hkl) = \sum_{j=1}^{N} f_j \exp\left[2\pi i\left(hx_j + ky_j + lz_j\right)\right] \qquad \textbf{Equation 2.6}$$

When collecting the information from the diffraction pattern, the intensity I_{hkl} of each reflection is measured. This allows us to know the amplitude of the diffracted X-ray beam, but does not give us any information about the phase of the wave, i.e. whether the amplitude is positive or negative. This is known as "the phase problem" in X-ray crystallography and means that F_{hkl} cannot be described as directly proportional to the intensity. Instead, the relationship is expressed as in Equation 2.7.

$$I_{hkl} \propto |F_{hkl}|^2 \qquad \textbf{Equation 2.7}$$

The process of calculating the hkl values and observed structure-factors is known as data reduction and was carried out using the software CrysAlisPro, by Agilent.[201] In order to calculate the electron density ρ for each atom, the reverse Fourier-transform of the structure factors must be performed for each atom. The transform is defined by the following equation, where V is the volume of the unit cell; this gives an average electron-density for each atom in the unit cell from the overall structure.

$$\rho(xyz) = \frac{1}{V}\sum_{hkl} F(hkl)\exp[-2\pi i(hx + ky + lz)] \qquad \textbf{Equation 2.8}$$

It must be remembered however that, because the phases are unknown, the electron density cannot be calculated from this equation alone. Higher symmetry in a unit cell makes this process quicker as electron density does not need to be calculated individually for atoms related by symmetry.

In order to solve the crystal structure, different methods can be used. These are either Patterson synthesis, where the structure is solved by focusing on the vectors

between pairs of atoms in the crystal structure and is most applicable when there is a small number of heavy atoms, such as transition metals, in the asymmetric unit. The asymmetric unit being the smallest unit in a crystal structure that cannot be reduced further by applying symmetry operations.

Another way of solving a structure is *via* direct methods, which use a combination of mathematical and statistical functions to assign phases to the diffracted waves. This method is carried out using software such as Sir92.[202]

The final method that can be used is charge flipping. Charge flipping involves flipping between direct and reciprocal space and is an iterative method that must converge on a structure solution, where there is a good agreement between the calculated structure-factors $|F_c|$ and observed structure-factors $|F_o|$. Charge flipping can also verify the symmetry of the structure and suggest a new space-group if the symmetry is found to be incorrect. Charge flipping has been used as the solution method in all structures described throughout this work, using the software Superflip.[203]

Once the structure has been solved, the resulting electron-density map must be used to determine the final structure of the crystal. This is done by comparing calculated structure factors F_{calc} to the observed structure factors F_o to give the *R* factor, expressed by Equation 2.9.

$$\boldsymbol{R} = \sqrt{\frac{\sum||\boldsymbol{F_o}|-|\boldsymbol{F_c}||}{\sum|\boldsymbol{F_o}|}} \qquad \textbf{Equation 2.9}$$

The resulting *R*-factor should be below 0.1, ideally between 0.02 and 0.05. As the structural model is changed during the refinement process, the least-squares method is used to find the new *R*-factor. It is also required for the ratio of shift over standard uncertainty (max e.s.d) to tend towards zero to show a stable refinement. Constraints and restraints can be applied to prevent the model from veering too far from the suggested model during the least-squares refinement cycles.

During refinement, vibrations within the crystal can cause electron density to be "smeared out", especially when there are relatively light atoms present in a structure containing heavy atoms. These light atoms can be constrained to be refined isotropically, so that they will be treated as if their thermal parameters are the same in all directions. Restraints are applied to bonds or planes of atoms, so that bond lengths cannot vary from an assigned value or cannot vary from being planar to one another. These tools are

extremely useful in structures such as the hybrid materials described in this work, which contain both inorganic and organic components.

For single-crystal X-ray diffraction; crystals were mounted on a loop in oil and fitted on the goniometer head of the diffractometer, before being aligned within the X-ray beam using a camera. Data for some structures were collected at 100 K, but the majority were collected at 150 K. Low temperatures are required to reduce vibrations in the crystal. Measurements were performed on an Oxford Gemini S Ultra diffractometer, which uses the Kα wavelength for molybdenum, which is λ=0.70926 Å. The integration carried out using CrysAlisPro.[5] Single-crystal X-ray data for a small number of structures were collected by the NCS (National Crystallography Service) at the University of Southampton.[204]

All structures were solved using Superflip and refined using the program CRYSTALS.[203, 205] Some C and N atoms were located using Fourier maps and refined isotropically. Some 4-MPy and aromatic rings have been constrained to be planar and their bonds constrained to 1.38 Å for C-C, 1.34 Å for C-N and 1.51 Å for methyl C-C. Other organic molecules have also had their bonds constrained. Hydrogen atoms were added geometrically and Platon SQUEEZE was used to remove residual electron density and locate voids in the structure relating to disordered solvent-molecules, where voids were present.[206]

CIFs are included of all single-crystal structures in the electronic supplementary-information, attached as a CD to the thesis.

2.2.3 **Powder X-Ray Diffraction**

Powder X-ray diffraction (PXRD) differs from single-crystal X-ray diffraction (SCXRD) as powder contains many randomly-oriented crystallites of varying sizes. Therefore, instead of producing a diffraction pattern of discrete spots, the intensities are averaged out over all atoms in an (hkl) plane. This gives an appearance of rings, each relating to a specific 2θ value. The output of the experiment is a graph consisting of peaks of varying intensity for each 2θ value (Figure 2.6). These 2θ values can be used along with the Bragg equation (Equation 2.4) to calculate the d-spacing and therefore lattice parameters for that structure. The peaks in the powder pattern vary in width based on the size of the crystallites; the crystallite sizes can be estimated by using the Scherrer equation.

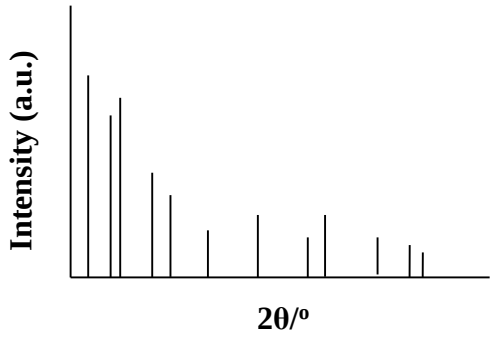

Figure 2.6 Example of a PXRD pattern

Powder-diffraction data were collected using a Bruker D8 Advance powder diffractometer or D8 Discover diffractometer. For the D8 Advance, data were collected for 1 hr over the range $5 \leq 2\theta/° \leq 60$. The instrument uses germanium-monochromated Cu-$K_{\alpha 1}$ radiation of $\lambda = 1.54056$ Å and Bragg-Brentano geometry. The samples were fixed to zero-background holders using a small amount of Vaseline©. For the D8 discover, multiple samples can be examined over short exposure times using only a small amount of sample. This instrument uses parallel beam geometry with Cu-$K\alpha_1$ radiation $\lambda = 1.54184$ Å, operated in transmission. Data were measured over the range $4 \leq 2\theta/° \leq 50$ and the exposure time of each sample was set to 30 minutes. Powder patterns were observed and compared using the Bruker DIFFRAC PLUS evaluation software EVA. In cases where comparisons have been made with simulated patterns, these have been simulated using the CCDC software Mercury.[207] In cases where lattice parameters have been refined against powder-diffraction data, this has been carried out using the software DASH, using the Pawley refinement method.[208]

2.2.4 **Elemental Analysis**

Elemental analysis was carried out externally by MEDAC Ltd using approximately 3 mg of crystals. The CHN analysis was carried out *via* combustion, where the CHN content is determined from the products of dynamic flash combustion of the sample. These combustion gases produced are then passed through a reduction tube, before being analysed by chromatography as N_2, CO_2 and H_2O.

This technique gives us information about the organic composition of the structure. SCXRD is the main characterisation-technique used, but generally does not

confirm all organics within the structure as a proportion of them will be disordered. The space that these molecules fill will be detected by PLATON squeeze as residual electron-density within the crystal structure. CHN analysis allows us to identify these molecules based on the relative percentages of carbon, hydrogen and nitrogen.

2.2.5 **Infrared Spectroscopy**

Fourier-transform infrared spectroscopy was used to identify the functional groups present in the organic components of the materials. When a compound is exposed to infra-red radiation, the different functional-groups undergo a transition such as a vibration, stretching or bending motion, which gives a characteristic absorption-frequency in the spectrum.[209] These measurements were carried out using a Perkin-Elmer Spectrum 100 FTIR Spectrometer using ATR and recorded over the range 550 – 4000 cm^{-1}. The data were collected from 32 scans at a resolution of 2 cm^{-1}.

2.2.6 **Thermogravimetric Analysis**

Thermogravimetric analysis was performed using the TA Instruments Q50 TGA on 7 -13 mg of ground sample, under an N_2 atmosphere, or on a TA Q600 DSC-TGA in air or N_2 on 3-6 mg of sample. The Q50 instrument measures the weight change of the sample as it is heated from room temperature up to approximately 800 ^oC using a heating rate of 5 ^oC min^{-1}. The TA Q600 DSC-TGA measures the weight change with temperature up to 1000 ^oC and also measures the heat flow during the experiment; making is easier to detect variations such as phase transitions.

This technique is used in order to confirm the organic species present in a material and determine the thermal stability and decomposition temperature of the compound. When the SCXRD and CHN data have been analysed to give a proposed identification of organic components in the structure, TGA can be used to verify that the weight changes on heating the material are consistent with the proposed structure. It is expected that neutral pore-organics will be removed first, followed by charged organics. Finally, any organics bonded to the inorganic components will be removed followed by full decomposition of the structure to the corresponding oxide or sulphide.

2.2.7 Diffuse Reflectance

Diffuse reflectance spectroscopy is a technique used to measure the absorption edge of a material and also to identify the specific absorptions of a material, which often give a material its colour.

The sample is exposed to radiation of varying wavelength from the visible to the UV region. If there is no absorbance from the sample, all of the incident light is reflected back into the detector. As the band gap of the sample is a measure of how much energy is required to excite electrons from the valence band into the conduction band, when the energy of the band gap is reached, the incident light is absorbed by the sample.

The reflectance data recorded by the instrument were converted into absorption data using the Kubelka-Munk relationship (Equation 2.10). Where R_∞ is the reflectance from an infinitely thick layer of sample, k is the total absorption coefficient and s is the total scattering factor.

$$R_\infty = \frac{(1-R_\infty)^2}{2R_\infty} = \frac{k}{s} \qquad \textbf{Equation 2.10}$$

When using $BaSO_4$ as a standard, the total absorption coefficient k=0, as all light will be reflected. To measure the diffuse reflectance for the sample, a sample of ground powder is flattened on to the compacted $BaSO_4$ standard. Diffuse-reflectance measurements were carried out using a Perkin Elmer Lambda 35 UV-Vis spectrometer with reflectance attachment. For these experiments a wavelength range of 1000 nm (visible region) to 200 nm (UV region) was used in each case.

The sulphide materials discussed in this work have different band-gaps, which can be determined from the absorption edge measured for the sample. The absorption edge is found by fitting a tangent line to the absorption band in the spectrum and determining the value at which the tangent line crosses the x-axis.

2.2.8 Scanning-Electron Microscopy (SEM) and Electron Dispersive X-Ray Analysis (EDX)

Scanning-electron microscopy was used both to observe single crystals of the materials at high magnification, but also select areas of interest for EDX analysis. In order to prepare the sample for EDX, single crystals of the samples were selected and fixed to a stub. The samples were all coated with carbon before carrying out SEM and EDX analyses, which were both carried out under high vacuum. A Cambridge 360 Stereoscan microscope was used for the examination of the coated samples.

Electron dispersive X-ray analysis (EDX) was used to determine relative gallium and germanium content in structures containing both metals, or those from reactions where both metals were used. Due to their very similar electronic structure, Ge and Ga cannot be distinguished by X-ray diffraction. Therefore, EDX was used to distinguish between them.

The sample is bombarded with an electron beam and the energy of the different emissions from the sample are measured. The radiation measured is produced when an electron is "knocked out" of the inner shell of an atom and an electron from a higher-energy shell transitions to the vacant lower-energy orbital. Most of the lines produced are the K_α lines; created when an electron drops from the L shell to the K shell. K_β lines are produced when an electron drops from the M shell to the K shell and are less common. The EDX measurements were carried out using the Oxford Instruments INCA X-ray analysis system, fitted to the Cambridge 360 Stereoscan microscope.

3 Hybrid Supertetrahedral Clusters Synthesised in 4-Methylpyridine

3.1 Introduction

There are currently a number of known structures based on the T3 gallium-sulphide supertetrahedron $[Ga_{10}S_{16}(L_4)]^{4-}$, where the corner S-atoms are replaced by amine ligands. These materials are described further in Section 1.4.5.[94, 113-115, 210-212] Ligands here are often aromatic nitrogen-based ligands based on substituted pyridine-rings. In this chapter, the solvent 4-methylpyridine (4-MPy) was mostly utilised (Figure 3.1). This solvent is present in a number of crystal structures, where it also acts as a structure-directing agent (SDA) and a countercation when protonated.

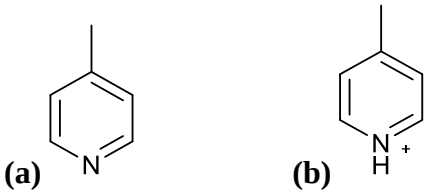

Figure 3.1 Structures of **(a)** 4-MPy and **(b)** protonated 4-MPy.

Successful reactions produced compounds (**1)** to **(7)** as described throughout this chapter. All of these structures are based on the $[Ga_{10}S_{16}(L_4)]^{4-}$ supertetrahedron, with different ways of linking and packing the clusters. Structures of different dimensionalities are described; in some cases where ditopic ligands link clusters together *via* the corners as previously demonstrated by Vaqueiro and described in Section 1.4.5.[113, 114, 211]

Synthesis was performed under a number of different reaction conditions, with a number of different reagents (Table 3.1). In all reactions, elemental gallium and sulphur powder were used as the Ga and S sources.

Table 3.1 Reaction parameters and reagents used in reactions carried out for chapter 3

Reaction Parameter	Variations Giving Materials (1) to (7)
Temperature/ ^{o}C	170, 200
Solvent	4-MPy, H_2O
Auxiliary Amine	Im, TMDPy
Auxiliary Imidazolium/ Phosphonium Salt	[BMMIm]Cl, [BMMIm]BF_4, [THTDP]Cl
Time/ Days	5, 6, 10

Initially work was carried out into using ionic liquids as potential solvents due to the milder conditions of these reactions. The possibility of linking SBUs together *via* different ligands, by taking initial products from solvothermal reactions and using them as reagents in an ionothermal reaction, was also investigated. These reactions are described in Sections 6.2.2 and 6.2.3.

In order to investigate other ways of using ionic liquids in these reactions, they were used as structure-directing agents; this proved more successful and materials created using this method are described in Sections 0 and 3.3.

Reactions were also carried out using traditional solvothermal-synthesis methods, using a basic solvent with gallium and sulphur. In some cases a structure-directing agent was used; in other cases the solvent also acted as the structure-directing agent. Reactions carried out throughout this work are included in Section 6.3 and Appendix 1.1.

Along with varying the parameters shown in Table 3.1, ratios between reagents were also varied; in some reactions water was added in order to aid crystallisation of the product. The ratios of Ga:S:SDA:4-MPy:H_2O was varied from 2:5:0.5:30:0 to 2.5:7:1:30:28 for amine-based SDAs and [BMMIm][BF_4], whereas ratios from 2:5:1.75:28:28 to 2:5:3.6:30:28:28 were used for the SDA [THTDP]Cl. All compounds described in this chapter were synthesised solvothermally as described in Section 2.1.1

Initial characterisation was carried out *via* SCXRD (Section 2.2.2). PXRD was used to confirm the purity of the samples (Section 2.2.3). In the event that a pure sample was produced, this was used for further measurements. In cases where samples contained impurities, crystals of the required material were handpicked in order to obtain a pure sample. The organic components and therefore the molecular formula of the structures were confirmed by CHN (Section 2.2.4), FTIR (Section 2.2.5) and TGA (Section 2.2.6) measurements. Optical band-gaps were measured for all of these compounds using UV-vis diffuse reflectance (Section 2.2.7) and photoluminescence data were collected for compounds **(1)** to **(5)**, as summarised in Section 3.6.

3.2 Zero-Dimensional Structures Synthesised in Ionic Liquids

3.2.1 $[C_6H_8N]_2[C_{12}H_{14}N_2][Ga_{10}S_{16}(NC_6H_7)_4]_2(C_{12}H_{12}N_2)(C_6H_7N)_2$ (1)

3.2.1.1 *Synthesis*

The title compound, **(1),** was synthesised from Ga metal (137 mg, 1.95mmol), S powder (143 mg, 4.46 mmol) and [THTDP]Cl (1.4 g, 2.70 mmol) in 4-MPy (2.7 ml, 25.8 mmol) and H_2O (0.5 ml, 28 mmol). The stoichiometric ratio of Ga:S:[THTDP]Cl:4-MPy:H_2O was 2:5:2.8:28:28. The reactants were sealed into the Teflon liner of a 23 ml autoclave and heated at 200 ^oC for 5 days. The product was a sample of orange crystals, which were identified as structure **(1)** by SCXRD (Section 3.2.1.2).

3.2.1.2 *Single-Crystal X-ray Diffraction*

Single-crystal X-ray diffraction data for **(1)** were collected by the NCS (National Crystallography Service) at the University of Southampton.[204] Crystal data are summarised in Table 3.2.

Table 3.2 Selected single-crystal X-ray diffraction data and refinement details for structure **(1)**

Crystallographically-Determined Formula	$C_{84}H_{94}Ga_{20}N_{14}S_{32}$
M_r	3724.26
Crystal habit	Red needle
Crystal system	Triclinic
Space group	P-1
T/K	100
a, b, c/Å	20.3058(14), 20.6427(14), 21.5230(15)
α, β, γ/º	109.033(3), 112.987(3), 101.268(2)
V/Å^3	7291.4(9)
Z	2
θ_{max}	27.543
ρ_{cal}/gcm^{-3}	1.694
μ/mm^{-1}	4.126
T_{min}, T_{max}	0.749, 0.884
Number of parameters	1085
Number of reflections used in refinement	34,222
Total number of reflections	56,787
R_{merge}	0.038
$R(I>3.0\sigma(I))$	0.0661
R_w	0.0737

3.2.1.3 *Structure Description*

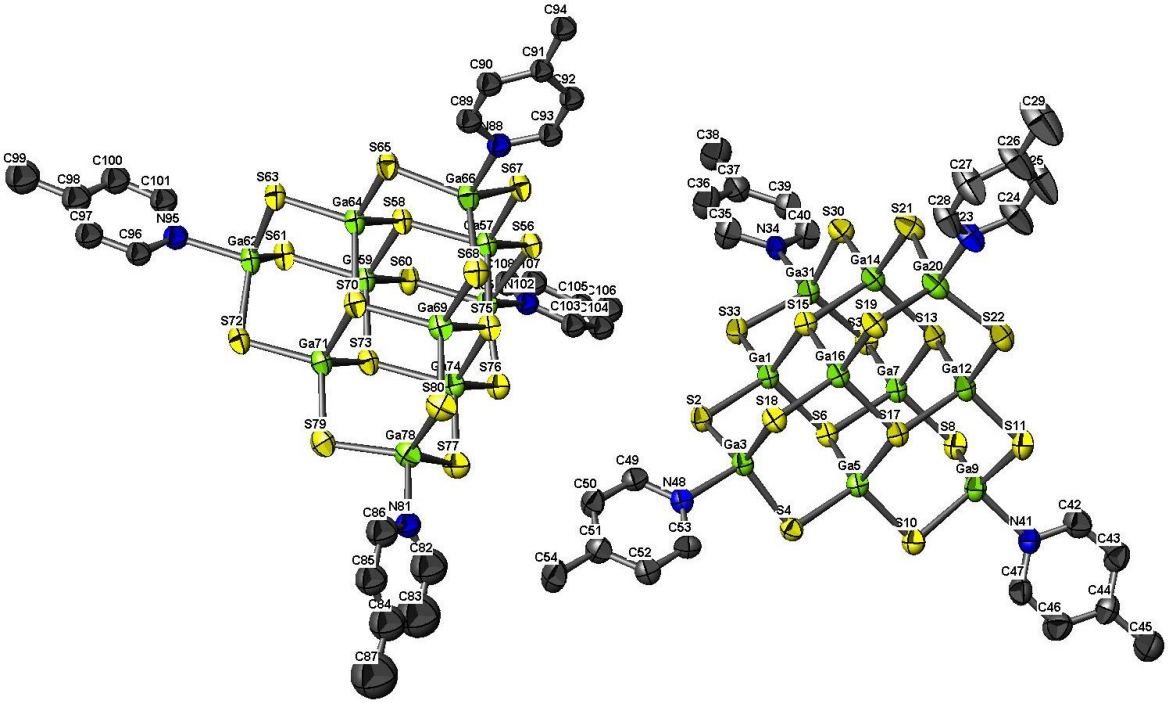

Figure 3.2 Asymmetric unit of **(1)** with solvent molecules and H-atoms omitted for clarity. Green =Ga, yellow = S, blue = N, grey = C.

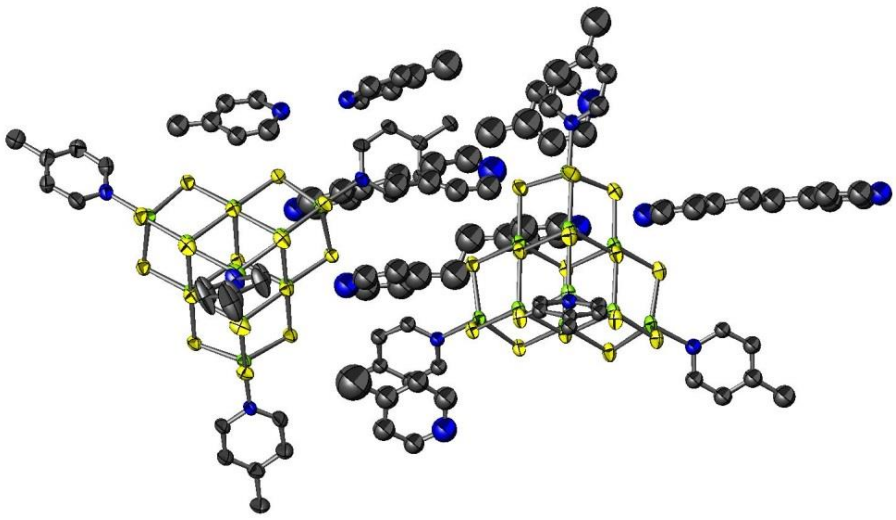

Figure 3.3 Asymmetric unit of structure **(1)** with ellipsoids at 50% probability, solvent molecules included and H-atoms omitted for clarity. Green =Ga, yellow = S, blue = N, grey = C.

Compound **(1)** has the overall formula $[C_6H_8N]_2[Ga_{10}S_{16}(NC_6H_7)_4]_2 \cdot [C_{12}H_{14}N_2](C_{12}H_{12}N_2)(C_6H_7N)_2$. This consists of $[Ga_{10}S_{20}]^{10-}$ clusters with 4-MPy units replacing the corner S-atoms to give a hybrid cluster of formula $[Ga_{10}S_{16}(NC_6H_7)_4]^{2-}$. The asymmetric unit (Figure 3.2 and Figure 3.3) contains two crystallographically - independent clusters. The charges of the clusters are balanced by different organic - cations; most of which have been located in the crystal structure.

Ga-S bond lengths are in the range of 2.222(2) – 2.343(2) Å and Ga-N bond lengths of 2.018(6) – 2.091(4) Å. S-Ga-S angles are between 106.66(6) and 118.36(7) º and S-Ga-N angles between 97.6(2) and 104.1(2) º. These are in the range expected for hybrid T3 gallium-sulphide supertetrahedra.[114, 115]

H-bonding is suggested to be present between the protonated amines that are not sharing an H-atom with another amine and the cluster, with an N-S distance of 3.21(2) Å. The N-S distance should be below *ca.* 3.85 Å. This distance is based on the method used by the Platon software, which uses the sum of the Van der Waals' radii of S (*ca.* 1.8 Å) and N (*ca.* 1.55 Å), followed by the addition of 0.5 Å.[206] Dance suggested in 2002 that the most stable intermolecular-distance for interaction is the sum of the Van der Waals' radii with an addition of 0.4 Å,[213] again consistent with the N-S distances in this work.

There are two protonated 4-MPy moieties ($[C_6H_8N]^+$) present, along with a dimerised form of the solvent; where formation of this has occurred *in-situ*. This dimer will occur on numerous occasions throughout this work and will be referred to as 4,4'-ethylenedipyridine (EDPy). Although the mechanism of this reaction cannot be proved, it can be speculated that it occurs *via* either radical formation, or through the formation of an organo-gallium intermediate.[214-217]

In order to balance the charge of the clusters in this structure, there must be four protons on the organic moieties. In this structure it is not uncommon for protons to be shared between more than one N-atom, but it cannot be determined exactly where these protons reside, due to the disorder of the organics in these types of compounds. One of the EDPy and all of the 4-MPy molecules have an occupancy of 0.5 i.e. they lie on that crystallographic site in half of the unit cells that repeat throughout the structure. Due to this and also the fact that H-atoms cannot be located, the exact location of the protons cannot be determined. Analytical data (Sections 3.2.1.5 and 3.2.1.7) indicated that a further protonated 4-MPy cation and two non-protonated 4-MPy moieties are present. This is also apparent when PLATON Squeeze is applied; confirming a void volume of *ca.* 89 $Å^3$ per unit cell (1.22 %); large enough to contain these species.

The discrete $[Ga_{10}S_{16}(NC_6H_7)_4]^{2-}$ clusters pack throughout the structure as shown in Figure 3.4. It can be deduced that the two crystallographically-independent clusters are oriented in different directions. Those in green (Figure 3.4) repeat along the *c*-axis, while those shown in magenta repeat along [100].

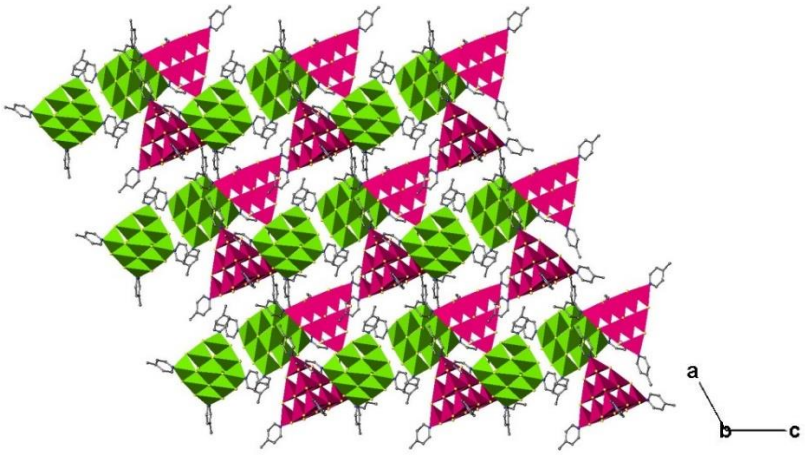

Figure 3.4 Structure of **(1)** viewed along the *b*-axis. Solvent molecules and H-atoms have been removed for clarity. Green and magenta show GaS_4 or GaS_3N tetrahedra. The different colours show crystallographically distinct polyhedra.

When the structure is viewed along [110] (Figure 3.5), it can be observed that the structure contains channels that propagate in this direction. Using the van der Waals' radii for all atoms, the channels can be seen to be of *ca*. 3 x 11 Å in size. (Figure 3.5 **(b)**)

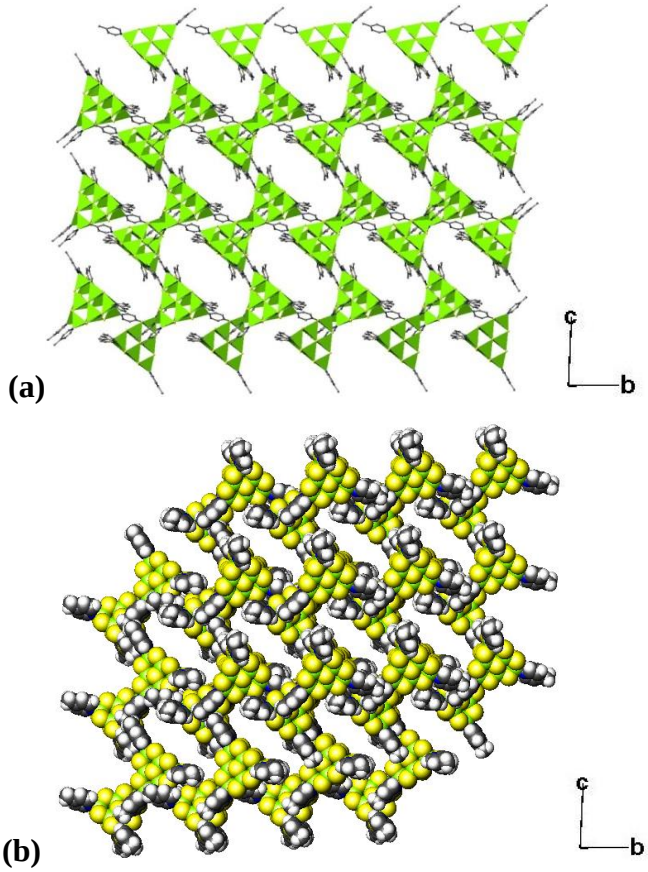

Figure 3.5 Structure of (1) viewed along [110]. (a) Green polyhedra show GaS_4 or GaS_3N tetrahedra. (b) View along [110] with Van der Waals' radii used for all atoms. Solvent molecules have been removed for clarity. Green =Ga, yellow = S, blue = N, grey = C.

An isostructural compound, which differs from **(1)** in the content of organic moieties, was previously synthesised by Romero *et al.*[119] While the previously-reported reaction produced a mixture of orange crystals and unreacted gallium, the synthesis reported here resulted in a sample containing only red-orange crystals of **(1).**

3.2.1.4 *Powder X-ray Diffraction*

Powder diffraction data were collected for compound **(1)**. Analysis of this data shows that the powder contains crystallites with the same structure as determined by SCXRD and the sample contains no impurities (Figure 3.6 and Table 3.3).

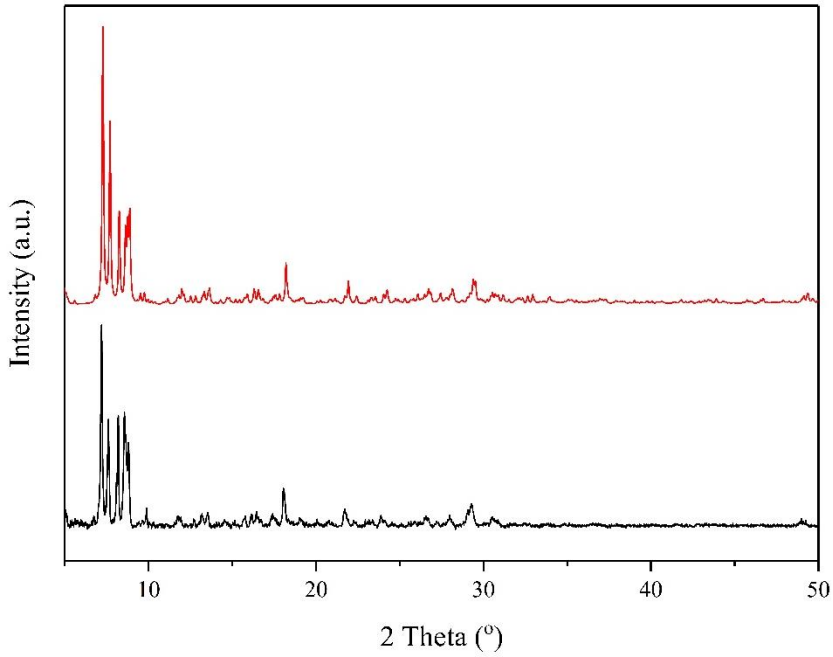

Figure 3.6 PXRD for the sample containing **(1).** Black = experimental, red = calculated from SCXRD.[218]

Table 3.3 Lattice parameters for **(1).** Parameters refined to PXRD data using DASH.[208]

SCXRD	***a*/ Å**	***b*/ Å**	***c*/ Å**	**α/ °**	**β/ °**	**γ/ °**
	20.3058(14)	20.6427(14)	21.5230(15)	109.033(3)	112.987(3)	101.268(2)
PXRD	***a*/ Å**	***b*/ Å**	***c*/ Å**	**α/ °**	**β/ °**	**γ/ °**
	20.102(5)	20.433(1)	21.640(2)	108.91(9)	112.63(2)	100.20(3)

3.2.1.5 *Elemental Analysis*

The experimental and calculated values for CHN analysis can be compared for **(1)**, based on the formula $[C_6H_8N]_2[C_{12}H_{14}N_2][Ga_{10}S_{16}(NC_6H_7)_4]_2(C_{12}H_{12}N_2)(C_6H_7N)_2$. (Experimental: C = 29.53 %, H = 2.77 %, N = 5.63 %. Calculated: C = 29.50 %, H = 2.84 %, N, = 5.73 %). This suggests that the proposed formula is in agreement with the experimental values for this compound.

3.2.1.6 *Infrared Spectroscopy*

FTIR confirms the presence of both protonated and non-protonated amines in this structure (Table 3.4 and Figure 3.7).

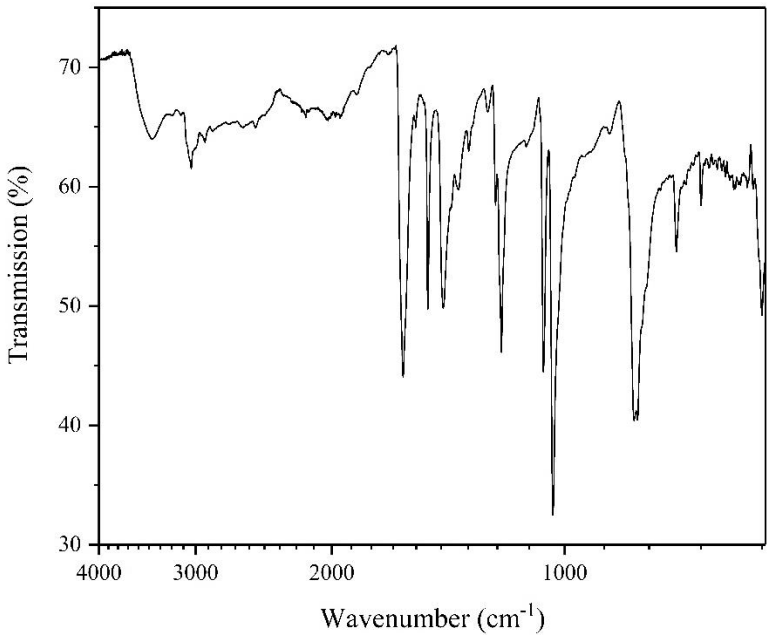

Figure 3.7 FTIR for **(1)**

Table 3.4 Key FTIR frequencies for structure **(1).** [219-222]

Wavenumber/ cm^{-1}	**Assignment**
3423	Aromatic ν (C-H) 4-MPy
3040	Aromatic ν (C-H) 4-MPy$[H]^+$
1618, 1502	Aromatic ν (C-C) 4-MPy$[H]^+$
1430	CH_3 ν (C-H) 4-MPy$[H]^+$
1205	δ (N-H) 4-MPy$[H]^+$
1064, 1035	Aromatic δ (C-H) 4-MPy$[H]^+$
814, 806	Aromatic γ (C-H)

3.2.1.7 *Thermogravimetric Analysis*

Thermogravimetric-analysis measurements were carried out on a sample of **(1)** in both air (Figure 3.8 **(a)**) and N_2 (Figure 3.8 **(b)**). It can be observed in Figure 3.8 **(b)** that the compound does not fully decompose when heated in an atmosphere of nitrogen, even when reaching temperatures of 1293 K. For the graph to reach a plateau, the sample must be heated in an oxidising atmosphere. This allows the compound to decompose into Ga_2O_3. The resulting weight is *ca.* 47.9 %, close to the final decomposition, which has a remaining weight of *ca.* 46 % (Figure 3.8 **(b)**).

The weight-change steps consist of the loss of non-protonated organic moieties (9.5 %), followed by the loss of the protonated ones (9.3 %); completed by the decomposition of the material into Ga_2O_3. It is proposed that sulphur is removed in the

form on SO_2 gas when the samples are heated in air. When the sample is heated under N_2, the sample is consistent with the loss of the neutral EDPy (*ca.* 5 %), followed by the removal of the charged organics (*ca.* 25 %), whereas this differs when the sample is heated in air. These measurements therefore suggest that the predicted formula from SCXRD and CHN measurements is correct.

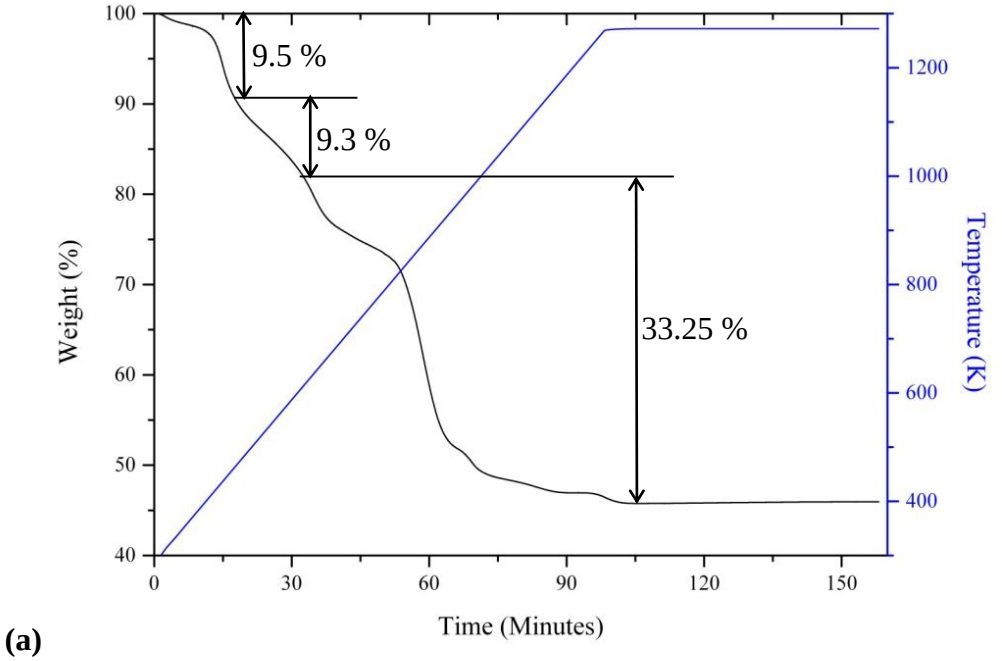

(a)

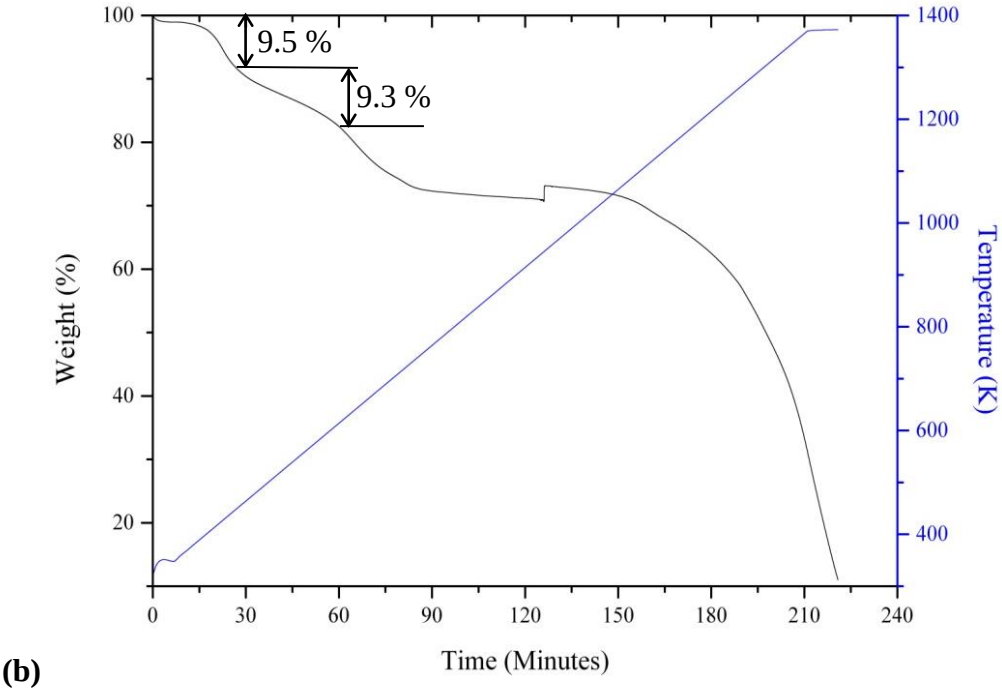

(b)

Figure 3.8 TGA data for **(1)** in **(a)** air and **(b)** N_2. Black line = weight percent vs time, blue = temperature vs time.

3.2.2 $[C_{12}H_{13}N_2]_{0.5}[C_6H_8N]_{1.5}[Ga_{10}S_{16}(NC_6H_7)_4]\ (C_6H_7N)_{0.5}$ (2)

3.2.2.1 *Synthesis*

Compound **(2)** was synthesised from Ga metal (137 mg, 1.95mmol), S powder (143 mg, 4.46 mmol), [THTDP]Cl (1.8 g, 3.47 mmol) in 4-MPy (2.9 ml, 29.8 mmol) and H_2O (0.5 ml, 28 mmol). The stoichiometric ratio of Ga:S:[THTDP]Cl:4-MPy:H_2O was 2:5:3.5:30:28 and the reaction was carried out at 200 ^oC for 5 days. This reaction can also be carried out in the absence of the ionic liquid to produce a compound with the same unit-cell. However, products of reactions carried out in the presence of the ionic liquid consist of orange crystals, while those synthesised without are yellow. All measurements were performed on the sample containing orange crystals, synthesised in the ionic liquid.

3.2.2.2 *Single-Crystal X-ray Diffraction*

Single-crystal X-ray Diffraction data for **(2)** were collected by the NCS (National Crystallography Service) at the University of Southampton.[204] Crystal data are summarised in Table 3.5.

Table 3.5 Selected single-crystal X-ray diffraction data and refinement details for **(2)**

Crystallographically-Determined Formula	$C_{42}H_{46}Ga_{10}N_7S_{16}$
M_r	1859.13
Crystal habit	Orange block
Crystal system	Monoclinic
Space group	$P2_1/n$
T/K	100
a, b, c/Å	12.9988(9), 26.1578(18), 20.9248(15)
β/º	105.6690(7)
V/Å^3	6850.5(8)
Z	4
θ_{max}	30.506
ρ_{cal}/gcm^{-3}	1.808
μ/mm^{-1}	4.402
T_{min},T_{max}	0.853,0.916
Number of parameters	587
Number of reflections used in refinement	13,403
Total number of reflections	20,855
R_{merge}	0.032
$R(I>3.0\sigma(I))$	0.0684
R_w	0.0691

3.2.2.3 *Structure Description*

Compound **(2)** has the overall formula $[C_{12}H_{13}N_2]_{0.5}[C_6H_8N]_{1.5}$ - $[Ga_{10}S_{16}(NC_6H_7)_4](C_6H_7N)_{0.5}$. The discrete $[Ga_{10}S_{16}(NC_6H_7)_4]^{2-}$ cluster resembles that in **(1)**. The asymmetric unit contains an EDPy moiety, where half is disordered over two sites, and modelled in Figure 3.9. Atoms C(64) to C(71), excluding N(66) and N(69), have occupancies of 0.5. This means that this species can occur either as EDPy or two separate 4-MPy moieties and that each case is equally likely, this has therefore been taken into account when giving the overall formula for this structure. However, EDPy and 4-MPy moieties differ by one H-atom only and therefore cannot be distinguished from one-another using CHN analysis (Section 3.2.2.5). There is also a second 4-MPy species present in the asymmetric unit.

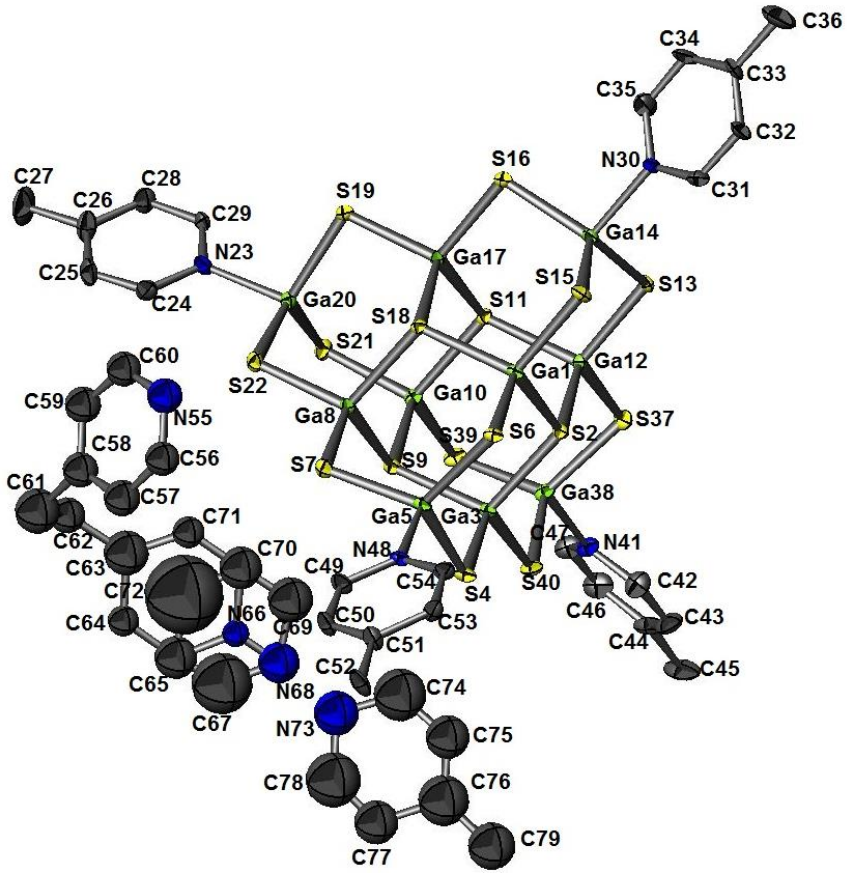

Figure 3.9 Asymmetric unit of **(2)**, with ellipsoids at 50% probability and H-atoms omitted for clarity. Green =Ga, yellow = S, blue = N, grey = C.

Ga-S bond lengths are in the range of 2.223(2) – 2.336(1) Å and Ga-N bond lengths of 2.025(4) – 2.038(5) Å. S-Ga-S angles are between 105.52(5) and 118.36(7) º and S-Ga-N angles between 99.3(1) and 104.7(1) º. These are in the range expected for hybrid T3 gallium-sulphide supertetrahedra.[114, 115] H-bonding cannot be observed between the cations located in the crystal structure and the cluster. π- π interactions do

appear to be present between one of the aromatic rings (N(55)-C(29), Figure 3.9) on the disordered EDPy moiety and one of the corner ligands (N(30) – C(35), Figure 3.10) with a distance of *ca.* 3.35 Å.

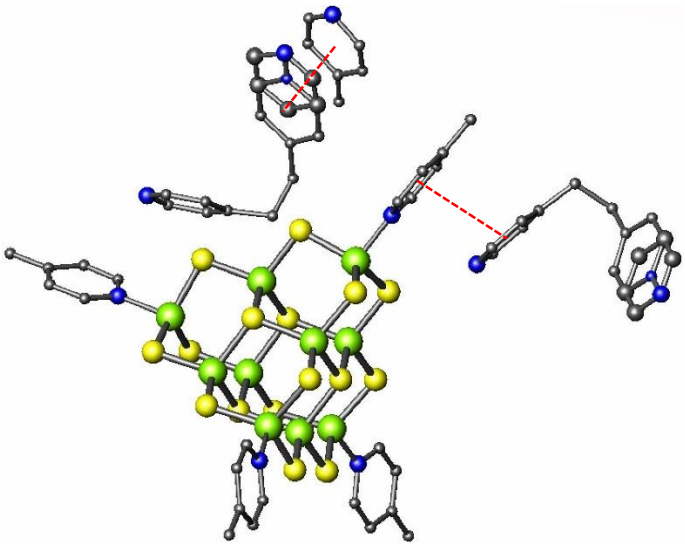

Figure 3.10 Cluster in **(2)**, showing π-π interactions (red dotted line).

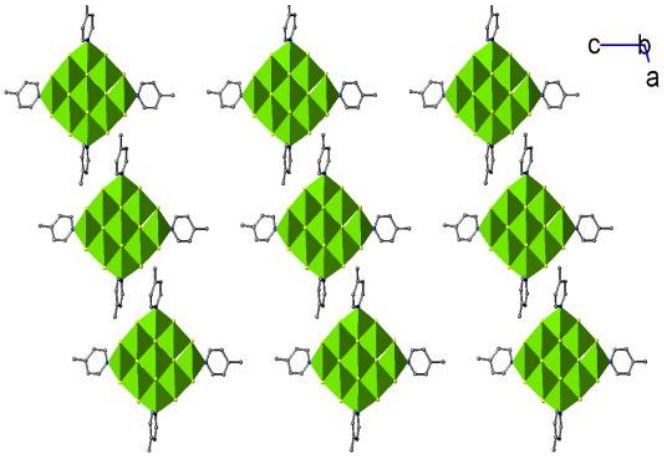

Figure 3.11 Packing of one layer of cluster in **(2)**, viewed along the *b*-axis.

The charges of two clusters are balanced by three protonated 4-MPy moieties, with another occurrence of protonated EDPy, shown in the asymmetric unit (Figure 3.9). Due to the close proximity of the EDPy to the 4-MPy, these must share a proton if either is protonated, therefore the EDPy has been described as monoprotonated. Platon SQUEEZE was performed during the refinement process and calculated a small void-space of 564.4 $Å^3$ per unit cell (8 %), this would allow the presence of the extra 4-MPy cation.

Figure 3.11 shows how the packing of clusters in **(2)** differs from that in **(1)**. The clusters are crystallographically equivalent; as confirmed by the fact that there is only one cluster in the asymmetric unit. They then align in the same direction and propagate along the *b*-axis.

Figure 3.12 illustrates how the clusters propagate along the *c*-axis**.** However, when the space-filling view is observed, it is evident that there are channels throughout the structure, propagating along the [100] direction (Figure 3.12 **(b)**). These channels are filled with the organic molecules described earlier in this section.

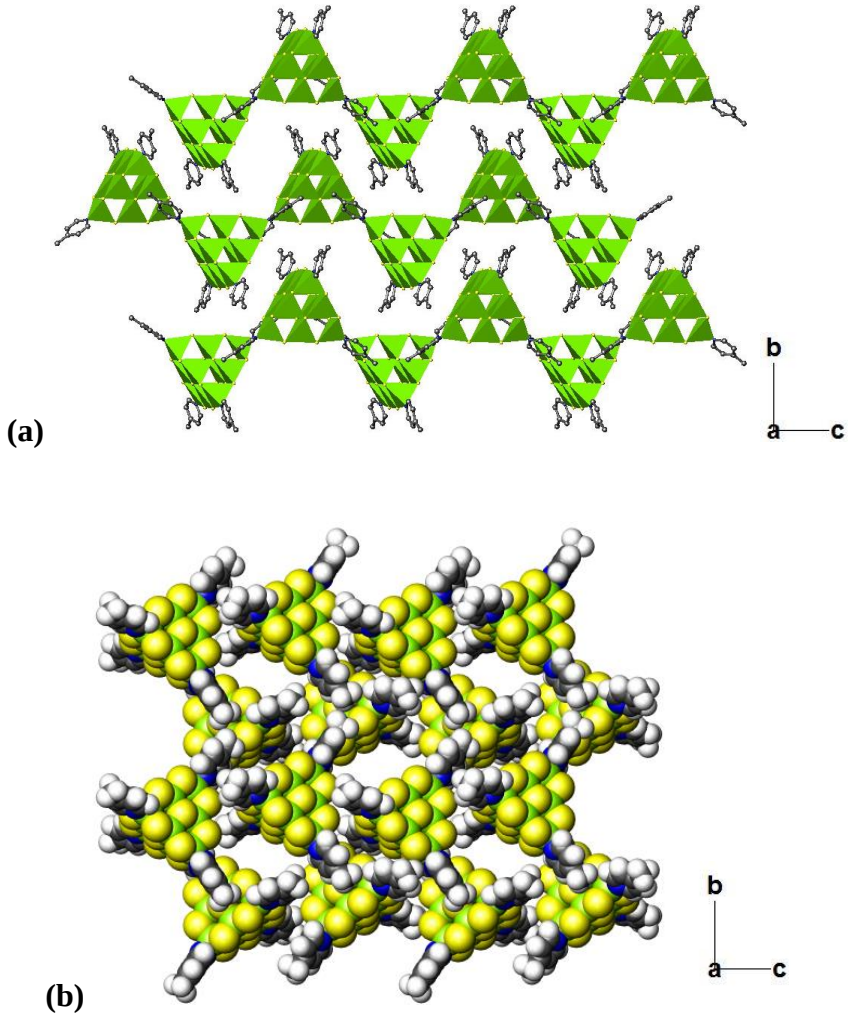

Figure 3.12 (2) viewed along [100]. Polyhedral view **(a)** and space-filling view **(b)**. Green polyhedra show GaS_4or GaS_3N tetrahedra. Green =Ga, yellow = S, blue = N, grey = C.

3.2.2.4 *Powder X-ray Diffraction*

Powder X-ray diffraction data were collected for **(2)** and show that the structure of the bulk is consistent with the crystal used for SCXRD and contains no impurities (Figure 3.13 and Table 3.6).

Table 3.6 Lattice parameters for **(2).** Parameters were refined against PXRD using DASH.[208]

SCXRD	***a*/ Å**	***b*/ Å**	***c*/ Å**	**α/ º**	**β/ º**	**γ/ º**
	12.9988(9)	26.1578(18)	20.9248(15)	90	105.6690(7)	90
PXRD	***a*/ Å**	***b*/ Å**	***c*/ Å**	**α/ º**	**β/ º**	**γ/ º**
	13.150(5)	26.382(5)	20.961(5)	90	105.44(5)	90

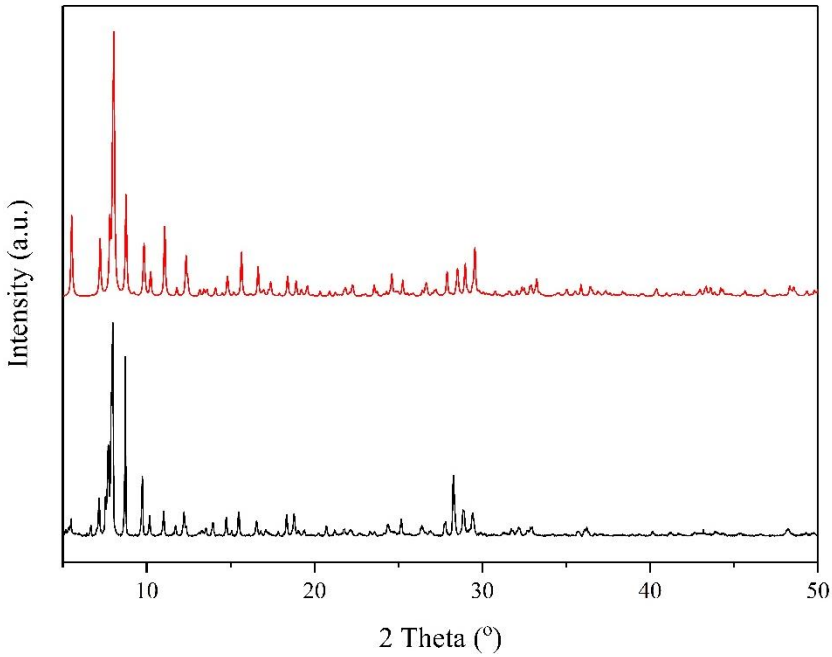

Figure 3.13 PXRD for **(2)**. Black = experimental, red = calculated from SCXRD.[218]

3.2.2.5 *Elemental Analysis*

The experimental and calculated values for CHN analysis can be compared. Experimental: C = 26.30%, H = 2.76%, N = 5.82%. Calculated: C = 27.11 %, H = 2.6 %, N = 5.27 %. There is good agreement between these values, which suggests the calculated formula of $[C_{12}H_{13}N_2]_{0.5}[C_6H_8N]_{1.5}$ $[Ga_{10}S_{16}(NC_6H_7)_4](C_6H_7N)_{0.5}$ is correct.

3.2.2.6 *Infrared Spectroscopy*

FTIR confirms the presence of the protonated amines in this structure (Figure 3.14 and Table 3.7).

Table 3.7 Key FTIR frequencies for **(2).** [219, 220]

Wavenumber/ cm^{-1}	Assignment
3443	Aromatic ν (C-H) 4-MPy
3000	Aromatic ν (C-H) 4-MPy$[H]^+$
1623, 1503	Aromatic ν (C-C) 4-MPy$[H]^+$
1442	CH_3 ν (C-H) 4-MPy$[H]^+$
1205	δ (N-H) 4-MPy$[H]^+$
814, 806	Aromatic γ (C-H)) 4-MPy$[H]^+$

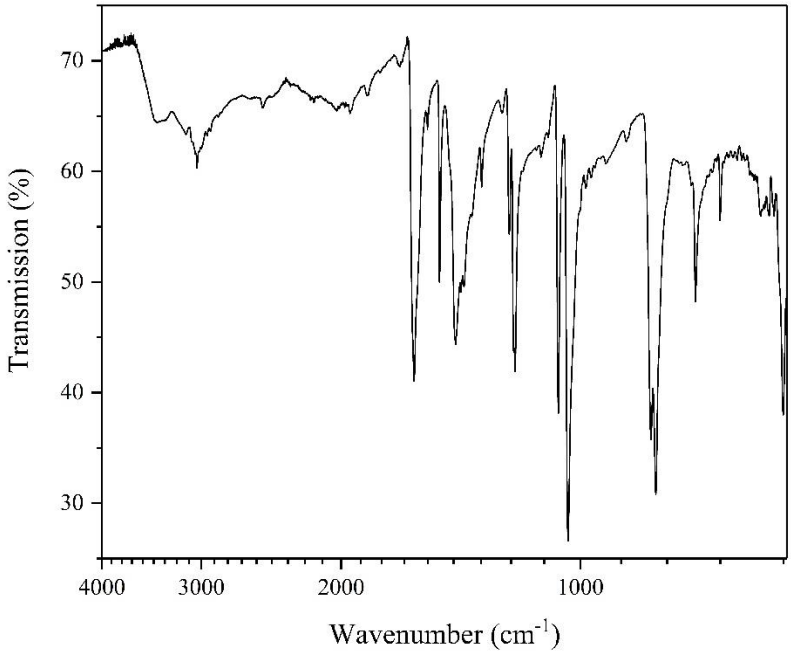

Figure 3.14 FTIR for **(2)**

3.2.2.7 *Thermogravimetric Analysis*

Thermogravimetric-analysis measurements were carried out on a sample of **(2)** in both air (Figure 3.8 **(a)**) and N_2 (Figure 3.8 **(b)**). Figure 3.15 **(b)** illustrates that this structure also does not fully decompose when heated in an atmosphere of nitrogen; in this case the sample was also heated up to 1293 K. The measurement was therefore repeated in an oxidising atmosphere of air; this is the case for all samples in this work where TGA has been performed.

Calculations show that for structure **(2)**, if it decomposes entirely to Ga_2S_3, the remaining weight would be 63.4 %; in this case lower than the plateau under N_2. When the structure decomposes further to Ga_2O_3, the resulting weight would be 50.4 %

corresponding to the final plateau when the sample decomposes under air. The small step close to full decompositon at *ca.* 70 minutes is thought to correspond to an intermediate of Ga_2O_2S.

The weight-loss steps are greater than would be expected from calculations. It can be seen that there are no well-defined organic-loss steps under N_2, thought to be due to both cations present in the structure being of the same nature. Loss of all pore organics would be expected to leave a remaining weight of *ca.* 85 %; compared with experimental values of 81 % in air and 74 % under N_2.

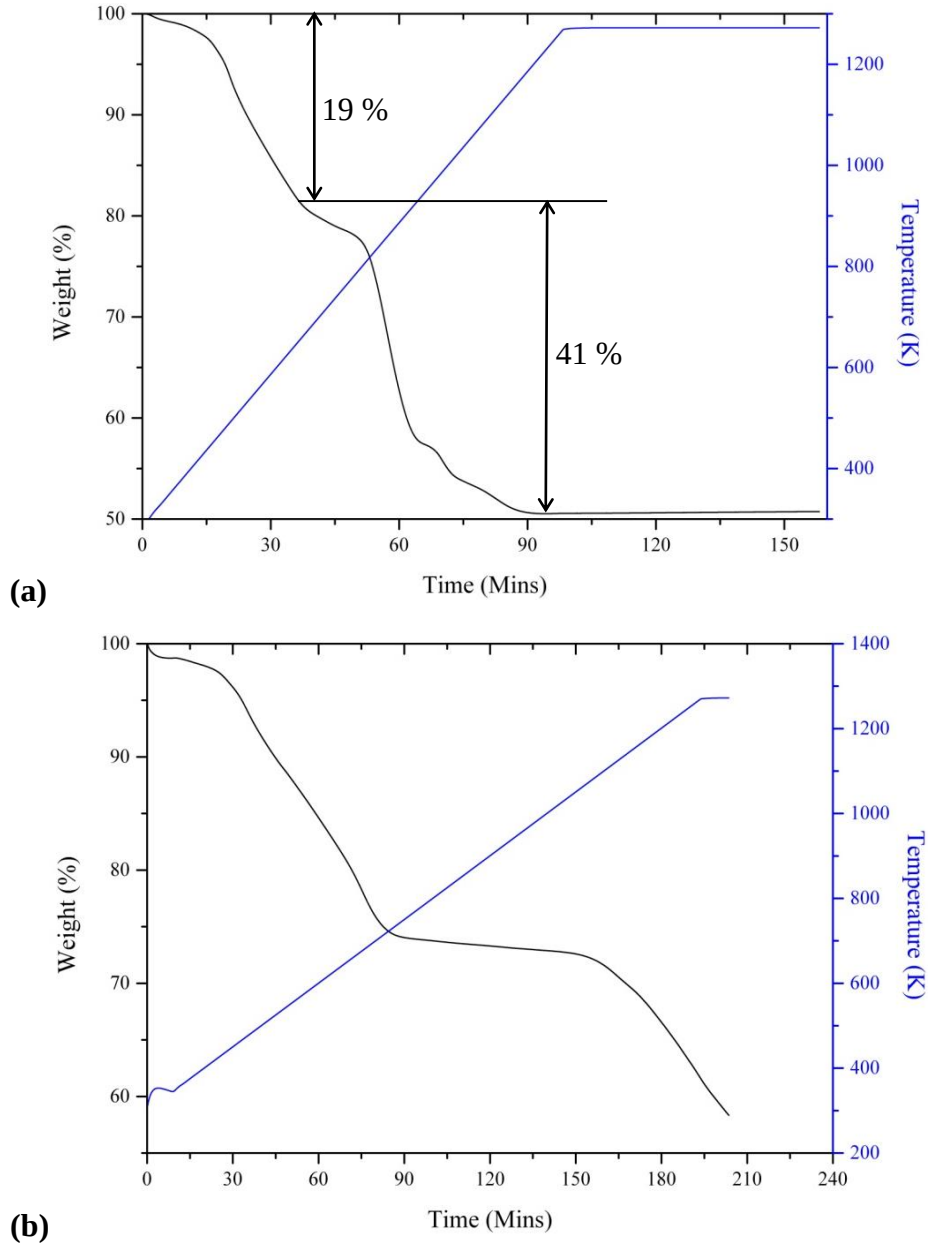

Figure 3.15 TGA data for **(2)** are shown in **(a)** air and **(b)** N_2. Black = weight percent vs time, blue = temperature vs time.

3.3 A Structure Containing Infinite Chains of Clusters

3.3.1 Synthesis

Compound **(3)** $[C_3H_3N_2C_4H_9CH_3][C_6H_8N][Ga_{10}S_{16}(NC_6H_7)_2(NC_6H_6)_2] \cdot (C_6H_7N)_{0.5}$ was synthesised from Ga metal (1.61 mmol, 113 mg), S powder (5.51 mmol, 176 mg) and [BMMIm][BF_4] (0.74 mmol, 178 mg) in 4-MPy (32.5 mmol, 2.9 ml). The reagents were heated at 200 ^oC in an autoclave for 6 days. Here the stoichiometric ratio of Ga:S:[BMMIm]BF_4:4-MPy was 2:7:1:30. The product contained only yellow blocks.

3.3.2 Structure and Characterisation

3.3.2.1 *Single-Crystal X-ray Diffraction*

Single crystal X-ray diffraction data were collected for **(3)** and are summarised in Table 3.5.

Table 3.6 Selected Single crystal X-ray diffraction data and refinement details for **(3)**

Crystallographically-Determined Formula	$Ga_{20}S_{32}C_{76}N_{14}H_{93}$
M_r	3622.97
Crystal habit	Yellow block
Crystal system	Orthorhombic
Space group	P*cca*
T/K	150
a, b, c/Å	36.4131(8), 20.0043(5), 18.4979(5)
V/Å^3	13474.2(6)
Z	4
θ_{max}	29.696
ρ_{cal}/gcm^{-3}	1.52
μ/mm^{-1}	4.460
T_{min}, T_{max}	0.739,0.915
Number of parameters	440
Number of reflections used in refinement	7462
Total number of reflections	16,815
R_{merge}	0.115
$R(I>3.0\sigma(I))$	0.0565
R_w	0.0617

Platon SQUEEZE was carried was applied on the crystallographically - determined structure, which established that a void space of 427.3 $Å^3$ per unit cell (3.17 %) was available.[206]

3.3.2.2 *Structure Description*

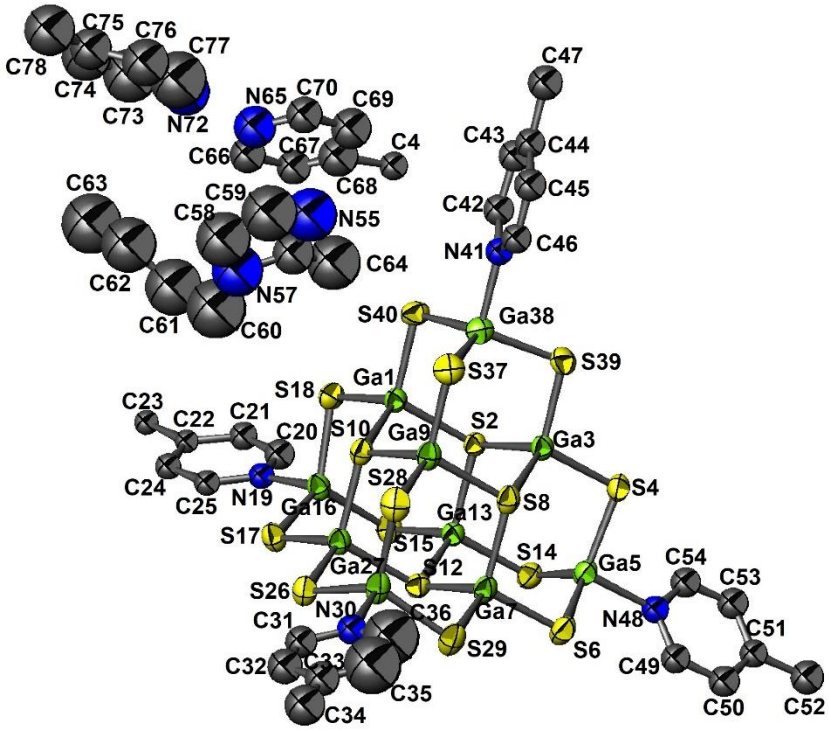

Figure 3.16 Ellipsoid view of **(3)**, with ellipsoids at 50% probability. Green =Ga, yellow = S, blue = N, grey = C.

The asymmetric unit of **(3)** contains two 4-MPy moieties, both with occupancies of 0.5 (Figure 3.16), along with a 1-butyl-2-methyl-imidazolium ($[C_3H_3N_2C_4H_9CH_3]^+$) cation; this suggests either rearrangement *in situ* or contamination of the starting material.

The organic moieties present in the crystal structure balance the -2 charge on the cluster, where both are protonated. Ga-S bond lengths are in the range of 2.215 (3) – 2.329(2) Å and Ga-N bond lengths of 2.024(8) – 2.029(8) Å. S-Ga-S angles are between 108.2(1) and 117.6(1) ^{o} and S-Ga-N angles between 96.9(2) and 104.4(2) ^{o}. These are in the range expected for hybrid T3 gallium-sulphide supertetrahedra.[114, 115] Unusually, as observed for **(2)** it does not appear that there are H-bonds present between the protonated-amine sites and the clusters; due to the 4-MPy moieties present sharing a proton between one-another.

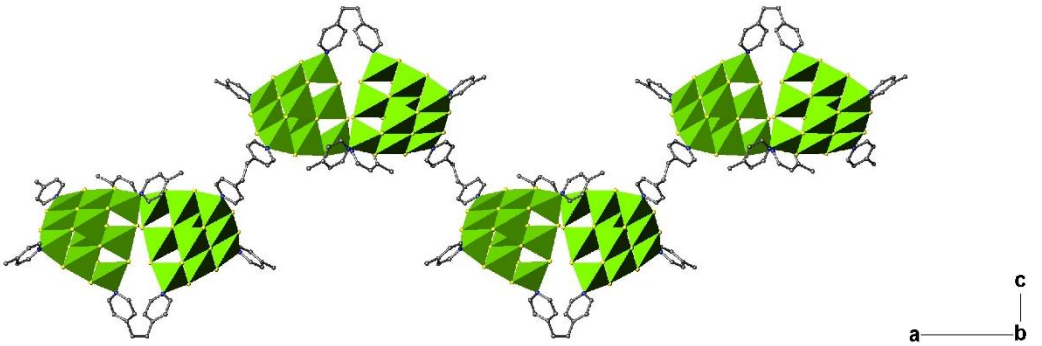

Figure 3.17 Perspective view of a zigzag chain running through structure **(3).** Green polyhedra show GaS_4or GaS_3N tetrahedra.

The negative charge of the $[Ga_{10}S_{16}(NC_6H_7)_2(NC_{12}H_{12})]^{2-}$ chains is balanced by protonation of the organic amines. The chains zigzag throughout the structure, due to the bending of alternating linkers (Figure 3.17) , and are packed in layers parallel to the [010] plane (Figure 3.18). An isostructural compound has been reported previously by Romero *et al.*,[211] but the material described here has been synthesised using the ionic liquid $[BMMIm][BF_4]$, and therefore contains different organic-species. The previously-reported structure contained two protonated 4-MPy moieties, whereas **(3)** contains 4-MPy and 1-butyl-2-methyl-imidazolium.

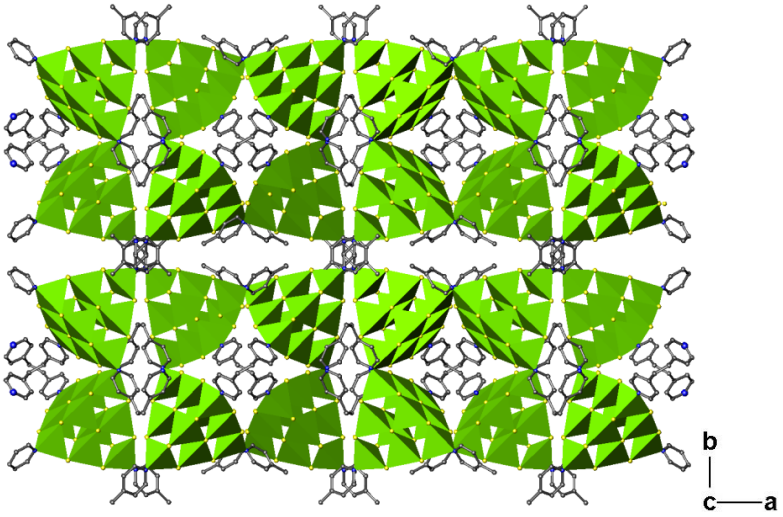

Figure 3.18 Structure of **(3)** viewed along [010]. Green polyhedra show GaS_4or GaS_3N tetrahedra.

3.3.2.3 *Powder X-ray Diffraction*

Powder X-ray diffraction (Figure 3.19 and Table 3.8) confirms the structure of the bulk matches that of the SCXRD and that the product is pure.

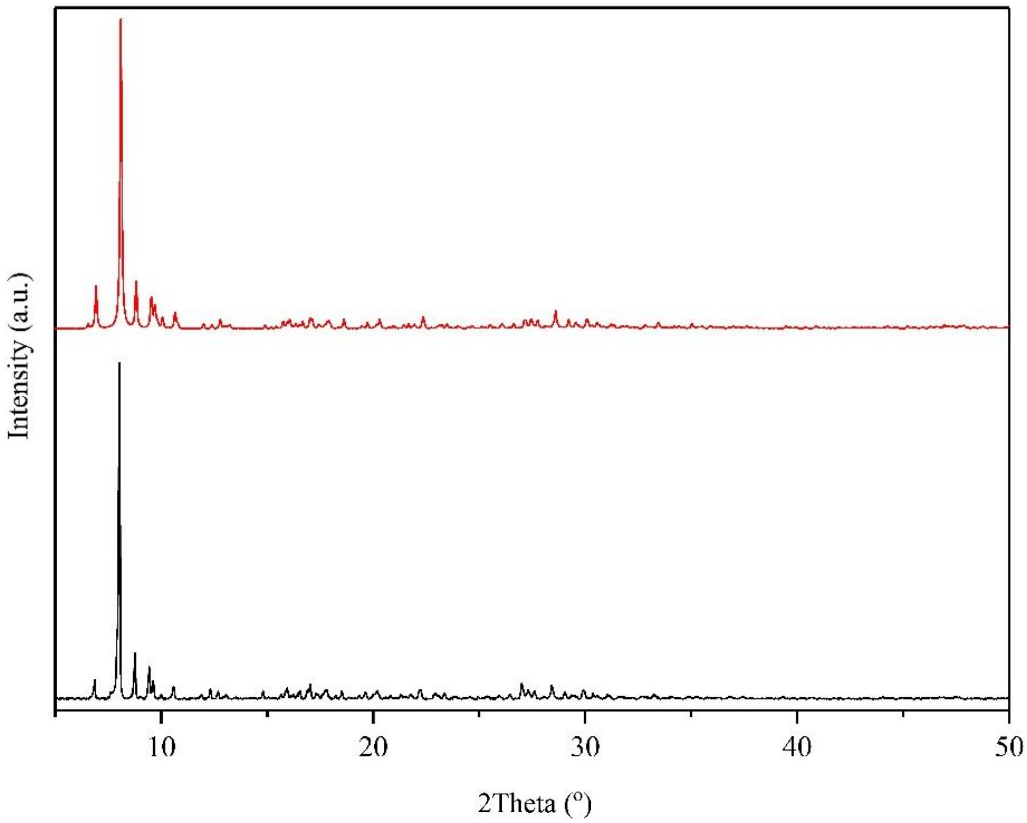

Figure 3.19 PXRD for **(3)**. Black = experimental, red = calculated from SCXRD.[218]

Table 3.8 Lattice parameters for **(3).** Parameters were refined against PXRD using DASH.[208]

SCXRD	***a*/ Å**	***b*/ Å**	***c*/ Å**	**α/ º**	**β/ º**	**γ/ º**
	36.4131(8)	20.0043(5)	18.4979(5)	90	90	90
PXRD	***a*/ Å**	***b*/ Å**	***c*/ Å**	**α/ º**	**β/ º**	**γ/ º**
	36.624(9)	20.0376(1)	18.612(8)	90	90	90

3.3.2.4 *Elemental Analysis*

Elemental-analysis results indicated that it was required to include an additional ½ of a 4-MPy moiety per formula unit to reach agreement between calculated and found contents (Experimental: C = 26.30%, H = 2.76%, N = 5.82%. Calc: C = 26.49 %, H = 2.77 %, N = 5.65 %). The final formula for this compound was therefore established to be $[C_3H_3N_2C_4H_9CH_3][C_6H_8N][Ga_{10}S_{16}(NC_6H_7)_2(NC_6H_6)_2](C_6H_7N)_{0.5}$.

3.3.2.5 *Infrared Spectroscopy*

FTIR was used to confirm the presence of amines within the structure (Figure 3.20). Key frequencies are listed in Table 3.9.

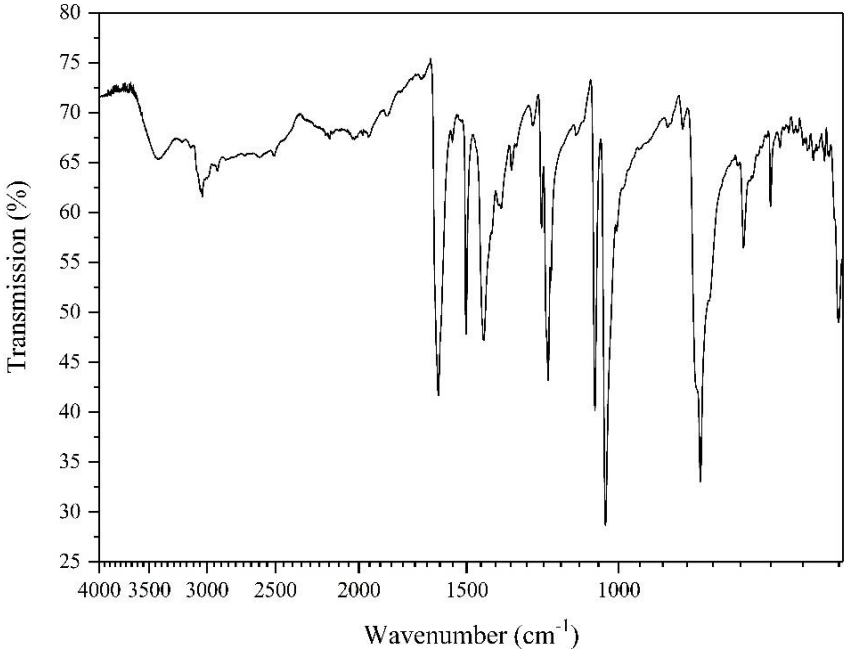

Figure 3.20 FTIR for **(3)**

Table 3.9 Key FTIR frequencies for **(3).** [219, 220]

Wavenumber/ cm^{-1}	Assignment
3443	Aromatic ν (C-H) 4-MPy
3056	Aromatic ν (C-H) 4-MPy$[H]^+$
1617, 1502	Aromatic ν (C-C) 4-MPy$[H]^+$
1434	CH_3 ν (C-H) 4-MPy$[H]^+$
1208	δ (N-H) 4-MPy$[H]^+$
812, 805	Aromatic γ (C-H)

3.3.2.6 *Thermogravimetric Analysis*

This compound does not fully decompose in nitrogen (Figure 3.21 **(b)**), like the previous samples, the structure was also heated up to 1293 K. In an oxidising atmosphere of air the material first loses the non-charged 4-MPy moiety (2.2 %), followed by the charged organics $[C_3H_3N_2C_4H_9CH_3]^+$ and $[C_6H_8N]^+$. The compound then fully decomposes into Ga_2O_3 (Figure 3.21 **(a)**).

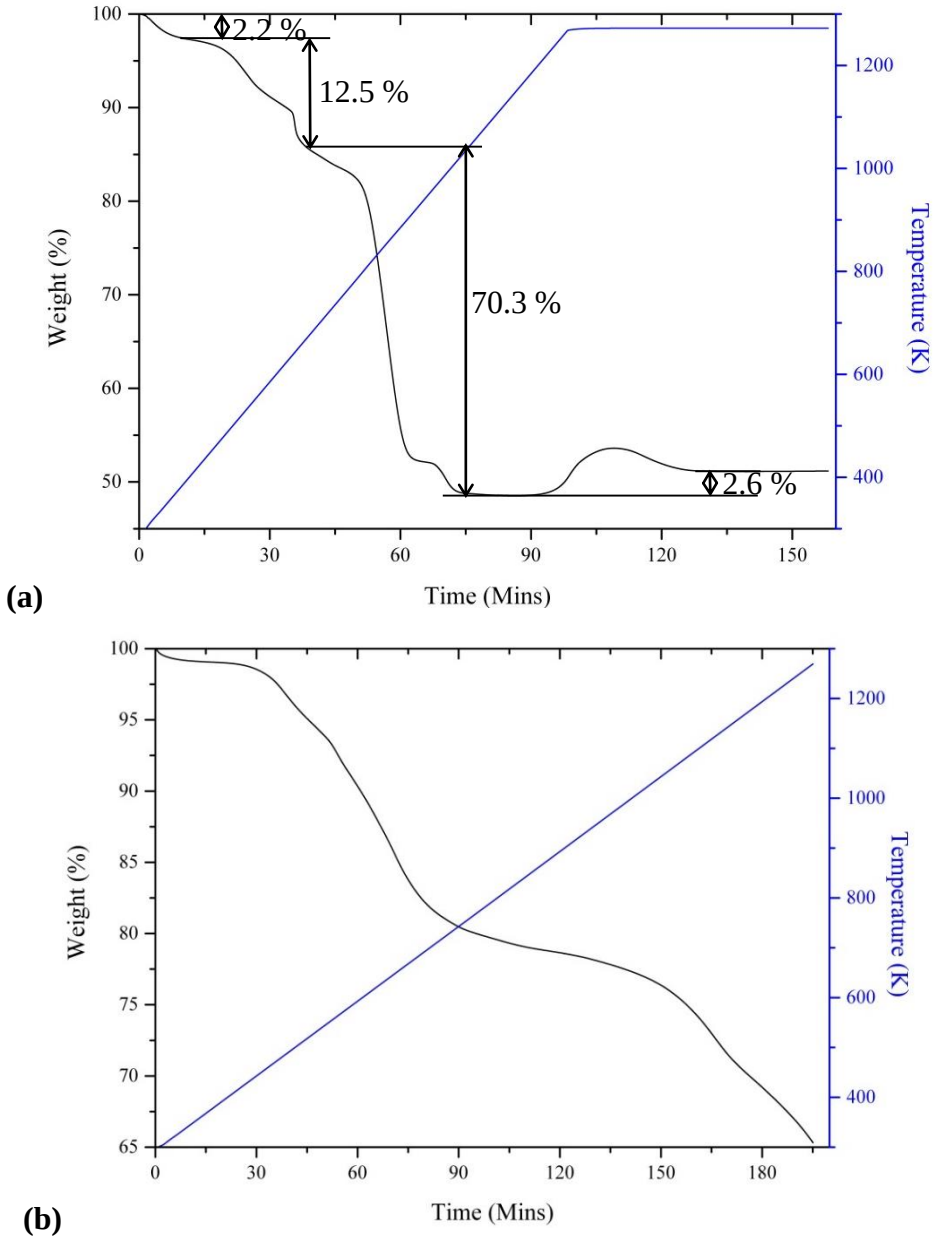

Figure 3.21 TGA data for **(3)** in **(a)** air and **(b)** N_2. Black = weight percent vs time, blue = temperature vs time.

Calculations show that for **(3)**, if it decomposes entirely to Ga_2S_3, the remaining weight would be 63.50 %; in this case lower than the minimum value when heated under N_2 of 65.5 %. When the structure decomposes further to Ga_2O_3, the resulting weight would be 50.6 % corresponding to the final plateau when the sample decomposes under air of 51.1 %.

3.4 Structures Containing Dimers of Clusters

3.4.1 $[NC_6H_8]_{2.5}[N_2C_4H_6][C_3H_5N_2]_{0.5}[Ga_{20}S_{32}(N_2C_{12}H_{12})_2(NC_6H_7)_5]$ (4)

3.4.1.1 *Synthesis*

Compound **(4)** was synthesised from Ga metal (1.95 mmol, 137 mg), S powder (4.97 mmol, 190 mg) and Im (1.04 mmol, 70.6 mg) with 4-MPy (29.8 mmol, 2.9 ml). The reaction was carried out at 200 ^oC for 6 days. The Ga:S:Im:4-MPy ratio was 2:6:1:30. This reaction gave a product consisting of yellow blocks and unreacted Ga. All further measurements were carried out on pure samples of handpicked crystals of **(4)**.

3.4.1.2 *Single-Crystal X-ray Diffraction*

Single crystal X-ray diffraction data were collected for **(4)** and are summarised in Table 3.10.

Table 3.10 Selected Single crystal X-ray diffraction data and refinement details for structure **(4).**

Crystallographically-Determined Formula	$C_{65.5}H_{73.5}Ga_{20}N_{13}S_{32}$
M_r	3463.41
Crystal habit	Yellow block
Crystal system	Monoclinic
Space group	$P2_1/n$
T/K	150
a, b, c/Å	13.6019(3), 20.1333(5), 46.7715(10)
β/º	93.767(2)
V/Å^3	12780.8(5)
Z	4
θ_{max}	31.946
ρ_{cal}/gcm^{-3}	1.800
μ/mm^{-1}	4.697
T_{min}, T_{max}	0.798,0.869
Number of parameters	1143
Number of reflections used in refinement	13,117
Total number of reflections	38,240
R_{merge}	0.076
$R(I>3.0\sigma(I))$	0.0530
R_w	0.0570

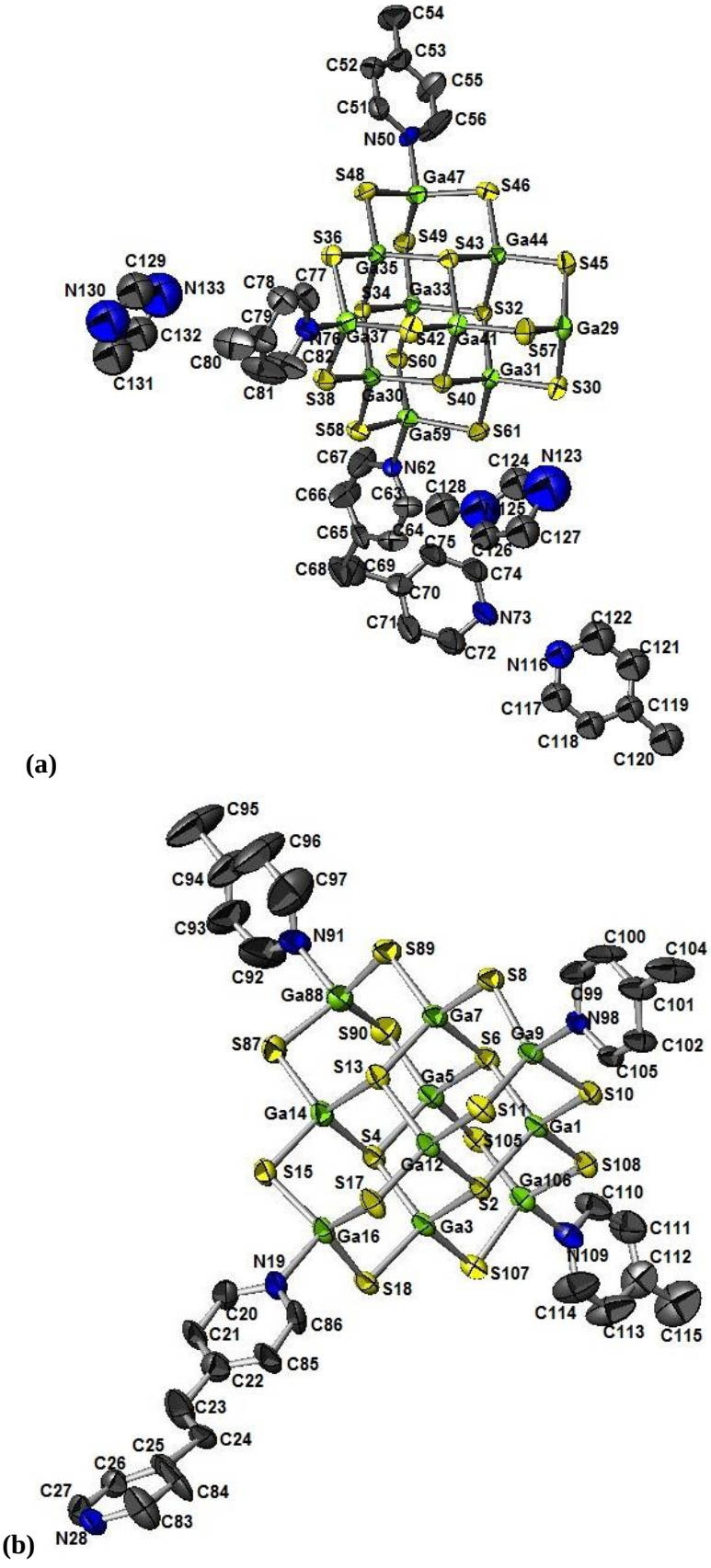

Figure 3.22 (a) and **(b)** ellipsoid views of the asymmetric unit of structure **(4).** Shown in two different figures for clarity of atom labels, with displacement ellipsoids at 50% probability. H atoms have been omitted for clarity. Green =Ga, yellow = S, blue = N, grey = C.

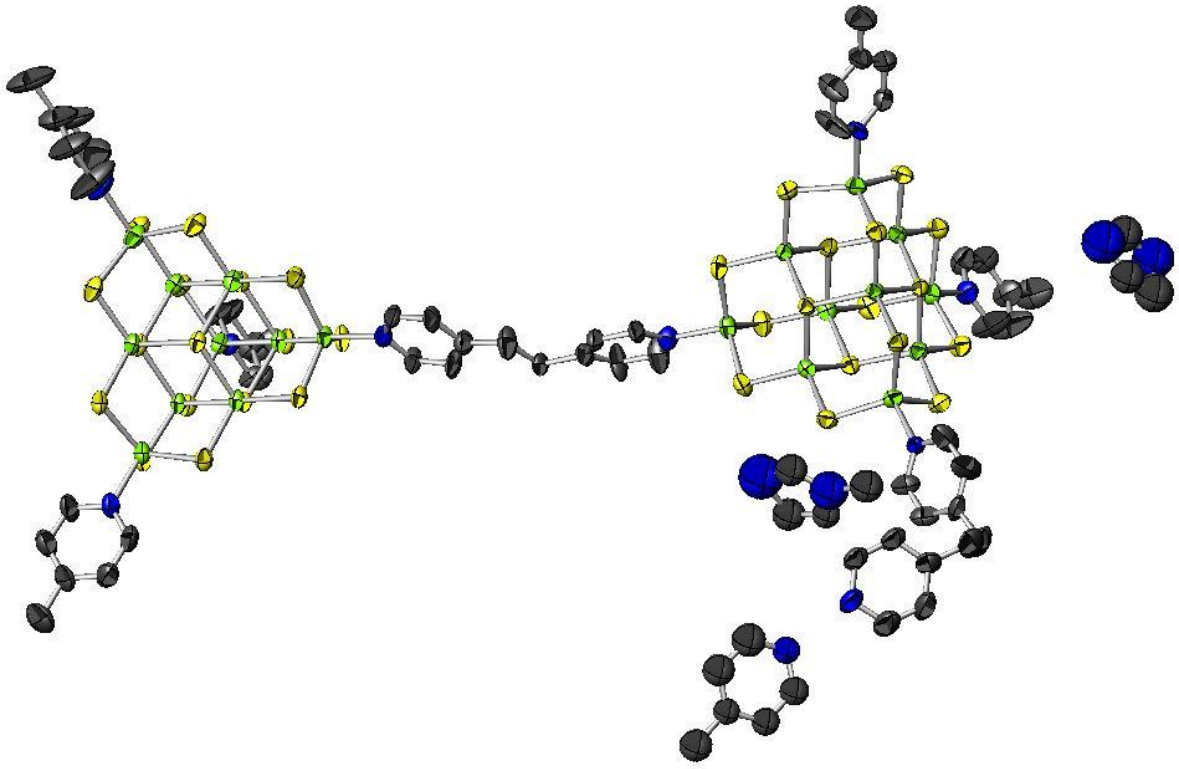

Figure 3.23 Ellipsoid view of the full asymmetric unit for structure **(4)**, with displacement ellipsoids at 50% probability. H atoms have been omitted for clarity. Green =Ga, yellow = S, blue = N, grey = C.

Compound **(4)** consists of dimeric anions, formed by linkage of two T3 supertetrahedral clusters, $[Ga_{20}S_{32}(N_2C_{12}H_{12})_2(NC_6H_7)_5]^{4-}$ (Figure 3.22 and Figure 3.23). One of the clusters in the dimer is terminated by 4-MPy ligands at three corners, with the final corner coordinated by an EDPy ligand, linking to another cluster. The three remaining-corners of the second cluster are terminated by two 4-MPy ligands and a bent EDPy ligand. One 4-MPy, one 1-methyl-imidazole and 1/2 an imidazole moiety are found in the asymmetric unit of this structure. Protonation of these species will result in an overall positive charge of +2.5. Charge balancing can be achieved through the incorporation of 1.5 protonated 4-MPy species in the void space, which has been estimated to be 380 $Å^3$ per unit cell using Platon SQUEEZE.[206]

Ga-S bond lengths are in the range of 2.233(3) – 2.333(3) Å and Ga-N bond lengths of 2.035(8) – 2.043(9) Å. S-Ga-S angles are between 107.23(9) and 118.1(1) º and S-Ga-N angles between 98.6(2) and 103.7(2) º. These are in the range expected for hybrid T3 gallium-sulphide supertetrahedra.[114, 115] A proton is shared between N(73) on the corner EDPy moiety and N(116) on the pore 4-MPy moiety, therefore H-bonds are not observed in the crystal structure.

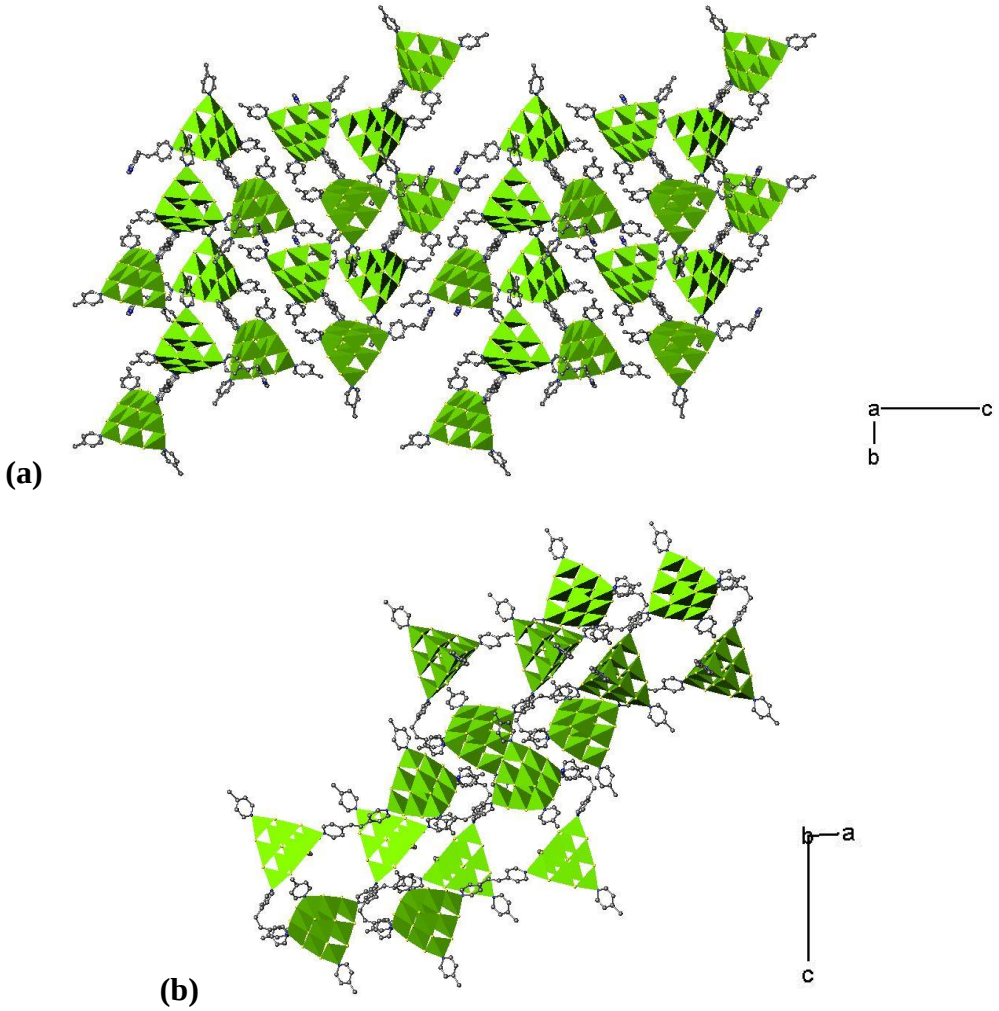

Figure 3.24 Polyhedral view of structure **(4)** viewed along **(a)** [001] and **(b)** [010]. H atoms and solvent molecules have been omitted for clarity. Green polyhedra = GaS_4or GaS_3N.

In **(4)**, dimers are packed in layers parallel to the (010) plane; **(a)** shows the structure viewed along [100], along the layers. Figure 3.24 **(b)** shows the structure of a layer, as viewed along [010]. An isostructural compound has been previously reported,[211, 223] but the terminal ligands on the dimers in **(4)** differ from those in the previously-reported material, where one of the corners was coordinated by a pyridine moiety and an extra corner was coordinated by EDPy. **(4)** also contains imidazolium and protonated 4-MPy, which were not present in the previously reported structure. The reagents used also differ greatly; in the previously-reported method tetraphenylphosphonium bromide and 1,2-di(4-pyridyl)ethylene were used instead of imidazole and 4-MPy.

3.4.1.3 *Powder X-ray Diffraction*

Powder diffraction data were collected for **(4)** in order to show that the structure of the bulk is consistent with the crystal used for SCXRD and that the product was pure. (Figure 3.25 and Table 3.11).

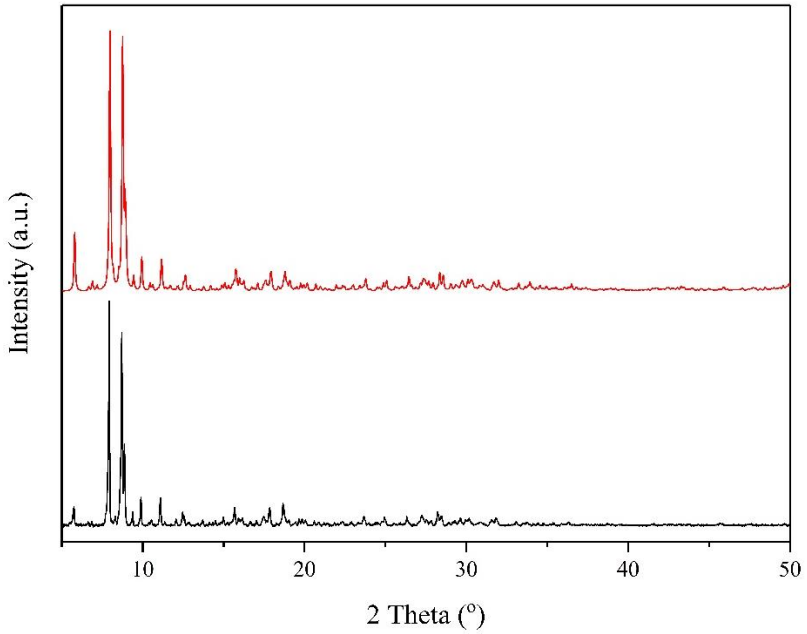

Figure 3.25 PXRD for structure **(4)**. Black = experimental, red = calculated from SCXRD.[218]

Table 3.11 Lattice parameters for **(4).** Parameters were refined against PXRD using DASH.[208]

SCXRD	***a*/ Å**	***b*/ Å**	***c*/ Å**	**α/ °**	**β/ °**	**γ/ °**
	13.6019(3)	20.1333(5)	46.7715(10)	90	93.767(2)	90
PXRD	***a*/ Å**	***b*/ Å**	***c*/ Å**	**α/ °**	**β/ °**	**γ/ °**
	13.625(1)	20.114(3)	47.151(2)	90	93.05(6)	90

3.4.1.4 *Elemental Analysis*

The proposed overall-formula, $[C_6H_8N]_{2.5}[C_4H_7N_2][C_3H_5N_2]_{0.5}$ $[Ga_{20}S_{32}$ - $(N_2C_{12}H_{12})_2(NC_6H_7)_5]$, is consistent with the elemental analysis when comparing the calculated and experimental values (Experimental: C = 24.19%, H = 2.67%; N = 5.54%. Calculated: C = 24.8 %, H = 2.47 %, N = 5.63 %).

3.4.1.5 *Infrared Spectroscopy*

FTIR for **(4)** confirms that aromatic amines are present within the structure (Figure 3.26). Table 3.9 shows the key frequencies in this sample.

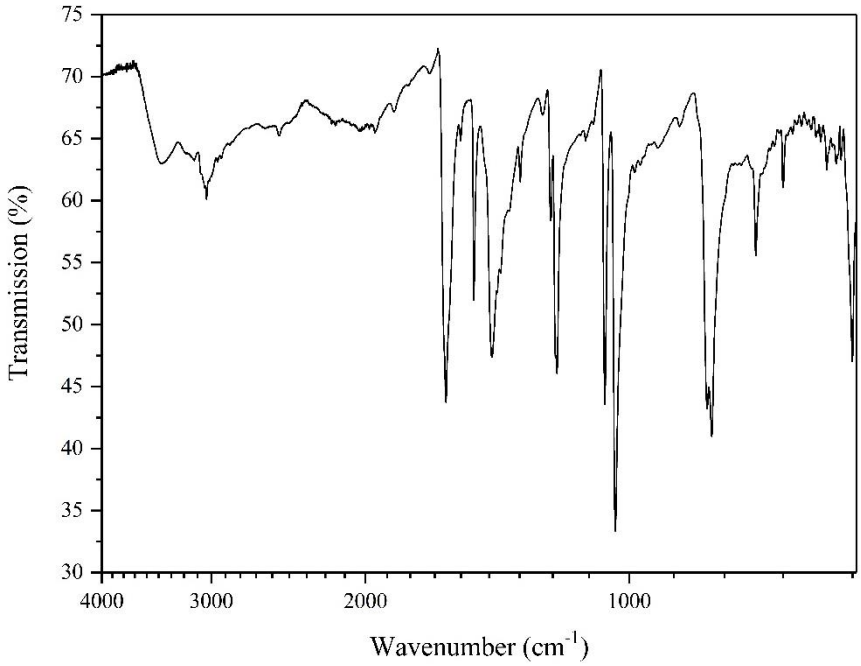

Figure 3.26 FTIR for **(4)**

Table 3.12 Key FTIR frequencies for **(4)**.[219, 220]

Wavenumber/ cm^{-1}	**Assignment**
3428	Aromatic ν (C-H) 4-MPy
3041	Aromatic ν (C-H) 4-MPy$[H]^+$
1620, 1505	Aromatic ν (C-C) 4-MPy$[H]^+$
1438	CH_3 ν (C-H) 4-MPy$[H]^+$
1208	δ (N-H) 4-MPy$[H]^+$
815, 806	Aromatic γ (C-H)

3.4.1.6 *Thermogravimetric Analysis*

Compound **(4)** is consistent with the other samples and shows that it does not fully decompose under a nitrogen atmosphere when held at 1273 K for 30 minutes. (Figure 3.27). Full decomposition of the structure to Ga_2S_3 would give a remaining weight of 66 %, suggesting that in this case the structure does begin to decompose further. This step is most likely to be attributed to oxidation by trace amounts of oxygen to Ga_2O_3.

The final plateau when the sample is heated in air has a final weight of 52.4 % for full decomposition into Ga_2O_3. Weight-loss steps in air are consistent with the loss of pore amines at 9.9 %. The following weight-loss step under N_2 is consistent with the loss of the corner 4-MPy ligands of 12.8 %. The remainder of the material decomposes

mainly in one step; although there is a small step before the plateau when the structure decomposes under air, again thought to correspond to an intermediate of Ga_2O_2S.

For the measurement under N_2, the loss of pores amines and corner 4-MPy moieties are consistent with a weight-loss step of 22.7 %. The material then continues to decompose but does not reach the final stage that occurs in air.

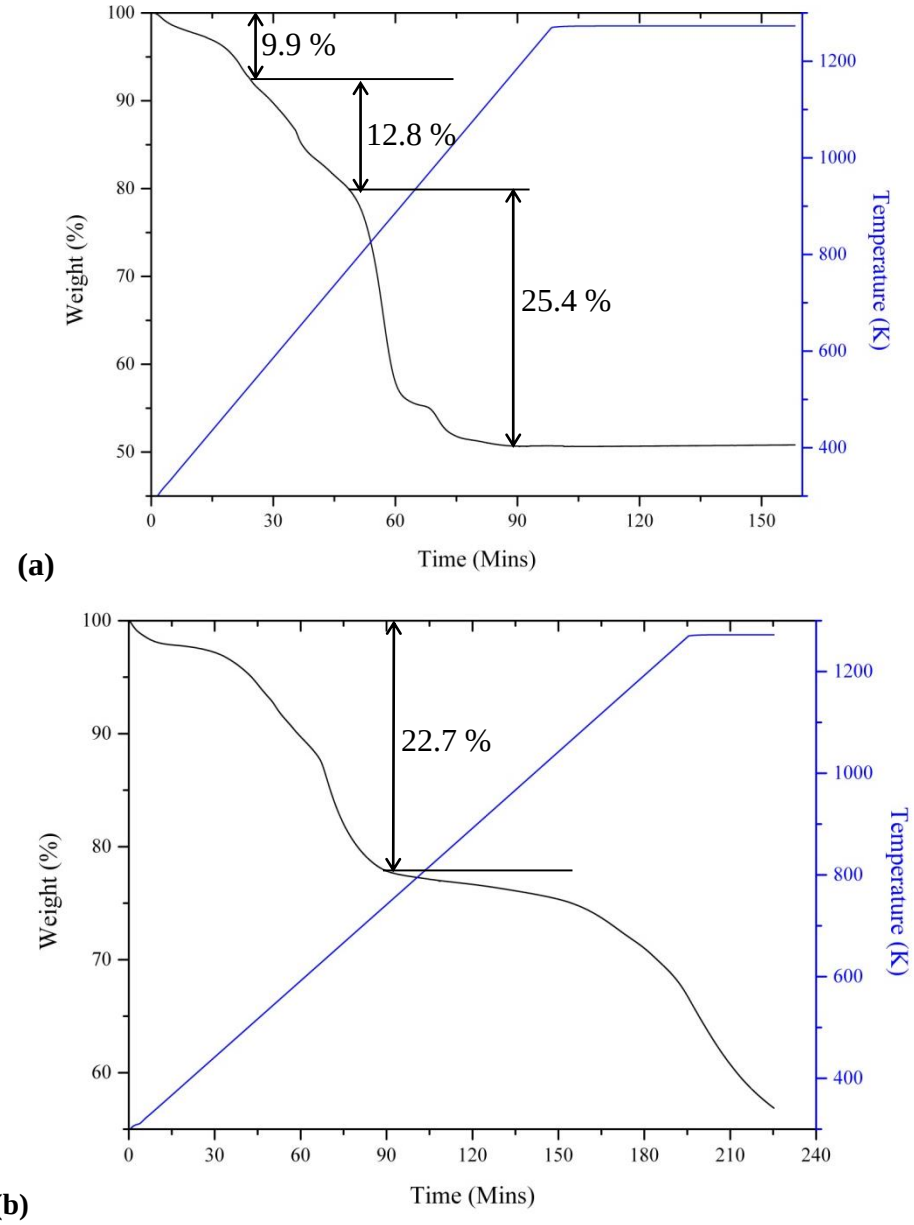

Figure 3.27 TGA data for **(4)** in **(a)** air and **(b)** N_2. Black = weight percent vs time, blue = temperature vs time.

3.4.2 **[$C_6H_8N]_4[Ga_{10}S_{16}(NC_6H_7)_3(NC_6H_6)][Ga_{10}S_{16}(NC_6H_7)_4](C_6H_7N)_2$ (5)**

3.4.2.1 *Synthesis*

Compound **(5)** was first synthesised from Ga (1.95 mmol, 137 mg), S powder (3.96 mmol, 127 mg) and Im (1.04 mmol, 70.6 mg) in 4-MPy (29.8 mmol, 2.9 ml) for 6 days at 200 °C. The Ga:S:Im:4-MPy ratio was 2:6:1:30; the sample consisted of yellow blocks of **(5)** and unreacted gallium. It was also synthesised from Ga metal (1.95 mmol, 137 mg) and S powder (5.94 mmol, 159 mg) in 4-MPy (29.8 mmol, 2.9 ml) and H_2O (27.8 mmol, 0.5 ml) at 170 °C for 6 days. The Ga:S:Im:4-MPy ratio was 2:6:1:30. This gave a sample containing only yellow plates of **(5)**.

3.4.2.2 *Single-Crystal X-ray Diffraction*

Single-crystal X-ray diffraction data were collected for **(5)** and are summarised in Table 3.13.

Table 3.13 Single crystal X-ray diffraction data for structure **(5).**

Crystallographically-Determined Formula	$C_{168}H_{180}Ga_{40}N_{28}S_{64}$
M_r	7432.51
Crystal habit	Yellow block
Crystal system	Monoclinic
Space group	$P2_1/n$
T/K	100
a, b, c/Å	13.4776(4), 44.8635(8), 22.6128(5)
β/°	99.233(2)
V/Å^3	13495.8(5)
Z	2
θ_{max}	30.485
ρ_{cal}/gcm^{-3}	1.829
μ/mm^{-1}	4.455
T_{min}, T_{max}	0.659,0.837
Number of parameters	1253
Number of reflections used in refinement	17,256
Total number of reflections	35,261
R_{merge}	0.063
$R(I>3.0\sigma(I))$	0.0578
R_w	0.0586

3.4.2.3 *Structure Description*

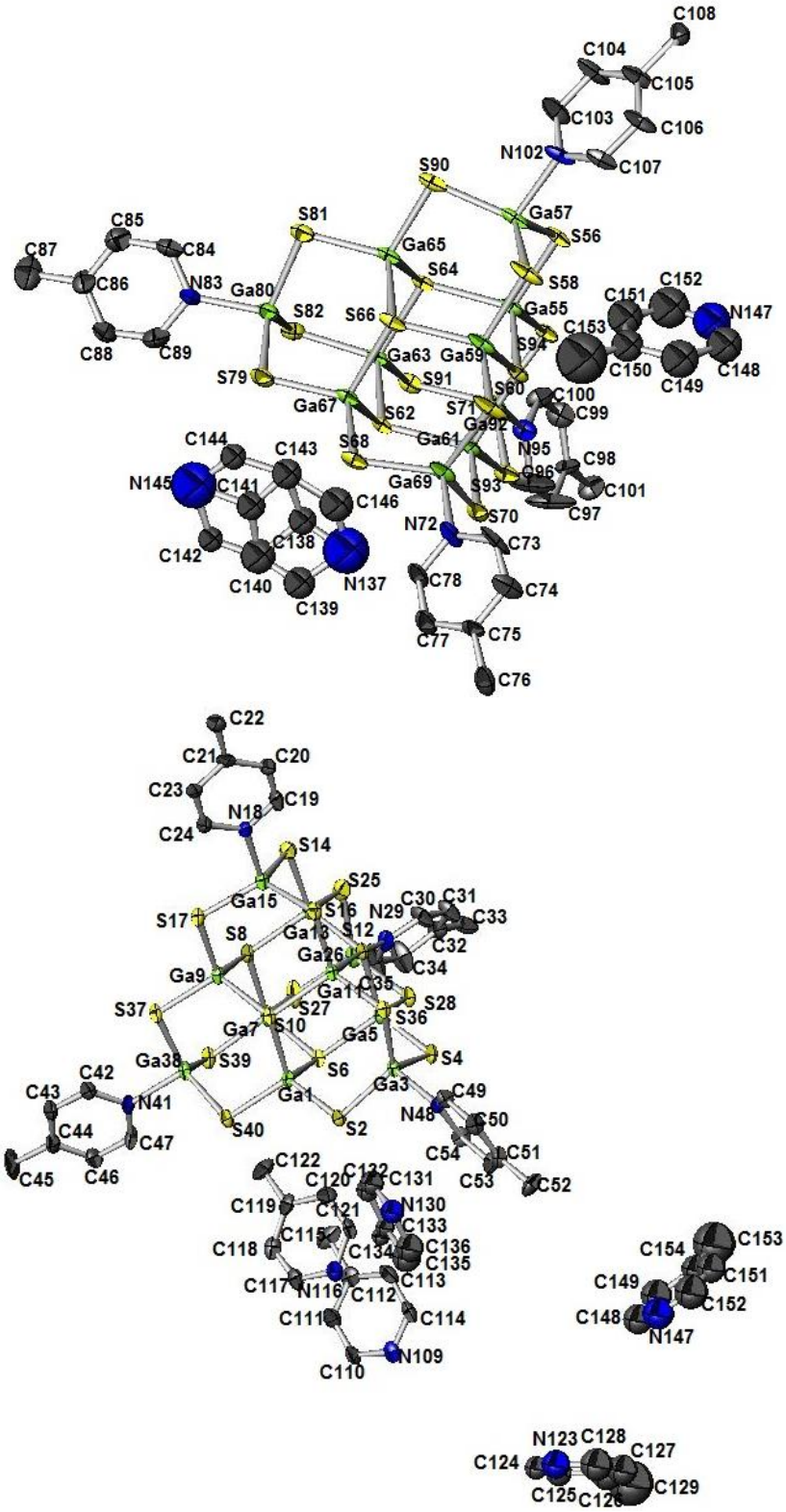

Figure 3.28 Ellipsoid view of the asymmetric unit for structure **(5)**, with displacement ellipsoids at 50% probability. Shown in two different figures for clarity of atom labels. H atoms have been omitted for clarity. Green =Ga, yellow = S, blue = N, grey = C.

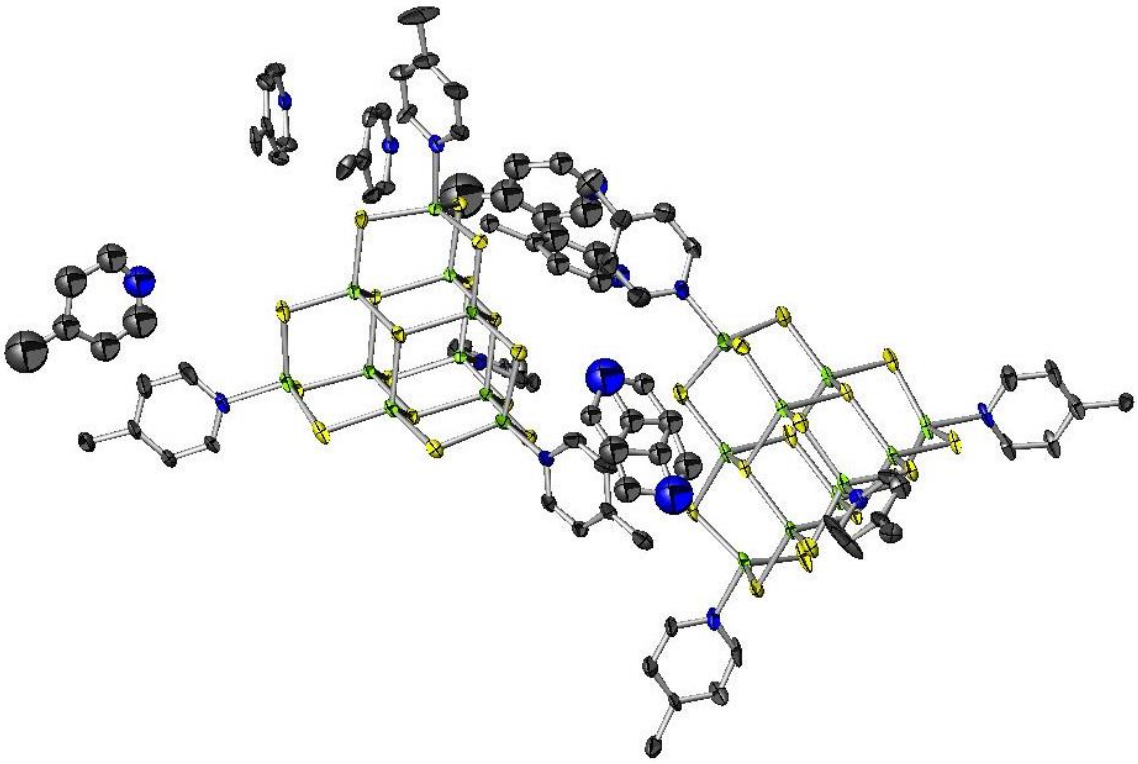

Figure 3.29 Ellipsoid view of the full asymmetric unit for structure **(5).** H atoms have been omitted for clarity. Green =Ga, yellow = S, blue = N, grey = C.

The asymmetric unit of **(5)** contains a single cluster and half of a dimer; giving a ratio of single:dimeric clusters of 2:1. The dimer linkage again occurs via an EDPy moiety. In this case the C-C bond is from C(108), to itself *via* symmetry (Figure 3.28). The dimers differ from those found in **(4)** in that both clusters in the dimer are terminated by 4-MPy ligands at three corners. The dimer can be therefore be formulated as $[Ga_{20}S_{32}(N_2C_{12}H_{12})(NC_6H_7)_6]^{4-}$, while the single cluster $[Ga_{10}S_{16}(NC_6H_7)_4]^{2-}$ is identical to those found in **(1)** and **(2)**. Each asymmetric unit contains six 4-MPy moieties; one of which is disordered between two overlapping-sites (Figure 3.28). Four of the 4-MPy units must be protonated to balance the negative charge from the clusters.

Ga-S bond lengths are in the range of 2.213 (2) – 2.330(2) Å and Ga-N bond lengths of 2.022(7) – 2.039(7) Å. S-Ga-S angles are between 106.35(8) and 119.21(8) º and S-Ga-N angles between 98.9(2) and 105.4(2) º. These are in the range expected for hybrid T3 gallium-sulphide supertetrahedra.[114, 115] An N-S bond distance of *ca.* 3.35 Å is observed between N(147) and S(16) and of *ca.* 3.32 Å between N(130) and S(81), indicating H-bonding.

The packing of **(5)** is such that the dimers align parallel to one another in alternating directions, in a herringbone-like arrangement (Figure 3.30 **(a)**). The single clusters reside in the remaining space, also alternating in direction (Figure 3.30 **(b)**).

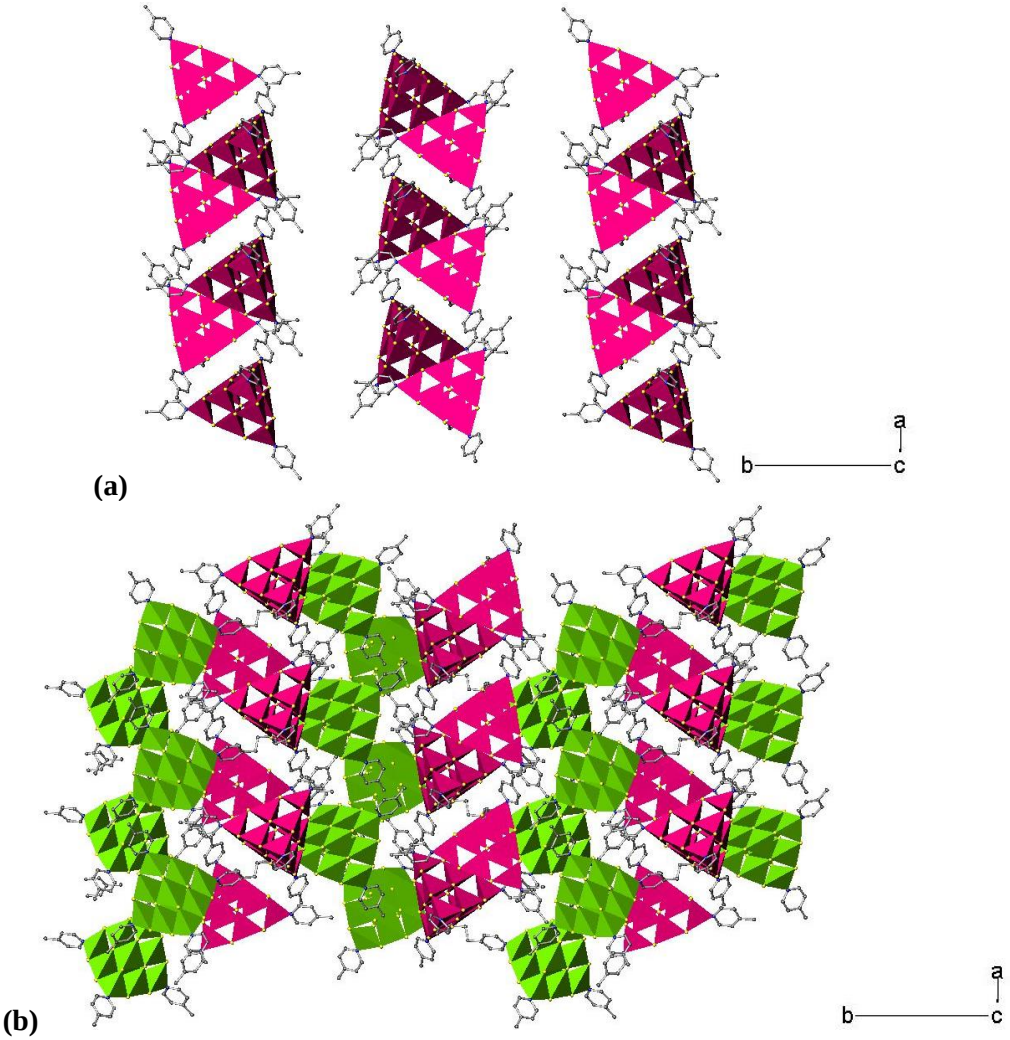

Figure 3.30 Polyhedral view of structure **(5)** viewed along the *c*-axis. **(a)** Shows dimers only (magenta). **(b)** Shows all clusters. Discrete clusters are shown in green. H atoms and solvent molecules have been omitted for clarity.

3.4.2.4 *Powder X-ray Diffraction*

Powder X-ray diffraction shows that the structure of the bulk material is pure and consistent with the SCXRD refinement.

Table 3.14 Lattice parameters for **(4).** Parameters were refined against PXRD using DASH.[208]

SCXRD	***a*/ Å**	***b*/ Å**	***c*/ Å**	**α/ º**	**β/ º**	**γ/ º**
	13.4776(4)	44.8635(8)	22.6128(5)	90	99.233(2)	90
PXRD	***a*/ Å**	***b*/ Å**	***c*/ Å**	**α/ º**	**β/ º**	**γ/ º**
	13.394(1)	45.384(1)	22.400(4)	90	99.29(8)	90

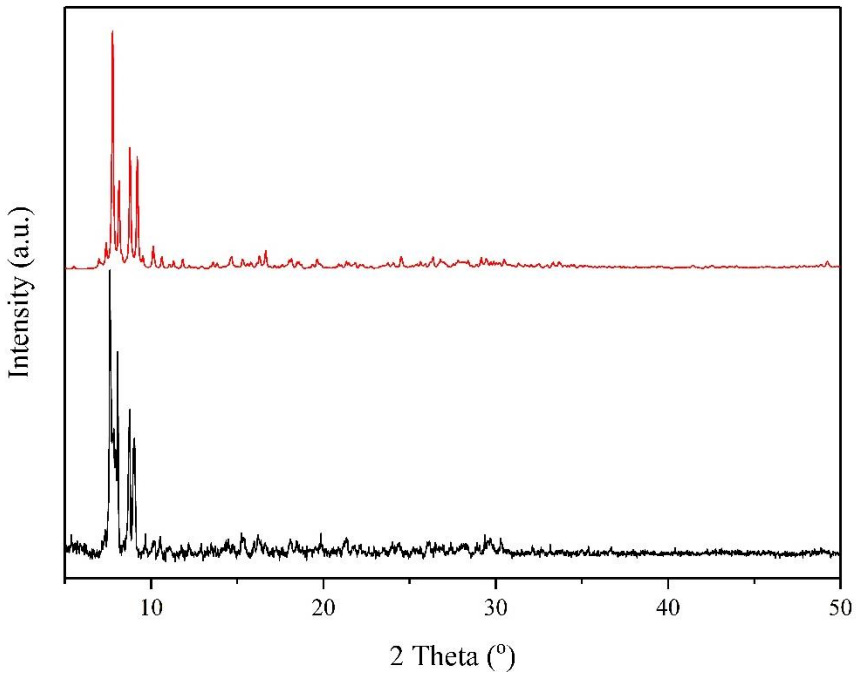

Figure 3.31 PXRD for sample containing **(5).** Black = experimental, red = calculated from SCXRD.[218]

3.4.2.5 *Elemental Analysis*

Elemental analysis data suggested that the proposed formula for **(5)** of $[C_6H_7N]_4[C_6H_8N]_8[Ga_{10}S_{16}(NC_6H_7)_4]_2[Ga_{20}S_{32}(N_2C_{12}H_{12})(NC_6H_7)_6]$ is correct. This is suggested by the comparison of calculated and experimental values from CHN analysis (Experimental: C = 26.42%, H = 2.87%, N = 5.37%. Calc: C = 27.07%, H = 2.73%, N = 5.26%).

3.4.2.6 *Infrared Spectroscopy*

FTIR (Figure 3.32) confirms the presence of amines in the voids of this structure; key frequencies are shown in Table 3.15.

Table 3.15 Key FTIR frequencies for **(5).**[219, 220]

Wavenumber/ cm^{-1}	**Assignment**
3447	Aromatic ν (C-H) 4-MPy
3055	Aromatic ν (C-H) 4-MPy$[H]^+$
1621, 1505	Aromatic ν (C-C) 4-MPy$[H]^+$
1438	CH_3 ν (C-H) 4-MPy$[H]^+$
1209	δ (N-H) 4-MPy$[H]^+$
803	Aromatic γ (C-H)

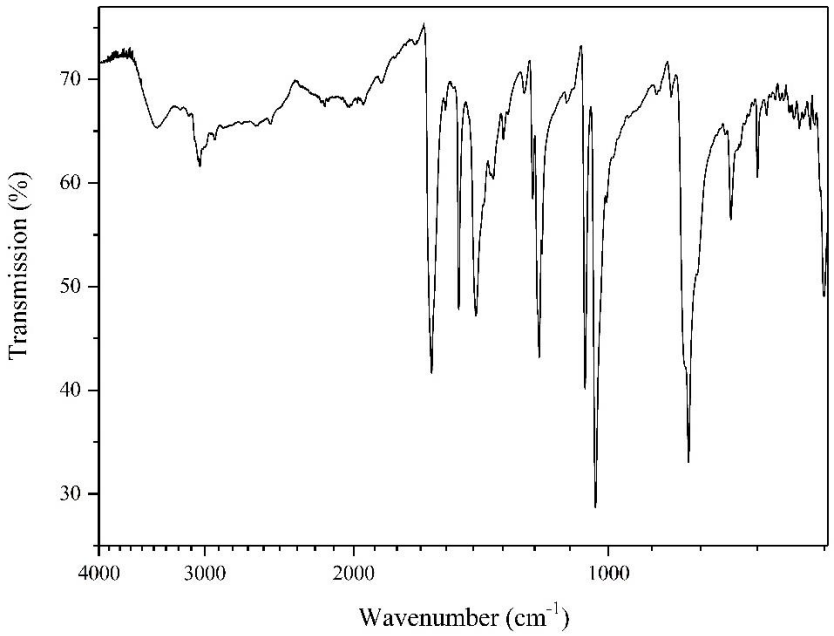

Figure 3.32 FTIR spectrum for **(5).**

3.4.2.7 *Thermogravimetric Analysis*

Following the same trend as the other samples, this compound does not decompose fully under N_2 (Figure 3.33). Full decomposition to Ga_2S_3 would give a final weight of 63.2 %, suggesting that decomposition does continue after holding the temperature at 1273 K for 30 minutes. There is however a weight-loss step at approximately this temperature when the structure decomposes in both air and nitrogen; to 68 and 66 % respectively.

The first weight-change step can be attributed to the loss of non-protonated 4-MPy moieties of *ca.* 5 %. Loss of the protonated 4-MPy cations, along with the corner ligands on the discrete clusters gives a further weight-loss of *ca.* 20 %. Finally there is a small weight-change of *ca.* 7.5 % associated with the loss of the corner amines from the dimers. The rest of the structure then decomposes to Ga_2S_3, followed by Ga_2O_3 in air; giving a remaining weight of 50.3 %, corresponding to the final plateau in air of *ca.* 52 %.

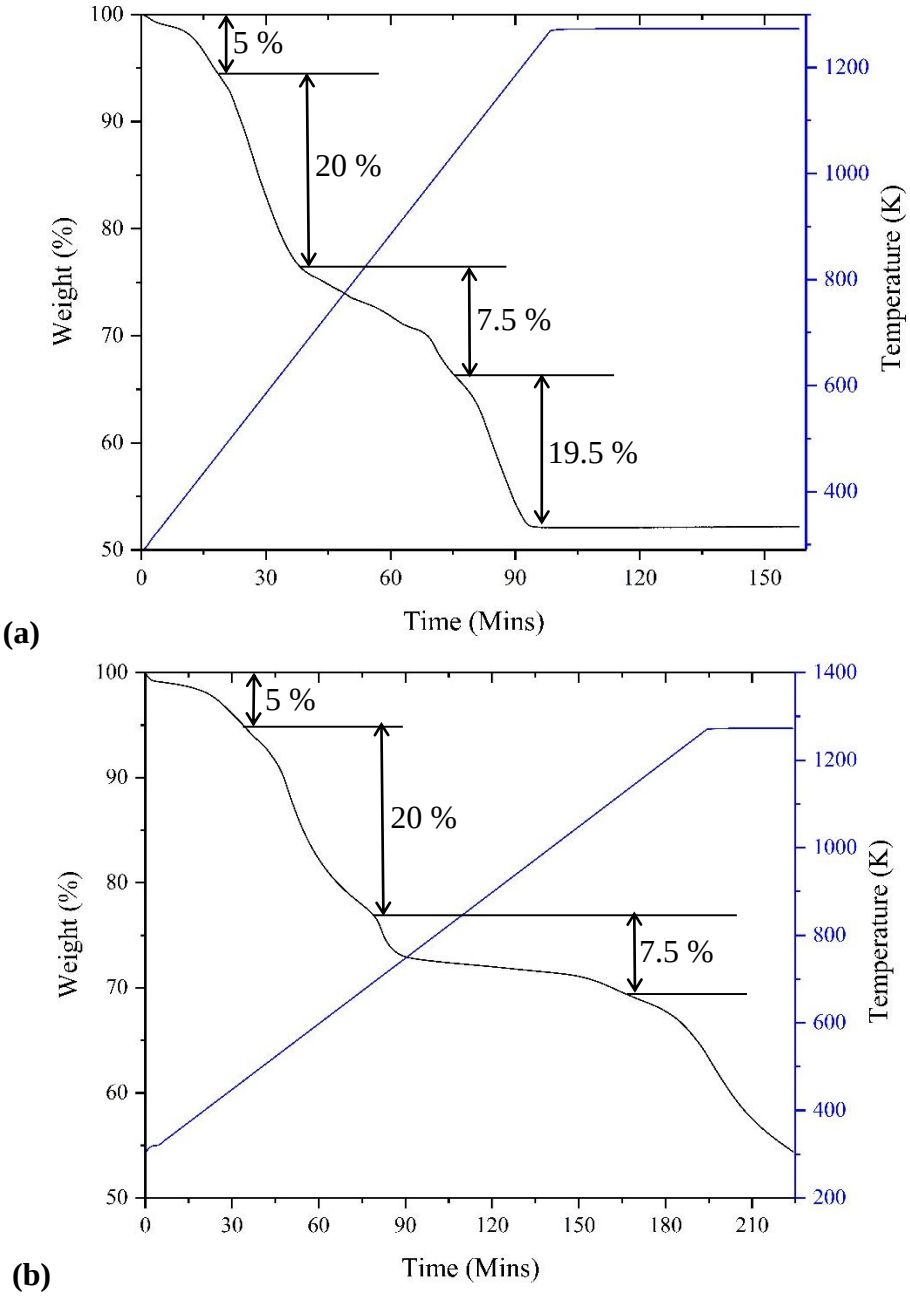

Figure 3.33 TGA data for sample **(5)** are shown in **(a)** air and **(b)** N_2. Black = weight percent vs time, blue = temperature vs time.

3.4.3 **[C_6H_8N]$_6$[$Ga_{20}S_{32}(NC_6H_7)_6(N_2C_{12}H_{12})$][$Ga_{10}S_{16}(NC_6H_7)_3(C_6H_6N)$]($C_6H_7N$)$_6$ (6)**

3.4.3.1 *Synthesis*

Compound **(6)** was first created from Ga metal (1.95 mmol, 137 mg), S powder (4.95 mmol, 159 mg) and TMDPy (1.04 mmol, 206 mg) in 4-MPy (29.8 mmol, 2.9 ml). The reaction was carried out for 6 days at 200ºC. Here the Ga:S:TMDPy:4-MPy ratio was 2:5:1:30. This reaction gave a mixture of light yellow plates and orange plates,

where orange plates were compound **(6)** and the yellow plates were a compound $[C_{12}H_{12}N_2]_2[C_{12}H_{14}N_2]_2[C_6H_7N]_6[Ga_{10}S_{16}(NC_6H_7)_4]_4$, previously reported by Romero *et al*. and isostructural with **(1)**.[223] Crystals of **(6)** were picked by hand using a microscope to carry out further measurements.

3.4.3.2 *Single-Crystal X-ray Diffraction*

Single crystal X-ray diffraction data were collected for **(6)** and are summarised in Table 3.16.

Table 3.16 Single crystal X-ray diffraction data for structure **(6)**

Crystallographically-Determined Formula	$C_{96}H_{106}Ga_{30}N_{16}S_{48}$
M_r	5114.46
Crystal habit	Orange Plate
Crystal system	Monoclinic
Space group	I2/*c*
***T*/K**	150
***a, b, c*/Å**	29.2955(8), 16.9999(4), 45.8025(13)
***β*/º**	107.717(3)
***V*/Å^3**	21728.7(11)
Z	4
θ_{max}	32.584
ρ_{cal}/gcm^{-3}	1.620
μ/mm^{-1}	4.146
T_{min},T_{max}	0.748,0.883
Number of parameters	843
Number of reflections used in refinement	11,130
Total number of reflections	35,044
R_{merge}	0.0839
$R(I>3.0\sigma(I))$	0.1113
R_w	0.1323

3.4.3.3 *Structure Description*

Compound **(6)** contains both chains and dimers (Figure 3.34 and Figure 3.35). Dimers have the formula $[Ga_{20}S_{32}(N_2C_{12}H_{12})(NC_6H_7)_6]^{4-}$ which describes two clusters linked *via* an EDPy ligand, where all other corners are terminated with 4-MPy. Chain clusters are linked *via* EDPy, as in structure **(3)**, but in this case chains are linear, unlike in **(3)** where they bend.

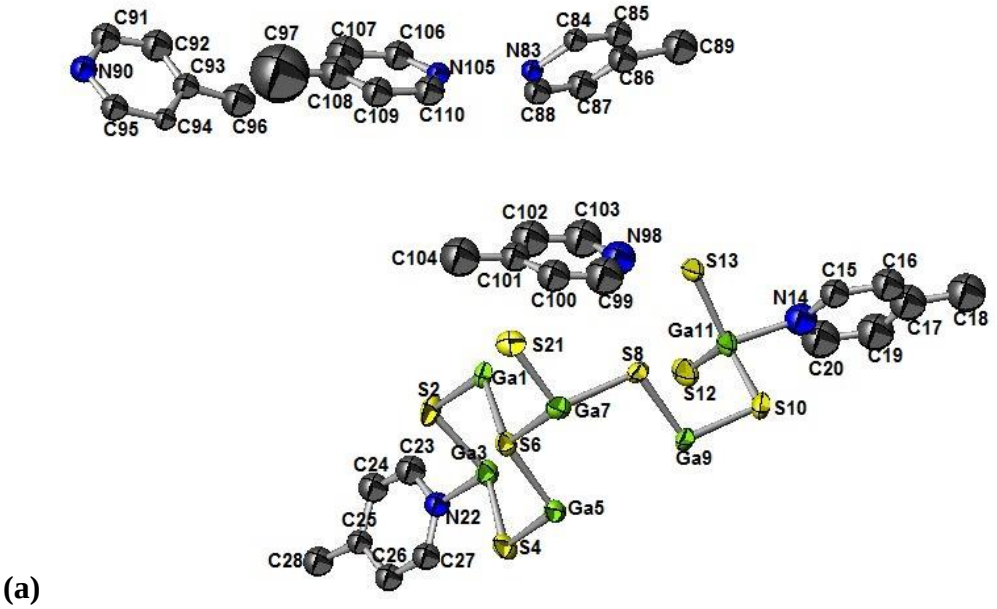

(a)

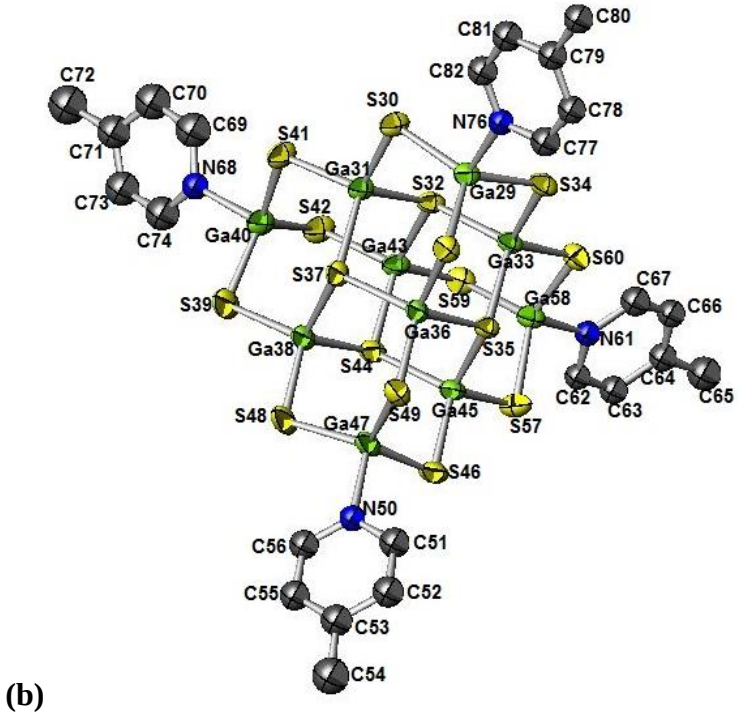

(b)

Figure 3.34 (a) and **(b)** Ellipsoid view of the asymmetric unit for structure **(6)**, shown in two different figures for clarity of atom labels. H atoms have been omitted for clarity. Green =Ga, yellow = S, blue = N, grey = C.

The asymmetric unit of **(6)** contains half of a dimer (i.e. one cluster) and half of the chain cluster, with the other halves related by a two-fold rotation along [010] and a glide-plane (010) (Figure 3.34 and Figure 3.35). Each asymmetric unit contains four 4-MPy moieties; each with an occupancy of 0.5; two of which have overlapping methyl-groups in the crystal structure. C-C distances are too short for this to be modelled as a

dimer. It has therefore been deduced that the charge is balanced by two 4-MPy cations, with an extra organic-cation needed to balance the net charge of -3.

Ga-S bond lengths are in the range of 2.221(3) – 2.346(3) Å and Ga-N bond lengths of 2.023(9) – 2.047(8) Å. S-Ga-S angles are between 106.4(1) and 117.4(1) º and S-Ga-N angles between 98.5(3) and 104.7(3) º. These are in the range expected for hybrid T3 gallium-sulphide supertetrahedra.[114, 115] Again, protonated N-atoms share protons between 4-MPy moieties, which prevents H-bonding with the clusters.

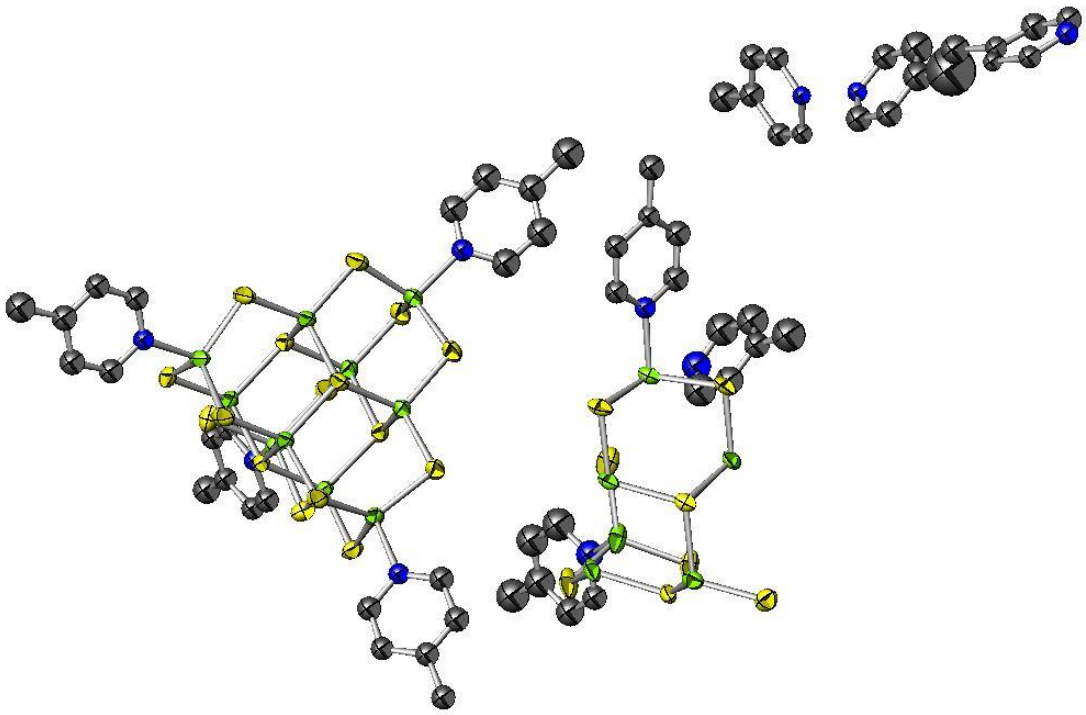

Figure 3.35 Ellipsoid view of the full asymmetric unit for structure **(6)**. H-atoms have been omitted for clarity. Green =Ga, yellow = S, blue = N, grey = C.

Dimers can align parallel to one another due to the fact that the linkers are not bent. Figure 3.34 shows how the dimers and chains form alternate layers to one another throughout the structure.

Compound **(6)** is structually related to a known material, synthesised by Romero,[223] but the unit cell here utilises the body-centred setting, rather than C-centred. The structure reported by Romero contained Py as a counter-cation, rather than 4-MPy, to balance the charge. There are also additional 4-MPy moeities present in structure **(6)**, as confirmed by CHN analysis (Section 3.4.3.5) and TGA (Section 3.4.3.7). The synthetic-method reported by Romero utilises 1,3-benzodiazole, not reported to be in either crystal structure.[223]

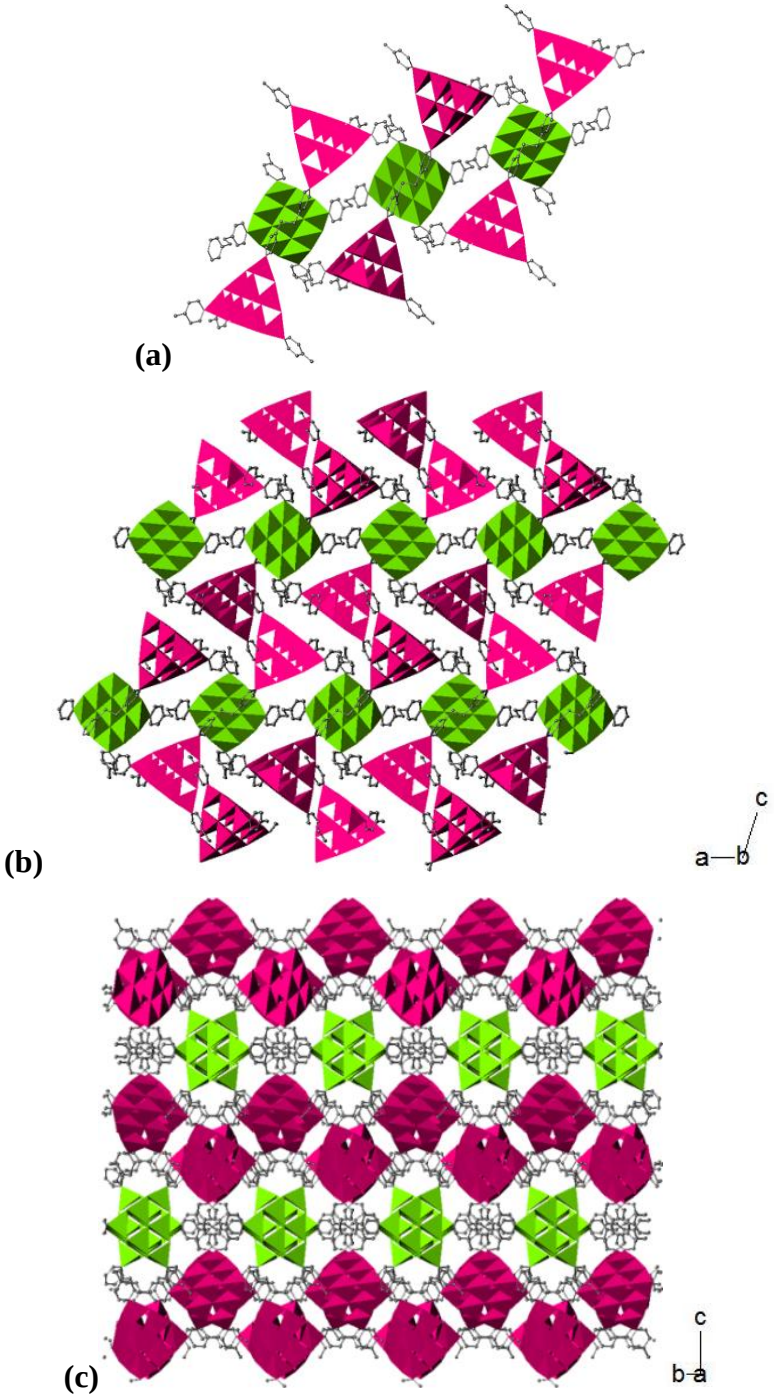

Figure 3.36 Polyhedral view of structure **(6)**. **(a)** Three dimers and a chain of three clusters, **(b)** packing along the *b*-axis and **(c)** packing along the *a*-axis. Dimers are shown in magenta and chains in green.

3.4.3.4 *Powder X-ray Diffraction*

Powder X-ray diffraction (Figure 3.37) shows that the sample contains two different phases; structure **(6)**, along with a phase isostructural to compound **(1)**,[211] which is the most frequently prepared material that has been synthesised during the exploration

of different synthesis-conditions. It is likely that this is the most stable phase that can be produced when reacting Ga and S in 4-MPy (Section 6.3.2.1).

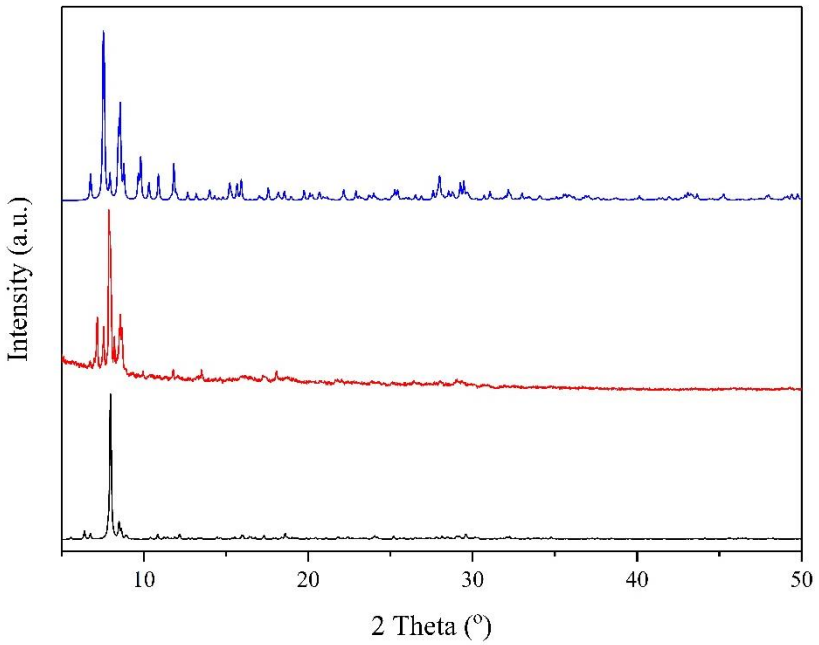

Figure 3.37 PXRD for sample containing **(6).** Black = calculated from SCXRD, red = sample containing **(6)** , blue = calculated pattern for known material, isostructural to **(1).**[211,218]

Table 3.17 Lattice parameters for **(6).** Parameters were refined against PXRD using DASH.[208]

SCXRD	***a*/ Å**	***b*/ Å**	***c*/ Å**	**α/ º**	**β/ º**	**γ/ º**
	29.2955(8)	16.9999(4)	45.8025(13)	90	107.717(3)	90
PXRD	***a*/ Å**	***b*/ Å**	***c*/ Å**	**α/ º**	**β/ º**	**γ/ º**
	29.382(1)	17.016(5)	45.209(3)	90	108.10(9)	90

3.4.3.5 *Elemental Analysis*

The formula of $[C_6H_8N]_6[Ga_{20}S_{32}(NC_6H_7)_6(N_2C_{12}H_{12})][Ga_{10}S_{16}(NC_6H_7)_3$-$(C_6H_6N)](C_6H_7N)_6$ gives calculated CHN values consistent with experimental elemental analysis results. (Experimental: C = 29.08 %, H = 2.68 %, N = 5.51 %. Calculated: C = 29.49 %, H = 2.89 %, N = 5.73 %).

3.4.3.6 *Infrared Spectroscopy*

FTIR confirms the presence of amines within the structure (Figure 3.38); key structure assignments are included in Table 3.18.

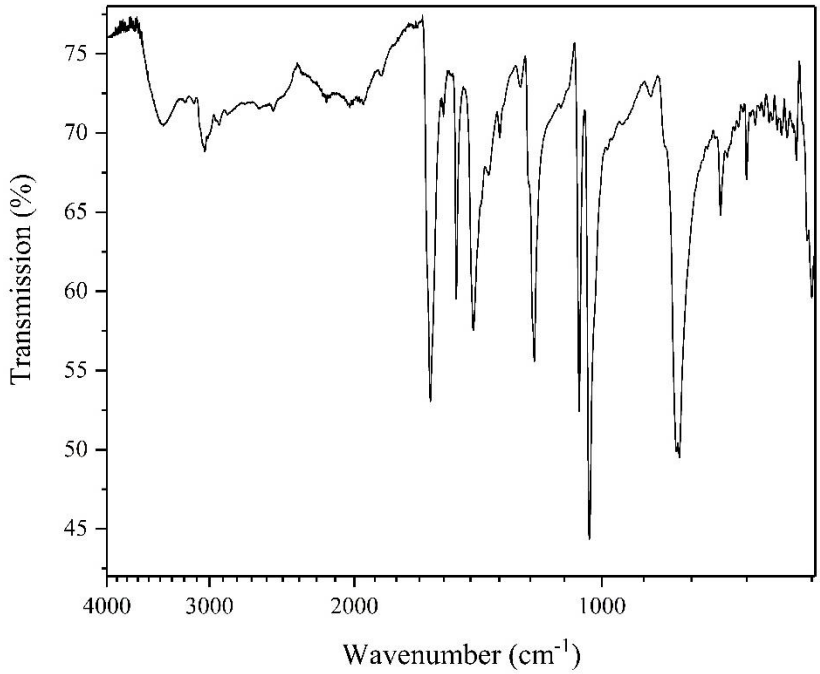

Figure 3.38 FTIR spectrum for compound **(6).**

Table 3.18 Key FTIR assignments for **(6).**

Wavenumber/ cm^{-1}	**Assignment**
3439	Aromatic ν (C-H) 4-MPy
3041	Aromatic ν (C-H) 4-MPy[H]$^+$
1621, 1505	Aromatic ν (C-C) 4-MPy[H]$^+$
1439	CH_3 ν (C-H) 4-MPy[H]$^+$
1207	δ (N-H) 4-MPy[H]$^+$
813, 805	Aromatic γ (C-H)

3.4.3.7 *Thermogravimetric Analysis*

Compound **(6)** does not fully decompose within N_2 (Figure 3.39 **(b)).** Full decomposition to Ga_2S_3 would leave a remaining weight of 60.3 %. Therefore, the compound must continue conversion into Ga_2O_3. It is concluded that there must be a small amount of oxygen present to oxidise the sample. The final plateau in air corresponds to full decomposition of the structure to Ga_2O_3 (Figure 3.39 **(a)**), leaving a remaining weight of 48.0 %.

The first weight-loss step in air corresponds to the removal of the unprotonated pore 4-MPy moieties of *ca.* 11 %, followed by another 12 % corresponding to the removal of the protonated analogues. The rest of the structure appears to decompose mostly in one step, with a small step at *ca.* 50 %; close to complete decomposition in air.

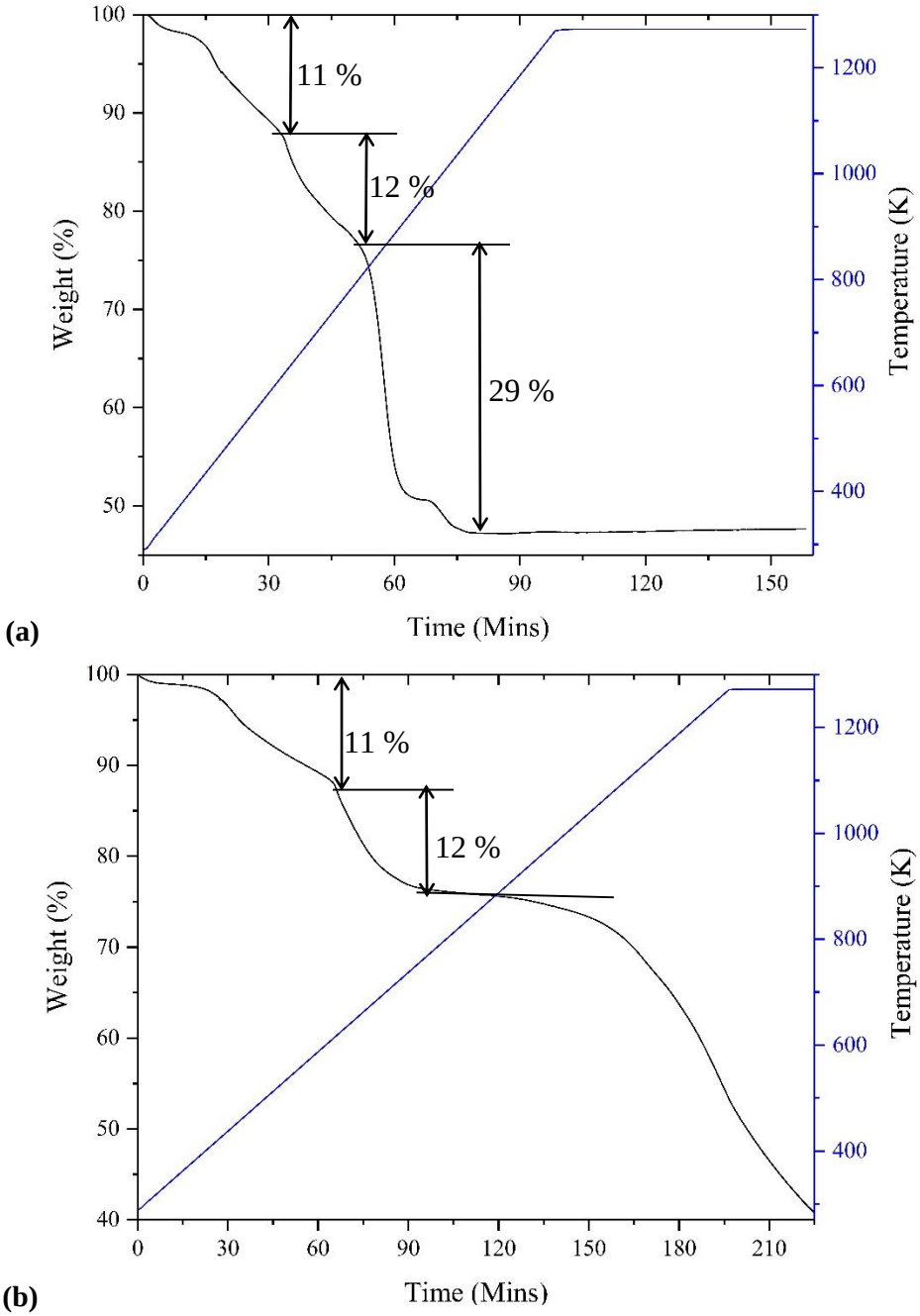

Figure 3.39 TGA data for sample **(6)** in **(a)** air and **(b)** N_2. Black line = weight percent vs time, blue = temperature vs time.

3.5 Hybrid Tetrahedra of Supertetrahedra **(7)**

3.5.1 **Synthesis**

Compound **(7)** **[**$C_6H_8N]_{14}[Ga_{10}S_{20}]_7(NC_2H_7)_4(NC_6H_7)_8(N_2C_{12}H_{12})_8$ was first synthesised by a previous student in the research group.[224] the synthetic method was optimised throughout this project to produce a higher yield of this compound, to allow physical properties to be measured.[225]

The material was initially synthesised by Tong using Ga metal (140 mg, 2.01 mmol, S powder (178 mg, 5.55 mmol), BenzIm (120 mg, 1.01 mmol) and 4-MPy (2.94 ml, 30.11 mmol); the reaction mixture was heated at 200 °C for 5 days.[224]

The method was optimised to Ga metal (170.6 mg, 2.5 mmol), S powder (158.5 mg, 5 mmol) and 4-methylpyridine (2.9 ml, 30 mmol); heated for 6 days at 200 °C; showing that BenzIm is not necessary to produce the desired product. The resulting sample consisted of a mixture of yellow cubes of **(7)** and orange needles isostructural with **(1)**. Crystals of **(7)** were separated by hand in order to carry out further measurements.

3.5.2 Structure and Characterisation

3.5.2.1 *Single-Crystal X-ray Diffraction*

Single-crystal X-ray data were collected by Sarah. J. Ewing at Heriot-Watt University. The solution and refinement process were also carried out by Ewing.[225] Data for single-crystal X-ray diffraction, carried out by Ewing on a crystal synthesised by Tong are shown in Table 3.19.

Table 3.19 Selected single crystal X-ray diffraction data and refinement details for **(7).**

Crystallographically-Determined Formula	$C_{192}H_{220}Ga_{70}N_{36}S_{112}$
M_r	11503.92
Crystal habit	Yellow Cube
Crystal system	Tetragonal
Space group	$I4_1/a$
T/K	100
a, b, c/Å	24.003(3), 24.003(3), 85.886(13)
V/Å^3	49,484(12)
Z	4
θ_{max}	26.571
ρ_{cal}/gcm^{-3}	1.544
μ/mm^{-1}	4.241
T_{min}, T_{max}	0.564,0.745
Number of parameters	640
Number of reflections used in refinement	11,982
Total number of reflections	25,427
$R(I>3.0\sigma(I))$	0.0643
R_w	0.0719

3.5.2.2 *Structure Description*

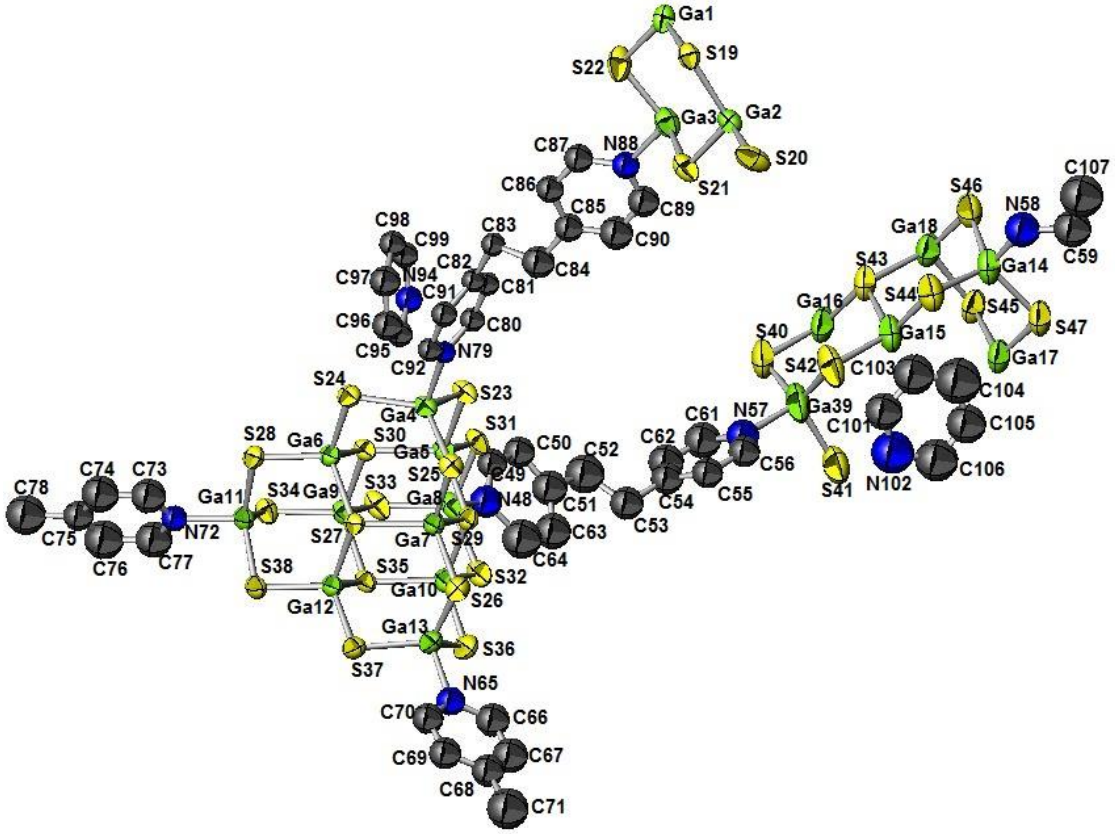

Figure 3.40 Ellipsoid view of the full asymmetric unit for structure **(7).** H atoms have been omitted for clarity. Green =Ga, yellow = S, blue = N, grey = C.

The asymmetric unit of structure **(7)** contains a full $[Ga_{10}S_{16}]^{4-}$ cluster, linked *via* EDPy moieties to both half a cluster and quarter of a cluster from the two remaining corners (Figure 3.40). This results in the formation of an SBU consisting of four clusters linked into a tetrahedron (Figure 3.41); which has been described as a "new class of super-supertetrahedron".[225] The distance along the edges of the tetrahedron formed is 37 Å, measured from the centres of adjacent clusters.

The resulting structure consists of 2-dimensional layers; with a large amount of void space available to contain the pore amines needed to balance the negative charge. A pore volume of 42 % was calculated using PLATON Squeeze.[206]

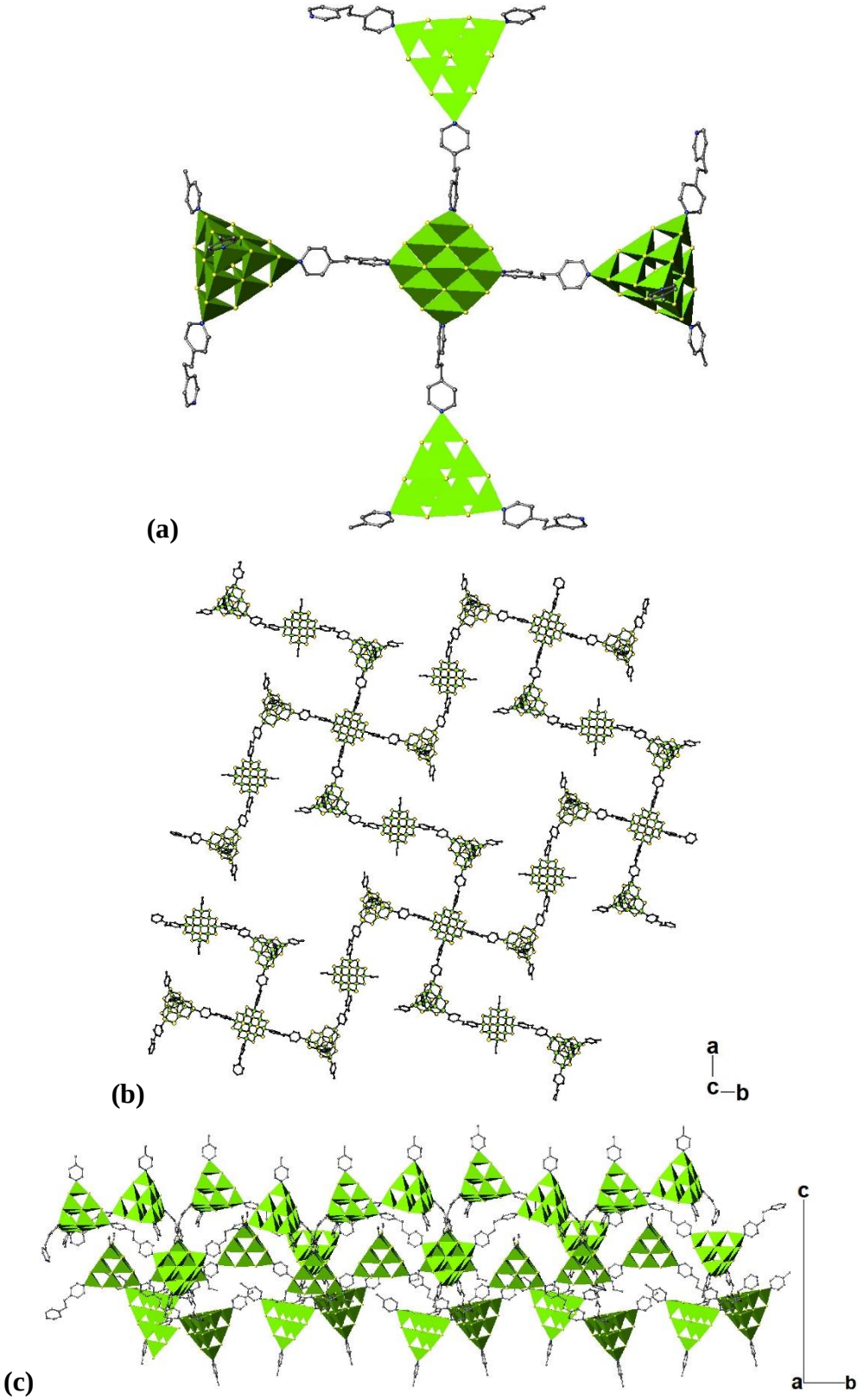

Figure 3.41 Polyhedral view of **(a)** the tetrahedron of supertetrahedra, **(b)** a 2D layer (along [001]) and **(c)** along [100] (a layer) in **(7).**

3.5.2.3 *Powder X-ray Diffraction*

Powder X-ray diffraction (Figure 3.42) shows that the sample contains two different phases; structure **(7)**, along with a phase isostructural to compound **(1).**[211]

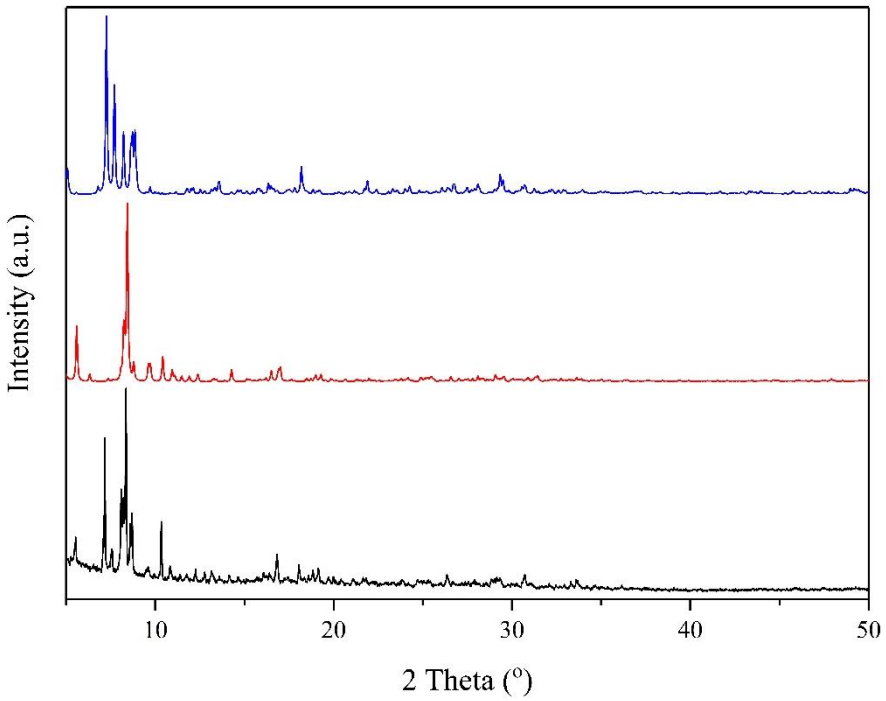

Figure 3.42 PXRD for black = sample containing **(7)**, red line = **(7)** calculated from SCXRD and blue = impurity phase **(1)**, calculated from SCXRD.[211,218]

Table 3.20 Lattice parameters for **(7)**. Parameters were refined against PXRD using DASH.[208]

SCXRD	***a*/ Å**	***b*/ Å**	***c*/ Å**	**α/ °**	**β/ °**	**γ/ °**
	24.003(3)	24.003(3)	85.886(13)	90	90	90
PXRD	***a*/ Å**	***b*/ Å**	***c*/ Å**	**α/ °**	**β/ °**	**γ/ °**
	23.916(1)	23.916(1)	84.284(2)	90	90	90

3.5.2.4 *Elemental Analysis*

Calculated CHN values from the suggested formula $[C_6H_8N]_{14}[(Ga_{10}S_{16})_7 - (NC_2H_7)_4(NC_6H_7)_8(N_2C_{12}H_{12})_8]$ are consistent with the experimental values from elemental analysis. Experimental: C = 26.09 %, H = 2.53 %, N = 4.68 %. Calculated: C = 23.26 %, H = 2.41 %, N = 4.83 %.

3.5.2.5 *Thermogravimetric Analysis*

TGA was carried out on a pure sample of **(7)** in atmospheres of both air and N_2. (Figure 3.43).

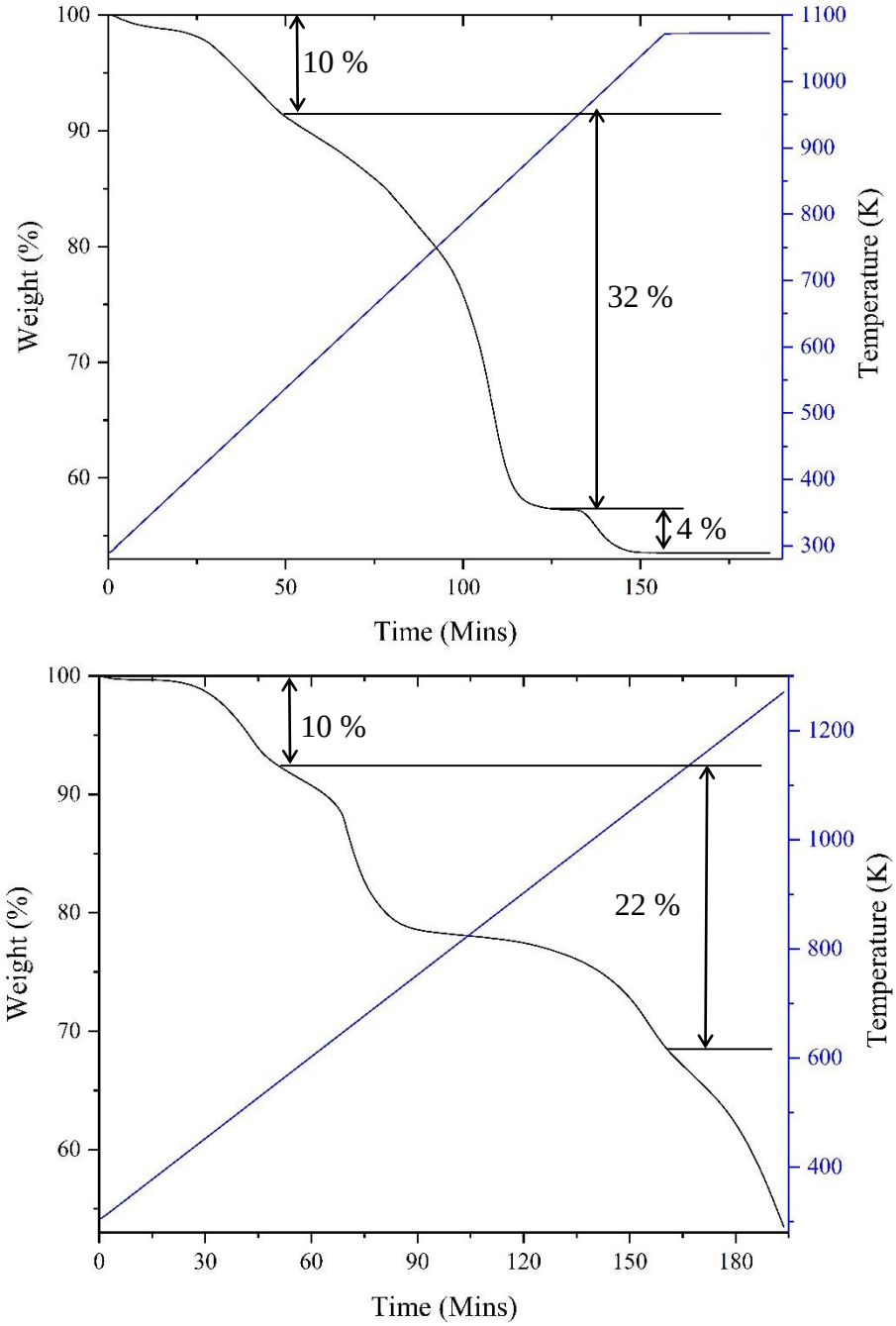

Figure 3.43 TGA data for compound **(7)** in **(a)** air and **(b)** N_2. Black line = weight percent vs time, blue line = temperature vs. time.

The first weight-loss step in the TGA for **(7)** can be attributed to the loss of pore amines (*ca.* 10 %). When the measurement is carried out in air (Figure 3.43 **(a)**) the rest of the structure decomposes mostly in one step, at 120 minutes there is a small step proposed to be due to formation of an intermediate product of Ga_2O_2S (58 %). before

full decomposition of the product is proposed to be to Ga_2O_3, leaving a remaining weight of 54 % .

Calculated weight-steps show that the corner 4-MPy amines weigh 7.6 % and the linking EDPy amines a further 12.1 %. The measurement under N_2 is therefore slightly outside of these values with steps of *ca.* 90 %, 78 % and 68 % (Figure 3.43).

3.6 Optical Properties of Compounds **(1)** to **(7)**

3.6.1 **Diffuse Reflectance**

Diffuse reflectance spectroscopy (Section 2.2.7) was used to determine the optical band-gaps of materials **(1)** – **(7).** Absorption edges have been measured and used to estimate the band gaps of the materials. Photoluminescence was used to further explore the electronic properties of all of the compounds described in this chapter; this is included in Section 3.6.2.

3.6.1.1 ***Diffuse Reflectance Measurements for (1)***

Diffuse reflectance was measured on red crystals of **(1)** (Figure 3.44**)**. The tangent line (red) shows the absorption edge, where it crosses the *x*-axis, is 3.18(2) eV, making this material a wide-gap semiconductor.

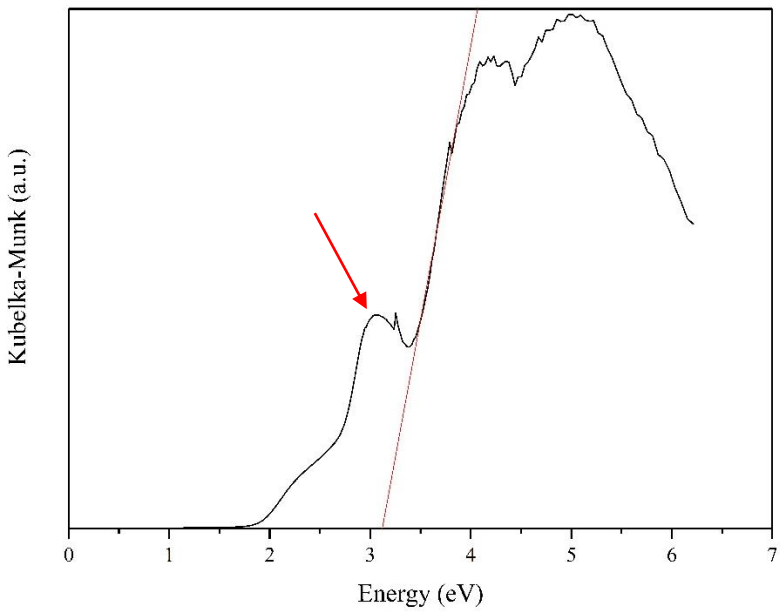

Figure 3.44 Diffuse reflectance for **(1).** Red line = tangent for absorption edge. Red arrow = charge transfer peak.

The red arrow shows a peak due to charge transfer, expected to be from the clusters to the ligands, although it is not trivial to prove this. The red colour of the crystals is suggested to be caused by charge transfer. Zhang *et al.* suggested that these types of materials form ion-pair charge-transfer (IPCT) salts.[226] In this case, the anionic clusters would be the electron donors and the aromatic organic-cations the electron acceptors.

3.6.1.2 *Diffuse Reflectance Measurements for (2)*

Diffuse reflectance for orange crystals of **(2)** is shown in Figure 3.45. The tangent-line (red) shows the absorption-edge of 3.44(4) eV, which would also classify this material as a wide-gap semiconductor. This compound also shows a charge transfer peak, considered to cause the orange colour of the crystals.

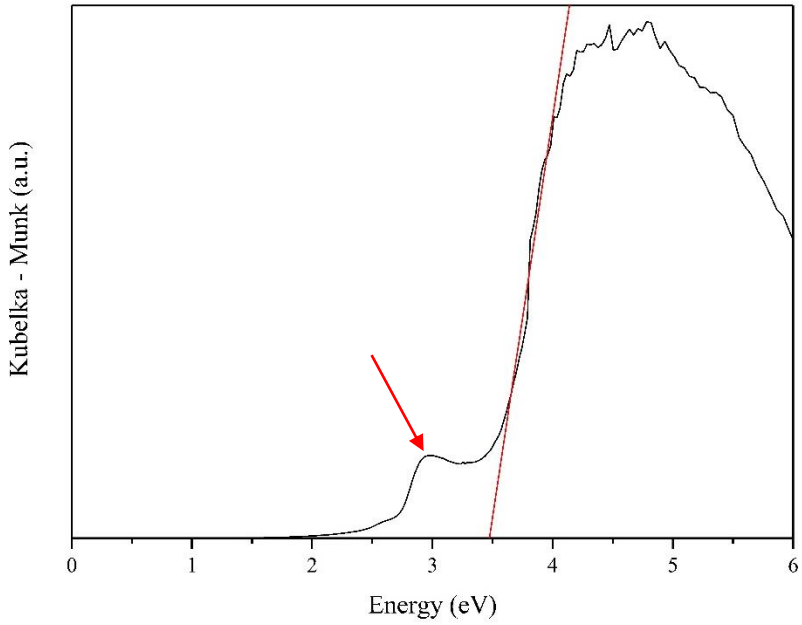

Figure 3.45 Diffuse reflectance graph for **(2).** Red line = tangent for absorption edge. Red arrow = charge transfer peak.

3.6.1.3 *Diffuse Reflectance Measurements for (3)*

The diffuse reflectance spectrum for **(3)** is shown in Figure 3.46. The tangent line (red) shows an absorption-edge of 3.14 (1) eV; again suggesting this material is a wide-gap semiconductor. This material shows a weak charge-transfer band and therefore was also measured for its photoluminescent properties (Section 3.6.2)

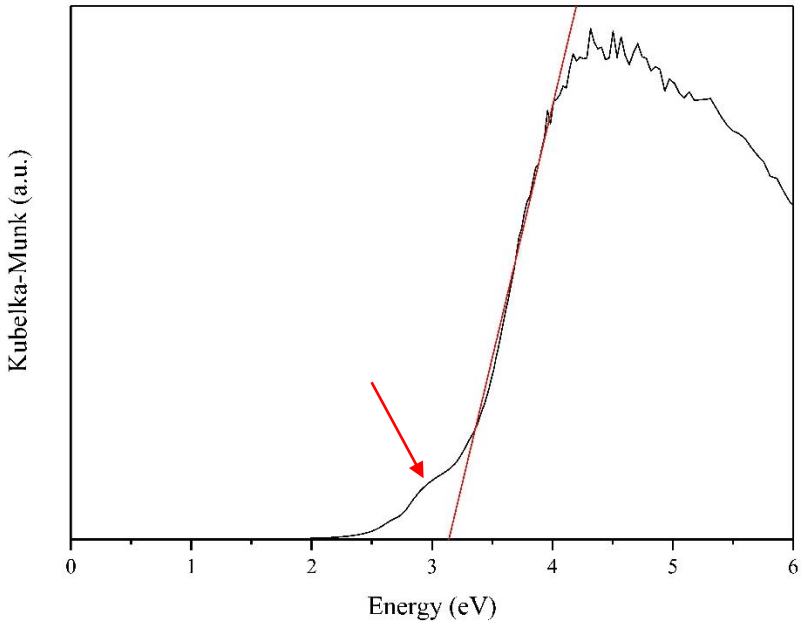

Figure 3.46 Diffuse reflectance graph for **(3).** Red line = tangent for absorption edge. Red arrow = charge transfer peak.

3.6.1.4 *Diffuse Reflectance Measurements for (4)*

Diffuse reflectance for structure **(4)** is shown in Figure 3.47. Suggesting a band gap for this compound of 3.22(2) eV; consistent with the wide-gap semiconducting behaviour of the other materials in this chapter. The spectrum also shows a charge-transfer band; photoluminescence properties are included in Section 3.6.2.

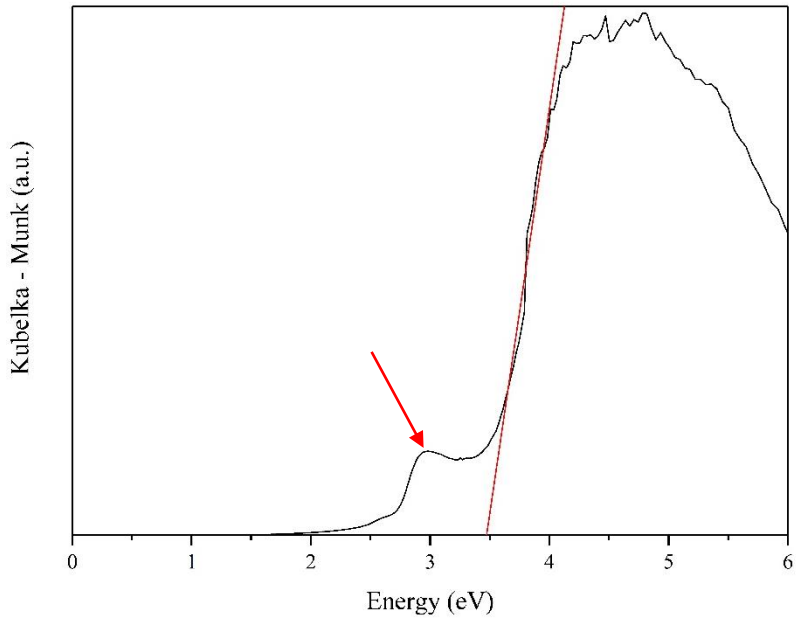

Figure 3.47 Diffuse reflectance graph for structure **(4).** Red line = tangent for absorption edge. Red arrow = charge transfer peak.

3.6.1.5 *Diffuse Reflectance Measurements for (5)*

The absorption edge for **(5)** was measured as 3.33(1) eV, suggesting that this material is also a wide-gap semiconductor (Figure 3.48).

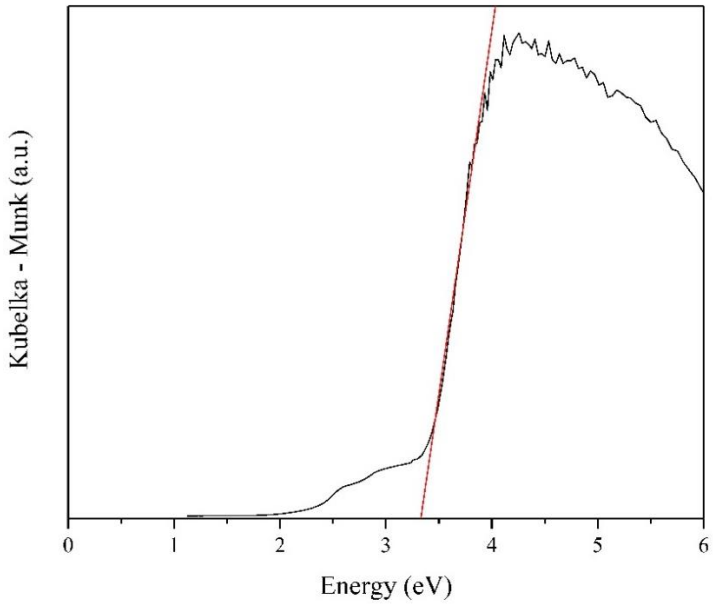

Figure 3.48 Diffuse reflectance graph for structure **(5**). Red line = tangent for absorption edge.

The charge-transfer peak is not as prominent in this material compared with structures **(1)** to **(4)**. Photoluminescence measurements for this material and also shown in Section 3.6.2.

3.6.1.6 *Diffuse Reflectance Measurements for (6)*

Diffuse-reflectance measurements for compound **(6)** (Figure 3.49) show that the materials has an absorption edge of 2.74(5) eV, making it also a wide-gap semiconductor. Unfortunately, due to the inability to obtain a sufficient amount of **(6)** as a single phase, photoluminescence measurements could not be carried out. The sharp peak in the spectrum is thought to be from instrumental error.

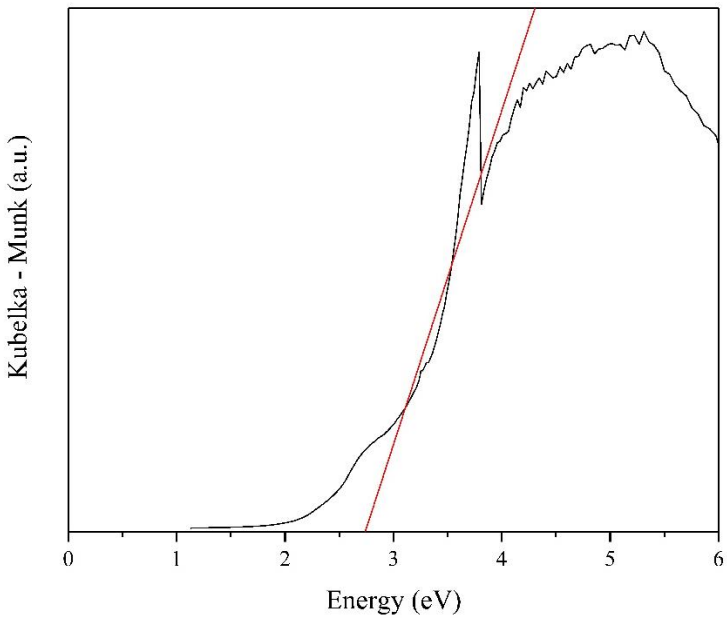

Figure 3.49 Diffuse reflectance for compound **(6)**. Red line = tangent for absorption edge.

3.6.1.7 *Diffuse Reflectance Measurements for (7)*

Diffuse-reflectance measurements (Figure 3.50) showed that the material has an absorption edge of 3.07(1) eV. There was not a sufficiently-pure sample of crystals to carry out photoluminescence measurements, although there is no charge-transfer band apparent in the diffuse-reflectance spectrum.

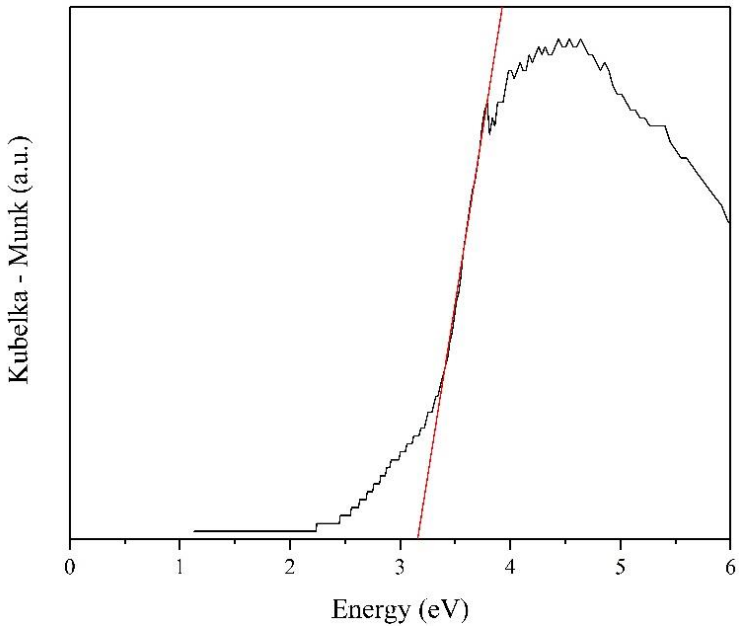

Figure 3.50 Diffuse reflectance graph for structure **(7)**. Red line = tangent for absorption edge.

3.6.2 **Photoluminescence Measurements**

Due to the fact that the diffuse-reflectance spectra of many of the materials presented in this chapter exhibit peaks that could be attributed to charge-transfer transitions, the optical properties were investigated further. Photoluminescence measurements were carried out at the University of Surrey, in the Research Group of Professor Richard Curry, in the Department of Electrical Engineering. It was discovered that the structures absorb radiation in the ultraviolet (UV) region and emit within the visible region. Different structures emit at different wavelengths with different lifetimes and quantum efficiencies.

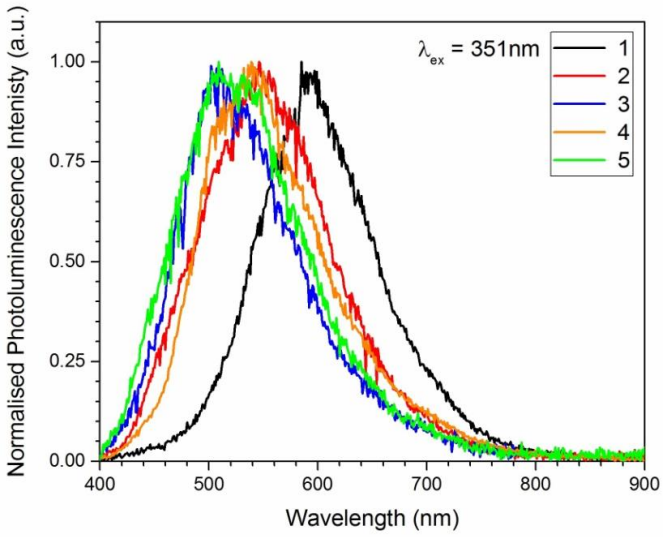

(a)

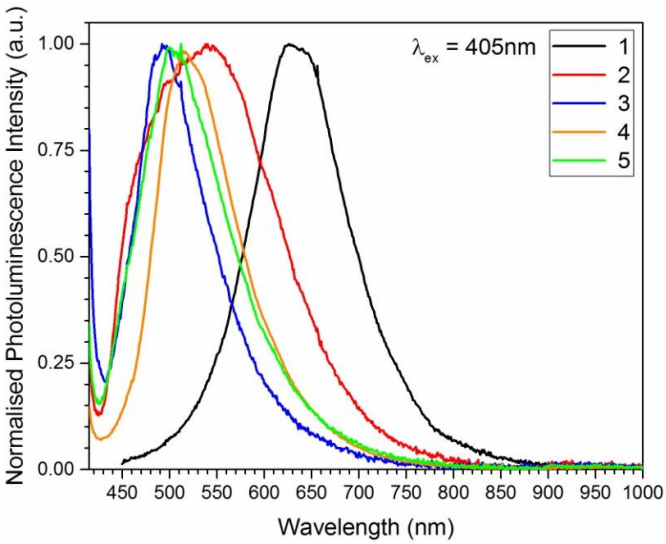

(b)

Figure 3.51 Emision wavelength vs. intensity graph for structures**(1)** to **(5),** with an excitation wavelength of **(a)** 351 nm and **(b)** 405 nm.

Photoluminescence intensities of compounds **(1)** to **(5)** were measured against emission wavelength at two different wavelengths of excitation. Figure 3.51 shows emission at excitation wavelengths of 351 and 405 nm respectively; corresponding to values at which charge-transfer bands appear on the diffuse-reflectance spectra (Table 3.21). These measurements showed that all samples emit at different wavelengths.

Table 3.21 Table of charge-transfer bands for structures **(1)** to **(5).**

Material	Charge Transfer Peak/ nm
(1)	414
(2)	424
(3)	422
(4)	416
(5)	426

Figure 3.51 shows that the emission wavelength of **(1)** is red shifted compared to the emission from other samples. This would potentially explain the red/orange colour of these crystals, compared to the yellow colour of the others. The sample with the widest spread of emission wavelengths is sample **(2)**, which was found to emit white light. Samples **(3)** to **(5)** all emit yellow light.

These results can be compared with those carried out previously by Vaqueiro *et. al*. A material $[C_5H_6N]_3[Ga_{10}S_{16}(OH)(N_2C_{13}H_{14})]$ consisting of layers of T3 gallium-sulphide clusters linked *via* EDPy and OH^-, emits at 430 nm when excited at 370 nm.[212] This is in the same region that emission occurs in compounds **(1)** to **(5)**. Photoluminescence of a material $[C_2H_8N]_2[Ga_{10}S_{16}(N_2C_{12}H_{12})(NC_2H_7)_2$, consisting of T3 gallium-sulphide clusters linked into a chain showed a very broad emission-band when excited at 360 nm.

A number of different materials based on supertetrahedral clusters have been reviewed by Levchenko.[227] These include the hybrid pentasupertetrahedral zinc-sulphide clusters $[Zn_8S(SPh)_{14}L_2]$, resembling those described in Section 1.4.5.[228] An emission band was observed at *ca.* 350 nm with L = 3-(2-thienyl)-pyridine or at 476 nm when L= 5-aminoquinoline. This showed that the nature of the corner ligands greatly influence the emission spectra of the materials. Clusters also showed no emission with L= 4,7-phenanthroline. The hybrid T5 cadmium-indium sulphide cluster $[Cd_{13}In_{22}S_{52}(MIm)_4]^{12-}$

(MIm = methylimidazole) reported by Feng *et. al* showed a broad emission-band at 512 nm and as described in the review, this is red shifted compared to the emission wavelengths of smaller clusters such as T4.[115]

The T5 materials synthesised in ionic liquids by Xiong *et. al*, as described in Section 1.5.1, also showed red-shifted emission values compared to T3 clusters.[155] The non-hybrid cluster $[Cu_5In_{30}S_{52}(SH)_2Cl_2]^{13-}$ showed emission at 540 nm, whereas the hybrid cluster $[Cu_5Ga_{30}S_52(SH)_2(Bim)_2]^{11-}$ showed broad emission at 630 nm. Doping by manganese(II) was carried out by Feng *et. al* and also showed a red-shifted emission of 630 nm, compared to the non-doped value of *ca.* 490 nm.[229] The clusters here were coreless T5 clusters, which had an Mn^{2+} ion inserted into the core site. The coreless nature of the non-doped clusters could affect the trend observed where the wavelength of emission increases with increasing cluster-size. Materials **(1)** – **(5)** are within the expected range for hybrid T3 clusters, when compared to materials described in the literature.

Table 3.22 Quantum efficiencies of structures **(1)** to **(5).**

Structure	Quantum Efficiency/ %
(1)	1.12
(2)	0.94
(3)	0.64
(4)	1.14
(5)	0.70

Quantum efficiencies were measured for samples **(1)** to **(5)** (Table 3.22), where quantum efficiency is the percentage of the energy of the exciting radiation that is reemitted as light.

3.7 Summary of Chapter

Materials **(1)** to **(7)** were synthesised in 4-MPy under different reactions conditions, as described. All of these materials have structures base on the hybrid supertetrahedron $[Ga_{10}S_{16}(L)_4]^{2-}$, where L = 4-MPy or EDPy and EDPy is the dimerised form of 4-MPy. **(1)** and **(2)** both contain the discrete cluster $[Ga_{10}S_{16}(C_6H_7N)_4]^{2-}$, where the clusters are packed in a different way in each case and were both synthesised using

the ionic liquid [THTDP]Cl. These materials consisted of red and orange crystals respectively and showed strong charge-transfer bands in their diffuse-reflectance spectra (Figure 3.44 and Figure 3.45), where charge transfer is proposed to originate between the formation of ion-pair charge-transfer (IPCT) pairs between the clusters and the pore amines. The other material that shows a strong charge-transfer band is **(4)** , which also consisted of crystal with an orange to red colour. **(4)** was synthesised solvothermally with Im as a structure-directing agent and consisted of $[Ga_{10}S_{20}(C_6H_7N)_4]^{2-}$ clusters linked *via* EDPy to form $[Ga_{10}S_{20}(C_6H_7N)_3(C_6H_6N)]^{2-}$, where C_6H_6N refers to half on an EDPy moiety.

The other materials described in this chapter did not show strong charge-transfer bands and consisted of yellow crystals. **(3)** contained chains of the T3 hybrid supertetrahedra, again linked *via* EDPy linkers into zigzag chains. **(5)** and **(6)** contained T3 units of varying dimensionalities; **(5)** contained both dimers and discrete clusters, whereas **(6)** contained both dimers and chains. All instances where clusters were linked together were *via* an EDPy moiety. **(3)** and **(5)** both contained weak charge-transfer bands.

(7) contains a novel SBU of a tetrahedron of supertetrahedra, first synthesised by Tong.[224, 225] The synthesis method was optimised and physical measurements were carried out. This material did not show evidence of charge-transfer in its diffuse-reflectance spectrum. Materials **(1)** to **(5)** were analysed using photoluminescence measurements. **(1)** was found to emit red light, whereas **(2)** was found to emit white. Samples **(3)** to **(5)** all emitted in the yellow region. Unfortunately, sufficient amounts of pure crystals for **(6)** and **(7)** could not be obtained for photoluminescence measurements.

4 Solvothermal Synthesis of Germanium and Germanium - Gallium Sulphides of Varying Dimensionalities

4.1 Introduction

The reactions described in this chapter and the products formed were initially investigated in attempts to create mixed-metal hybrid-supertetrahedra with both gallium and germanium present. In the literature, there are so far a number of examples of gallium-sulphide supertetrahedra,[94, 113, 114, 211, 212, 225] there is also evidence that other main-group metals form these types of clusters, as described in Sections 1.4.3 and 1.4.4.[155]

Throughout this chapter, germanium oxide was combined with gallium metal and sulphur in reactions carried out in 4-MPy solvent, in attempts to form these clusters. The organic reagents used throughout this chapter were the 4-MPy solvent, along with TMDPy, Im, BenzIm and Bipy. Ionic liquids [BMMIm]Cl and [BMMIm]BF_4 were also utilized when investigating these reactions.

Many germanium-based chalcogenide compounds that are synthesised solvothermally consist of T2 units, also known as adamantane units. These are common units when a metal with an oxidation state of 4+ is used,[173, 175, 230] they are therefore also common in tin-based chalcogenide structures.[174, 231, 232]

Here, the influence that germanium has on these reactions compared to gallium will become apparent; with the affinity that gallium has towards forming T3 hybrid clusters being overpowered by the excess charge and ionic nature of germanium. Structures are described here based on the T2 adamantane cluster favoured by germanium, along with a novel framework-material, containing different linkages of tetrahedra.

4.2 Trimers of T2 Germanium Sulphide Clusters

4.2.1 **Synthesis**

Compound **(8)** $[NC_6H_8]_8[Ge_{12}S_{28}]$ was synthesised from Ga metal (71.5 mg, 1 mmol), GeO_2 (109 mg, 1 mmol), S powder (178 mg, 5.50 mmol) and TMDPy (209 mg, 1 mmol) reacted in 4-MPy (2.9 ml, 30 mmol). The molar ratio of Ga:GeO_2:S:TMDPy:4-MPy was 1:1:5.5:1:30 and the reaction was carried out at 200 °C for 7 days. The resulting product was a mixture of orange crystals and Ga metal.

4.2.2 **Structure and Characterisation**

4.2.2.1 *Single-Crystal X-Ray Diffraction*

Single-crystal X-ray diffraction was carried out **(8)** and data are summarized in Table 4.1.

Table 4.1 Selected single crystal X-ray diffraction data and refinement details for **(8)**.

Crystallographically-Determined Formula	$[Ge_{12}S_{28}][NC_6H_8]_4$
M_r	2141.44
Crystal habit	Orange Plate
Crystal system	Monoclinic
Space group	$P2_1/m$
T/K	150
a, b, c/Å	9.5856(5), 44.8304(15), 9.6819(7)
β/°	117.774(8)
V/Å^3	3681.2(4)
Z	2
θ_{max}	30.581
ρ_{cal}/gcm^{-3}	1.932
μ/mm^{-1}	5.641
T_{min}, T_{max}	0.763,0.893
Number of parameters	316
Number of reflections used in refinement	5443
Total number of reflections	11,459
R_{merge}	0.0427
$R(I>3.0\sigma(I))$	0.0702
R_w	0.0580

Residual electron-density was modelled during the refinement of the crystal structure of **(8)** using Platon SQUEEZE.[206] Platon calculated a void space of 442.6 $Å^3$ per unit cell (12 %).

4.2.2.2 *Energy-Dispersive X-Ray Analysis*

Both Ga and GeO_2 were used in the reaction and Ga and Ge cannot be distinguished from one-another *via* SCXRD due to the difference of only one electron. EDX (Electron Dispersive X-ray Analysis) was carried out on crystals of the material in order to determine the Ga and Ge content of the material.

Table 4.2 EDX Data for **(8)** showing molar % by element.

Element	Molar %	Molar %	Molar %	Molar %
O	18.33	0	0	0
S	52.14	69.37	70.31	73.3
Ge	29.54	30.63	29.69	26.7

These showed that this phase contains only germanium and sulphur, with trace amounts of oxygen. This information was taken into account for the refinement of the single-crystal data, where Ga was not included. The EDX results are also consistent with an approximate Ge:S ratio of 3:7, as determined by single-crystal X-ray diffraction (Table 4.1).

4.2.2.3 *Structure Description*

The asymmetric unit for **(8)** contains one and 1/2 T2 germanium-sulphide supertetrahedra $[Ge_4S_{10}]^{2-}$ (Figure 4.1), linked through an μ_2-S bridge and symmetry-related by a mirror plane. These adamantane units have previously been described in a number of cases, as described in Section 1.4.3.[175, 233, 234] In this case, in the asymmetric unit, the formula of the full inorganic component would be $[Ge_7S_{15}]^{2-}$. Ge-S bond lengths are in the range of 2.2043(19) Å - 2.2786 (16) Å, with the longer bond lengths corresponding to those involving bridging sulphur atoms. S-Ge-S angles are in the range of 96.15(6) – 114.56(7) °, where the smallest angles involve bridging S-atoms. These values are consistent with literature values for T2 $[Ge_4S_{10}]^{4-}$ clusters.[103]

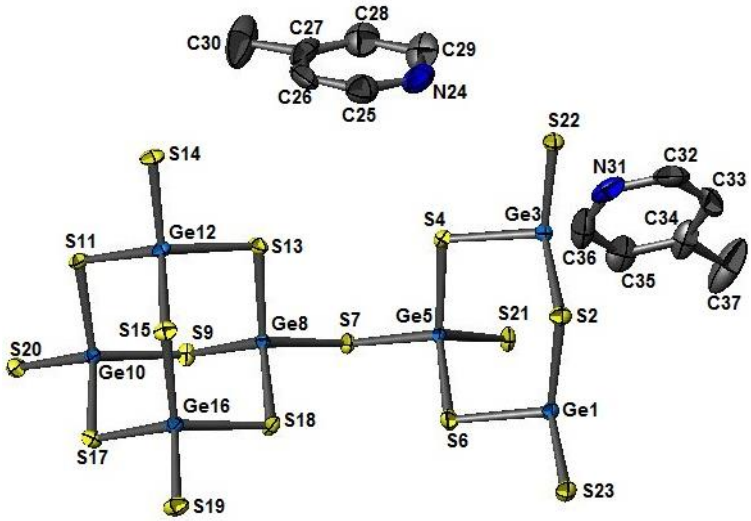

Figure 4.1 Asymmetric unit of **(8)**. Light blue = Ge, yellow = S, dark blue = N

Two cations per cluster are required to balance the charge of the anionic species; the cations are present in the form of two protonated 4-MPy moieties, which can be found in the crystal structure. These organics can be found in the crystal structure due to the ordering caused by these interactions; therefore the resulting formula of this compound is $[Ge_{12}S_{28}][NC_6H_8]_4$, where there are four protonated 4-MPy moities per cluster; two H-bonding (N-S = 3.19(4) Å) with S(22) and two H-bonding (N-S = 3.18(1) Å) with S(23) (Figure 4.1 and Figure 4.2). However, due to the void space calculated by Platon SQUEEZE,[206] it is very likely that there are further disordered amine-moities present in the material that reside in this space.

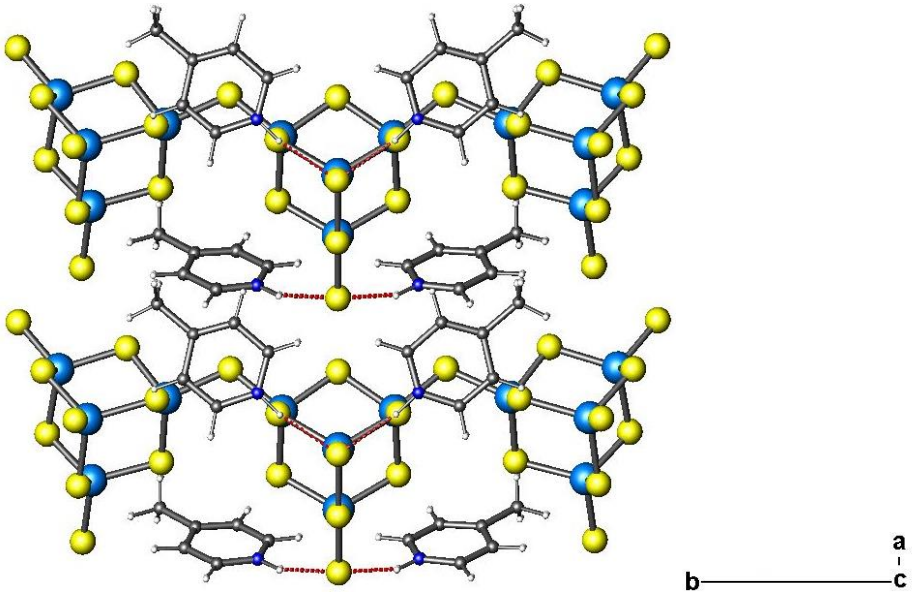

Figure 4.2 Two trimers in **(8)** viewed along the *c*-axis. Light blue = Ge, yellow = S, grey = C, dark blue = N, white = H. H-bonds are shown as red dotted lines.

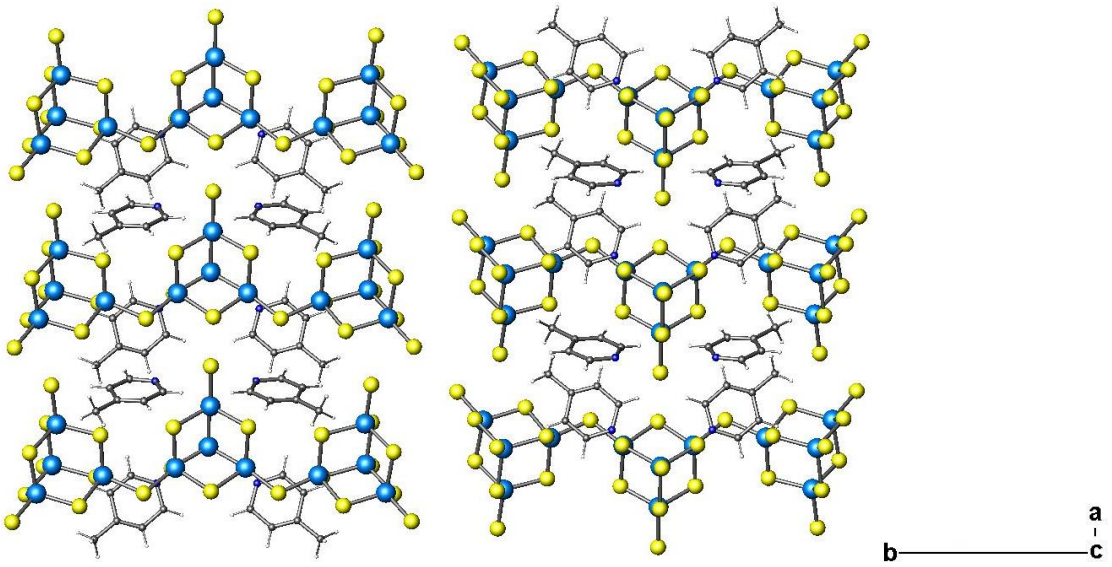

Figure 4.3 Two columns of trimers in **(8)** viewed along the *c*-axis. Light blue = Ge, yellow = S, grey = C, dark blue = N, white = H.

Packing of the trimers is shown in Figure 4.3; demonstrating that they line up along the *a*-axis, while alternating in direction as they propagate along the *b*-axis. The spacing between adjacent trimers is *ca.* 3 Å when measured from the centre of adjacent sulphur atoms and approximately 1 Å when the van der Waals' radii of atoms are used.

Polyhedral views of **(8)** are shown along both the (101) plane and [010] in Figure 4.4 and Figure 4.5 respectively. When viewed along (101) it can be seen that the trimers form layers throughout the structure; with spacing as shown between the two columns (Figure 4.4**)**. Packing when viewed along [010] (Figure 4.5), shows that the trimers are offset along the *c*-axis. The trimers are related to one another *via* a 2_1 screw axis, along [010].

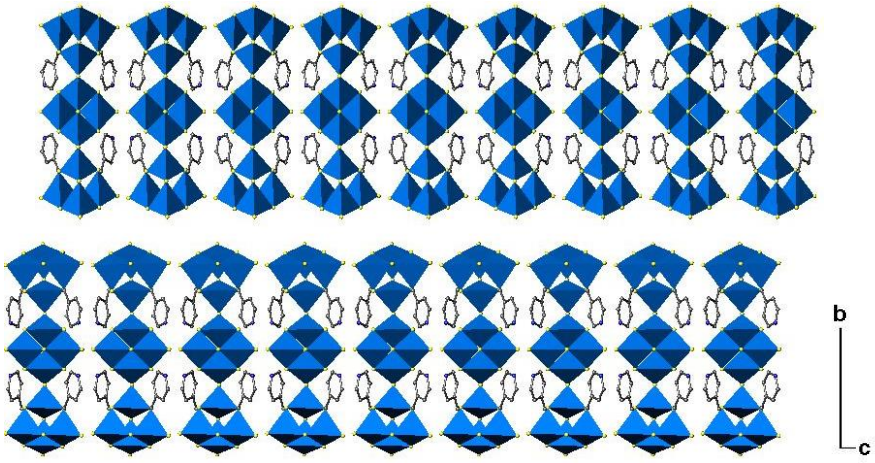

Figure 4.4 Polyhedral view of **(8)** viewed along the (101) plane. Light blue polyhedra = Ge, yellow = S, grey = C, dark blue = N. H atoms have been removed for clarity.

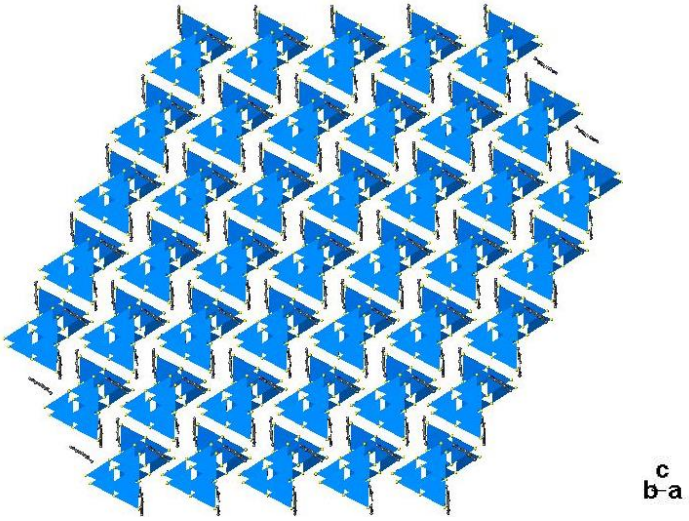

Figure 4.5 Polyhedral view of **(8)** viewed along [010]. Light blue polyhedra = Ge, yellow = S, grey = C, dark blue = N. H atoms have been removed for clarity.

4.2.2.4 *Powder X-ray Diffraction*

PXRD (Figure 4.6) suggests that the sample contains both **(8)** and a second phase (peaks below 2θ = 10 º); consisting of powder present in the product, which unfortunately could not be identified. Refined lattice-parameters for **(8)** are shown in Table 4.3.

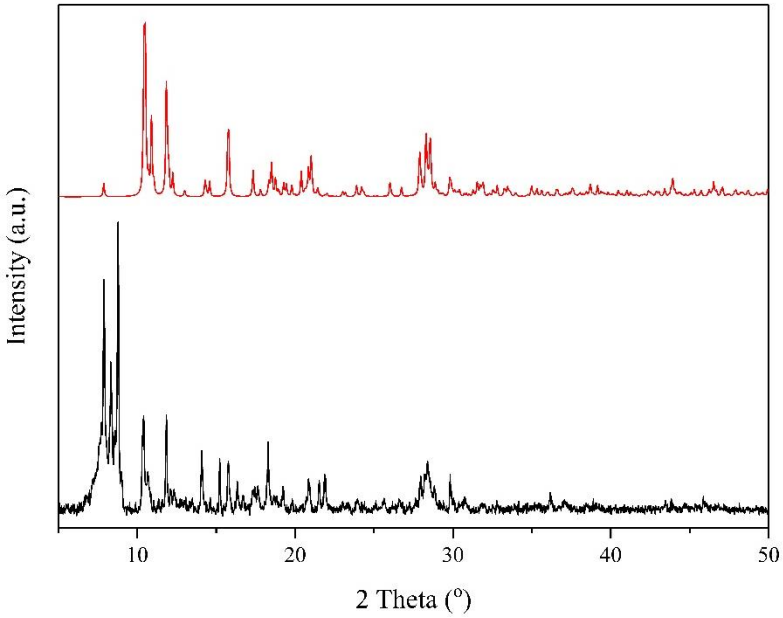

Figure 4.6 PXRD for structure **(8)**. Experimental = black, calculated from SCXRD = red.

Table 4.3 Lattice parameters from PXRD of **(8).** Parameters were refined against PXRD using DASH.[208]

SCXRD	***a*/ Å**	***b*/ Å**	***c*/ Å**	**α/ º**	**β/ º**	**γ/ º**
	9.5856(5)	44.8304(15)	9.6819(7)	90	117.774(8)	90
PXRD	***a*/ Å**	***b*/ Å**	***c*/ Å**	**α/ º**	**β/ º**	**γ/ º**
	9.591(8)	44.847(7)	9.682(9)	90	117.87(2)	90

4.2.2.5 *Issues with Reproducibility*

This structure could not be reproduced and the original sample was not suitable for further measurements. The reaction was repeated a number of times; including repeating the reactions with the same parameters and also adjusting parameters in an attempt to reproduce the structure (Table 4.4). Summaries of all reactions carried out in this work are listed in Appendix 1.2.

Table 4.4 Reaction conditions used in attempts to reproduce **(8)**. Reaction conditions used in initial reactions are in bold.

Reaction Parameter	Variations Used
Metal Sources	GeO_2, **Ga + GeO_2**
Temperature/ ^oC	150, **170**, 200
Auxiliary Amine	**TMDPy,** no amine
Time/ Days	**5**, 6, 7
Ga:GeO_2:Amine:4-MPy Ratio	1:1:6:1:30, **1:1:5.5:1:30**, 1:1:5:1:30, 1:1:4:1:30, 1:1:5.5:4:30:, 1:1:10:4:30, 2.5:1:4:1:30, 0:2:5.5:1:30, 0:2:5:4:30, 2.5:1:4:0:60

4.3 Chains of T2 Germanium Sulphide Clusters

4.3.1 **Synthesis**

Compound **(9)** $[NC_6H_8]_2[Ge_4S_9](C_6H_7N)_{0.5}$ was synthesised from Ga metal (69.2 mg, 1 mmol), GeO_2 (102 mg, 1 mmol) and S powder (127 mg, 3.95 mmol) in 4-MPy (2.9 ml, 30 mmol). The stoichiometric ratio was 1:1:4:30 and the reaction was carried out for 5 days at 170 ^oC. The resulting product contained orange plates and powder. A pure sample of **(9)** was prepared by handpicking crystals, in order to carry out further measurements.

4.3.1.1 *Energy-Dispersive X-Ray Analysis*

EDX analysis was also carried out on single crystals of **(9)**, this also determined germanium to be the only metal present in the compound (Table 4.5).

Table 4.5 EDX Data for (9) showing molar % by element.

Element	Molar %	Molar %	Molar %	Molar %	Molar %	Average Molar %
S	59.25	57.18	75.08	71.25	61.23	65(8)
Ge	40.75	42.82	24.92	28.75	38.77	35(8)

In this case, the relative percentages of Ge and S vary, suggesting that there could be some areas of the crystals where the percentages are slightly different. The calculated Ge:S ratio is 4:9, whereas the experimental ratio ranges from 4:6 to 4:12, which means that the calculated ratio is still in range determined experimentally.

4.3.2 Structure and Characterisation

4.3.2.1 *Single-Crystal X-Ray Diffraction*

SCXRD was carried out on an orange plate of **(9)** (Table 4.6). Platon SQUEEZE was used to model residual electron-density in the single-crystal refinement for **(9)**.[206] Platon calculated a void space of 1351.5 $Å^3$ per unit cell (43.7 %).

Table 4.6 Selected single-crystal X-ray diffraction data and refinement details for **(9).**

Crystallographically-Determined Formula	$[Ge_4S_9](NC_6H_8)$
M_r	672.11
Crystal habit	Orange Plate
Crystal system	Monoclinic
Space group	$P2_1/n$
T/K	150
a, b, c/Å	13.9587(6), 10.3898(4), 22.159(1)
β/°	105.773(5)
V/Å^3	3092.7
Z	4
θ_{max}	30.540
ρ_{cal}/gcm^{-1}	1.444
μ/mm^{-1}	4.449
T_{min},T_{max}	0.480,1.000
Number of parameters	181
Number of reflections used in refinement	2716
Total number of reflections	8307
R_{merge}	0.0748
$R(I>3.0\sigma(I))$	0.0686
R_w	0.1097

4.3.2.2 *Structure Description*

The asymmetric unit (Figure 4.7) consists of a $[Ge_4S_9]^{2-}$ unit. The $[Ge_4S_9]^{2-}$ unit is a germanium-sulphide T2 supertetrahedron, where the corner sulphur-atoms are shared between two T2 clusters giving a μ_2-S linkage.

Based on the charge of the cluster, two positively-charged organic cations are needed per asymmetric unit. In the asymmetric unit, one 4-MPy moiety can be found per cluster; this implies that there must be another disordered positively-charged moiety per $[Ge_4S_9]^{2-}$ supertetrahedron. The Ge-S bond-lengths are in the range of 2.091(3) to 2.266(3) Å. Short distances correspond to terminal Ge-S bonds and longer distances correspond to those with bridging S atoms. These are again in the range expected for a T2 cluster of this nature.[103]

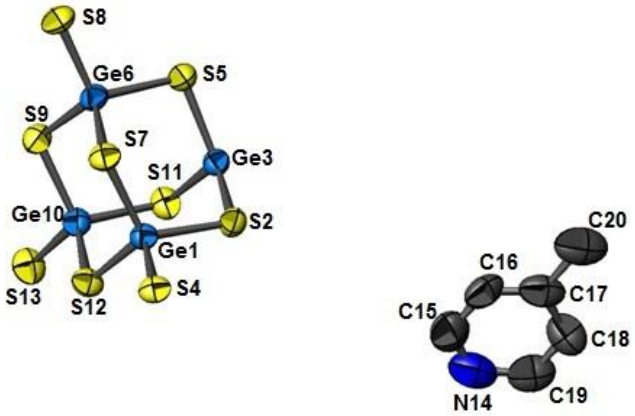

Figure 4.7 Asymmetric unit of **(9).** Light blue = Ge, yellow = S, dark blue = N, grey = C. H-atoms are omitted for clarity.

The T2 supertetrahedra link along the *b*-axis into zigzag chains *via* the μ_2-linkage (Figure 4.8). N-S distances of 3.167 Å suggest that there are H-bonding interactions between the H atoms on the protonated 4-MPy cations and terminal S atoms on the adamantane units. This interaction explains why this 4-MPy cation can be found in the crystal structure. The 4-MPy moieties that are H-bonding with the inorganic components are ordered throughout the structure, while the remaining cations are disordered. Chains pack throughout the material as shown in Figure 4.9

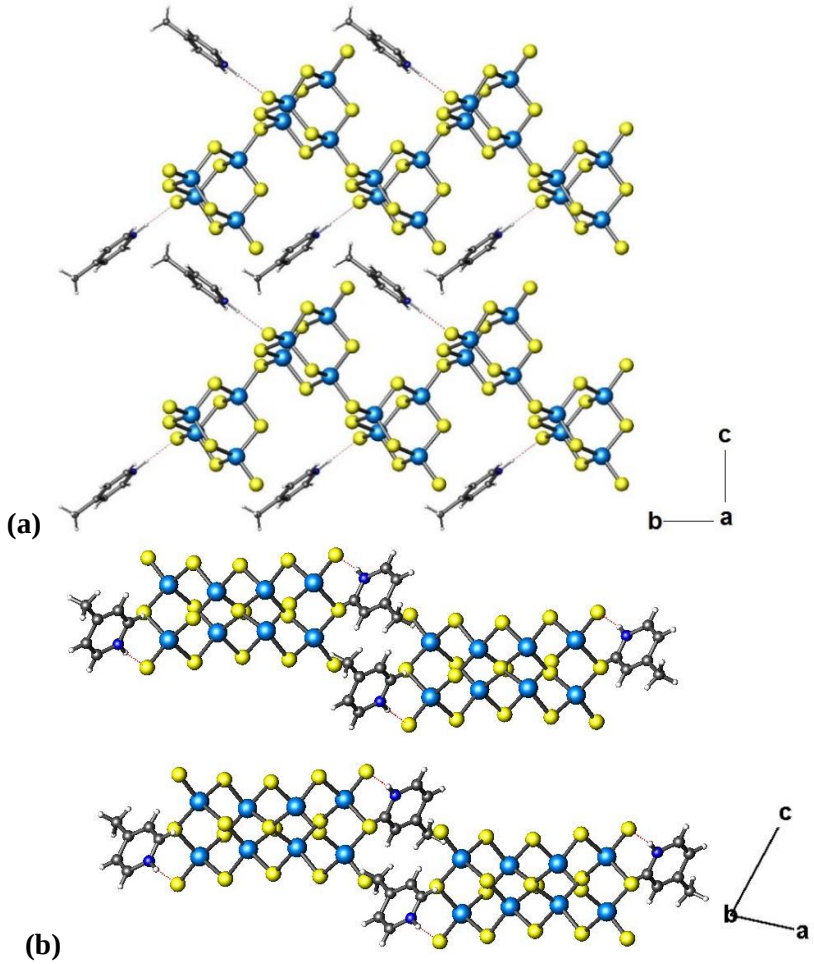

Figure 4.8 Chains in **(9)** viewed along **(a)** the *a*-axis and **(b)** the *b*-axis. H-bonding interactions are indicated by red dashed lines.

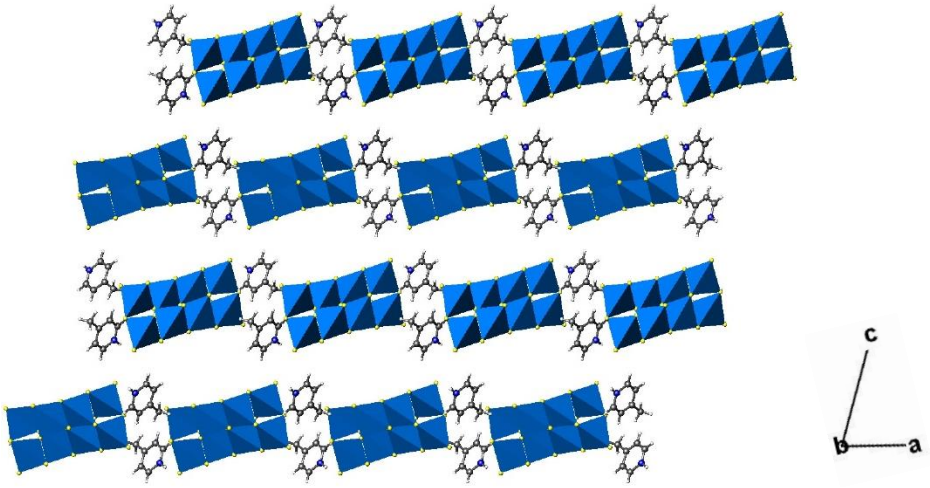

Figure 4.9 Polyhedral view of chains in **(9),** viewed along the *b*-axis

The crystal structure consists of zigzag chains oriented along the *b* –axis (Figure 4.8 **(a)**); the 4-MPy cations alternate in orientation to support the zigzag pattern of the chains. Chains alternate in direction, as observed in Figure 4.10.

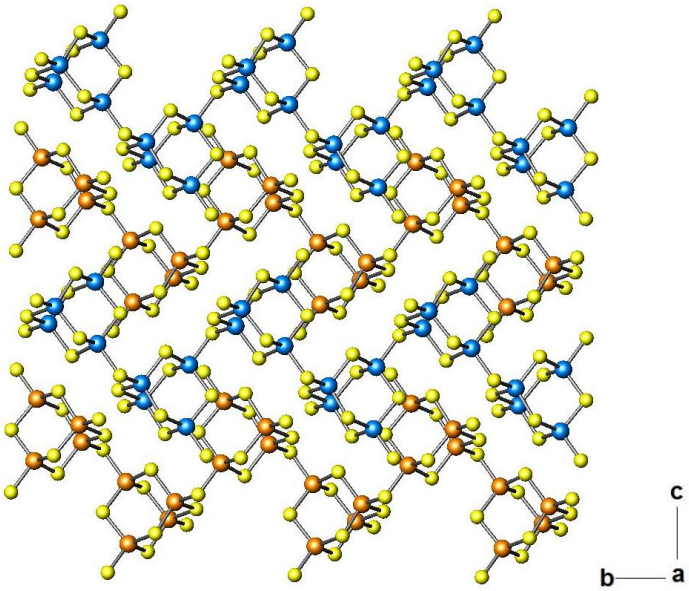

Figure 4.10 Structure of **(9)** viewed along the *a*-axis with organic moieties omitted for clarity. Yellow = S, blue/orange = Ge, in order to distinguish between $[Ge_4S_9]^{2-}$ chain orientations.

This structure is isostructural with a material produced by Parise *et al.* in 1995.[230] The structure in the literature contains the amine DPA (dipropylammonium), with two protonated-equivalents of these moieties balancing the negative charge of each cluster. The given formula for this structure was $Ge_4S_9(C_3H_7)_2NH_2(C_3H_7)NH_2(C_2H_5)$, where $(C_3H_7)NH_2(C_2H_5)$ is an organic species formed *in situ*. No physical-property measurements were carried out on the material reported by Parise.[230]

Previously, there has been no evidence of germanium sulphides based on adamantane clusters synthesised in 4-MPy, although there is an example of a material containing Bipy. Another example discussed donor-acceptor interactions when these clusters were present in a structure with a pophyrin.[234, 235] The clusters in these materials are held together by strong H-bonding networks; rather than linking *via* corner-sharing S-atoms. These adamantane clusters are mostly found either as discrete units or corner sharing in 3-dimensional networks.[101, 132, 233] They can also be observed to link into structures of higher dimensionalities through transition-metal centres,[102, 103, 236] as described in Sections 1.4.3 and 1.4.4.

4.3.2.3 *Powder X-Ray Diffraction*

PXRD shows that the bulk is consistent with that of **(9)** (Figure 4.11) and is pure. Lattice parameters were refined against the powder data (Table 4.7). Differences in the intensities between the calculated and experimental data could be attributed to preferred orientation, as the crystals are plates.

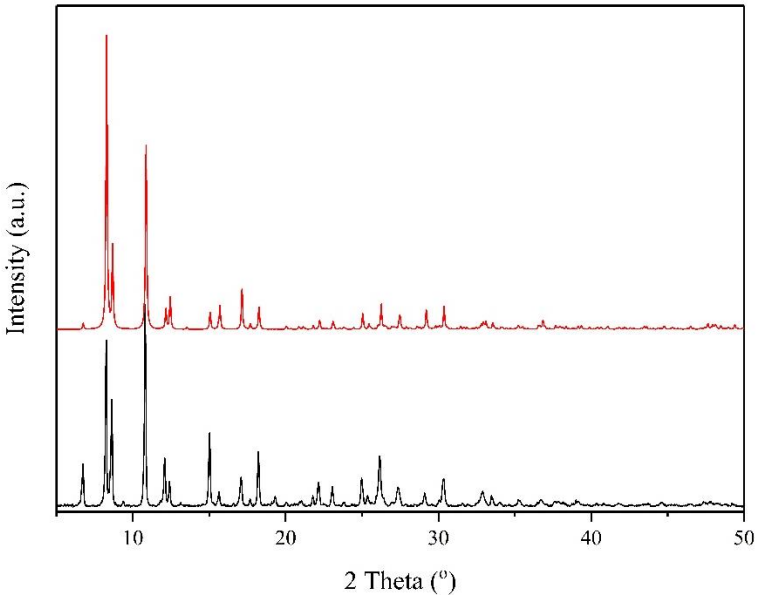

Figure 4.11 PXRD for **(9).** Experimental=black, simulated=red.

Table 4.7 Lattice parameters for **(9).** Parameters were refined against PXRD using DASH.[208]

SCXRD	***a*/ Å**	***b*/ Å**	***c*/ Å**	**α/ º**	**β/ º**	**γ/ º**
	13.9587(6)	10.3898(4)	22.159(1)	90	105.773(5)	90
PXRD	***a*/ Å**	***b*/ Å**	***c*/ Å**	**α/ º**	**β/ º**	**γ/ º**
	14.000(3)	10.420(3)	22.316(5)	90	105.77(3)	90

4.3.2.4 *Elemental Analysis*

The proposed formula of **(9)** is $[C_6H_8N]_2[Ge_4S_9](C_6H_7N)_{0.5}$, which is in good agreement with the values obtained from CHN elemental analysis (Experimental : C = 23.65, H = 2.69, N = 4.55, Calculated: C = 23.77, H = 2.60, N = 4.20). The disordered organic species would be located in the void space calculated by Platon SQUEEZE as 1351.5 $Å^3$ per unit cell (43.7 %).[206]

4.3.2.5 *Infrared Spectroscopy*

FTIR data were recorded for compound **(9)** and confirmed the presence of protonated amines within the structure (Figure 4.12 and Figure 4.12). When compared with the FTIR spectra for the T3 hybrid-supertetahedral clusters described in Chapter 3, there are differences in intensity of the peaks, suggested to be mainly due to the smaller proportion of non-protonated 4-MPy in the material.

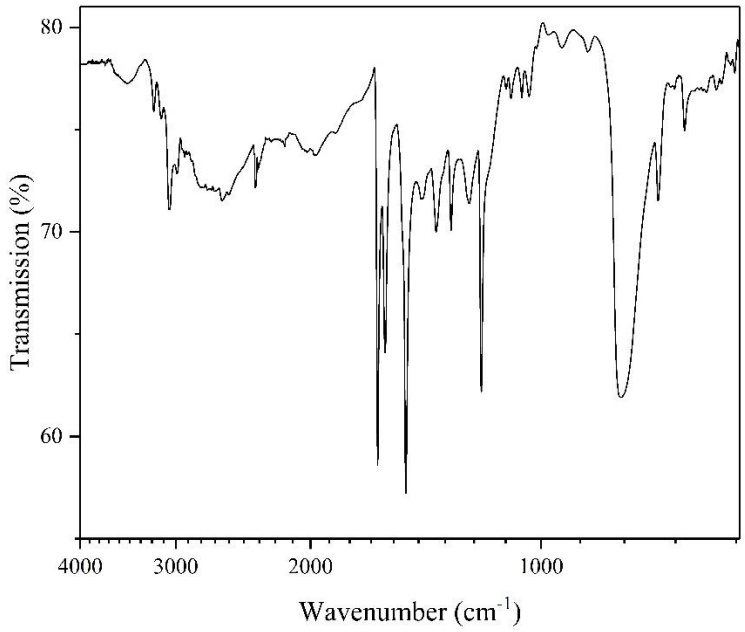

Figure 4.12 FTIR for **(9)**

Figure 4.13 Key FTIR frequencies for **(9).**[219, 220]

Wavenumber/ cm^{-1}	Assignment
3519	Aromatic ν (C-H) 4-MPy
3056	Aromatic ν (C-H) 4-MPy$[H]^+$
1635	Aromatic δ (C-N) 4-MPy$[H]^+$
1502	Aromatic ν (C-C) 4-MPy$[H]^+$
1420	CH_3 ν (C-H) 4-MPy$[H]^+$
1197	δ (N-H) 4-MPy$[H]^+$
791	Aromatic γ (C-H)

4.3.2.6 *Thermogravimetric Analysis*

TGA was carried out on a pure sample of **(9)** in atmospheres of both air and N_2. (Figure 4.14). Compound **(9)** loses more weight when it is heated under nitrogen (Figure 4.14 **(b)**) than when it is heated in air (Figure 4.14 **(a)**). Calculations show that loss of the non-protonated organic component $(C_6H_7N)_{0.5}$ from $[C_6H_8N]_2[Ge_4S_9](C_6H_7N)_{0.5}$ causes an initial weight-loss of *ca.* 10 %; shown in both TGA graphs. This step is

followed by the loss of the protonated organic-components $[C_6H_8N]_2$, and conversion to GeS_2 (23 %) leaving a remaining weight of *ca.* 67 %; as observed when the sample is heated in air, however this step is not observed under N_2.

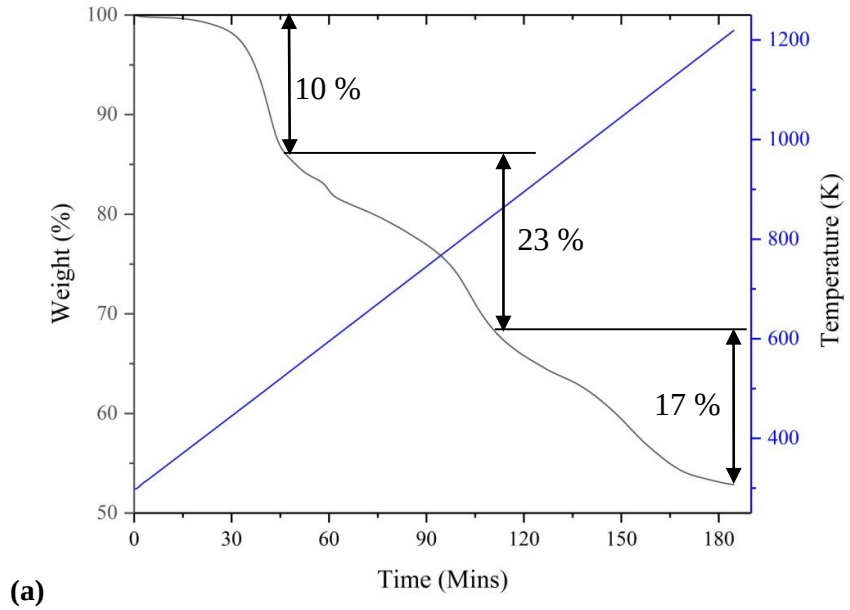

(a)

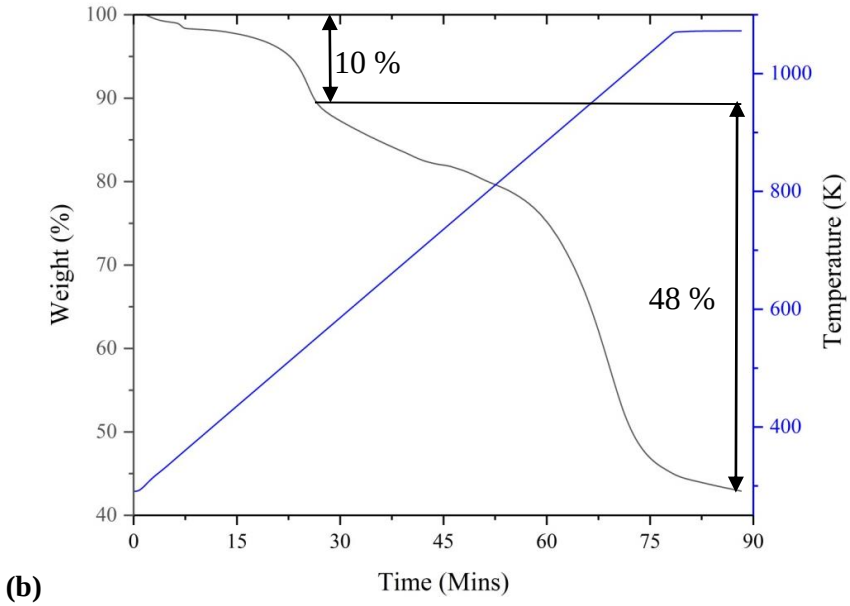

(b)

Figure 4.14 TGA data for **(9)** are shown in **(a)** air and **(b)** N_2. Black line = weight percent vs time, blue line = temperature vs time.

The final weight-loss step for the decomposition of **(9)** would be conversion to the oxide of the metal present. The final weight present in air corresponds to GeO_2, with a value of *ca.* 50 %. Usually, it would be expected that the final product when the product is heated under N_2 would be GeS_2, due to the lack of oxygen to form GeO_2. In fact, the weight loss is greater in this case when the sample is heated under nitrogen. It is thought

that this is due to the formation of GeO; produced when germanium is heated in a limited amount of oxygen and Germanium(IV) is reduced to Germanium(II); due to the lack of sufficient oxygen for the sample to decompose to GeO_2. When the entire sample decomposes to GeO, the resulting weight would be *ca.* 42 %; consistent with the final weight (Figure 4.14 **(b)**.

4.3.2.7 *UV-Vis Diffuse Reflectance Spectroscopy*

Diffuse reflectance was measured on orange crystals of **(9)** (Figure 4.15**)**. The tangent line (red) shows the absorption edge is at 3.36(1) eV, making this material a wide-gap semiconductor. Compared with materials containing discrete clusters, as described by Sun *et al.* with band gaps of 1.65 – 2.21 eV, due to the presence of a methylviologen cation, this is wider.[237] However, 3-dimensional mesoporous materals containing these clusters, as described by Wachhold *et al.,* have band gaps in a similar region to **(9)** at 3.2 – 3.4 eV.[173]

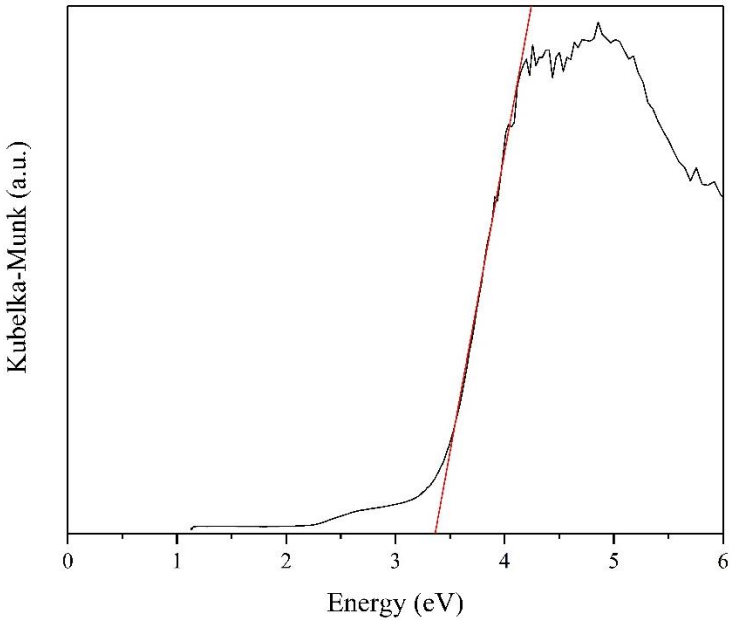

Figure 4.15 Diffuse reflectance graph for **(9)**. Red tangent line shows absorption edge.

4.3.3 **Discussion**

When compared with **(8)** (Section 4.2), **(9)** has a higher dimensionality; increasing from the zero-dimensional trimer in **(8),** to the 1-dimensional chains in **(9)**. As described, a number of reactions were carried out in attempts to reproduce **(8)**. In many reactions, **(9)** was formed preferentially (Section 6.3.3.1); this suggests that the 1-dimensional structure is more stable. Compound **(8)** was synthesised at 200 ^{o}C over 7 days; with a Ga:GeO_2:S:TMDPy:4-MPy ratio of 1:1:5.5:1:30, whereas **(9)** can be formed

by numerous different methods. Compound **(9)** can be synthesised under temperatures from 150 - 200 ºC and times of 5-7 days; it has also been synthesised in the absence of of gallium.

4.4 A Germanium-Gallium Sulphide Framework Based on T2 Supertetrahedra

4.4.1 Synthesis

Yellow crystals of **(10)** $[C_6H_8N]_2[Ga_2Ge_2S_8]$ were synthesised from a mixture of Ga (1 mmol, 68 mg), GeO_2 (1 mmol, 102 mg), S (4 mmol, 127 mg) and Im (1 mmol, 70.8 mg) in 4-methylpyridine (2.9 ml, 30 mmol). The reaction was performed in a 23 ml Teflon-lined autoclave, at 200 ºC for 6 days. There are a number of different ways of synthesising this material (Section 6.3.3.1), but the synthesis described above gives the purest product. This product consisted of yellow plates of **(11)**.

4.4.2 Structure and Characterisation

4.4.2.1 *Energy-Dispersive X-Ray Analysis*

The reaction mixture to produce **(10)** contained both GeO_2 and Ga; therefore EDX was carried out on single crystals of this sample. This indicated that **(10)** contains both Ga and Ge in a *ca.* 1:1 ratio. Results for five different measurements and their average are displayed in Table 4.8. This was also repeated on a second crystal, which gave values in the same region (Appendix 2.1). Final stoichiometric values were calculated to be Ga = 1.8(2), Ge = 2.2(2) and S = 7.9(2).

Table 4.8 EDX Data for **(10)** showing molar % by element.

Element	Molar %	Molar %	Molar %	Molar %	Molar %	Average Molar %
O	9.83				10.92	10.38
S	62.01	67.64	66.46	64.54	58.25	63.78
Ga	11.96	13.63	16.14	15.16	15.22	14.42
Ge	16.2	18.73	17.4	20.3	15.6	17.65

4.4.2.2 *Single-Crystal X-Ray Diffraction*

The crystal structure of **(10)** contains one crystallographically-distinct metal site. During the single-crystal refinement for **(10)**, the results of the EDX analysis were taken into account. Occupancies for this site were set as 50% Ge and 50% Ga. Selected crystallographic data are given in Table 4.9.

Platon SQUEEZE was used to model the residual electron-density in the structure.[206] The void space was calculated to be 1364 $Å^3$ (~57 %) per unit cell.

Table 4.9 Selected single crystal X-ray diffraction data and refinement details for **(10).**

Crystallographically – Determined Formula	$Ga_4Ge_4S_{16}$
M_r	1082.30
Crystal habit	Yellow Plate
Crystal system	Tetragonal
Space group	*I*-42d
***T*/K**	150
***a, b, c*/Å**	11.2495(15), 11.2495(15), 19.032(3)
***V*/Å^3**	2408.6(6)
Z	2
θ_{max}	30.333
ρ_{cal}/gcm^{-3}	1.492
μ/mm^{-1}	5.350
T_{min},T_{max}	0.774,0.948
Number of parameters	30
Number of reflections used in refinement	405
Total number of reflections	1589
R_{merge}	0.164
$R(I>3.0\sigma(I))$	0.0687
R_w	0.0679

4.4.2.3 *Structure Description*

The asymmetric unit of **(10)** has a formula of MS_3 (Figure 4.15). Due to the fact that the metal site has a 1:1 ratio of Ge:Ga, this can be expressed as $[GeGaS_6]_{0.5}^{2.5-}$. This asymmetric unit represents ¼ of a corner-sharing T2 unit $[Ge_2Ga_2S_8]^{2-}$.

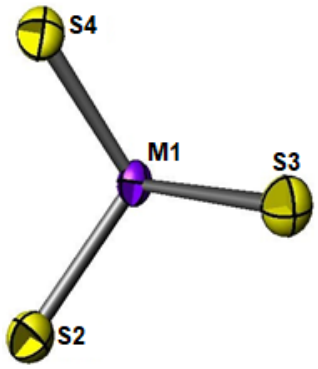

Figure 4.16 Asymmetric unit of **(10).** Purple = Ge/Ga, yellow = S.

Each T2 cluster shares four of their corners with adjacent T2-clusters (Figure 4.17) The resulting formula of the framework is therefore $[Ga_2Ge_2S_8]^{2-}$. Ge/Ga-S bond lengths are in the range of 2.223(9) to 2.230(7) Å. This is consistent with either a Ge-S or Ga-S bond.[103, 238] Two cations per cluster are needed to balance the charge. In this case, no organic-components have been found within the crystal structure. This suggests that all of the organic cations are disordered throughout the void space, which was calculated by Platon SQUEEZE as 1364 $Å^3$ (~57 %).[206]

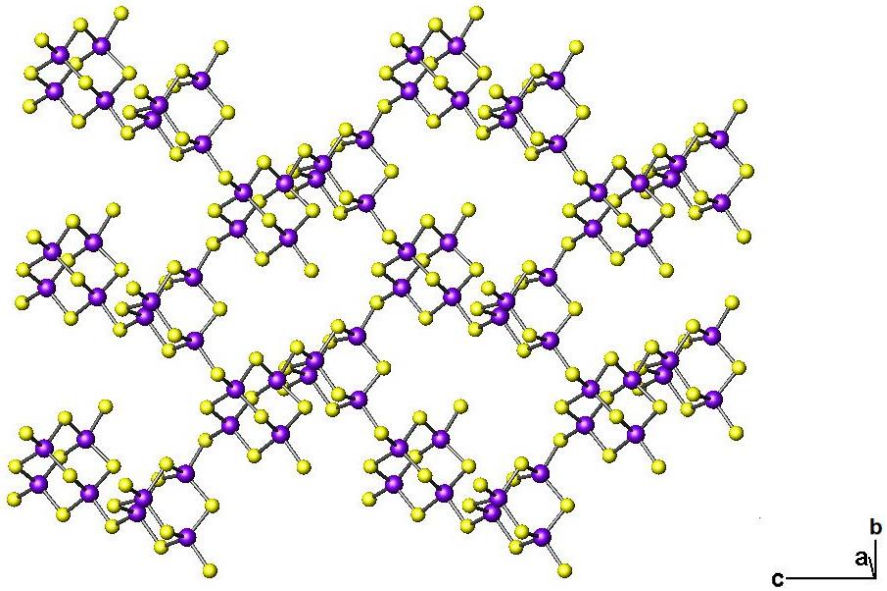

Figure 4.17 Perspective view of framework in **(10).** Purple = Ge/Ga, yellow = S.

In the structure of **(10)**, channels run along the *b*-axis (Figure 4.18) and the *a*-axis (Figure 4.17), whereas there are no accessible-channels along the *c*-direction. The size of the channels is estimated to be 3 x 5 $Å^2$ when van der Waals' radii are used.

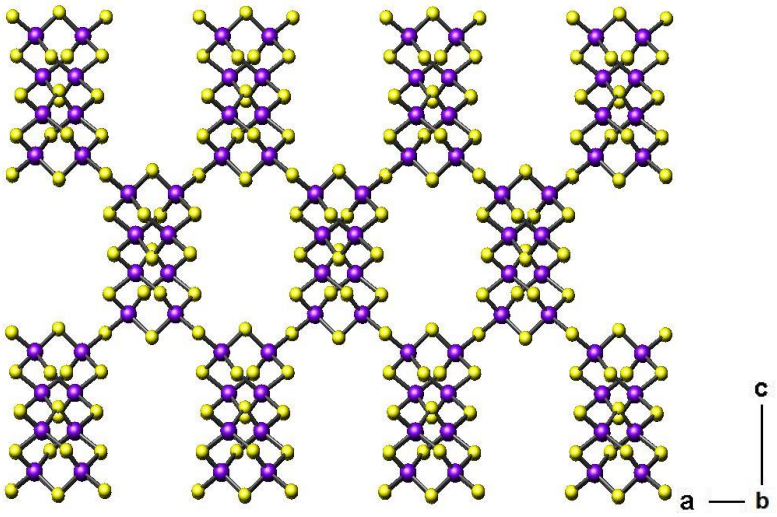

Figure 4.18 The structure of **(10)** viewed along the *b*-axis. Purple = Ge/Ga, yellow = S.

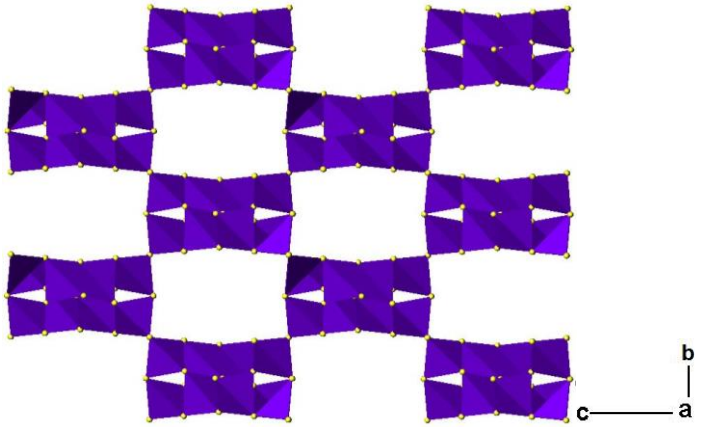

Figure 4.19 Polyhedral view of structure of **(10)**, along the a-axis. Purple = Ge/Ga, yellow = S.

(10) is isostructural with a material first synthesised by Feng *et al;* the compound is referred to in this publication as UCR-21GaGeS-APO.[104] In this case APO (1-amino-2-propanol, C_3H_9NO) was used as the amine and a ratio of Ga:Ge of 3.3:0.7 is reported. Therefore, although the crystal structure appears the same, the metal content is different; this means that the charge of the framework is altered from the previously-reported structure. Organic cations will also be different, because firstly, the framework has a lower negative-charge and secondly, a different solvent has been used. Photoluminescence is published for some materials reported by Feng *et al.*,[104] although these data are not included for UCR-21GaGeS-APO.[104]

Both structures have the double-diamond topology, as described for a number of materials in Section 1.4.4. In many cases, networks of this nature are interpenetrating, whereas **(10)** is not. However, due to the fact that the material consists of T2 clusters, the resulting pore-diameter is relatively small (*ca.* 3 x 5 $Å^2$)

4.4.2.4 *Powder X-Ray Diffraction*

PXRD for **(10)** shows that the sample contains only this phase (Figure 4.19); the powder pattern matches those of both crystal structures, from **(10)** and UCR-21GaGeS-APO.

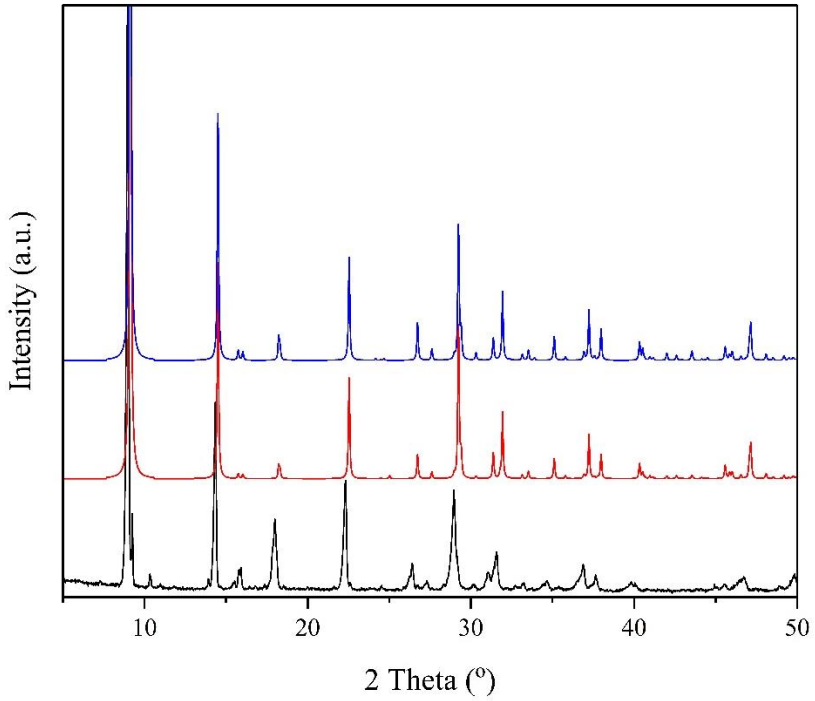

Figure 4.20 PXRD for **(10)**, black = experimental for **(10)**, red = simulated for **(10)**, blue = simulated for UCR-21GaGeS-APO [104]

Table 4.10 Lattice parameters for **(10).** Parameters were refined against PXRD using DASH.[208]

SCXRD	***a*/ Å**	***b*/ Å**	***c*/ Å**	**α/ º**	**β/ º**	**γ/ º**
	11.2495(15)	11.2495(15)	19.032(3)	90	90	90
PXRD	***a*/ Å**	***b*/ Å**	***c*/ Å**	**α/ º**	**β/ º**	**γ/ º**
	11.397(8)	11.397(8)	19.147(5)	90	90	90

4.4.2.5 *Elemental Analysis*

Elemental analysis suggests that the pores contain 2 protonated 4-MPy moieties per cluster (Experimental: C= 17.79 %, H = 2.02 %, N = 3.79 %. Calculated: C = 19.76 %, H = 2.21 %, N = 3.84 %). The formula has therefore been deduced to be $[C_6H_8N]_2[Ga_2Ge_2S_8]$. However, the calculated percentage of carbon is slightly higher

than the experimental value. This might indicate that this material also contains water, as it is present in the reaction mixture. For example, adding 4 moles of water per formula unit, which would result in $[C_6H_8N]_2[Ga_2Ge_2S_8](H_2O)_4$ and lead to calculated values of C = 17.98 %, H = 3.02 %, N = 3.5 %.

4.4.2.6 *Infrared Spectroscopy*

FTIR of **(10)** could confirm the presence of water (Figure 4.21), but the key frequencies that suggest the presence of lattice water are in the same region that other interactions occur for 4-MPy (Table 4.11), so this cannot be used to fully confirm this. The FTIR confirms the presence of protonated 4-MPy within the material.

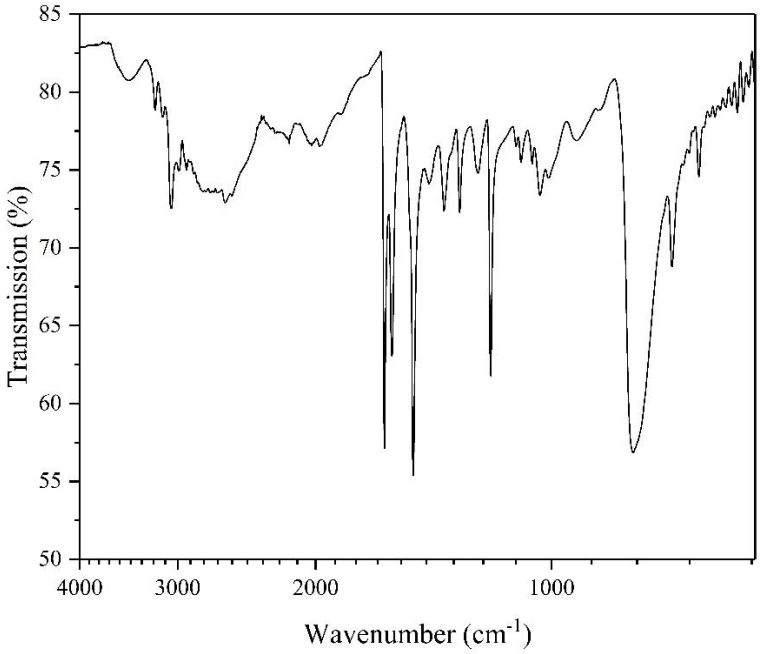

Figure 4.21 FTIR for **(10).**

Table 4.11 Key FTIR frequencies for structure **(10).**[219, 220, 239]

Wavenumber/ cm^{-1}	Assignment
3483	Water ν(O-H), Aromatic ν (C-H) 4-MPy
3056	Aromatic ν (C-H) 4-MPy$[H]^+$
1632	Aromatic δ (C-N) 4-MPy$[H]^+$, Water γ(H-O-H)
1596	Water γ(H-O-H)
1502	Aromatic ν (C-C) 4-MPy$[H]^+$
1430	CH_3 ν (C-H) 4-MPy$[H]^+$
783	Aromatic γ (C-H)

4.4.2.7 *Thermogravimetric Analysis*

TGA data have been measured for compound **(10)** (Figure 4.22). When the sample is heated in air the weight-loss steps are as follows. The initial weight-loss of *ca.* 9 % would refer to the loss of water from the sample. This weight loss is followed by the loss of the organic components, to give a remaining weight of *ca.* 67.5 %. If GeS_2 and Ga_2S_3 were the final products, the remaining weight would be *ca.* 64 %; corresponding to the final weight when the material is heated in air (Figure 4.22 (a)).

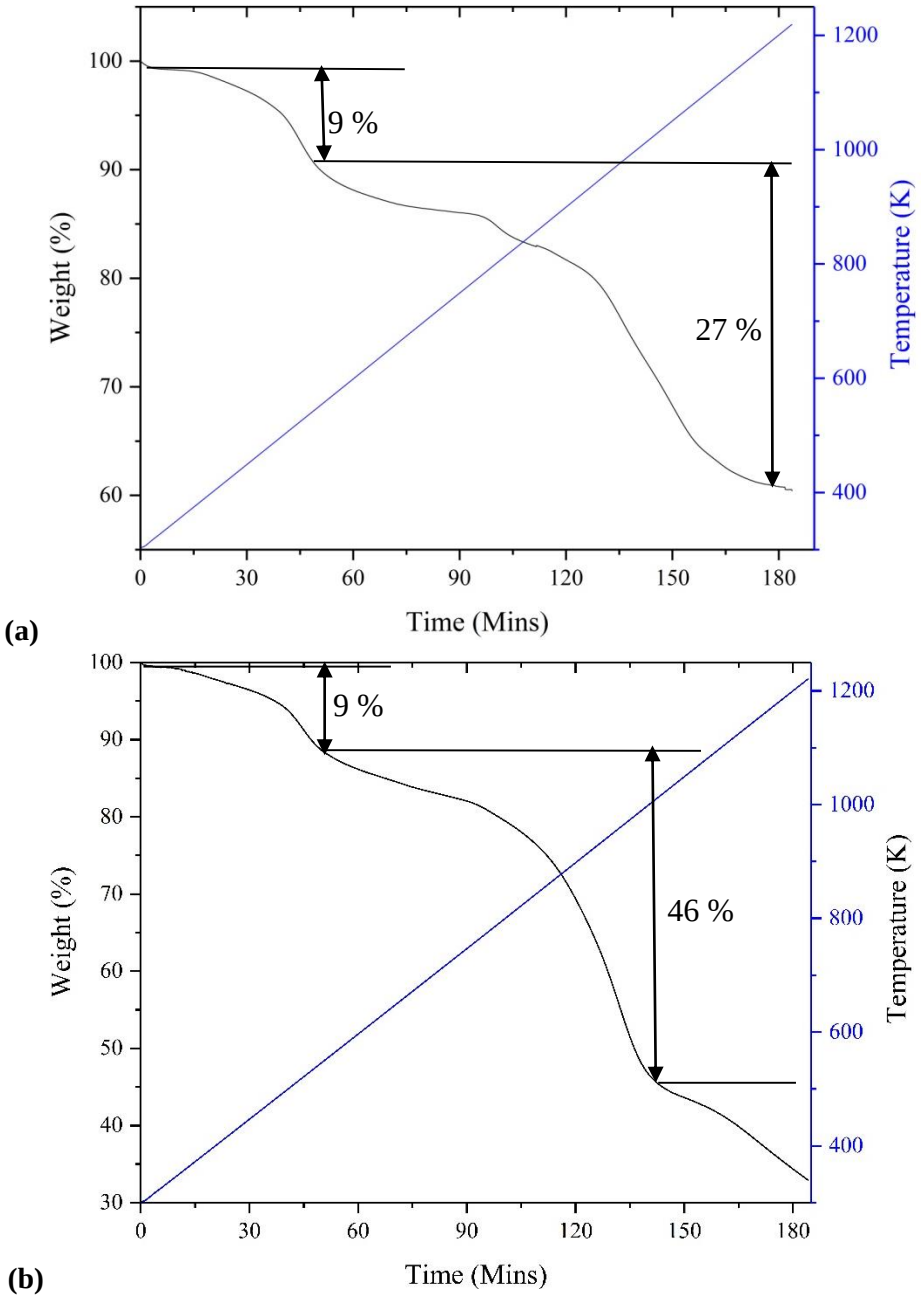

Figure 4.22 TGA data for **(10)** are shown in **(a)** air and **(b)** N_2. Black = weight percent vs time, blue = temperature vs time.

As described for **(9)** (Section 4.3), when germanium is heated in a limited supply of oxygen, GeO can be formed. It is suspected that this has occurred during the TGA measurement for **(10)**. Giving products of GeO and Ga_2O_3, with a weight of *ca.* 45 %.

4.4.2.8 *UV-Vis Diffuse Reflectance*

UV-Vis diffuse reflectance (Figure 4.23) shows that the absorption edge for **(10)** is 3.10(5) eV. This compound is therefore a wide-gap semiconductor; consistent with the other materials described. However, this band gap is narrower than the band gap of **(9)** and also narrower than those described for $[Ge_4S_{10}]^{2-}$ clusters linked *via* metal centres at 3.2 – 3.4 eV.[173] Zheng *et al.* reported the band gap for UCR-20 (Figure 1.14), a material also based on T2 gallium-germanium sulphide clusters, to be *ca.* 3.6 eV.[190] However, UCR-20 has a Ge:Ga ratio of 2:1 rather than 1:1, which would be expected to affect the band gap of the material. Unfortunately Zheng *et al.* do not quote the band-gaps of the other materials that they have produced based on these clusters.

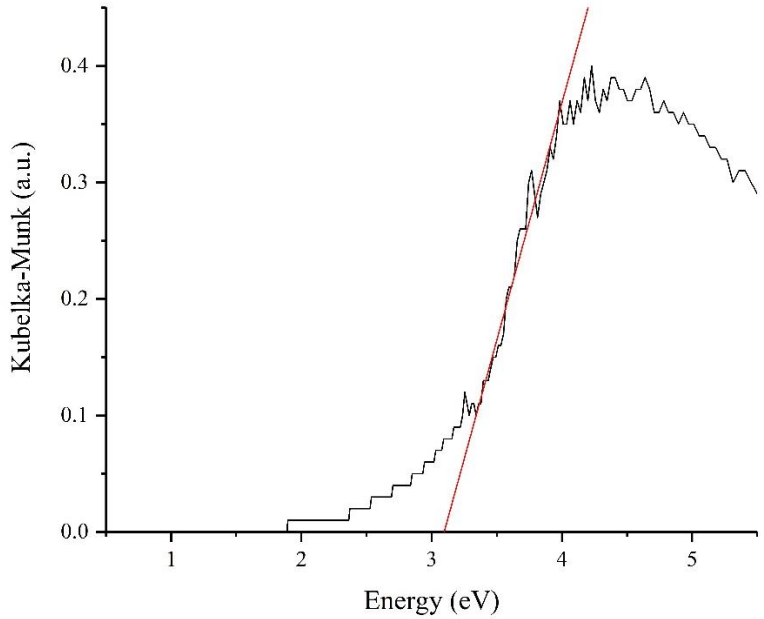

Figure 4.23 Diffuse reflectance graph for **(10)**. Red tangent line shows absorption edge.

4.4.3 **Discussion**

When compared with **(8)** and **(9)**, this structure has a higher dimensionality; going from the 1-dimensional chains shown in structure **(9)** to the 3-dimensional framework described here. The main difference here is that gallium has also been incorporated into this structure.

There are a number of different ways of synthesising this framework, as is apparent due to the fact that isostructural materials have been previously reported.[104] During the course of this work it was synthesised numerous times while exploring different reaction-parameters. Different reaction-conditions that could form structure **(10)** are described in Section 6.3.3.1**.**

4.5 A Germanium-Gallium Sulphide Framework Based on Single Tetrahedra

4.5.1 **Synthesis**

$[NC_6H_8][GaGe_3S_8](NC_6H_7)(H_2O)_5$ was synthesised from a mixture of Ga (1 mmol, 71 mg), GeO_2 (1 mmol, 110 mg) and S (5.5 mmol, 170 mg) in 4-MPy and H_2O (30 mmol, 0.5 ml). The reaction was carried out at 200 ^oC for 6 days. This material can also be synthesised without water, by adding 4,4'-trimethylenedipyridine or imidazole to the reaction mixture, but the synthesis described above gives the purest product. The sample contained pale-yellow octahedral-crystals of **(11)** and powder. Crystals of **(11)** were handpicked under a microscope to carry out further measurements on the material.

4.5.2 **Structure and Characterisation**

4.5.2.1 ***Energy Dispersive X-Ray Analysis***

As in the materials previously described, the reaction mixture for **(11)** contained sources of both gallium and germanium metals. EDX analysis was used to determine the ratio of the two metals within the crystals and the results are shown below (Figure 4.24 and Table 4.12). The data showed that there is a Ge:Ga ratio of 2.9(1):1.1(1) in this structure, which has been simplified to 3:1.

Table 4.12 EDX Data for **(11)** showing molar % by element.

Element	Molar %	Molar %	Molar %	Molar %	Average Molar %
O	6.3	2.6			4.5
S	67.3	61.7	68.0	63.5	67.3
Ga	8.5	7.8	11.0	9.0	8.8
Ge	19.3	17.8	24.7	19.3	23.2

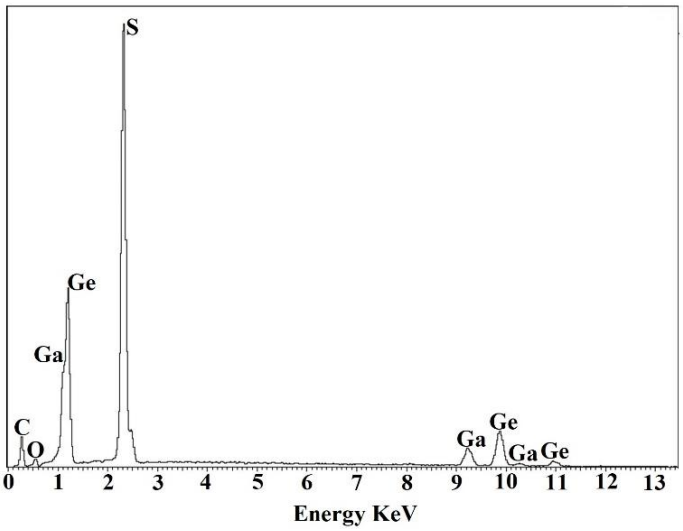

Figure 4.24 EDX spectrum for **(11).**

4.5.2.2 *Single-Crystal X-Ray Diffraction*

During structure refinement, the ratio of Ge:Ga metal sites was taken into account. Occupancies were set as 75 % and 25 % for Ge and Ga respectively. Their atomic coordinates and thermal parameters were constrained to be equal to each other. Selected crystallographic data are given in Table 4.9.

Table 4.13 Selected single-crystal X-ray diffraction data and refinement details for **(11).**

Crystallographically-Determined Formula	$GaGe_3S_8$
M_r	544.02
Crystal habit	Yellow Octahedra
Crystal system	Tetragonal
Space group	$I4_1/a$
T/K	150
a, b, c/Å	23.997(1), 23.997(1), 10.308(8)
V/Å^3	5936.4(6)
Z	12
θ_{max}	32.553
ρ_{cal}/gcm^{-3}	1.826
μ/mm^{-1}	6.670
T_{min},T_{max}	0.577,0.766
Number of parameters	82
Number of reflections used in refinement	2500
Total number of reflections	4841
R_{merge}	0.092
$R(I>3.0\sigma(I))$	0.0398
R_w	0.0383

Platon SQUEEZE was used to model the residual electron-density and calculated a potentially accessible void-space of 2719.3 $Å^3$ per unit cell (45 %).

4.5.2.3 *Structure Description*

The asymmetric unit of structure **(11)** has a formula of M_3S_6 where M = Ga^{3+} or Ge^{4+}, as the ratio between these metals has been confirmed as 3:1 Ge:Ga, this can be expressed as $[GaGe_3S_8]^-$.(Figure 4.25). Selected bond-lengths and angles for **(11)** are shown in Table 4.14

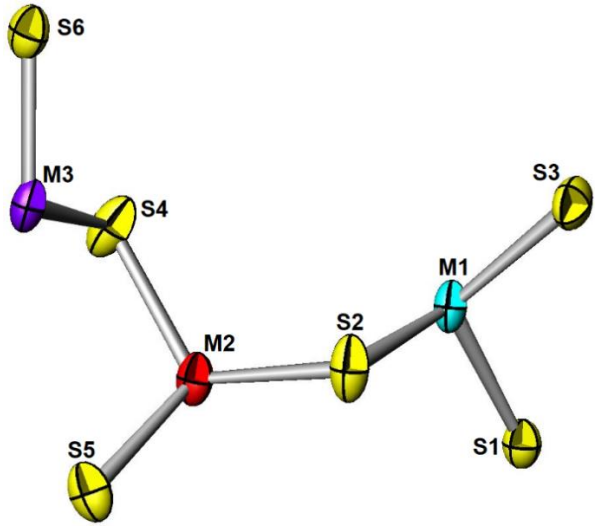

Figure 4.25 Asymmetric unit of **(11)**. Purple, teal, red = Ge/Ga, yellow = S.

Table 4.14 Selected bond-lengths and angles for **(11).**

Bond	Bond Length/ Å	Bond Angle	Bond Angle / º
M(1) - S(3)	2.2261(16)	S(1) - M(1) – S(2)	107.60(7)
M (1) - S(2)	2.2245(15)	S(1) - M(1) – S(3)	111.62(6)
M (1) - S(1)	2.2290(17)	S(2) - M(1) – S(3)	107.83(6)
M (2) - S(2)	2.2382(15)	S(2) – M(2) – S(4)	115.73(7)
M (2) - S(4)	2.2365(19)	S(2) – M(2) – S(5)	109.24(6)
M (2) - S(5)	2.2413(16)	S(4) -M(2) – S(5)	110.33(6)
M (3) - S(4)	2.2192(16)	S(4) –M(4) – S(6)	102.59(7)
M (3) - S(6)	2.2215(18)		

The structure consists of $[MS_4]^{4.25-}$ tetrahedra, with different linkages throughout the structure (Figure 4.25**)**. The structure of **(11)** is built from four-membered rings of $[M(1)S_4]^{4.25-}$ tetrahedra, linked *via* their vertexes (Figure 4.26 **(b)**) and capped by four further $[M(2)S_4]^{4.25-}$ tetrahedra (Figure 4.26 **(a)** and **(c)**). These are linked together into

a framework *via* helical chains of $[M(3)S_4]^{4.25-}$(Figure 4.26 **(d)**); these helical chains run along [001] and result from a 4_1 screw-axis that runs through the centre of the helix and the 4-membered ring, also along [001]. The presence of a glide-plane (001) supports the alternating direction of the helix rotation, resulting in a non-chiral structure; confirmed by the spacegroup of the material. An alternative view of the structure is shown in Figure 4.27, displaying how the helical chains link the capped four-membered rings to form the channels along the *c*-axis.

The material has a potentially accessible void-volume of approximately 45 %,[206] however the actual accessible void-space is less than this, due to the width of the channels being small, with a diameter of *ca.* 2.5 Å.

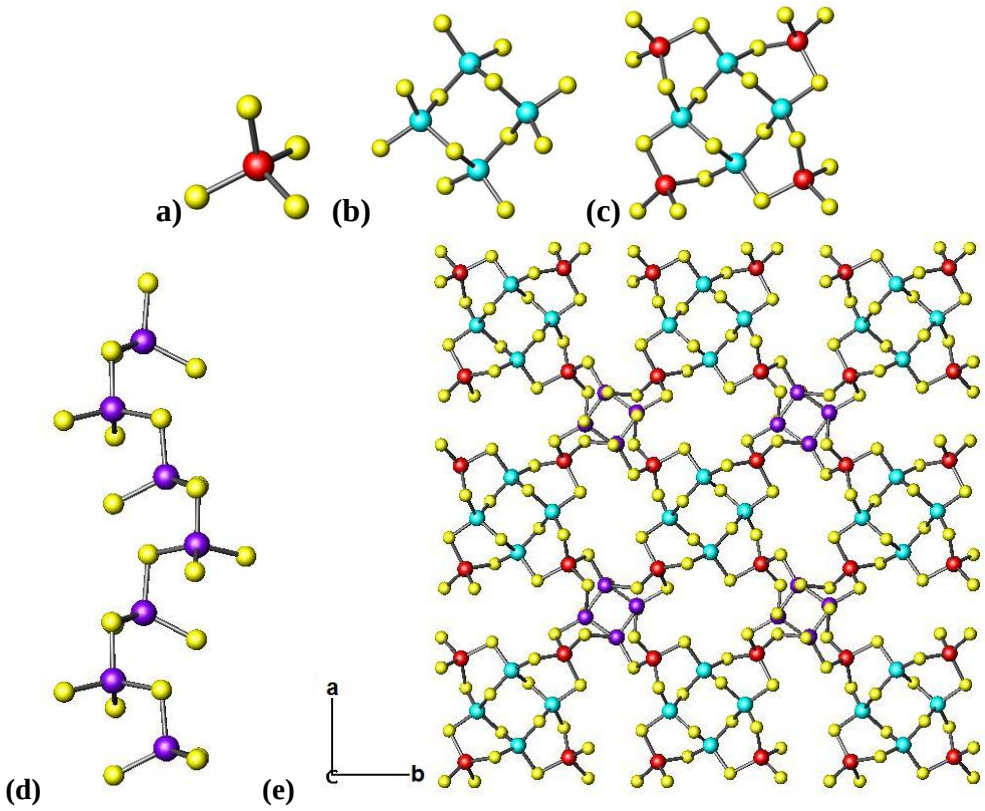

Figure 4.26 Structural units in **(11) (a)** tetrahedron, **(b)** 4-membered ring, **(c)** capped ring, **(d)** helical chain of tetrahedra **(e)** framework, viewed along the *c*-axis. Purple, teal, red = Ge/Ga, yellow = S.

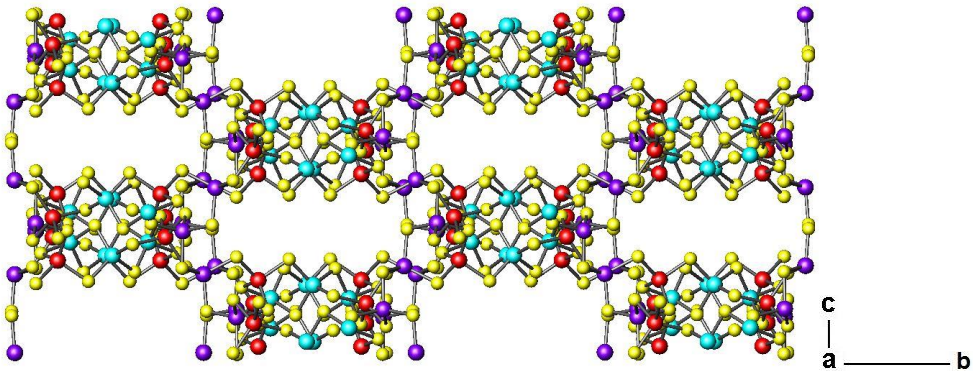

Figure 4.27 Framework in **(11)**, viewed along the *a*-axis. Purple, teal, red = Ge/Ga, yellow = S.

4.5.2.4 *Bond-Valence Calculations*

Table 4.15 Bond valence sums for **(11)**.[240]

	Bond Length 1 (Å)	Bond Length 2 (Å)	Bond Length 3 (Å)	Bond Length 4 (Å)	Bond Valence Ga^{3+}	Bond Valence Ge^{4+}
M(1)	2.2261(16)	2.2245(15)	2.2290(17)	2.2318(14)	3.36	3.88
M(2)	2.2382(15)	2.2365(19)	2.2413(16)	2.2502(17)	3.24	3.75
M(3)	2.2192(16)	2.2215(18)	2.2266(15)	2.2225(15)	3.41	3.94

Bond-valence sums were performed on all three metal-sites and these show little preference for each metal (Table 4.15). A typical Ge-S bond would be in the range of *ca.* 2.19-2.23 Å,[241] whereas Ga-S would be closer to *ca.* 2.27 Å.[238, 240]

4.5.2.5 *Powder X-Ray Diffraction*

PXRD was carried out on **(11)** (Figure 4.28). The sample contained a large amount of unidentified powder, along with crystals of **(11).**

Table 4.16 Lattice parameters for **(11)**. Parameters were refined against PXRD using DASH.[208]

	***a*/ Å**	***b*/ Å**	***c*/ Å**	**α/ º**	**β/ º**	**γ/ º**
SCXRD	23.997(1)	23.997(1)	10.308(8)	90	90	90
PXRD	***a*/ Å**	***b*/ Å**	***c*/ Å**	**α/ º**	**β/ º**	**γ/ º**
	23.83(1)	23.83(1)	10.31(7)	90	90	90

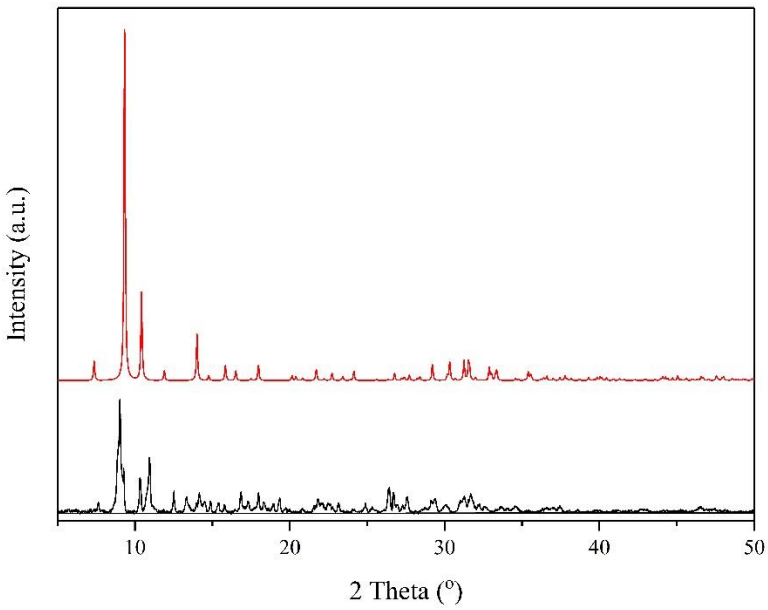

Figure 4.28 PXRD for **(11),** black line = sample containing **(11)** and red line = calculated from SCXRD of **(11).**

4.5.2.6 *Elemental Analysis*

With the overall charge of the given formula for the framework $[GaGe_3S_8]^-$, only one cation per formula unit is needed to balance this. Elemental analysis indicated that an extra non-protonated solvent molecule per formula unit is also present, along with six water-molecules. (Experimental: C = 17.17 %, H = 3.24 %, N = 3.34 %; calculated: C = 17.57 %, H = 2.95 %, N =3.41 %). Taking this into account, the overall formula of **(11)** can be given as $[NC_6H_8][GaGe_3S_8](NC_6H_7)(H_2O)_6$.

4.5.2.7 *Infrared Spectroscopy*

FTIR measurements were carried out on **(11)** (Figure 4.29). The FTIR indicates that there is potentially water in the structure, along with both protonated and non-protonated 4-MPy moities. However, as is seen for **(10),** key IR frequencies for lattice water are in the same region as key amine-frequencies.

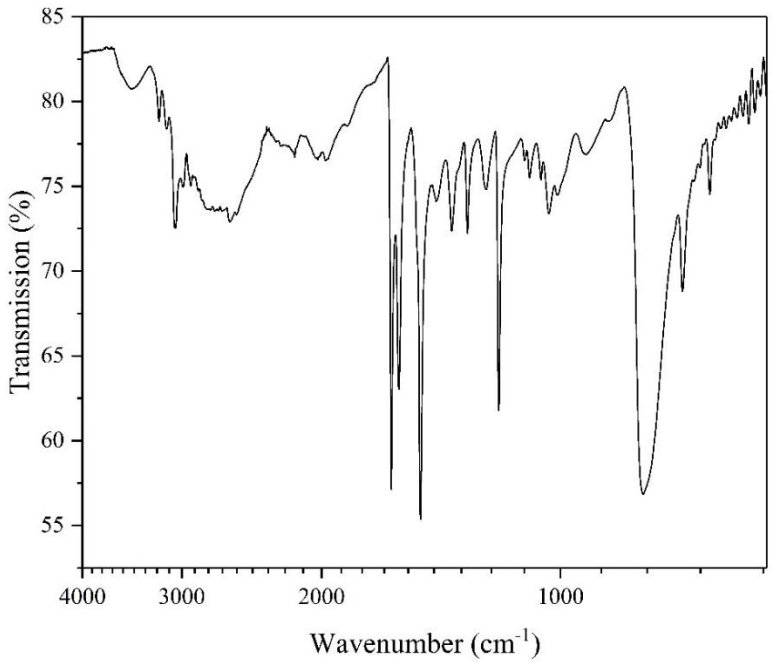

Figure 4.29 FTIR for structure **(11)**

Table 4.17 Key FTIR frequencies for structure **(11)**. [219, 220, 239]

Wavenumber/ cm^{-1}	**Assignment**
3473	Water ν(O-H), Aromatic ν (C-H) 4-MPy
3070	Aromatic ν (C-H) 4-MPy$[H]^+$
1633	Aromatic δ (C-N) 4-MPy$[H]^+$, γ(O-H)
1596	Water γ(O-H)
1500	CH_3 ν (C-H) 4-MPy$[H]^+$
1368	CH_3 ν(C-H)
786	Aromatic γ (C-H)

4.5.2.8 *Thermogravimetric Analysis*

TGA was carried out on **(11)** (Figure 4.30) in air and N_2**.** The small initial weigh-loss of *ca* 2 % at the beginning of both measurements may be arising from the removal of surface water from the sample. The following step is a weight-loss of a further *ca.* 13 %. This corresponds to the loss of water from the pores 6(H_2O). The next weight-loss of *ca.* 9 % corresponds to the loss of organic solvent (NC_6H_7). This leaves the 4-MPy cations; which should be more difficult to remove.

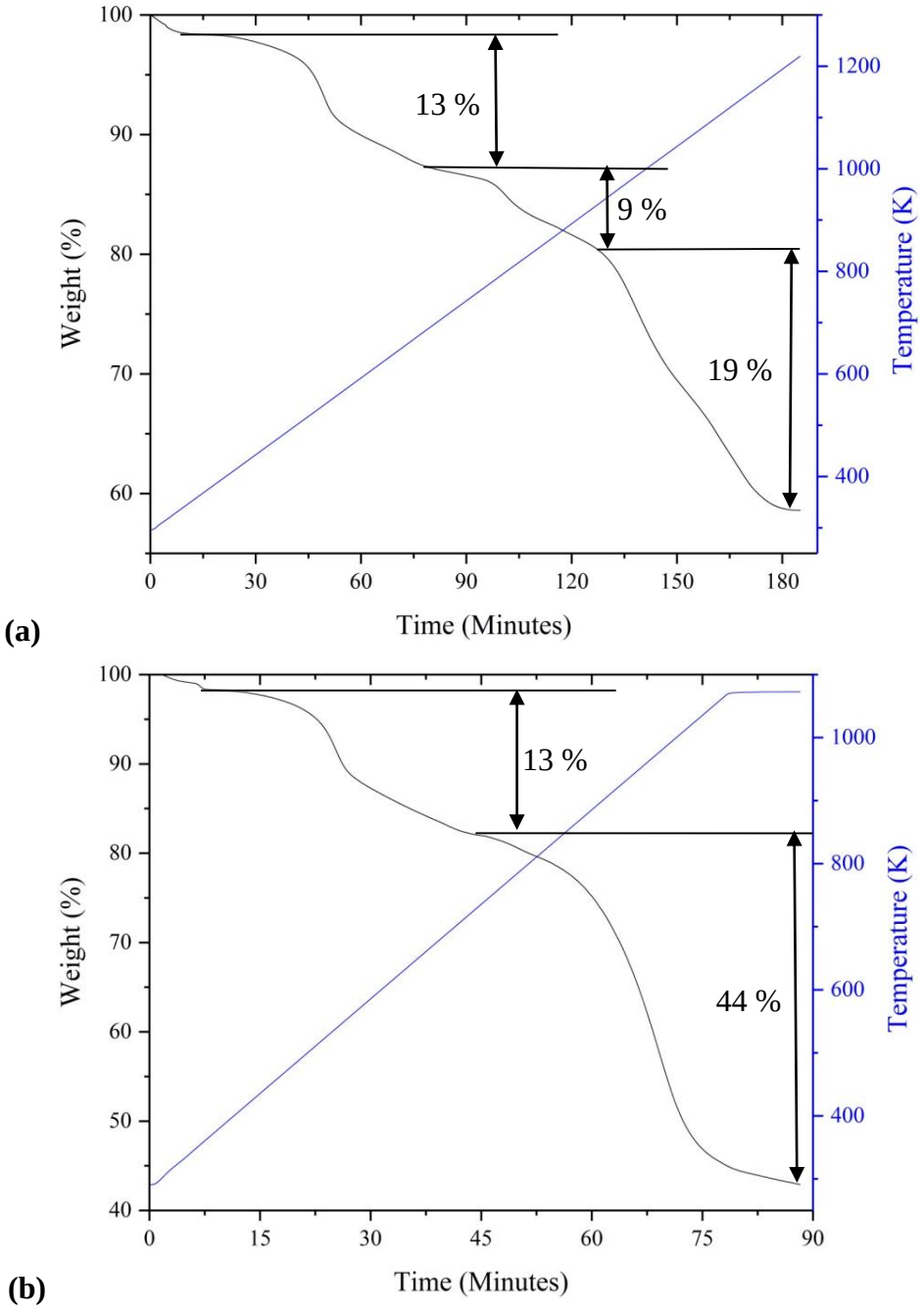

Figure 4.30 TGA data for sample **(11)** in **(a)** air and **(b)** N_2. Black shows weight percent vs time, blue shows temperature vs time.

When the sample is heated in air, it can be observed that the final weight is 59 %; consistent with a mixture of GeS_2, GeS and Ga_2S_3, although there is not enough sample remaining to analyse this using PXRD (Figure 4.30 **(a)**).. The temperature may not be sufficiently high to decompose the GeS_2 and Ga_2S_3 into GeO_2 and Ga_2O_3.

When the sample is heated under N_2, the final weight-loss is greater (Figure 4.30 **(b)**). This implies conversion of GeS and GeS_2 to GeO, as described for structures **(9)** and **(10)** when germanium is heated to high temperatures in a limited amount of oxygen.

A mixture of Ga_2S_3 and GeO would give the remaining weight of 43 %, matching the final weight-percent measured.

4.5.2.9 *UV-Vis Diffuse Reflectance*

Diffuse reflectance data were recorded on a sample of hand-picked crystals of **(11)** (Figure 4.31). The absorption edge of 3.37(2) eV, confirmed material **(11)** to be a wide-gap semiconductor. Compared with the values previously reported, this material has a wider band-gap than both **(10)**, at 3.10(5) eV and of a very similar value to **(9)** at 3.36(1) eV. This could suggest that the band gap increases with increasing dimensonaility and decreases with increasing Ga:Ge ratio. However, due to the fact that **(11)** does not consist of T2 clusters like materials **(9)** and **(10)** this is not fully conclusive.

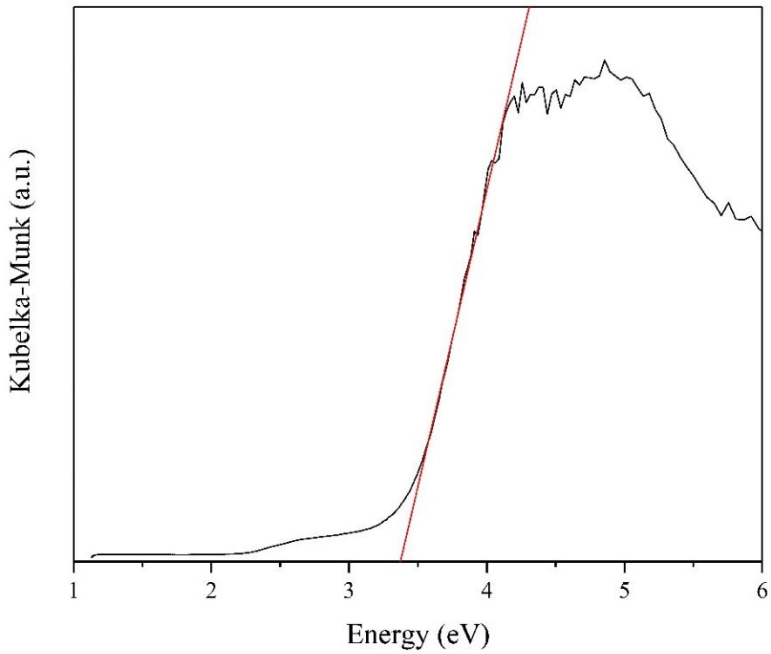

Figure 4.31 Diffuse reflectance graph for structure **(11)**. The absorption edge is shown by the red tangent-line.

4.5.3 **Discussion**

(11) can be formed under different sets of conditions, as described in more detail in Section 6.3.3.1. It has already been discussed that, although the structure does contain water, it can be formed without water present in the reaction mixture. It may end up in the pores of the structure during the washing step, as the structure has been measured to contain accessible void-space. To the best of our knowledge, this is the first 3-dimensional gallium-germanium sulphide that is not built from T2 supertetrahedra.

4.6 Discussion of Chapter

This chapter describes four different materials, synthesised with both gallium and germanium metals in the reaction mixtures. At the outset, the initial goal was to create hybrid supertetrahedra containing both metals; as this has not been done before with gallium and germanium existing in the same hybrid clusters. However, inorganic-frameworks based on gallium-sulphide supertetrahedra are well documented, as described in Section 1.4.4.[104, 184] From this work, it would appear that germanium does not favour forming hybrid-clusters, as these do not exist in the literature, except where post-synthetic modification of the clusters has been carried out.[120, 242]

Materials **(8)** to **(10)** illustrate that germanium favours the formation of T2 supertetrahedra; with the trimer **(8)** being a novel SBU, which unfortunately cannot be reproduced. It is unknown the specific reason why this has formed only once. The chains of T2 units **(9)** are previously known, however this is the first time the chains have been stabilized by $[4\text{-MPyH}]^+$.

Changing the reaction conditions can result in gallium being incorporated into the structure. In this case, a framework **(10)** based on mixed-metal T2 supertetrahedra can be formed, as previously described by Feng *et al.* with different amines.[104] When a specific Ga:Ge:S ratio is used, a novel germanium-gallium sulphide framework **(11)** is produced. To the best of our knowledge this is the first example of a gallium-germanium sulphide framework that is not based on T2 supertetrahedra. Although the pores of this structure are not large, there is accessible void-space, which appears to contain a mixture of 4-MPy cations and water. Materials **(9)** to **(11)** were synthesised on a number of occasions, as detailed in Section 6.3.3

Compounds **(9), (10)** and **(11)** were all found to be wide-gap semiconductors, in line with the yellow colours of the crystals and previously-reported band-gaps for germanium and gallium sulphides.[173, 237] If a framework such as **(11)** were to be formed with larger pores, this would give the structure potential to be used in catalysis, i.e. if pores were large enough to perform ion-exchange measurements.

5 Gallium Sulphides Synthesised using Superbases

5.1 Introduction

This chapter describes materials synthesised using the superbases DBU and DBN. The conjugate acids of these amines have higher pK_a values compared with the other amines used throughout this work (Section 2.1), such as 4-MPy (pK_a = 5.98) and Im (pK_a=6.95).

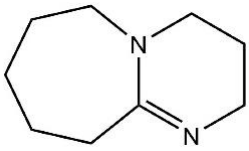

1,8-Diazabicyclo[5.4.0]-undec-7-ene (DBU) pK_a = 12.5

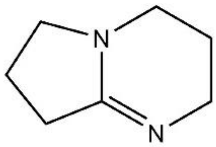

1,5-Diazabicyclo[4.3.0]-non-5-ene (DBN) pK_a = 12.7

Figure 5.1 Structures of superbases DBU and DBN.

Investigation of these amines was chosen based on the success of these in the production of the ISC (isolated supertetrahedral cluster) and SCIF (supertetrahedral chalcogenide imidazole framework) series by Feng *et al.*,[115, 116] as described in Section 1.4.5. In these cases DBU was used as a templating agent, in a solvent system of 2-amino-1-butanol and acetonitrile. There has not been much investigation into whether superbases can act as solvents for forming supertetrahedral-clusters.[116]

Superbases were used as both structure-directing agents and solvents, as described in Section 6.4 and outlined in Section 2.1.1. Both of these instances are featured here, although the materials produced differ substantially. Superbases were also used over weaker amines in surfactant-thermal synthesis reactions due to the milder conditions produced by using PEG rather than a basic solvent, as described in further detail in Sections 2.1.3 and 6.6.2.2.

5.2 T3 Clusters Synthesised with DBU and PEG-400

5.2.1 **Introduction**

Here, one crystal structure **(12)**, containing a T3 gallium-sulphide supertetrahedron is described. However, three different colours of crystals have been produced: colourless **(12a)**, yellow **(12b)** and red **(12c)**, all with the same unit-cell. Here, single-crystal data for the colourless crystals only are included, but other data are included for the different colours of crystal.

5.2.2 **Synthesis**

Compound **(12a)** $[C_9H_{18}N_2]_6[Ga_{10}S_{16}(SH)_4]$ was synthesised from Ga metal (133 mg, 2 mmol), TAA (389 mg, 5.2 mmol), DBU (0.5 ml, 3.35 mmol) and PEG-400 (4 ml). The reaction was carried out at 140 ^oC for 6 days. The resulting product was a mixture of colourless crystals of **(12a)** and unreacted Ga metal.

Material **(12b)** was synthesised from Ga metal (133 mg, 2 mmol), TAA (389 mg, 5.2 mmol), DBU (0.5 ml, 3.35 mmol) and PEG-400 (4 ml). The reaction was heated at 160 ^oC for 6 days. The resulting product consisted of yellow crystals of **(12b)**. The same product was formed when the amount of DBU was doubled to 1 ml (6.7 mmol).

(12c) was produced by the reaction of Ga metal (133 mg, 2 mmol), S powder (172 mg, 5.37 mmol) and DBU (1 ml, 6.7 mmol) in PEG-400 (4 ml). This reaction was carried out at 160 ^oC for 6 days. The product consisted of a mixture of brown/red crystals of **(12c)** and unreacted Ga metal.

In all cases where further measurements have been carried out, these have been taken from samples of handpicked crystals.

5.2.3 **Structure and Characterisation**

5.2.3.1 ***Single-Crystal X-Ray Diffraction***

Single-crystal data (Table 5.1) for **(12a)** were collected by the NCS,[204] due to the fragility of the crystals. When attempts were made to collect this data at the University, crystals were found to gradually degrade during data collection, meaning that the structure could not be solved from the data obtained. Solvent molecules were located using Fourier difference maps. Two of the DBU moieties were refined isotropically due to disorder, whereas the other four were refined anisotropically. Many of the C-C and C-

N bonds have been restrained in the isotropic DBU moieties, based on the literature values for bond lengths in DBU.[243] All H-atoms were added geometrically and Platon SQUEEZE was used to confirm that all solvent molecules had been found.[206]

Table 5.1 Selected Single-Crystal X-ray Diffraction Data and Refinement Details for **(12a).**

Formula	$[C_9H_{18}N_2]_6[Ga_{10}S_{16}(SH)_4]$
Mr	2257.88
Crystal habit	Colourless Octahedral
Crystal system	Monoclinic
Space group	$P2_1$
***T*/K**	100
***a, b, c*/Å**	14.1675(3), 14.1898(3), 21.3007(4)
***β*/º**	90.5730(18)
***V*/Å^3**	4281.95(15)
Z	2
θ_{max}	27.485
ρ_{cal}/gcm^{-3}	1.751
μ/mm^{-1}	3.623
T_{min},T_{max}	0.805,0.947
Number of parameters	755
Number of reflections used in refinement	17,010
Total number of reflections	19,636
R_{merge}	0.0606
$R(I>3.0\sigma(I))$	0791
R_w	0.0762
Flack Parameter	0.064(10)

5.2.3.2 *Structure Description*

The asymmetric unit of **(12)** contains a T3 $[Ga_{10}S_{20}]^{10-}$ supertetrahedron (Figure 5.2) and six DBU moieties. Unlike those described in Chapter 3, the cluster in **(12)** does not have ligands co-ordinating to the corner gallium-sites; therefore is an inorganic cluster. Due to the cluster containing four more sulphur atoms compared to the hybrid clusters, it has a greater negative-charge. This is thought to be the reason for the large solvent-content within the structure; due to the large number of DBU cations required to balance the charge of 10-. As each of the six DBU moieties can only be monoprotonated, four further protons are needed in order to balance the anionic cluster. It is therefore proposed that the corner S-atoms are protonated, giving a formula of $[Ga_{10}S_{16}(SH)_4]^{6-}$ for

the cluster. Including the DBU cations, the overall formula for **(12)** is $[Ga_{10}S_{16}(SH)_4][C_9H_{18}N_2]_6$.

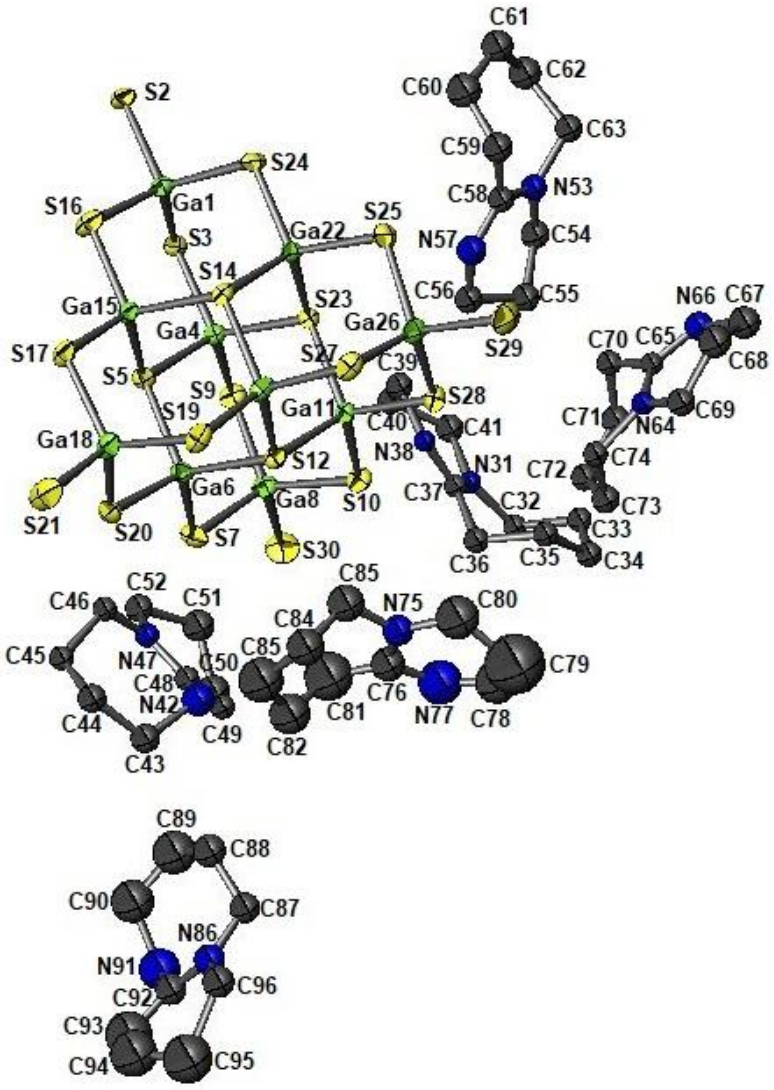

Figure 5.2 Asymmetric unit of **(12).** Green = Ga, yellow = S, blue = N, grey = C. H-atoms have been omitted for clarity.

Ga – S bonds are in the range of 2.217(2) -2.333(2) Å, where those in -Ga-S-H groups are in the range of 2.279(2) – 2.292(3) Å.[114] This can be compared to a material previously reported by Vaqueiro *et al.* where the Ga-S bond-lengths were reported to be 2.2681(7) Å. Although the bonds reported here are slightly longer than previously reported, the material in comparison is the compound $(C_7H_{10}N)_6$ - $[Ga_{20}S_{34}H_2(NC_7H_9)_4(N_2C_{12}H_{10})]$, which consists of dimers or hybrid T3 clusters, linked through a bipy moiety. As only one of the corners on each supertetrahedron contains the –Ga-S-H linkage and the others consist of a Ga-N bond, this could cause a difference in this bond length. S-Ga-S angles are in the range of 100.21 – 115.66 °, where the angles

most distorted from the ideal tetrahedral-value of 109.5 º occur at the corners of the clusters. i.e. S(2)-Ga(1)-S(3) =100.21(8) º, S(3)-Ga(1)-S(16) = 115.16(9), S(9)-Ga(8)-S(30) = 102.69(9) º, S(7)-Ga(8)-S(9) = 115.13(9) º, S(19)-Ga(18)-S(21) = 101.30(11) º, S(19)-Ga(18)-S(20) = 115.48(9) º, S(27)-Ga(26)-S29 = 103.15(10) º and S(28)-Ga(26)-S(29) = 105.66(10) º.

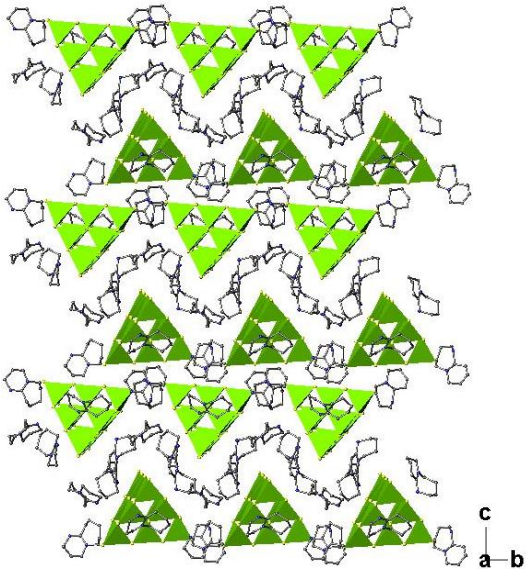

Figure 5.3 Structure of **(12)**, viewed along the *a*-axis. Green tetrahedra = $[GaS_4]^{5-}$, yellow = S, blue = N, grey = C. H-atoms have been omitted for clarity.

When the structure of **(12)** is viewed along the *a*-axis (Figure 5.3), it can be observed that the supertetrahedra propagate along the *b*-axis, with DBU moieties separating the rows of clusters. The organic molecules also appear to propagate in this direction; while aligning with the edges of the clusters.

It is a possibility that the DBU moieties have been templated to form this pattern by the long-chain PEG-400 surfactant, which could have directed the DBU cations to align along the *b*-axis. The DBU moities are also arranged in this way running along the *a*-axis. The DBU cations also exhibit H-bonding with the clusters; with N-S distances of between 3.20(1) and 3.85(1) Å.

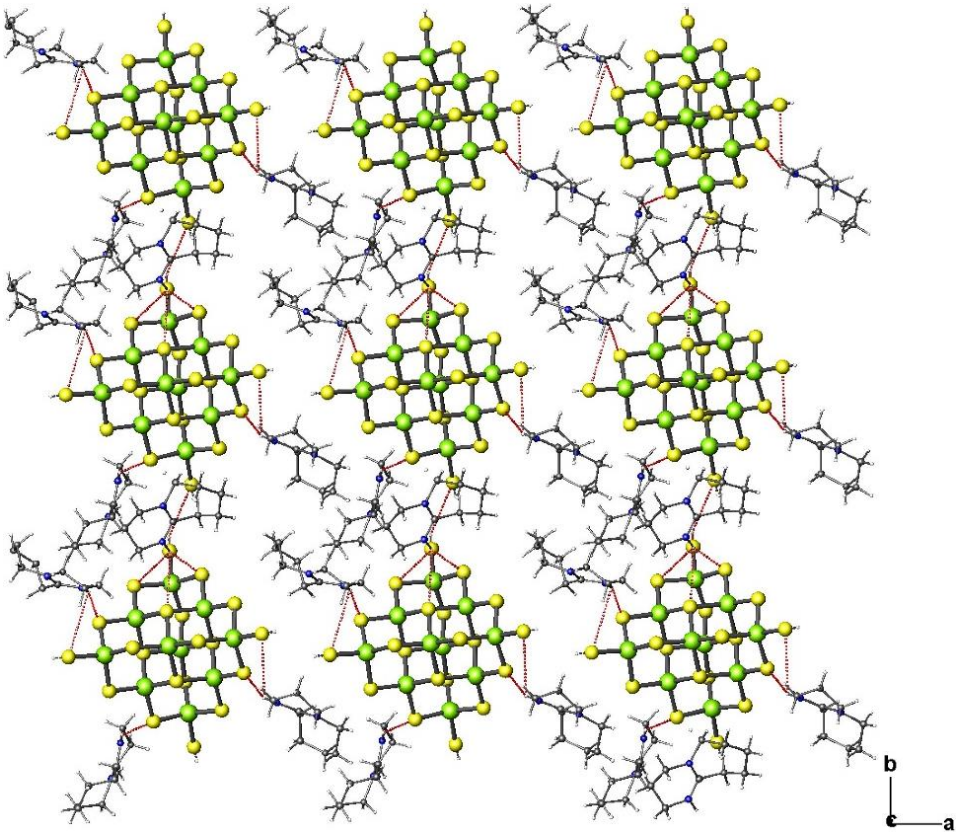

Figure 5.4 H-bonding network in **(12)**, viewed along the *c*-axis. Green = Ga^{-}, yellow = S, blue = N, grey = C, red dotted lined = H-bonds.

5.2.3.3 *Powder X-Ray Diffraction*

PXRD was carried out on **(12a)**, **(12b)**, and **(12c)** (Figure 5.5). These measurements suggest that all samples consist of the same phase; that of **(12)**, as determined from the SCXRD. Refining lattice parameters (

Table 5.2) showed a good agreement between all three samples.

Table 5.2 Lattice parameters for **(12).** Parameters were refined against PXRD using DASH.[208]

SCXRD	***a*/ Å**	***b*/ Å**	***c*/ Å**	**α/ º**	**β/ º**	**γ/ º**
	14.1675(3)	14.1898(3)	21.3007(4)	90	90.5730(18)	90
PXRD (12a)	***a*/ Å**	***b*/ Å**	***c*/ Å**	**α/ º**	**β/ º**	**γ/ º**
	14.294(1)	14.255(6)	21.306(1)	90	90.86(6)	90
PXRD (12b)	***a*/ Å**	***b*/ Å**	***c*/ Å**	**α/ º**	**β/ º**	**γ/ º**
	14.293(5)	14.251(3)	21.300(3)	90	90.83(7)	90
PXRD (12c)	***a*/ Å**	***b*/ Å**	***c*/ Å**	**α/ º**	**β/ º**	**γ/ º**
	14.213(8)	14.189(8)	21.300(7)	90	90.79(5)	90

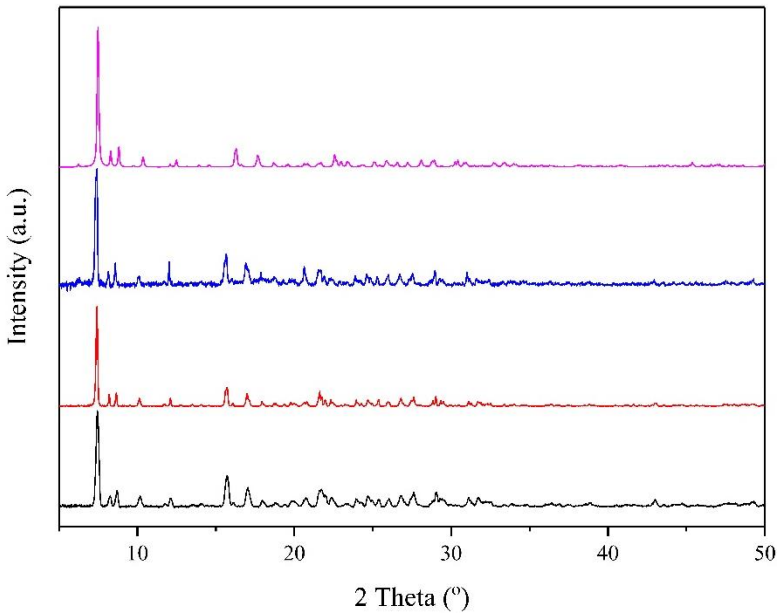

Figure 5.5 PXRD of **(12) (a)** (black line), **(b)** (red line), **(c)** (blue line) and simulated from SCXRD (magenta line).

The small increase in the lattice parameters for the PXRD compared with the SCXRD could be due to the fact that SCXRD measurements were carried out at 150 K, whereas PXRD was carried out at room temperature.

5.2.3.4 *Elemental Analysis*

CHN analysis was carried out on **(12) (a)**, **(b)** and **(c).** Data from clear crystals of **(12a)** agree with the experimental data, confirming the formula $[Ga_{10}S_{16}(SH)_4][C_9H_{18}N_2]_6$ (Experimental: C = 28.62 %, H = 4.68 %, N = 7.30 %. Calculated: C = 28.6 %, H = 4.98 %, N = 7.41 %). There are no distinct differences between the elemental analyses of the colourless and yellow crystals. Yellow crystals of **(12b)** gave values to support the crystallographically-determined formula (Experimental: C = 28.3 %, H = 4.61 %, 7.23 %).

Unfortunately, due to the presence of large amounts of Ga metal on the surface of crystals of **(12c)**, elemental analysis could not be carried out on the pure material. CHN analysis was attempted on this material on two occasions. One of these samples contained a number of crystals; but analysis indicated that the sample was non-homogenous. A second sample was sent for analysis, after sonication in ethanol, which was thought to have had all Ga removed. This sample was ground into powder when sent for CHN analysis and gave percentage values of C = 24.0 %, H = 3.77 %, N = 6.00 %. This is inconsistent with the calculated values for this material; however, it

shows the same ratio of C:H:N of *ca.* 6:1:1.5. This is consistent with not only the values calculated for **(12)**, but also all values measured from the non-homogenous sample. This could imply that the sample is still contaminated with Ga metal and in all cases this greatly affected the result.

5.2.3.5 *Infrared Spectroscopy*

FTIR was carried out on **(12) (a)**, **(b)** and **(c)** (Figure 5.6). Key FTIR frequencies for these materials are shown in Table 5.3.

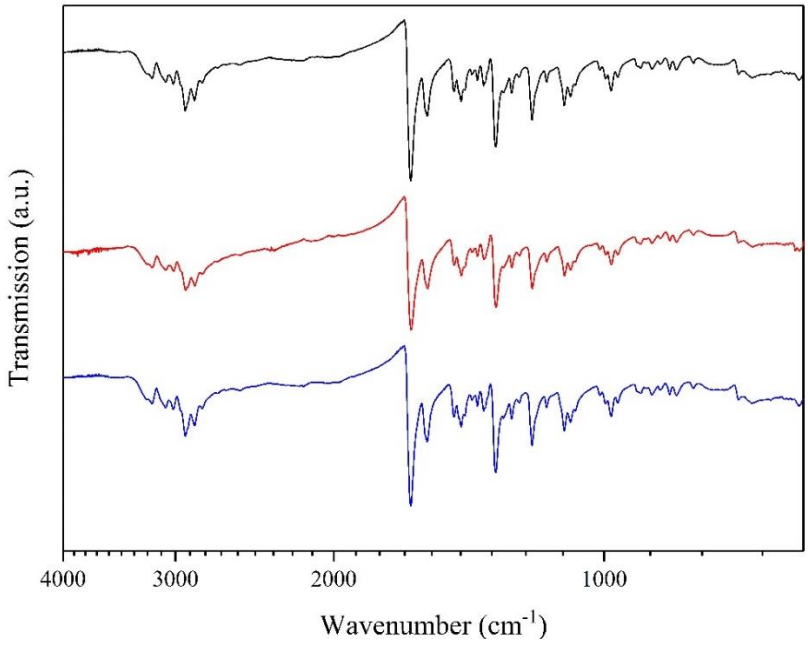

Figure 5.6 FTIR of **(12) (a) (**black line**), (b)** (red line), and **(c)** (blue line).

It can be observed (Figure 5.6) that there appear to be no differences between the FTIR spectra of the three materials. The frequencies in the spectra correspond to the amine DBU (Table 5.3) and N-H stretches present in the spectra indicate the presence of protonated DBU moieties, along with the other characteristic frequencies for DBU. The –S-H frequency would be expected to occur at *ca.* 2600 cm^{-1} and is usually very weak so therefore cannot be observed in this spectrum.

Table 5.3 Key FTIR frequencies in **(12) (a), (b)** and **(c).**

Wavenumber/ cm^{-1}	**Assignment**
3204, 3083, 3008	ν (N-H)
2922, 2853	ν (C-H)
1567, 1636	ν (C-N)
1330-1440	CH_2 γ (C-H)

5.2.3.6 *Thermogravimetric Analysis*

TGA measurements were carried out on samples of **(12a)** and **(12b)** (Figure 5.6). Due to the issue of Ga metal contamination in **(12c)** (Section 5.2.3.3) TGA was not possible for this material. The measurements performed on **(12a)** and **(12b)** show consistency between the colourless and yellow crystals; confirming what was suggested by CHN analysis (Section 5.2.3.4).

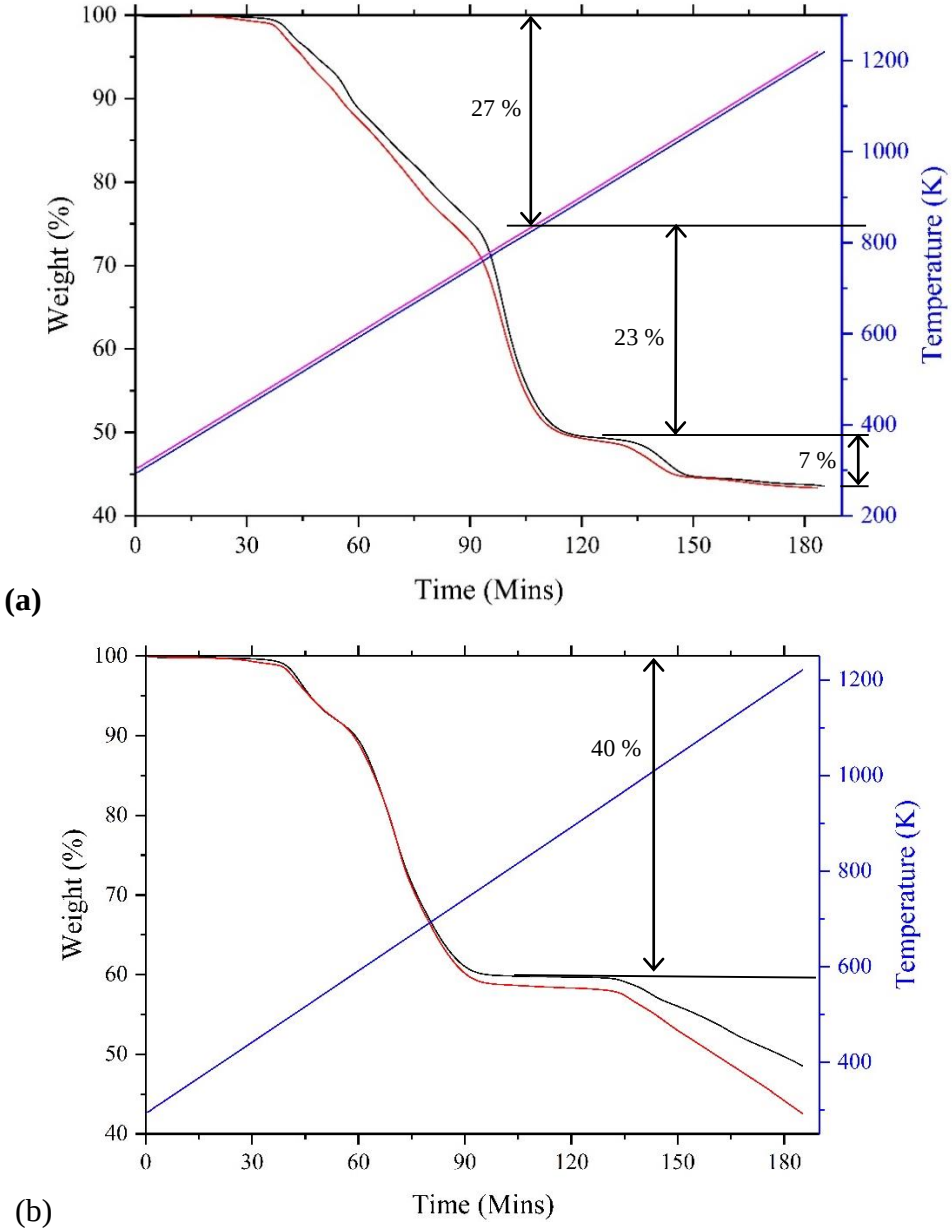

Figure 5.6 TGA in **(a)** air and **(b)** under N_2. Weight % vs. time = black line for **(12a)** and red line for **(12b)**. Temperature vs. time = blue line for both **(12) (a)** and **(b)** under N_2 and **(12a)** only in air. Temperature vs. time = magenta for **(12b)** in air.

The measurements in air (Figure 5.6 **(a)**) show three weight-loss steps. The first of these corresponds to the loss of the non H-bonded protonated DBU species

4$[C_9H_{18}N_2]^+$. The following weight-loss step corresponds to the removal of the H-bonded protonated DBU species 2$[C_9H_{18}N_2]^+$. This leaves a remaining product of Ga_2S_3 at *ca.* 50 %. This then decomposes further into Ga_2O_3; accounting for the final weight-difference of 7 % and leaving a final weight of *ca.* 43 %.

When TGA was carried out under N_2 (Figure 5.6 **(b)**), not all of the weight-loss steps are present and the material has not fully decomposed at 1200 K. The weight loss of 40% observed corresponds to the loss of all protonated DBU moieties. The next decomposition step has not been completed at the final temperature.

5.2.3.7 *UV-Vis Diffuse Reflectance*

Diffuse-reflectance measurements were carried out on all three colours of crystals of **(12)** (Figure 5.7) to confirm the colour differences and also to determine the optical band-gaps of the materials.[115]

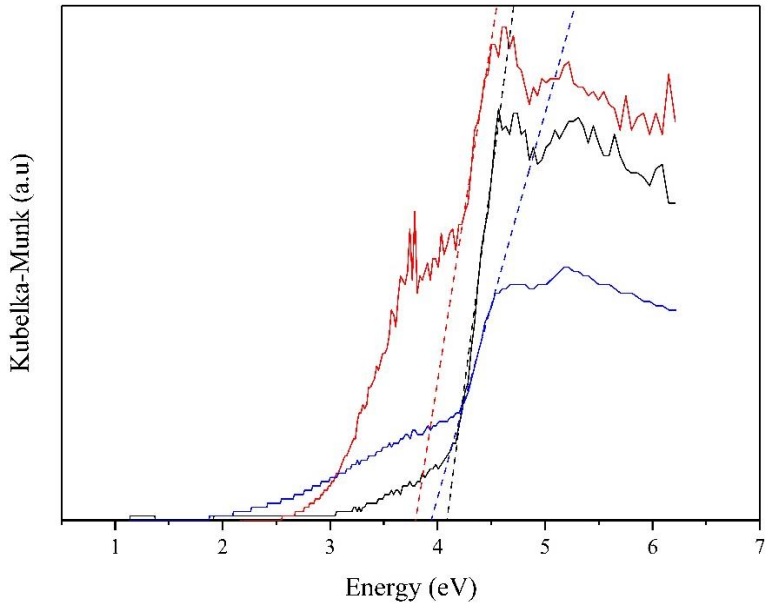

Figure 5.7 UV-vis diffuse reflectance of **(12) (a)** (black line), **(b)** (red line), and **(c)** (blue line). Corresponding dashed-lines show the absorption edges for each material.

UV-Vis diffuse reflectance data (Figure 5.7) showed that the absorption edge for colourless crystals of **(12a)** is 4.10(1) eV; this band gap is in the region where the material could be considered to be an insulator and confirms the colourless nature of the crystals.

Yellow crystals of **(12b)** and red crystals of **(12c)** displayed absorption edges of 3.75(4) and 3.95(2) eV respectively. These band gaps are in the region where yellow-colourless crystals would be expected. However, it can be observed in Figure 5.6 that both materials show additional bands at lower energies. It is suggested that these are charge-transfer bands of a similar nature to those described in Section 3.6.1. In this case,

there are no ligands coordinated to the corners of the clusters; therefore charge transfer would have to occur between the clusters and the organics within the material. Although **(12b)** and **(12c)** appear to be of different colours, based on the small change in band gap and similarity in the positions of the charge-transfer peaks, it is possible that the colour appears to be stronger due to the large size of the crystals of **(12c)** compared with **(12b)**.

It could be suggested that the varying colour comes from defects in the yellow and red crystals. Pathak *et al.* described this effect in $ZnAl_2O_4$, which has the spinel structure,[244] where different colours were observed and said to arise from defects in the material and are observed as shifts in the diffuse-reflectance peaks from the materials.

5.2.4 **Discussion**

Data for material **(12)**, for which the structure has been determined from colourless crystals of **(12a)**, were collected on crystals of three different colours. **(12b)** and **(12c)** were found to appear yellow and red colours respectively. It is possible that the appearance of different colours stems from the difference in size between the crystals in the two samples. Although **(12c)** contains larger crystals; the large amounts of Ga metal present in the sample prevented in-depth analysis on this sample. It is possible that this large amount of Ga is key to the formation of large crystals in the sample, which may grow on the surface of the metal.

Materials reported by Wu *et al.* were synthesised with DBN, in the absence of a surfactant.[115] There were a number of materials reported in this publication, of which some were similar to **(12)**. The material ISC-3 consisted of T3 indium-sulphide clusters, with DBN coordinated to the corners. This material is also reported to be colourless. It is stated in this work that when DBU is used, it does not coordinate to the corners due to its size. The only material reported to contain DBU contains a T5 cluster and it is not stated that attempts to create T3 clusters with DBU were carried out.[115] This could imply that coordination of the superbase to the corners of the cluster would not necessarily cause a colour change, however the difference in metal and superbase here make it a difficult comparison to make.

The only difference between reaction parameters when producing the yellow or colourless crystals is the reaction temperature; **(12a)** is formed at 140 ^{o}C, whereas **(12b)** is formed at 160 ^{o}C. This temperature difference could affect the crystallisation of the product and cause a difference in solvent arrangement; however solvent location has not been determined from SCXRD for **(12b)**.

As described in Sections 1.4.3 and previously for this material. Currently, gallium-sulphide T3 supertetrahedra exist in either corner-sharing interpenetrating lattices or as hybrid supertetrahedra.[105, 113, 119] Although clusters with –SH terminating the corners do exist, [114, 245] this is the first example of a T3 gallium-sulphide supertetrahedral cluster that exists as a discrete unit with no organic-ligands coordinated to the corners.

5.3 Chains Synthesised in DBN

5.3.1 Synthesis

(13) was synthesised from Ga metal (70 mg, 1 mmol), GeO_2 (109 mg, 1 mmol), S powder (178 mg, 5.6 mmol) and TMDPy (206 mg, 1 mmol) in DBN (3 ml, 24 mmol). The reaction resulted in a mixture of brown crystals of **(13)** and a large amount of Ga metal.

5.3.2 Structure and Characterisation

5.3.2.1 *Energy-Dispersive X-Ray Analysis*

As both Ga and GeO_2 were used in the reaction mixture, EDX was carried out to determine the metal content in **(13)**. EDX showed that the structure only contained Ga and no Ge. Figure 5.8 shows an example spectrum recorded on **(13)** and the region on which it was measured is shown in Figure 5.9. A total of eight spectra were recorded from two different crystals, with four different areas on each crystal explored. All of these sites showed that the sample contained no germanium.

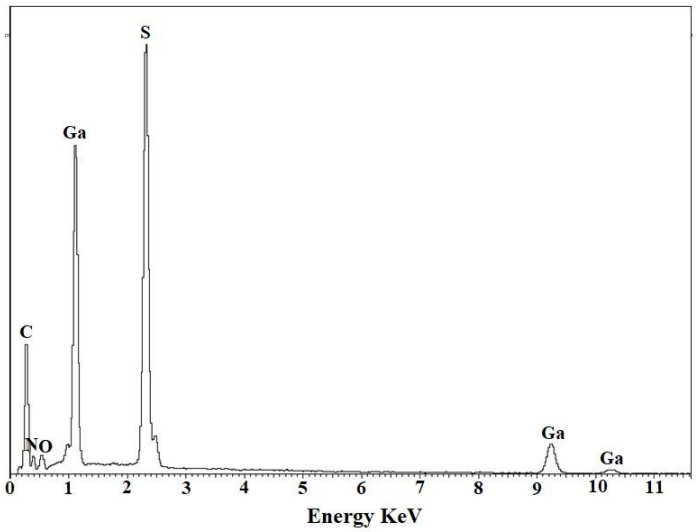

Figure 5.8 EDX data for **(13)**

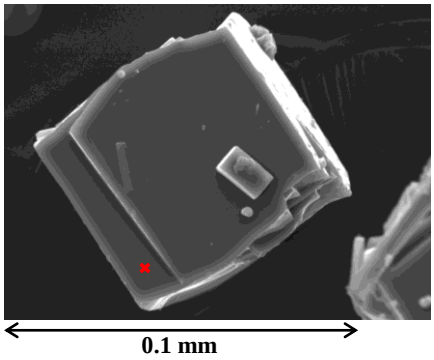

Figure 5.9 SEM image of **(13)** showing the area from which the measurement was taken (red).

5.3.2.2 *Single-Crystal X-Ray Diffraction*

SCXRD was carried out on a single crystal of **(13) (**Table 5.4**)**. Some C, N and H atoms were placed using the Fourier difference map. The DBN moiety, which is disordered over two sites, was modelled isotropically. The disordered DBN moiety is found in two opposite orientations within the asymmetric unit; each of the orientations has been modelled with an occupancy of 0.5.

Table 5.4 Selected single-crystal X-ray diffraction data and refinement details for **(13).**

Formula	$[C_7H_{13}N_2][GaS_2]$
Mr	274.05
Crystal habit	Brown Block
Crystal system	Orthorhombic
Space group	P*ccn*
***T*/K**	150
***a, b, c*/Å**	12.7557(5), 12.7673(5), 6.0362(2)
***V*/Å^3**	983.03(6)
Z	4
θ_{max}	32.158
ρ_{cal}/gcm^{-3}	1.852
μ/mm^{-1}	3.179
T_{min},T_{max}	0.826,0.881
Number of parameters	51
Number of reflections used in refinement	1030
Total number of reflections	1556
R_{merge}	0.0371
$R(I>3.0\sigma(I))$	0.0505
R_w	0.0497

5.3.2.3 *Structure Description*

The asymmetric unit of **(13)** (Figure 5.10) contains one Ga atom and one S atom, with a Ga-S bond length of 2.2905(10) Å and resulting in a S-Ga-S angle of 115.71(4) °. Along with the inorganic component, the unit contains half of a DBN moiety. It can be observed (Figure 5.8) that the DBN is disordered over two sites with opposite orientations. Therefore, the moiety has been modelled as described in Section 5.3.2.1.

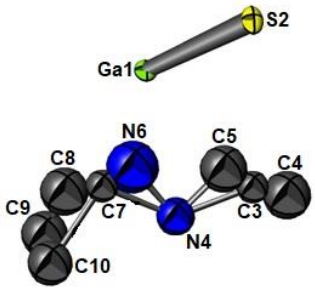

Figure 5.10 Asymmetric unit of **(13).** Green = Ga, yellow = S, blue = N, grey = C. H-atoms have been omitted for clarity.

The Ga and S atoms are bonded into a $[GaS_4]^{5-}$ tetrahedron, with each tetrahedron corner-sharing two S atoms with the adjacent cluster (Figure 5.11). This creates a chain of edge-sharing $[GaS_4]^{5-}$ tetrahedra with a resulting formula of $[GaS_2]^-$. The negative charge of the chains is balanced by one protonated DBN moiety per Ga site (Figure 5.11 and Figure 5.12). This gives a resulting formula of $[GaS_2][C_7H_{13}N_2]$.

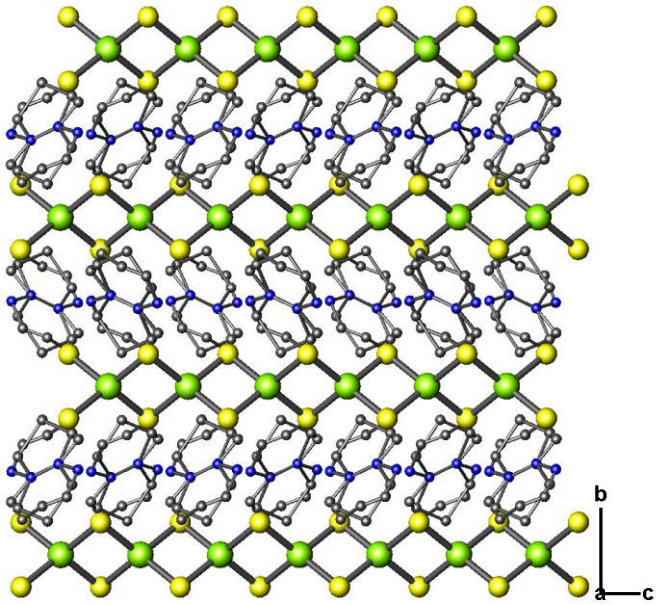

Figure 5.11 (13) viewed along the *a*-axis. Green = Ga, yellow = S, blue = N, grey = C. H-atoms have been omitted for clarity.

Figure 5.12 shows **(13)** viewed along the *c*-axis, along which the $[GaS_2]^{n-}_n$ chains propagate. The N-S distances between the N-H groups and the sulphur atoms on the chains are 3.74(5) Å and therefore H-bonding is apparent in the material.

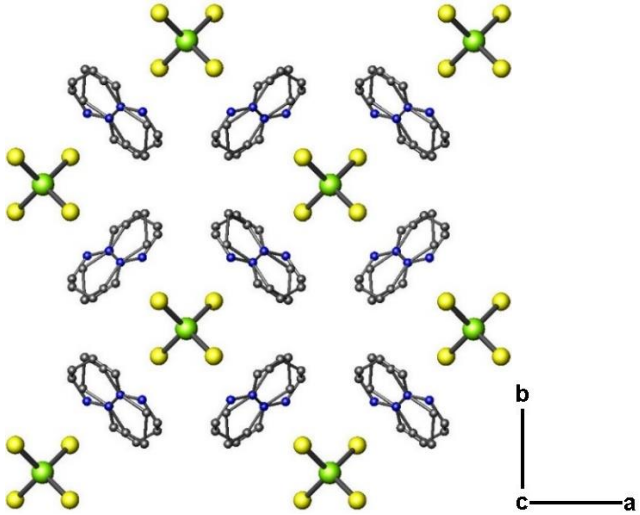

Figure 5.12 (13) viewed along the *c*-axis. Green = Ga, yellow = S, blue = N, grey = C. H-atoms have been omitted for clarity.

Chains of this nature have been synthesised on a number of occasions for different metal-chalcogenides, as described in Section 1.4.6.[123, 126, 129]

5.3.2.4 *Powder X-Ray Diffraction*

PXRD was carried out on the bulk sample of **(13)** (Figure 5.13). This showed that the structure of the bulk sample is consistent with that determined from SCXRD.

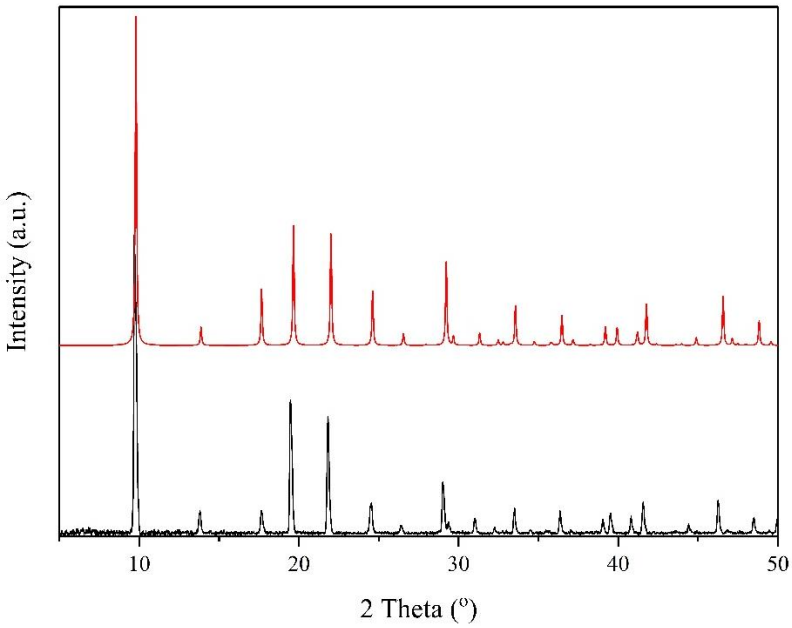

Figure 5.13 PXRD of **(13)** (black line) and simulated from SCXRD (red line).

Table 5.5 Lattice parameters for **(9).** Parameters were refined against PXRD using DASH.[208]

SCXRD	***a*/ Å**	***b*/ Å**	***c*/ Å**	**α/ º**	**β/ º**	**γ/ º**
	12.7557(5)	12.7673(5)	6.0362(2)	90	90	90
PXRD	***a*/ Å**	***b*/ Å**	***c*/ Å**	**α/ º**	**β/ º**	**γ/ º**
	12.833(4)	12.762(1)	6.0410(1)	90	90	90

5.3.2.5 *Elemental Analysis*

CHN analysis was carried out on **(13)**, however samples containing **(13)** also contained a large amount of Ga metal; mainly on the surface of the crystals. As described for **(12c)**, this made collecting a pure sample of crystals extremely difficult. Samples were sonicated in ethanol in an attempt to remove the Ga metal from the crystals and a sample was sent for analysis.

Two different samples were submitted; one of crystals which was found to be non-homogenous and one in which crystals were ground. It was thought that all Ga had been removed by sonication in this case. Values for **(13)** were calculated to be C = 32.46 %, H = 5.06 %, N = 10.81 %, which differ from the experimental values of C = 29.14 %, H = 4.11 % and N = 8.68 %. The C:H:N ratio from the sonicated sample was found to be 7.25:1:2.13, compared with 6.5.1:2 calculated for DBN. It is therefore possible that the sample is contaminated with Ga metal, which will not show up in PXRD as it is a liquid just above room temperature.

5.3.2.6 *Infrared Spectroscopy*

FTIR spectroscopy was carried out on **(13)** (Figure 5.14). Key frequencies are listed in Table 5.6 and support the evidence that protonated DBN cations balance the charge of the anionic chains in **(13)**.

Table 5.6 Key FTIR frequencies in **(13)**

Wavenumber/ cm^{-1}	**Assignment**
3187, 3097	ν (N-H)
2935, 2863	ν (C-H)
1677, 1584	ν (C=N)
1378-1447	CH_2 γ (C-H)

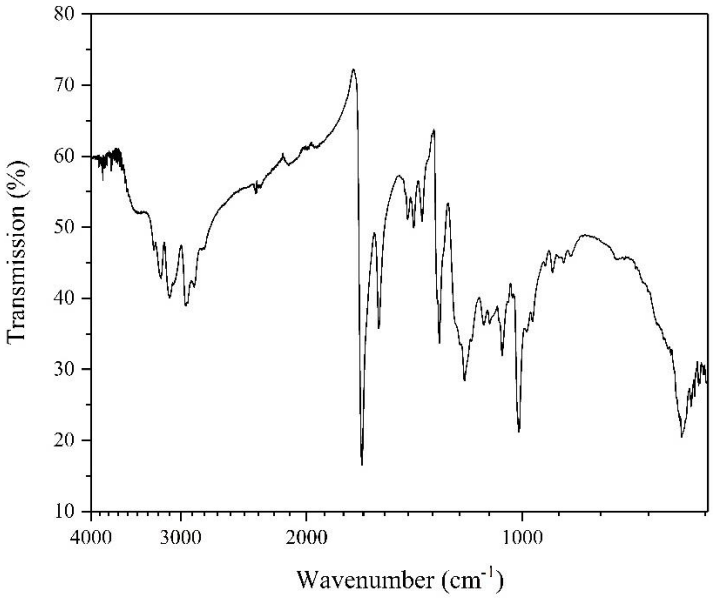

Figure 5.14 FTIR of **(13).**

5.4 Discussion

(13) was synthesised from Ga metal and S in DBU; with the auxiliary amine TMDPy. The material produced was a one-dimensional gallium-sulphide chain, whose negative charge is balanced by protonated DBN moieties, disordered over two sites. Due to the large amounts of Ga metal on the surface of the crystals, as described in Section 5.3.2.5, it was not trivial to obtain pure samples of crystals of **(13)**. This meant that a sufficiently-pure sample could not be obtained for TGA or diffuse-reflectance measurements.

This material resembles a number of compounds previously reported by Vaqueiro *et al.*. These include $[M(en)_3]_{0.5}[GaS_2]$ (M=Co, Mn, Ni),[123] where the chains are charge balanced by organometallic complexes and also both indium and gallium-sulphide chains balanced by 1,4-bis(3-aminopropyl)piperazine (APP) cations.[125] Alongside the sulphide chains; Ewing has also reported the formation of indium-selenide chains with the same connectivity. In this case; chains were charge balanced by ammonium cations, though synthesis was carried out in 3,5-Lut.[124] Those described in Section 1.4.6 show different packing to **(13)**, along with the material synthesised by Romero *et al.* These materials show rotation of the chains with respect to each other throughout the structure, whereas the packing in **(13)** resembles the material $KFeS_2$, a material for which the crystal structure was reported in 1942.[246, 247] In this case the chains are always aligned, as shown in Figure 5.12.

6 Overview of Synthesis Methods and Unexpected Syntheses

6.1 Introduction

6.2 Ionothermal Synthesis

6.2.1 **Introduction**

Reactions were carried out to investigate whether new hybrid gallium-sulphide materials can be produced using ionothermal synthesis. Compounds **(1)** and **(2)** contain the discrete clusters $[Ga_{10}S_{16}(NC_6H_7)_4]^{2-}$, as described in Section 0 and were synthesised using ionic liquids as templates. Research was carried out to determine whether a reaction of a compound containing discrete supertetrahedral-clusters, in a mixture of ionic liquid and a chosen ditopic-ligand, would allow clusters of this type to be linked into structures of higher dimensionalities.

Xiong *et al.* reported synthesising new hybrid T5 gallium-copper sulphides in the ionic liquid 1-butyl-3-methylimidazolium chloride ([BMMIm]Cl),[155] as described in Section 1.5.1. using the precursor $[enH]_2[Ga_4S_7(en)_2]$ (en = ethylenediamine), first synthesised by Vaqueiro (Sections 1.4.6.1 and 6.2.2.3).[123]. The resulting structures did not contain SBUs from the original material, which broke down during the reaction. In this chapter, syntheses based on this method are presented, where the precursor used by Xiong was substituted with the material $[C_6H_8N]_6[C_{12}H_{10}N_2]_2[Ga_{10}S_{16}(NC_6H_7)_4]_4 \cdot (C_{12}H_{12}N_2)_2$ containing discrete T3 hybrid clusters (Section 6.2.2.2). This material is isostructural to **(1)** (Section 6.2.2.2) and was initially synthesised by Romero.[119]

Reactions were also carried out using the same precursor used by Xiong *et al.* (Section 6.2.2.3). For both precursors, different auxiliary-amines were explored. Time, temperature and stoichiometry were also varied throughout (Table 6.1). The aim here was to explore whether new structures could be made based on this method, either by substituting the starting material with one containing a T3 supertetrahedron and/or changing other parameters.

6.2.2 Reactions Using the Precursors $[C_6H_8N]_6[C_{12}H_{10}N_2]_2[Ga_{10}S_{16}(NC_6H_7)_4]_4$ and $[enH]_2[Ga_4S_7(en)_2]$

6.2.2.1 *Synthesis*

Reaction conditions were used for these reactions as specified in Table 6.1. A full list of reactions carried out during this work is included in Appendix 1.

The precursor $[enH]_2[Ga_4S_7(en)_2]$ was synthesised using a modified reaction-method reported by Xiong *et al.*[155] It was produced from gallium metal (3.4 mmol, 237 mg) and sulphur (6.8 mmol, 218 mg) in ethylenediamine (50.9 mmol, 3.4 ml). The reagents were heated in an autoclave for 5 days at 170°C, confirmed by PXRD (Figure 6.5).

Table 6.1 Parameters changed while using $[C_6H_8N]_6[C_{12}H_{10}N_2]_2[Ga_{10}S_{16}(NC_6H_7)_4]_4$ and $[enH]_2[Ga_4S_7(en)_2]$ as precursors.

Parameter Varied	Used
Solvent	[BMMIm]Cl, $[BMMIm]BF_4$
Auxiliary Amine	DMA (40 % in H_2O), TMDPy, Im, en, DMM, 4-MPy
Temperature/ °C	160,170, 200
Time/ Days	6, 13

TMDPy = 4,4'-trimethylenedipyridine, Im = imidazole,
DMM = 2,6-dimethylmorpholine (Figure 6.1).

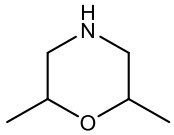

2,6-Dimethylmorpholine
DMM

Figure 6.1 Structure of 2,6-dimethylmorpholine

6.2.2.2 *Results and Discussion from Precursor $[C_6H_8N]_6[C_{12}H_{10}N_2]_2[Ga_{10}S_{16}(NC_6H_7)_4]_4$*

$Cu(NO_3)_2$ has been used in these reactions. During initial experiments, a number of reactions were carried out in the absence of copper(II) nitrate (Appendix 1.6). In the reactions where it was omitted, no solid product was formed. This implies that in the absence of $Cu(NO_3)_2$, solubility of the product is too high. The amount of ionic liquid was halved to determine whether this would solve this; however there was still no product formed. In order to determine whether it is the nitrate species that is important for the

formation of solid during the reaction, $Cu(NO_3)_2$ was replaced with $Ga(NO_3)_3$. The reactions gave no products, therefore $Cu(NO_3)_2$ is needed to give a solid.

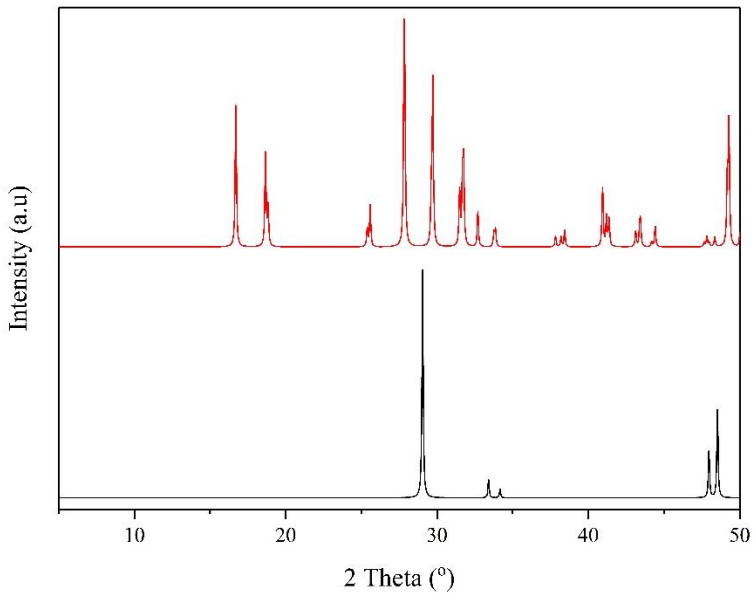

Figure 6.2 Calculated PXRD of gallite (black line) and monoclinic α- Ga_2S_3 (red line).

The products of these reactions are poorly crystalline, but analysis of the powder X-ray diffraction data suggest that the peak positions in many of these products correspond Ga_2S_3, for which a simulated powder-pattern in shown in Figure 6.2. Peaks could also correspond to the mineral gallite, with the formula $CuGaS_2$ (Figure 6.2); a possible product of reactions containing sulphur, gallium and copper nitrate. The need for $Cu(NO_3)_2$ to form a solid is consistent with the formation of gallite rather than Ga_2S_3.

Figure 6.3 **(b)** shows the results of reactions using TMDPy as the auxiliary amine. These samples are weakly crystalline (Figure 6.3 **(b)**). It is suggested that gallite has begun to form in these samples. The pattern corresponding to the reaction carried out in en appears to contain peaks from the starting material, unlike those in DMM or DMA (Figure 6.3). Other specific sets of conditions investigated are described in Appendix 1.6. All other reactions using TMDPy with this precursor gave amorphous samples.

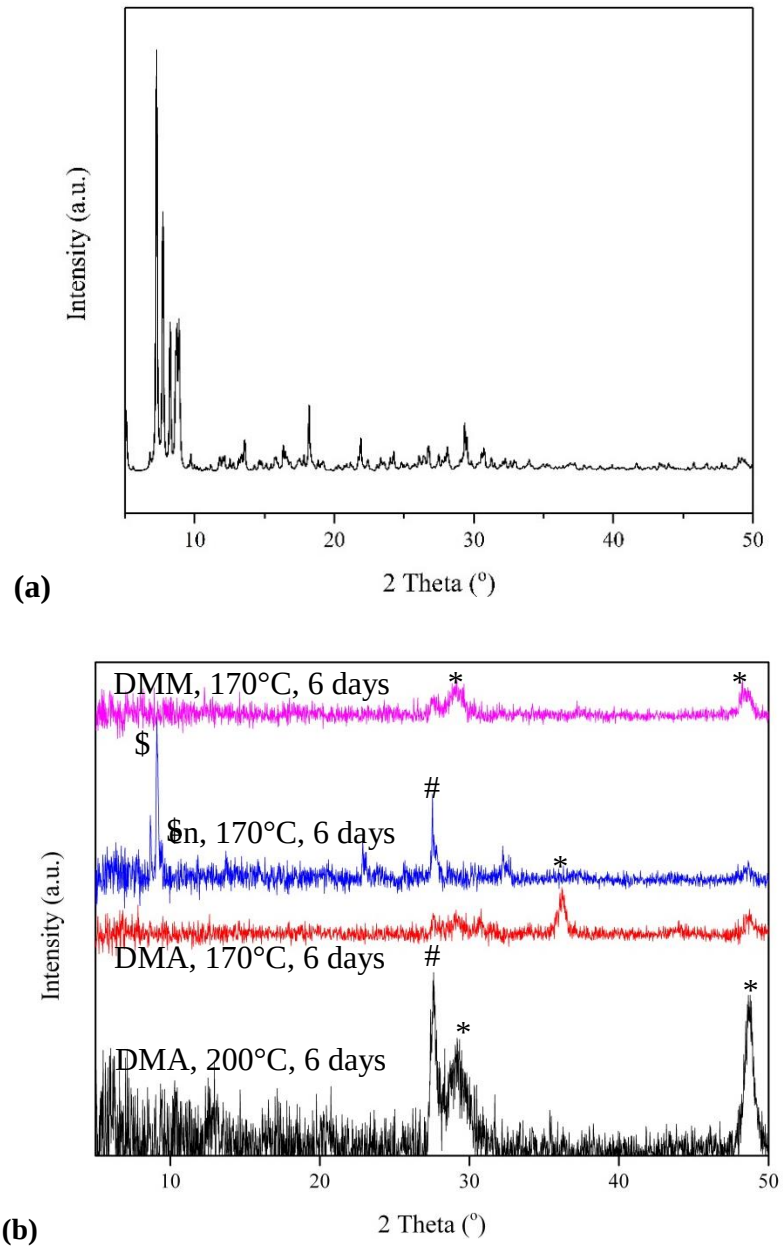

Figure 6.3 PXRD of **(a)** precursor $[C_6H_8N]_6[C_{12}H_{10}N_2]_2[Ga_{10}S_{16}(NC_6H_7)_4]_4$, **(b)** products of with precursor and TMDPy. Keys to symbols: $CuGaS_2$,*; Ga_2S_3[#], precursor[$].

PXRD was measured on products of reactions when TMDPy was substituted with Im (Figure 6.3). The pattern from the precursor is present when the reaction is carried out at 160 °C and 170 °C with different amines. The pattern disappears when the reaction is carried out at 200 °C (Figure 6.4). It is thought that Ga_2S_3 begins to form in these reactions (Figure 6.2 and Figure 6.4). It is proposed that the precursor decomposes and the gallium and sulphur react to form Ga_2S_3.

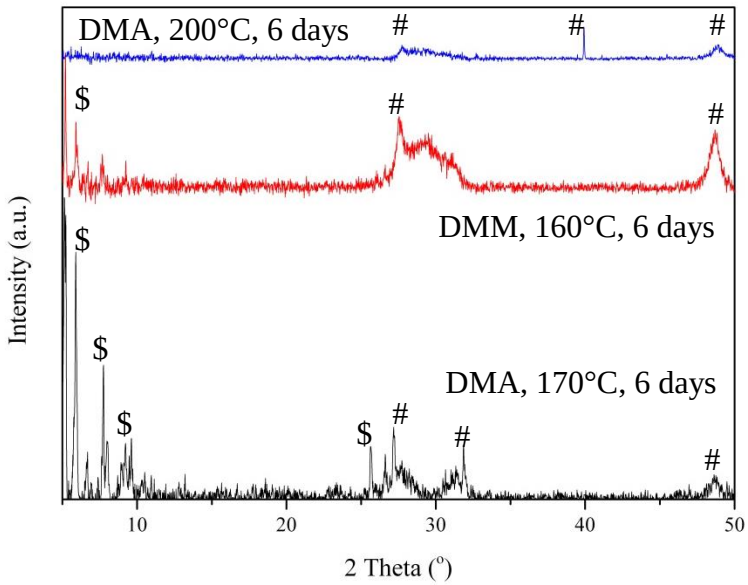

Figure 6.4 PXRD of products with precursor and Im, described in Table 6.3. Keys to symbols: Ga_2S_3[#], precursor[$].

6.2.2.3 *Results and Discussion from Precursor $[enH]_2[Ga_4S_7(en)_2]$*

PXRD for a sample of the precursor synthesised prior to the reactions described is shown in Figure 6.5.

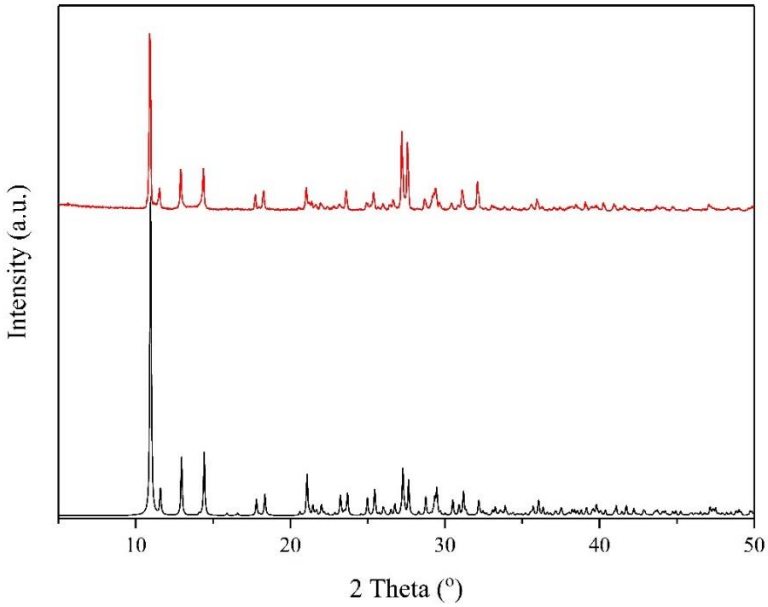

Figure 6.5 PXRD of a sample containing the precursor $[enH]_2[Ga_4S_7(en)_2]$ (black line) and the precursor simulated from SCXRD, provided by Vaqueiro (red line).[123]

PXRD patterns from products synthesised in [BMMIm]Cl (Figure 6.6) are similar to the patterns described in Section 6.2.2.2 (Figure 6.3 and Figure 6.4). These show decomposition of the precursor (Figure 6.5), along with the formation of gallite (Figure

6.2). The same result was seen as for Precursor 1 when $Cu(NO_3)_2$ was omitted from the reactions when using $[enH]_2[Ga_4S_7(en)_2]$ as a precursor. Therefore, copper nitrate was included in all reactions.

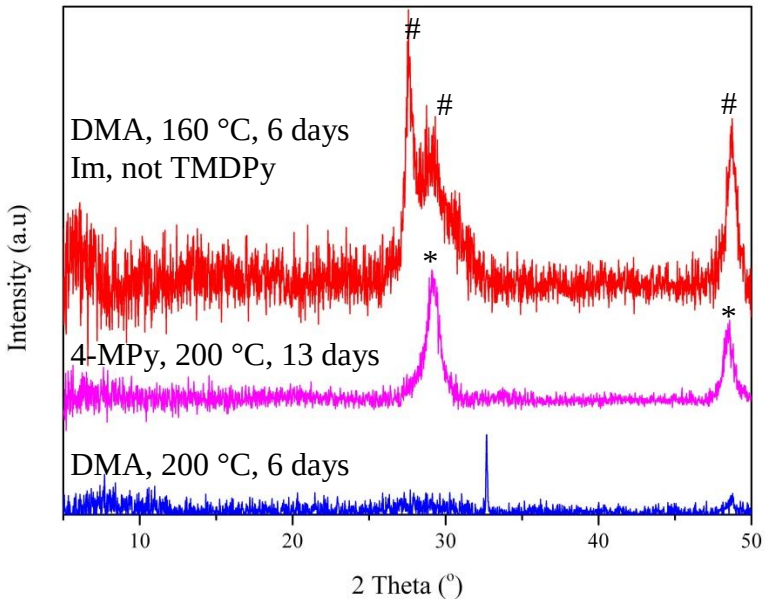

Figure 6.6 PXRD of products in [BMMIm]Cl. Keys to symbols: $CuGaS_2$,*; Ga_2S_3#.

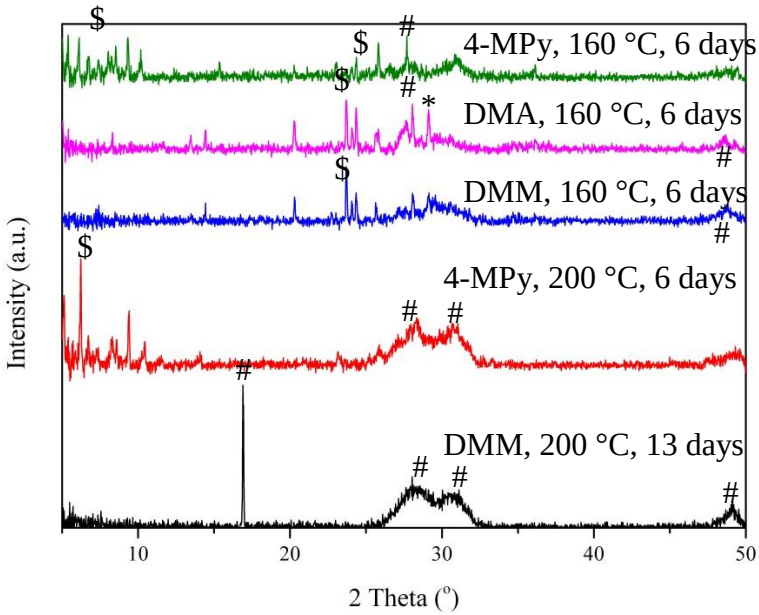

Figure 6.7 PXRD of products in $[BMMIm]BF_4$. Keys to symbols: $CuGaS_2$,*; Ga_2S_3#, precursor$.

When reactions take place in $[BMMIm]BF_4$, the products appear to contain more sharp peaks (Figure 6.7), although extra peaks seem to correspond to the precursor (Figure 6.5). The samples also differ in appearance when $[BMMIm]BF_4$ is used; the powders are green-brown rather than orange-brown. This suggests a higher copper-

content in the powder in the case where the product is green. It would seem that peaks are more intense because larger amounts of precursor remain in the product, rather than a new crystalline-phase forming.

6.2.3 **Reactions Using Elemental Reagents**

6.2.3.1 ***Synthesis***

Investigations were carried out into whether products could be obtained from gallium and sulphur starting-reagents in the ionothermal syntheses. This method would save time by eliminating the solvothermal-synthesis step but would remove the possibility of systematically linking known building-units. An example procedure is shown below:

Gallium metal (0.25 mmol, 17.2 mg) was added with sulphur powder (0.41 mmol, 13.2 mg), $Cu(NO_3)_2.3H_2O$ (0.18 mmol, 43 mg), thioacetamide (2.48 mmol, 187 mg), TMDPy (1.74 mmol, 346 mg) and [BMMIm]Cl (5.99 mmol, 1.135 g) into the Teflon liner of a steel autoclave using an auxiliary amine of dimethylamine (0.3 ml, 23.5 mmol, 40% in H_2O). The mixture was stirred magnetically for approximately 10 minutes, before sealing into the autoclave and heating in an oven at 160^oC for 6 days.

Table 6.2 Parameters Changed Throughout this Investigation

Parameter Varied	Used
Gallium Source	Ga, $Ga(NO_3)_3$
Solvent	[BMMIm]Cl, $[BMMIm]BF_4$,
Auxiliary Amine	DMA (40 % in H_2O), TMDPy, en, DMM, 4-MPy
Sulphur Source	Thioacetamide, Sulphur
Temperature/ ^oC	160,170, 200
Time/ Days	6, 13

6.2.3.2 ***Results and Discussion***

The powder patterns displayed in Figure 6.8 are consistent with the formation of gallite during reactions that take place in [BMMIm]Cl. However, when the temperature is decreased to 160 ^oC the powder is amorphous.

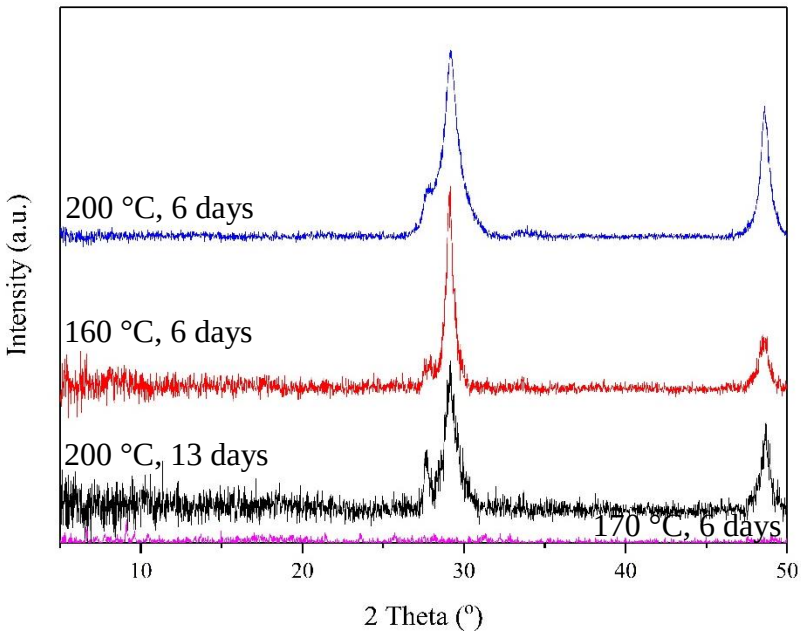

Figure 6.8 PXRD of products with elemental reagents in [BMMIm]Cl with DMA.

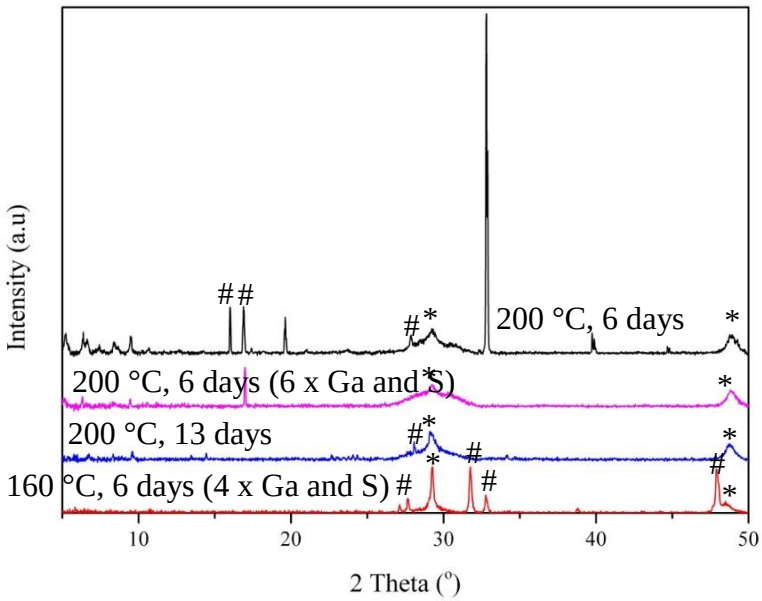

Figure 6.9 PXRD of products with elemental reagents in [BMMIm]BF_4 with DMA. Keys to symbols: $CuGaS_2$,*; Ga_2S_3#.

When [BMMIm]Cl is substituted for [BMMIm]BF_4, more peaks appear in the diffraction pattern (Figure 6.9). This is proposed to be caused by the formation of Ga_2S_3 along with gallite in some cases (Figure 6.2). It is worth noting that, when the amounts of gallium and sulphur are increased relative to the other reactants, the number of peaks reduces. In this case, changing the temperature creates peaks at different 2θ values. The most important features of the patterns from products formed at 200 °C are the peaks at

low-angle. These peaks suggest the formation of a material with a large unit cell. Unfortunately, due to the absence of single crystals, the structure of this material could not be determined; as observed in Figure 6.9, extending the time and varying the ratios of Ga and S did not promote the growth of single crystals.

6.2.4 Reactions Using Ionic Liquids as Structure-Directing Agents

Due to the fact that ionothermal syntheses described above were unsuccessful for preparing new phases, reactions were modified so that the ionic liquids would be used as templating agents or auxiliary salts in the reactions, rather than as solvents. This proved to be a more successful method of obtaining new crystalline-phases.

Reactions leading to the formation of the compounds **(1)**, **(2)** and **(3)** have been described in Chapter 3. General trends when carrying out these syntheses will be described in this chapter, along with some known structures, previously synthesised through a different method.

6.2.5 Overview of Reactions with Ionic Liquids

6.2.5.1 *Synthesis*

Reactions were carried out using ionic liquids as templating agents, different parameters explored are shown in Table 6.3. Some reactions were performed using only gallium metal; however some were carried out using a mixture of gallium and germanium.

Table 6.3 Parameters changed throughout this investigation

Parameter Varied	Used
Metal Source	Ga, GeO_2 (hexagonal form)
Solvent	4-MPy, H_2O
Auxiliary Amine	TMDPy, bipy, no amine
Ionic Liquid	[THTDP]Cl, [BMMIm]Cl, [BMMIm]BF_4
Temperature/ ^oC	170, 200
Time/ Days	6

[THTDP]Cl = Trihexyltetradecylphosphonium chloride

The solvent 4-MPy was used due to the fact that current research suggests that this is the most promising amine for producing hybrid-structures. It has been proven to dimerise in numerous cases (Chapter 3) and is favoured by gallium-sulphide T3 clusters

to co-ordinate to the corners.[119, 223] TMDPy and bipy were used as auxiliary amines as they are both ditopic. For the purposes of this investigation, linking clusters into a porous network was desired. Therefore, auxiliary amines were chosen with a structure that would allow this when co-ordinating corners of adjacent clusters.

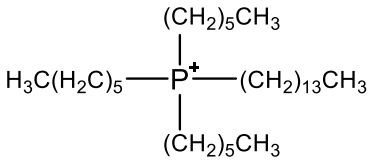

Trihexyltetradecylphosphonium
$[THTDP]^+$

Figure 6.10 Structure of trihexyltetradecylphosphonium.

[THTDP]Cl was chosen as a templating agent due its large size, it was thought that this may encourage the clusters to form a network containing larger pores. [BMMIm]Cl and $[BMMIm]BF_4$ were used due to the similarity of the imidazolium cations to amines previously used in these types of reactions. Different stoichiometries were also investigated when using these templating agents, the main components varied were the amounts of sulphur, ionic liquid and water (Appendix 1).

6.2.5.2 *Results and Discussion*

The most successful of these reactions gave materials **(1)** to **(3)** described in Chapter 3, from products containing single crystals. Aside from one reaction that produced powder containing **(1)**, and **(14)**, which is described in the following section.

In some cases, no solid product was obtained after filtration; this is thought to be due to the solubility of the reaction mixture being too high. Reactions that gave no solid products contained relatively high amounts of ionic liquid (at least *ca.* 3.5 mmol), although a high amount of ionic liquid did not always mean no solid would be formed and in some cases gave samples of single crystals (Chapter 3, Appendix 1.1 and Appendix 1.5).

A sample of orange powder, isostructural with **(1)** (Section 3.2.1) was produced from Ga metal (136 mg, 2 mmol), S powder (156 mg, 5 mmol), [THTDP]Cl (448 mg, 0.86 mmol) and 4-MPy (2.9 ml, 30 mmol).

When GeO_2 was added into the reactions, materials isostructural to **(10)** or **(11)** were formed (Sections 4.4 and 6.3.3). These materials were synthesised using either [BMMIm]Cl or [BMMIm]BF_4 in 4-MPy at 200 ^oC (Appendix 1.2 and Appendix 1.5).

6.2.6 A Material Synthesised with [THTDP]Cl in the Absence of Liquid Amine

A number of reactions were carried out using the ionic liquid [THTDP]Cl. To create this material, the reaction was carried out in the absence of 4-MPy, therefore the hybrid supertetrahedra described in Chapter 3 would be more difficult to form, unless the TMDPy were to co-ordinate the corners of the clusters. The product formed here was a framework material consisting of purely-inorganic T3 clusters **(14)**.

6.2.6.1 *Synthesis*

The reaction to produce **(14)** $[(CH_3(CH_2)_5)_3P(CH_2)_{13}CH_3]_{0.25}[NH_4]_{5.75}[Ga_{10}S_{18}]$-$(NH_3)$ was carried out using Ga metal (137 mg, 2 mmol), S (143 mg, 4.5 mmol), [THTDP]Cl (1.77 mmol, 1 g) TMDPy (206 mg, 1 mmol) and H_2O (0.6 ml, 34 mmol). Here, the water is in molar excess and can therefore be considered the solvent; although by volume there is more of the ionic liquid. The product of this reaction was colourless single-crystals of **(14)**.

6.2.6.2 *Single-Crystal X-Ray Diffraction*

SCXRD was carried out on a single crystal of **(14)**, submitted to the National Crystallography Service.[204] Raw data were supplied and solution and refinement were carried out.

Residual electron-density was modelled during the refinement of the crystal structure of **(14)** using Platon SQUEEZE.[206] Platon calculated a void space of 5384.5 $Å^3$ per unit cell (52.8 %).

Table 6.4 Single crystal X-ray diffraction data for **(14)**.

Crystallographically-Determined Formula	[Countercation]$_n$[$Ga_{10}S_{18}$]
M_r	1274.28
Crystal habit	Colourless Prism
Crystal system	Orthorhombic
Space group	P*bca*
***T*/K**	100
***a, b, c*/Å**	18.6203(3), 18.5985(3), 29.430(2)
***V*/Å^3**	10191.9(7)
Z	8
θ_{max}	27.484
ρ_{cal}/gcm^{-3}	1.661
μ/mm^{-1}	5.932
T_{min},T_{max}	0.708,0.743
Number of parameters	254
Number of reflections used in refinement	8451
Total number of reflections	11,646
R_{merge}	0.058
$R(I>3.0\sigma(I))$	0.0513
R_w	0.0541

6.2.6.3 *Structure Description*

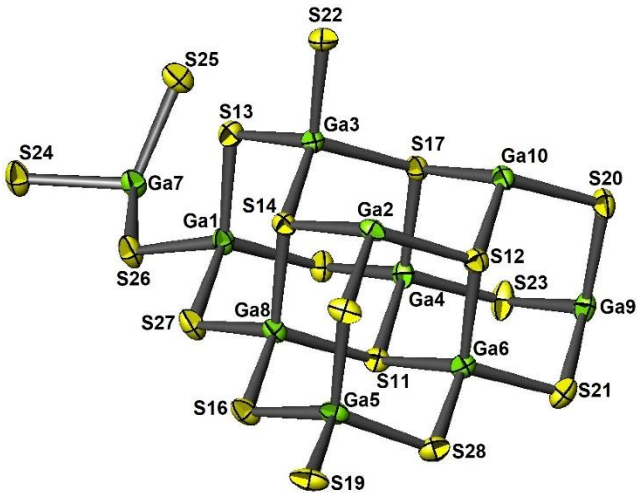

Figure 6.11 Asymmetric unit of **(14)**. Green = Ga, yellow = S.

The asymmetric unit of **(14)** consists of a T3 cluster with two corner sulphur-atoms missing. This is due to the corner sharing of the sulphurs on the vertices of the clusters within the structure (Figure 6.12). The $[GaS_4]^{5-}$ Ga-S bond-lengths are in the range of 2.219(2) – 2.322(2) Å, with most of the Ga-S-Ga angles range from

104.52(6) - 114.17(7) º. However, some of the angles at the corner- sharing clusters are very low i.e. S(26)-Ga(1)-S(27) = 96.45(6) º, S(15)-Ga(5)-S(19) = 97.26(6) º, S(24) - Ga(7) - S(26) = 98.57(7) º and S(19)_c - Ga(9) - S(23) = 97.86(7) º. This shows a distortion from the ideal tetrahedral shape at the corners.

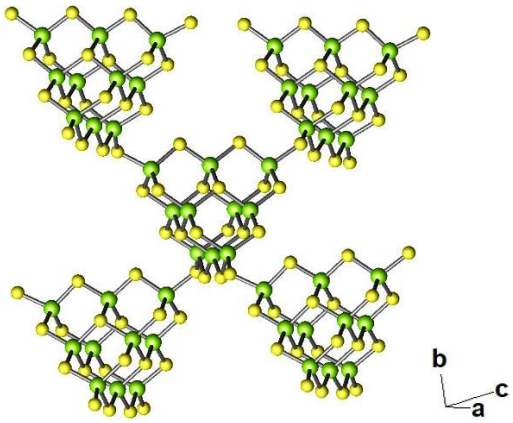

Figure 6.12 Perspective view of five clusters in **(14).** Green = gallium, yellow = sulphur.

T3 supertetrahedra are linked through the four corners (Figure 6.12). The corner-sharing T3 supertetrahedra create a 3-dimensional doubly-interpenetrating network with the double-diamond net, where each carbon-atom would be replaced by a T3 unit (Figure 6.13).

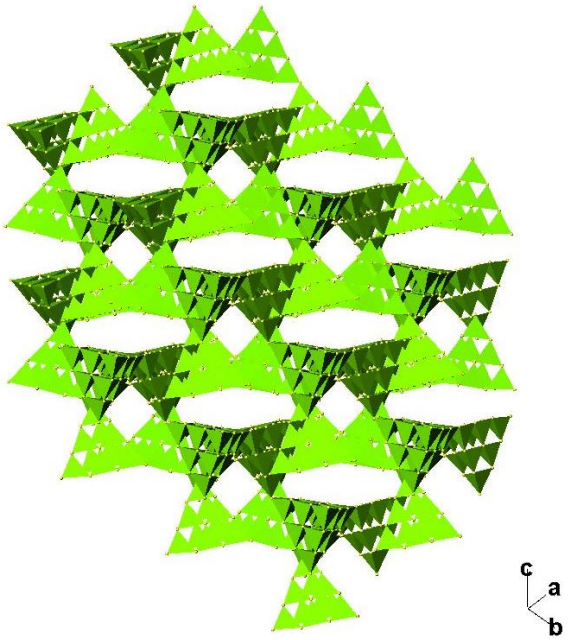

Figure 6.13 The two interpenetrating-networks in **(14)** viewed along [111]**.** Green tetrahedra = GaS_4.

The structure resembles the indium sulphide ASU-32, reported by Li *et al.*[82] It is also structurally related to a material synthesised by Romero in DEA, with the structure $[C_4H_{12}N]_6[Ga_{10}S_{18}]$, which also has a doubly-interpenetrating double-diamond lattice.[223] Corner-sharing T3 clusters have been frequently reported by Feng *et al.*, mostly containing more than one different metal, with the double-diamond structure (Section 1.4.4). [104, 248]

Although **(14)** displays a doubly-interpenetrating framework; the space-filling representation confirms the indication from Platon that there is remaining void-space in the material. Two different sizes of channels run along [111] (Figure 6.14) *ca.* 2 x 1 Å and 2 x 6 Å in diameter, providing space in which the countercations reside.

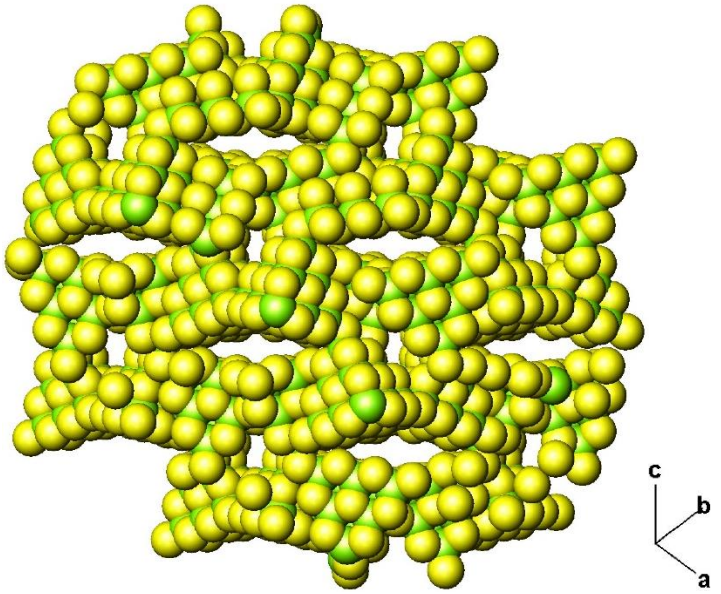

Figure 6.14 Space-filling representation of **(14)** viewed along [111]. Green = Ga, yellow = S.

6.2.6.4 *Powder X-Ray Diffraction*

Powder diffraction of **(14)** (Figure 6.15) shows that the bulk matches the pattern calculated from the SCXRD data, although there is a slight offset in 2θ. It also appears to have the same structure as the material synthesised by Romero.[223] Due to the fact that the unit cells have very similar parameters, this is not an unexpected result. It is proposed that there is a difference in the solvents of the two structures, which causes **(14)** to crystallise with a lower symmetry orthorhombic unit cell, compared with the tetragonal structure reported by Romero in space group $P4_32_12$.[223]

Table 6.5 Lattice parameters for **(14).** Parameters were refined against PXRD using DASH.[208]

SCXRD	***a*/ Å**	***b*/ Å**	***c*/ Å**	**α/ º**	**β/ º**	**γ/ º**
	18.6203(3)	18.5985(3)	29.430(2)	90	90	90
PXRD	***a*/ Å**	***b*/ Å**	***c*/ Å**	**α/ º**	**β/ º**	**γ/ º**
	18.728(5)	18.594(1)	29.622(4)	90	90	90

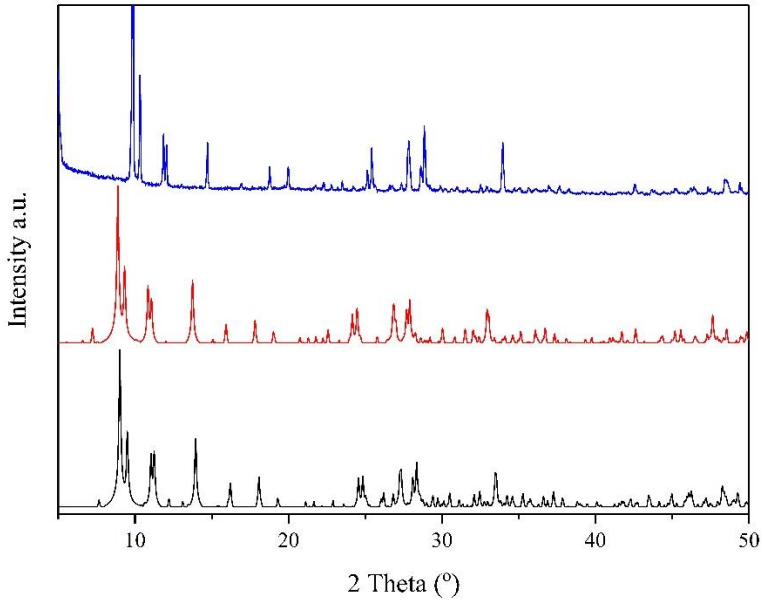

Figure 6.15 PXRD of bulk sample containing **(14)** (blue line); calculated pattern for material previously synthesised by Romero[223](red line) and calculated pattern from SCXRD on **(14)** (black line).

6.2.6.5 *Elemental Analysis*

CHN elemental analysis was required on this material to determine the overall formula of the product, due to the fact that none of the countercations could be located in the Fourier maps from SCXRD data. Experimental results for CHN content showed: C = 6.58 %, H = 3.03 %, N = 6.18 %. These values show a low percentage of carbon and high percentage of nitrogen, compared to the results found for other materials throughout this work. If C and N were only present in the form of TMDPy, the C:N ratio (5:1) would not be consistent with the experimental results (8:7).

The high nitrogen-content suggests the presence of ammonium ions that would have been produced *in-situ*. This gives calculated values of: C = 6.30 %, H = 2.84 % and N = 5.28 %, when ammonium is alongside the phosphonium species and water is also present in the pores. The presence of water is suggested by the lower percentage of hydrogen when water is omitted and also by the FTIR spectrum (Figure 6.16), TGA can be used to work out how many water molecules are expected to be present in the pores. The resulting formula is suggested to be $[(CH_3(CH_2)_5)_3P(CH_2)_{13}CH_3]_{0.25}[NH_4]_{5.75}$ -

$[Ga_{10}S_{18}](H_2O)_{1.5}$, assuming that the phosphonium species is still intact. The void space of 5384.5 $Å^3$ per unit cell (52.8 %) calculated by Platon SQUEEZE suggests that there is enough space for the phosphonium species to occupy.

6.2.6.6 *Infrared Spectroscopy*

FTIR spectroscopy was carried out on **(14)** (Figure 6.16), this suggests that the presence of ammonium cations in the pores is correct (Table 6.6), along with the presence of water. It also implies that alkyl chains are present in the structure.

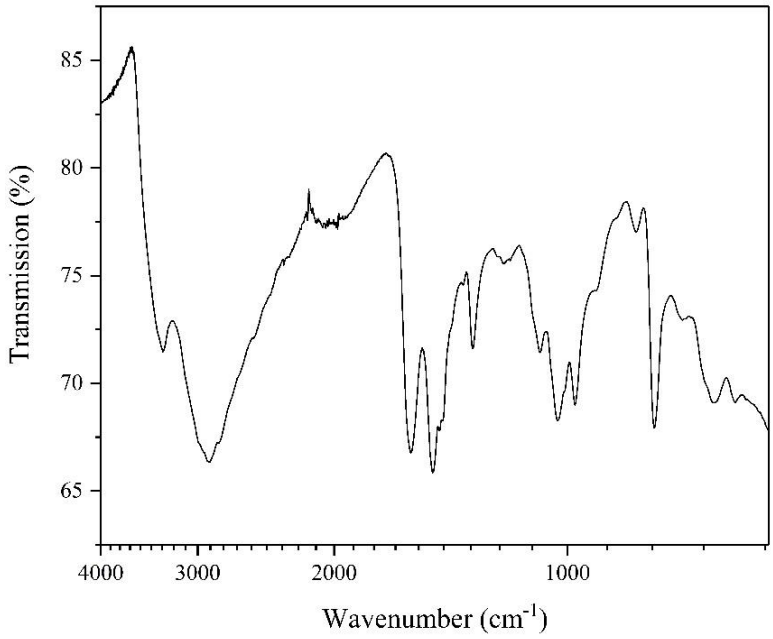

Figure 6.16 FTIR of **(14).**

Table 6.6 Key FTIR assignments **(14).**

Wavenumber/ cm^{-1}	**Assignment**
3327	Water, ν (O-H)
2900	Ammonium, ν (N-H) Symmetric
1595	Water γ(O-H)
1495	Ammonium, δ (N-H) Asymmetric
1326	Alkyl Chains, ω (C-H), CH_3, CH_2
773	Alkyl Chains, ρ (C-H), CH_2

6.2.6.7 *Thermogravimetric Analysis*

TGA measurements were carried out on **(14)** in both air and N_2 (Figure 6.17) in order to confirm the content in the pores and to determine the thermal stability of the compound.

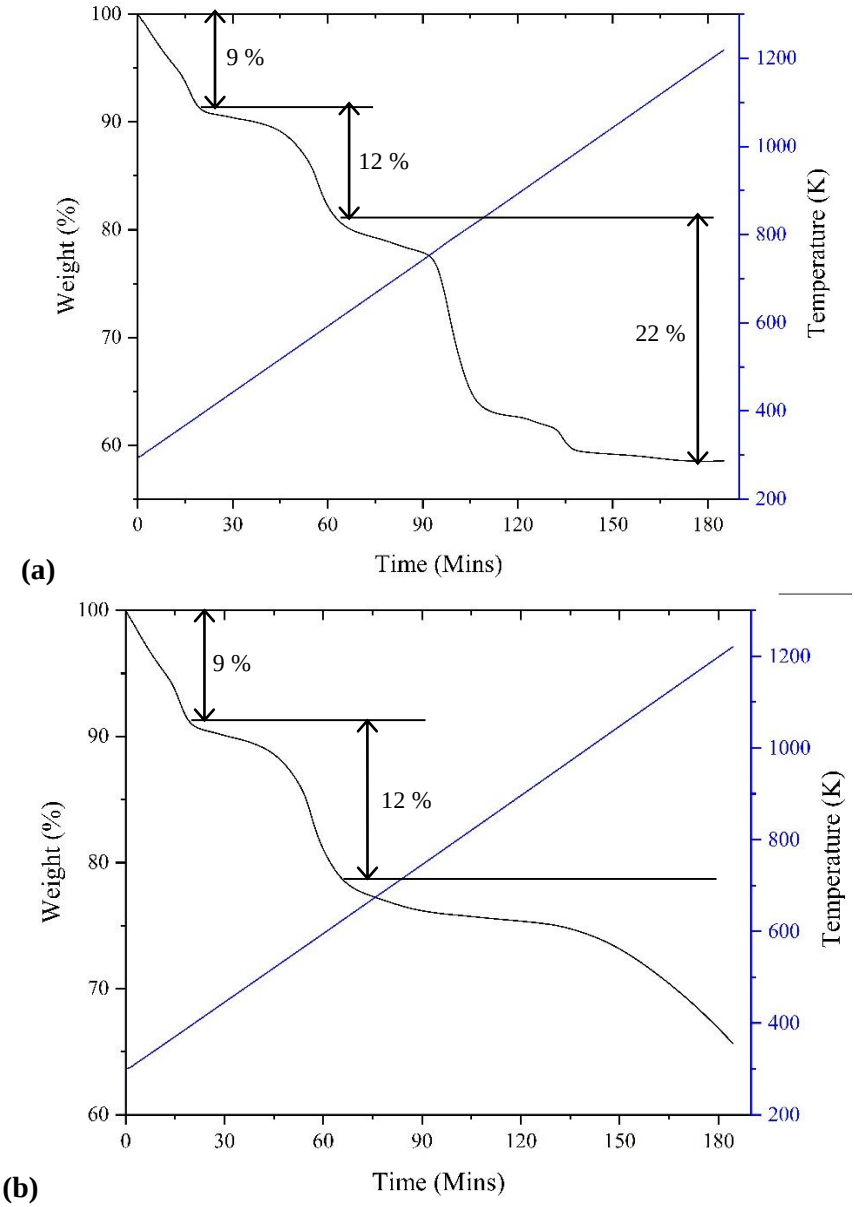

Figure 6.17 TGA for **(14)** in **(a)** air and **(b)** N_2. Black line = weight change vs. time, blue line = temperature vs. time.

Weight transitions for **(14)** decomposing in air (Figure 6.17 **(a)**) begin with the loss of the water and ammonium moieties from the sample, giving a weight loss of *ca.* 9 % corresponding to $1.5H_2O$ and $5.75[NH_4]^+$. The following weight-loss of *ca.* 12% arises from the loss of the phosphonium moiety $0.25[(CH_3(CH_2)_5)_3P(CH_2)_{13}CH_3]^+$. The remaining product is Ga_2O_3, leaving a remainder of *ca.* 60 %.

The decomposition of **(14)** does not appear to change when heated under N_2 (Figure 6.13 **(b)**), except for the fact that the decomposition of the inorganic framework is slower and it does not fully compose when heated up to 1000 ^oC.

6.2.6.8 *UV-Vis Diffuse Reflectance*

UV-Vis diffuse reflectance was carried out on **(14)** (Figure 6.18). The absorption edge for **(14)** is at 4.14(7) eV. This confirms the colourless nature of the crystals, the material as just outside the range to be classified as a wide-gap semiconductor (*ca.* 2-4 eV).

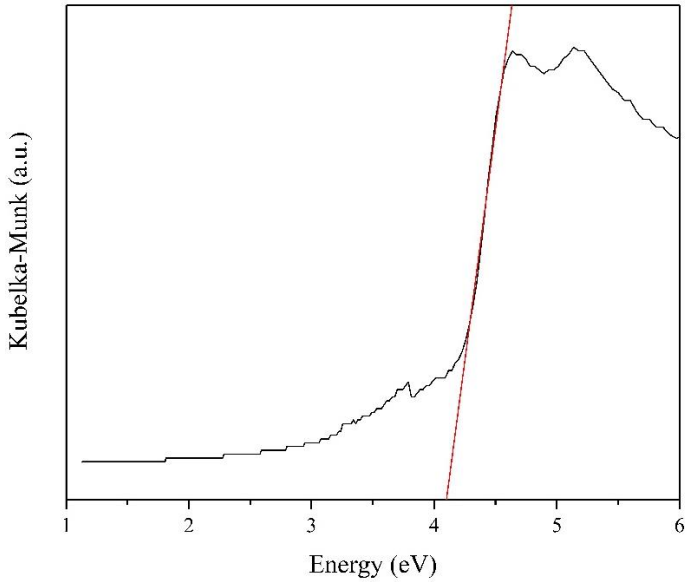

Figure 6.18 Diffuse reflectance of **(14),** red line shows absorption edge.

6.2.6.9 *Discussion*

The material **(14)** described here is the only material discussed in this work that has been synthesised using an ionic liquid in the absence of 4-MPy. In this reaction, the water is in molar excess, with the [THTDP]Cl stoichiometrically the lowest-concentration reactant. In this case, water is therefore considered to be the solvent and [THTDP]Cl the structure-directing agent. It is suggested from elemental analysis and FTIR that ammonium ions and are formed *in-situ* in order to balance the negative charge of the clusters and fill the large amount of void space in the structure, given that $[THTDP]^+$ has a low size:charge ratio.

Although the material is built from the T3 clusters described in Chapter 3, it is not co-ordinated by 4-MPy but links through the corners to form a double-diamond lattice (Figure 6.13) This is observed in a material synthesised by Romero,[223] along with the UCR series reported by Feng *at al.*[86, 104, 105, 116] Although the lattice is doubly interpenetrating, it is indicated from Platon SQUEEZE,[206] CHN analysis, TGA and in

order to charge balance, that there is pore space in the material. This is also indicated by the space-filling representation of the structure (Figure 6.14).

This structure therefore differs from the double-diamond T3-based structures previously-reported as it contains no amine-based SDA in the pores. It has also been synthesised using an IL as the SDA and appears to contain the IL, or fragments of the IL, in the pores of the material.

6.3 Solvothermal Synthesis with Gallium and Germanium Reagents in Different Amines

6.3.1 **Introduction**

As ionothermal synthesis did not prove to be a promising way of creating many novel crystalline phases, different amines were explored using solvothermal synthesis. Reactions were explored using amines that are known to give hybrid materials; 2,6-Lut, 3,5-Lut (Figure 6.19) and .4-MPy have been used previously by Vaqueiro in the synthesis of T3 hybrid gallium-sulphides,[113, 114, 119, 210] whereas en has been used to produce other crystalline gallium-sulphides, as described in Sections 1.4.4 and 1.5.1.[123]

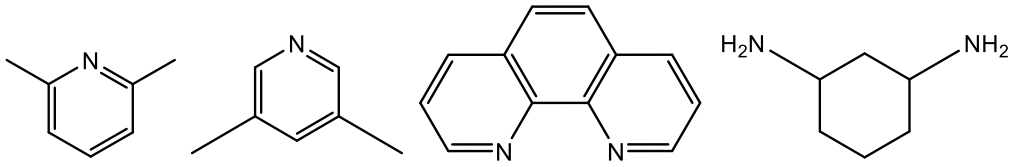

Figure 6.19 Structures of solvents and auxiliary amines used in this section.

Auxiliary amines were chosen for various different reasons. Im and BenzIm were chosen due to their use in forming 3-dimensional frameworks from supertetrahedral clusters in the past; as reported by Feng *et al* and described in Section 1.4.5.[116] Bipy and TMDPy were also chosen for their ditopic nature; Bipy has been used previously by Vaqueiro to link T3 gallium-sulphide clusters,[114] whereas TMDPy resembles the EDPy formed *in situ* from 4-MPy in a number of reactions described in Chapter 3. DACH (Figure 6.19) is also ditopic and has been explored previously in reactions carried out by Romero and Ewing.[124, 129, 223, 249, 250] Phenanthroline (Figure 6.19) was chosen due to its bulky nature; it was hoped that incorporating this into 3-dimensional structure could increase the size of the pores.

Reactions included those with gallium and sulphur-based starting materials. Reactions were also carried out with a mixture of gallium and germanium; in line with those described throughout Chapter 4.

Table 6.7 Parameters changed throughout this investigation

Reaction Parameter	Variations Used
Metal Sources	Ga, $Ga(NO_3)_3$, Ga_2O_3, GeO_2, $Cu(NO_3)_2$
Sulphur Sources	S, TAA
Temperature/ ^oC	150, 160, 170, 200
Solvent	4-MPy, 2,6-Lut, 3,5-Lut, en, H_2O
Auxiliary Amine	Im, TMDPy, BenzIm. BiPy, Phenan, DACH, no amine
Time/ Days	5, 6, 10

Successful reactions producing single crystals are described in Chapters 3 and 4. These consist of materials **(4)** to **(6)** synthesised from Ga and S and **(8)** to **(11)** synthesised from both Ga and GeO_2 with S. A gallium-sulphate material synthesised in 2,6-Lut is described in Section 6.3.4.

There are a number of materials that were produced repeatedly with varying reaction-conditions. Those cases where samples had similar powder-patterns and unit-cell parameters but were synthesised using different amines, could contain different organic-countercations. Single-crystal structures were not determined in all cases, in order to avoid repetition of data collections.

6.3.2 **Reactions Using Ga, Ga_2O_3 or $Ga(NO_3)$**

Materials isostructural with **(1)** and **(4)** were synthesised frequently, implying that these are particularly stable compounds (Sections 6.3.2.1 and 6.3.2.5, Appendix 1.1). Using $Ga(NO_3)_3$ did not prove to be a good route for synthesising new gallium-sulphide materials. In most cases, products were amorphous or poorly crystalline. The only reaction with $Ga(NO_3)_3$ that produced single crystals is that of **(15)**, described in Section 6.3.4.

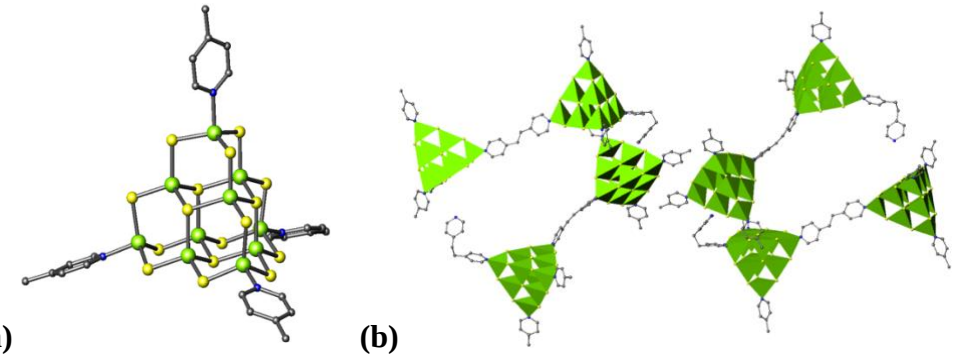

Figure 6.20 Perspective of views of **(a)** a discrete cluster from **(1), (b) dimers** in **(4).** Green = Ga, yellow = S, blue = N, grey = C. H-atoms have been removed for clarity.

6.3.2.1 *Different Reactions Producing Materials Isostructural with (1)*

A number of different reaction-conditions and auxiliary amines could be used to synthesise **(1) (**Figure 6.20 **(a)**), aside from the IL [THTDP]Cl used in the synthesis described in Section 3.2.1.1 (Table 6.8). Powder patterns from samples using each different auxiliary-amine are illustrated in Figure 6.21. In the PXRD pattern for the sample synthesised with BenzIm, there is an extra peak in the pattern, thought to correspond to small amounts of yellow crystals of **(4)** present in the sample.

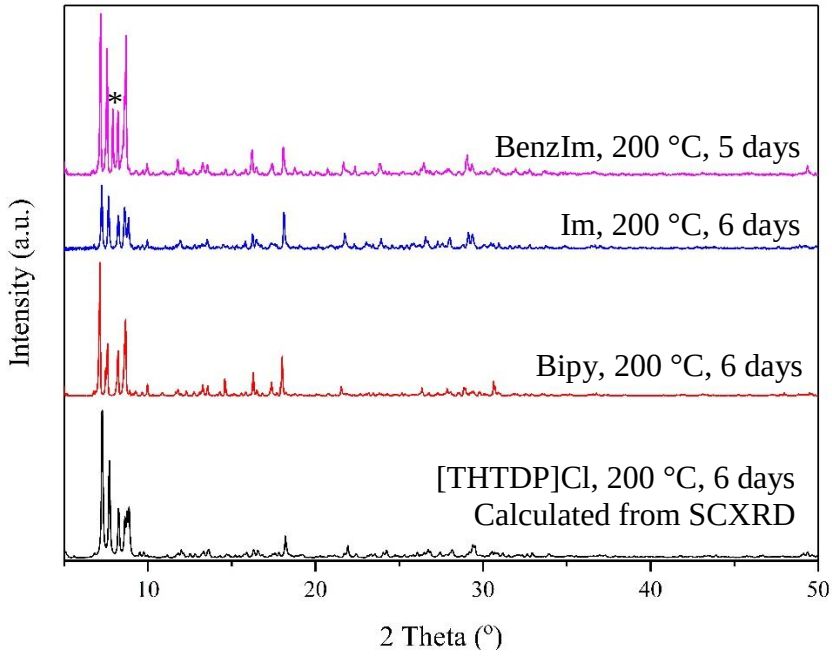

Figure 6.21 Powder patterns of different samples containing **(1)**, synthesised in different amines. Key to symbols: * = **(4)**.

Table 6.8 Reaction conditions producing materials with lattice-parameters corresponding to **(1).**

Reaction Parameter	Variations Used
Metal Sources	Ga
Sulphur Sources	S
Temperature/ ^{o}C	170, 200
Solvent	4-MPy, 4-MPy + H_2O
Auxiliary Amine/ IL	Im, BenzIm, Bipy, TMDPy, no amine, [THTDP]Cl
Time/ Days	5, 6, 10

6.3.2.2 *Different Reactions Producing Materials Isostructural with (3)*

The T3-based chain compound **(3)** could also be synthesised in the absence of the ILs [BMMIm]Cl or [BMMIm]BF_4 in the presence of TMDPy, as indicated by PXRD (Figure 6.22).

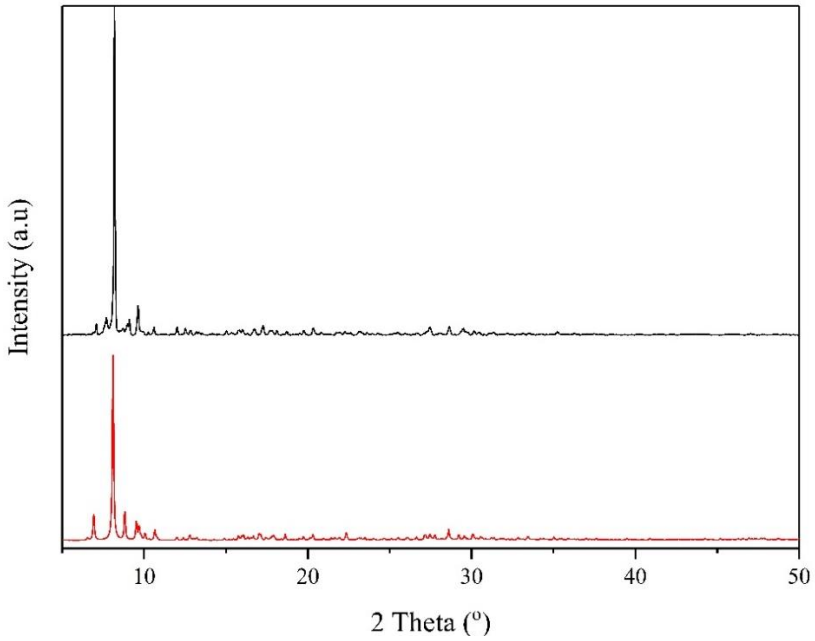

Figure 6.22 Powder patterns of different samples containing **(3)**. Calculated from SCXRD of **(3)** (red line) and sample synthesised in TMDPy (black line).

6.3.2.3 *Different Reactions Producing Materials Isostructural with (4)*

Like compound **(1)**, the T3-based dimer compound **(4)** was also synthesised using many different amines and conditions (Appendix 1.1). These two materials were also often both synthesised in the same reaction. It is not trivial to determine a pattern between when **(1)** will form, **(4)** will form or a mixture of both **(1)** and **(4).** It is suggested here that the reaction is affected by small changes in stoichiometry and pH. Therefore, when changing the amine, reactions cannot be directly compared. However, reactions with the same amine can be compared.

Table 6.9 Reaction conditions producing materials with lattice-parameters corresponding to **(4).**

Reaction Parameter	Variations Used
Metal Sources	Ga
Sulphur Sources	S
Temperature/ ^{o}C	200
Solvent	4-MPy, 4-MPy + H_2O
Auxiliary Amine	Im, TMDPy, BenzIm no amine
Time/ Days	5, 6

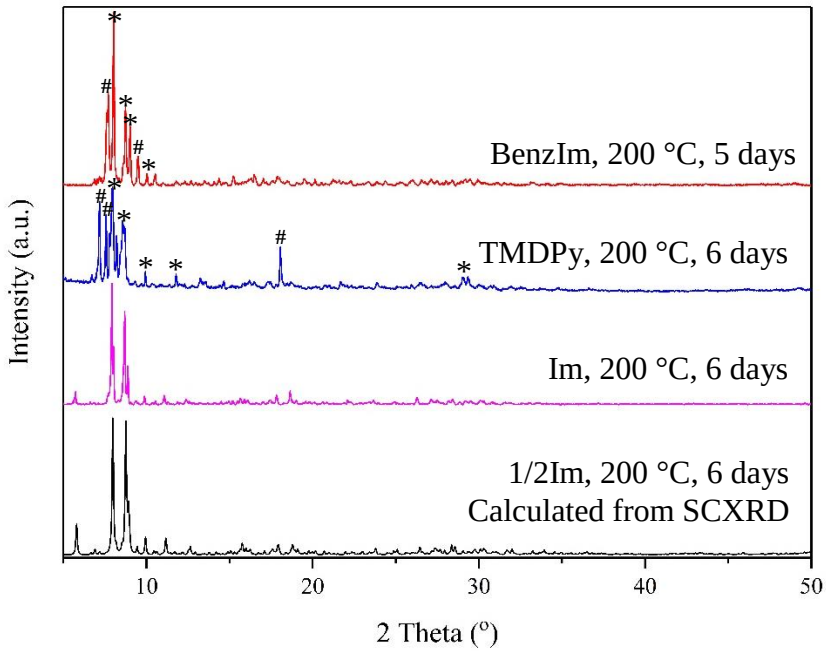

Figure 6.23 Powder patterns of different samples containing **(4)**, synthesised in different amines. Key to symbols: # = **(1)**,* = **(4).**

When reactions are carried out using Im, where the stoichiometric ratio of Ga:S:Amine:4-MPy has a relative amount of S greater than 2:6:1:30, **(4)** and **(1)** are both produced (Figure 6.23). Below this amount, only **(1)** is produced. **(4)** could be isolated by halving the relative amount of Im, or where the relative amount of S is exactly 6. Reactions with TMDPy show the opposite effect, where the amount of S must be 6 or lower to produce a mixture of both phases **(1)** and **(4)**, rather than **(1)** only. BenzIm was used in reactions in order to create **(7)** from the previously-known method used by Tong.[225] Therefore, an alternative ratio of 2:5:0.66:30 was used, which produced **(1)** in some cases and a mixture of **(1)** and **(4)** in others. This could be due to the effect of any residue present in the Teflon liner from previous reactions affecting the outcome. As described in Section 3.5, an optimised synthesis-method was developed to produce compound **(7)**.

6.3.2.4 *Different Reactions Producing Materials Isostructural with (5)*

Aside from the reaction described in Section 3.4.2.1, compound **(5)** that contains both single T3-clusters and T3-based dimers, is formed in two other cases. Along with synthesis using Im as the auxiliary amine, it can also be synthesised in the absence of auxiliary amine or, if water is added to the mixture; at 170 °C rather than 200 °C (Figure 6.24, Appendix 1.1, Section 3.4.2.1). The PXRD pattern for the product synthesised with no amine shows a difference in intensity of the lowest angle peaks, this is suggested to be from preferred orientation of the crystallites.

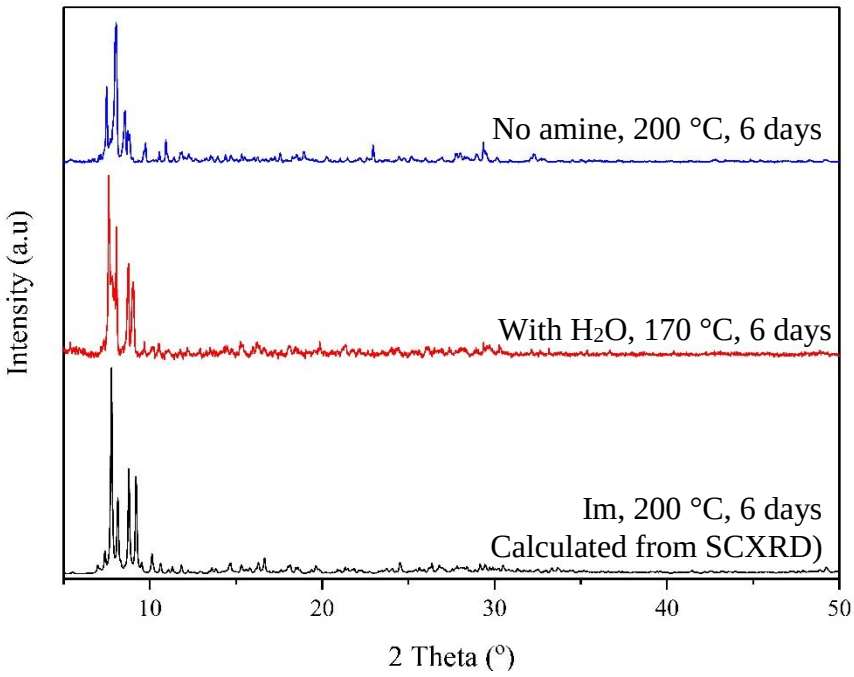

Figure 6.24 Powder patterns of different samples containing **(5)**, synthesised in different amines.

6.3.2.5 *Different Reactions Producing Materials Isostructural with (6)*

In the case of **(6)**, no samples containing this material alone were produced and all samples also contained crystals with the same unit cell as **(1)**. As explained in Section 3.6.1.6, this meant that not enough of the pure material could be obtained to carry out photoluminescence measurements. However, mixtures of **(1)** and **(6)** were described in one other case, where reaction conditions were unchanged aside from the addition of water to the reaction (Figure 6.25).

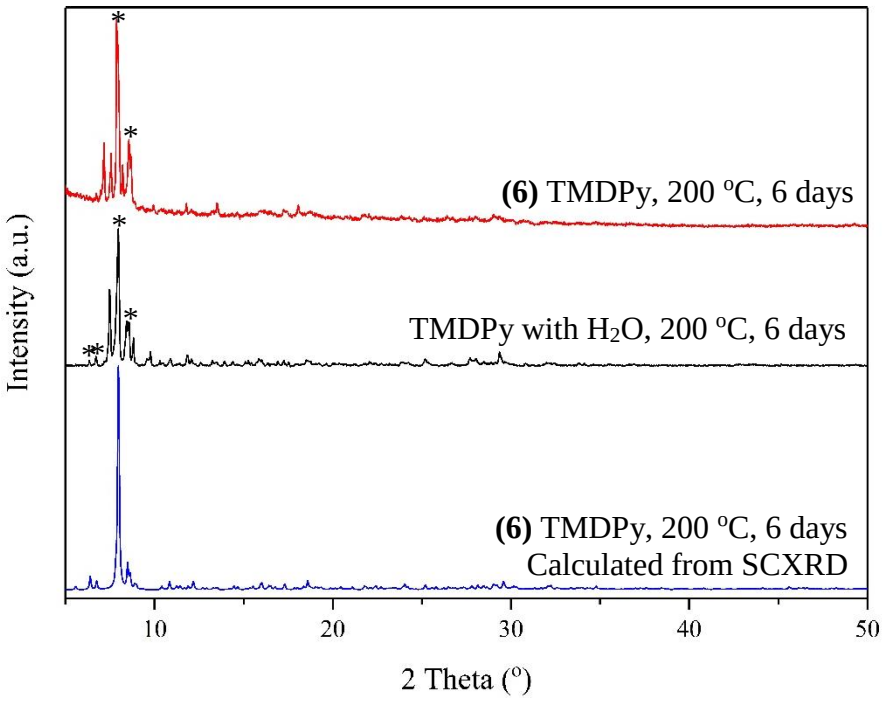

Figure 6.25 Powder patterns of different samples containing **(6)**, synthesised in different amines. Key to symbols: # = **(1)**,* = **(6).**

6.3.3 **Reactions Using Ga and GeO_2**

6.3.3.1 ***Reactions in 4-MPy***

Ga, GeO_2 and S in 4-MPy, with varying auxiliary-amines, gave four different products. A number of materials isostructural to **(10)** (Section 4.4 and Figure 6.16 **(a)**) and therefore resembling phases previously synthesised by Feng *et al.*, were produced frequently at temperatures of 200, 170 and 160 °C (Figure 6.26), a sample synthesised with BenzIm at 150 °C also contained crystals of **(10)** in the sample. (Appendix 1.2).[104]

Table 6.10 Reaction conditions producing materials with lattice-parameters corresponding to **(10).**

Reaction Parameter	Variations Used
Metal Sources	Ga and GeO_2
Sulphur Sources	S
Temperature/ °C	150, 160, 150, 200
Solvent	4-MPy, 4-MPy + H_2O
Auxiliary Amine/ IL	Im, TMDPy, BenzIm, no amine, [BMMIm]Cl, [BMMIM]BF_4
Time/ Days	5, 6, 7

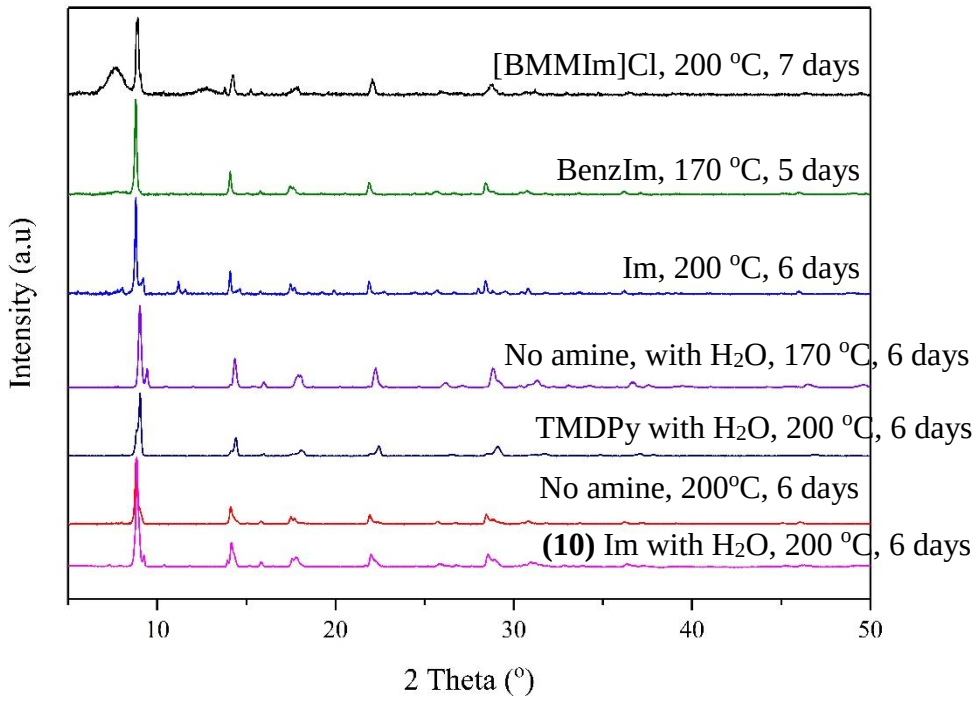

Figure 6.26 Powder patterns of different samples containing **(10)**, synthesised in different amines.

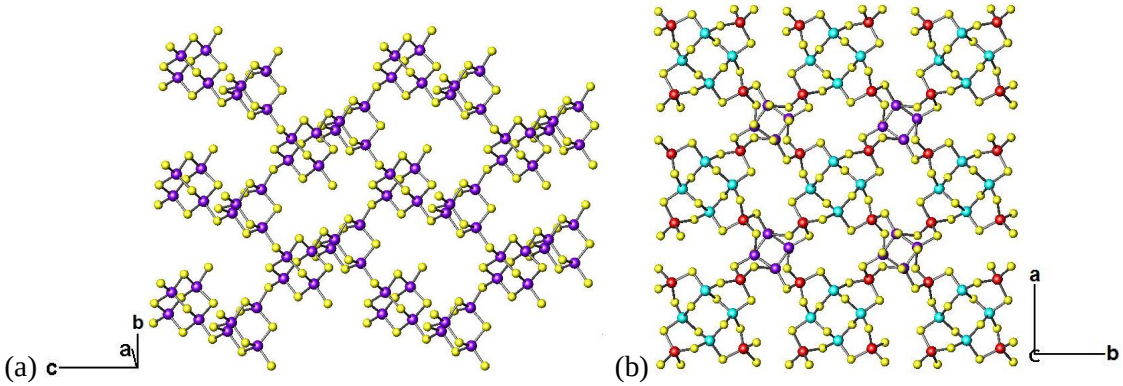

Figure 6.27 Framework in **(a) (10)** as shown in Section 4.4.2.3 and **(b) (11)** viewed along the *c*-axis, as shown in Section 4.5.2.3. Purple = Ge/Ga, red = Ge/Ga, teal = Ge/Ga, yellow = S.

At 200 °C, the other material produced is **(11)** (Section 4.5 and Figure 6.27 **(b)**) and these two materials can both formed in the same reaction. PXRD patterns for a number of samples containing **(10)** are shown in Figure 6.26 and those containing **(11)** or mixtures of **(10)** and **(11)** are shown in Figure 6.28.

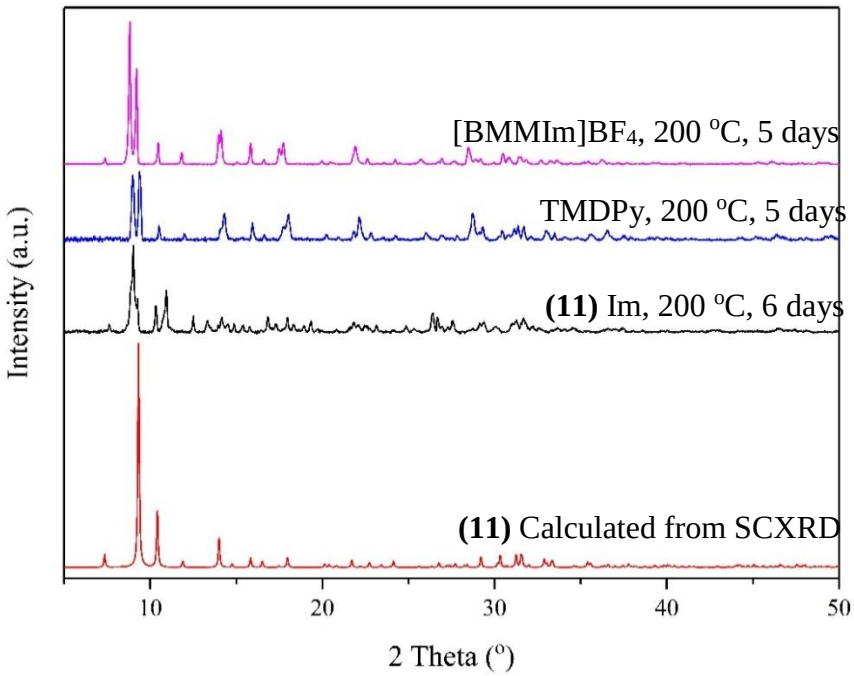

Figure 6.28 Powder patterns of different samples containing **(11)**, synthesised in different amines.

Aside from these two materials, GeO_2 remained the only solid when a Ge:Ga ratio of higher than 1:1 was used. On one occasion, the T2- trimer based germanium-sulphide material **(8)** (Section 4.2) was produced. As this could not be reproduced, it is unclear what happened during the reaction to cause the formation of this product. Using Phenan as an auxiliary amine did not give a solid product.

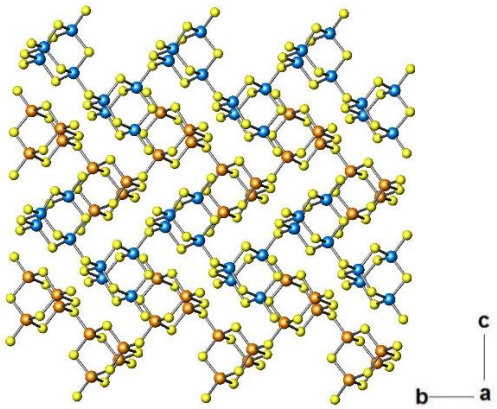

Figure 6.29 (9) viewed along the *a*-axis with organic moieties omitted for clarity, as shown in Section 0. Yellow = S, blue/orange = Ge, in order to distinguish between chain orientations.

At 150 and 170 °C **(11)** is not produced, but the T2-chain based germanium sulphide **(9)** (Section 4.3 and Figure 6.29) was formed on a number of different occasions. In some cases, GeO_2 was also present in the final product (Figure 6.31).

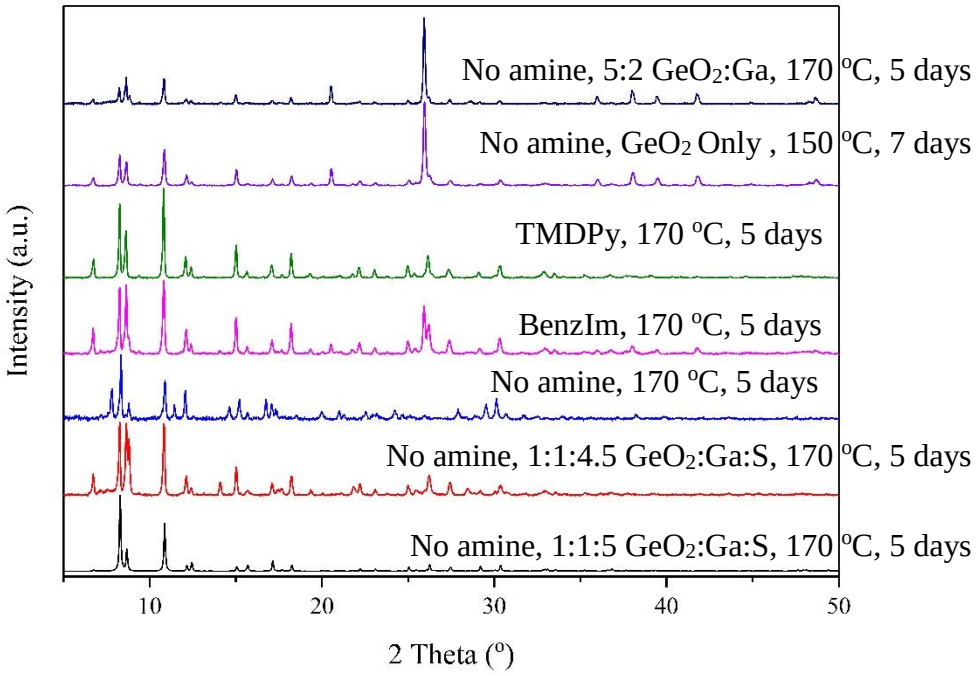

Figure 6.30 Powder patterns of different samples containing **(9)**, synthesised in different amines.

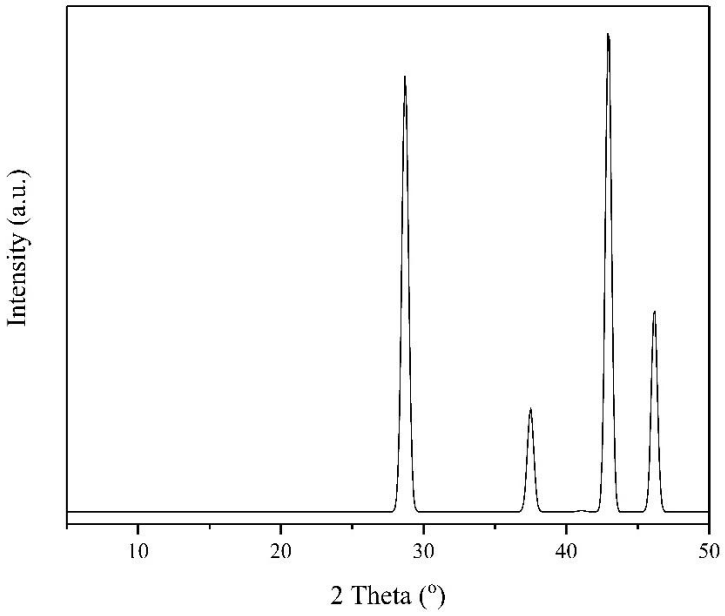

Figure 6.31 PXRD for GeO_2.

The fact that the framework materials **(10)** and **(11)** are synthesised mainly at higher temperatures and the chain structure **(9)** at lower temperatures is consistent with what would be expected with these types of materials,[251, 252] as described by Cheetham *et al* and reviewed by Sun *et al.* Higher temperatures tend to produce materials with higher dimensionalities and vice-versa.

In a number of cases, amorphous products were formed at 150 °C from various auxiliary amines and in some cases no solid product was formed (Appendix 1.2). When using only GeO_2, the only material created is **(9)**; other reactions give amorphous samples. When water was added, no solid product was formed and when TAA was used as a sulphur source GeO_2 remained.

Copper nitrate was added as a reagent in a number of reactions; copper was used in an attempt to create mixed-metal gallium copper sulphide clusters. As described in Section 1.4.2, Pauling's electrostatic valence rule determines that cations with oxidation states smaller than 3+ are required to form clusters larger than T3.[86] This has been proven by Xiong *et al.* through the synthesis of T5 clusters containing Ga(III) or In(III) with Cu(I)[155, 253, 254] (Section 1.5.1) and T4 clusters with In(III) and Cd(II) or Zn(II) (Section 1.4.5).[89, 116, 255] More recently, the T6 cluster $[Zn_{25}In_{31}S_{84}]^{25-}$ has been produced, further demonstrating how increasing the number of monovalent or divalent cations in a cluster increases its size.[253]

Reactions were carried out with both Ga and $Cu(NO_3)_2$ in 4-MPy at 200 °C for 6 days in order to investigate whether copper could be incorporated into the materials. Stoichiometric ratios were varied and the reaction was carried out both with and without the auxiliary amine TMDPy. A mixture of CuS and CuGaS was produced in each reaction.

6.3.3.2 *Reactions in Other Amines*

Reactions were carried out in en at 150 and 170 °C for 6 and 5 days respectively. TMDPy was investigated as an auxiliary amine at 170 °C and Im at 150 °C, with reactions carried out in the absence of an auxiliary amine at both temperatures. Reactions produced white/yellow unidentified powders of varying crystallinities; unfortunately no single-crystals were produced to determine these structures.

Reactions were carried out in 3,5-Lut and 2,6-Lut at 170 °C. An auxiliary amine of Im was used in reactions with 2,6-Lut in both the presence and absence of water. In the presence of water an unidentified grey powder was formed. In the absence of water an unidentified brown-powder was produced, this was also the case when no Im was added to this reaction mixture. When 3,5-Lut was used as the solvent, in the absence of water, an unidentified black-powder was produced. When water was added the product contained colourless-needles; these showed no diffraction when mounted for SCXRD.

6.3.4 A Layered Gallium-Sulphate

6.3.4.1 *Synthesis*

The reaction was carried out using $Ga(NO_3)_3{\cdot}xH_2O$ (388 mg, 1.5 mmol), S (96 mg, 3 mmol) and 2,6-Lut (7 ml, 6 mmol). The product was a mixture of small, brown crystals of **(15)** and brown powder.

6.3.4.2 *Single-Crystal X-Ray Diffraction*

Single crystal X-ray data were collected on a single brown block of **(15)**; all countercations were found in the Fourier Map.

Table 6.11 Single crystal X-ray diffraction data for **(15).**

Formula	$[NH_4][Ga_3(SO_4)_2(OH)_6]$
M_r	1022.58
Crystal habit	Brown block
Crystal system	Hexagonal
Space group	$R\bar{3}m$
T/K	150
a, b, c/Å	7.1659(7), 7.1659(7), 17.7397(19)
V/Å^3	521.37
Z	3
θ_{max}	31.888
ρ_{cal}/gcm^{-1}	3.229
μ/mm^{-1}	8.115
T_{min}, T_{max}	0.747,0.922
Number of parameters	25
Number of reflections used in refinement	220
Total number of reflections	317
R_{merge}	0.029
$R(I>3.0\sigma(I))$	0.0462
R_w	0.0449

6.3.4.3 *Structure Description*

The asymmetric unit of **(15)** contains a unit with formula $GaSO_3$ and an N-atom, thought to belong to an ammonium moiety (Figure 6.32). The structure consists of $[GaO_6]^{9-}$ octahedra, which are linked along the *a*- and *b*-axes (Figure 6.33).

There are three different oxygen-sites (Figure 6.32); it would be expected that the oxygen site that links the 6-coordinate gallium atoms to one-another is protonated to give an OH^- group, whereas those on the tetrahedral sulphate moiety are non-protonated. The ammonium cations reside in the voids between the layers to balance the negative charge of the network.

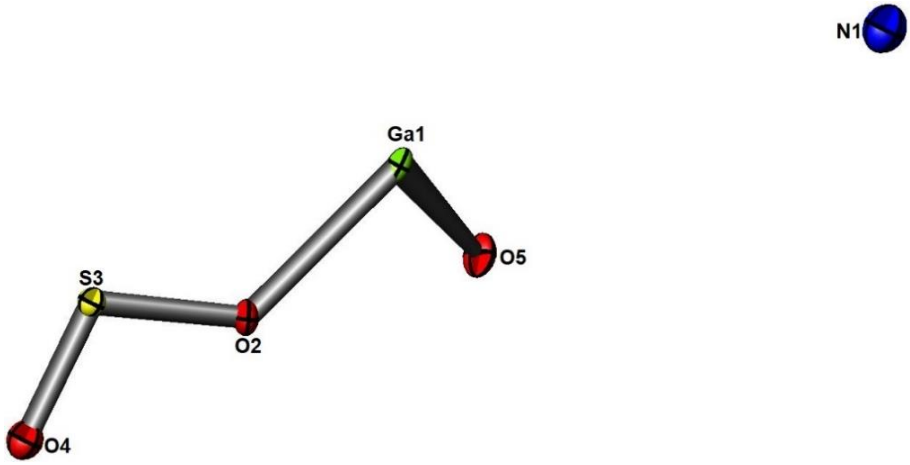

Figure 6.32 Asymmetric unit of **(15).** Green = Ga, yellow = S, red, = O, blue = N. H-atoms omitted for clarity.

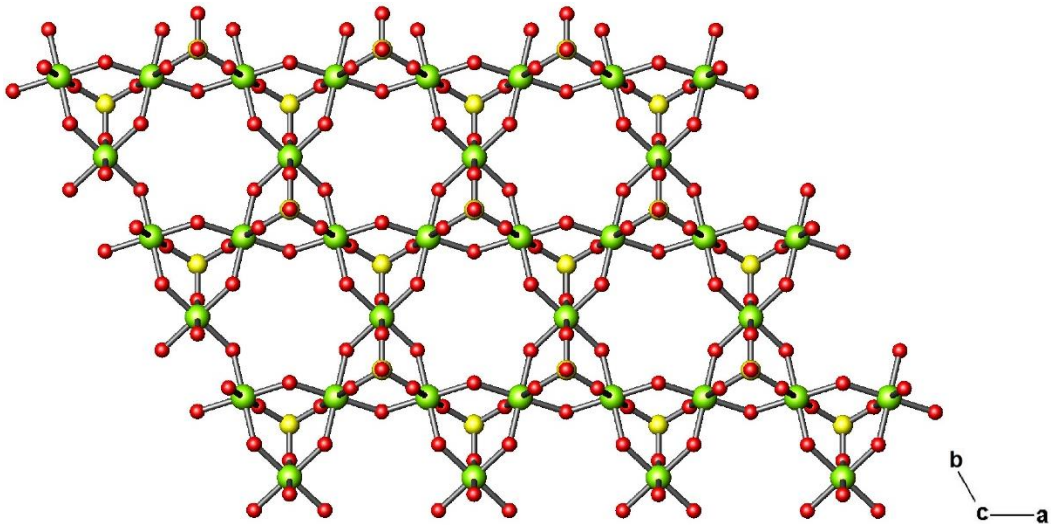

Figure 6.33 Structure of **(15)**, viewed along the *c*-axis. Green = Ga, yellow = S, red, = O, blue = N. H-atoms omitted for clarity.

The Ga-OS bond-length is 1.944(3) Å and the Ga-OH bond-length is 2.039(5) Å. These are in the region expected for shared and non-shared Ga-O bonds respectively.[256] The S-O bond length is 1.446(11), where as the S-O-Ga bond length is 1.481(6), in the region that would be expected in sulphate materials (*ca.* 1.430 – 1.501 Å).[257, 258]

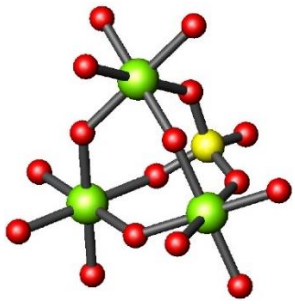

Figure 6.34 SBU in **(15).** Green = Ga, yellow = S, red, = O, blue = N. H-atoms omitted for clarity.

The SBU in **(15)** (Figure 6.34) consists of three octahedral $[GaO_6]^{9-}$ units and one $[SO_4]^{2-}$, linked *via* their corner O-atoms into a ring. In this case, it is expected that O-atoms that are not co-ordinated to sulphur are protonated. This gives the SBU an overall formula of $[Ga_3(OH)_{12}(SO_4)$. These SBUs are linked, alternating in orientation, into 6-membered rings *via* the sharing of the octahedral gallium units, resulting in a 2-dimensional framework $[Ga_3(SO_4)_2(OH)_6]^-$ (Figure 6.33 and Figure 6.35), where the negative charge is balanced by extra-framework ammonium cations.

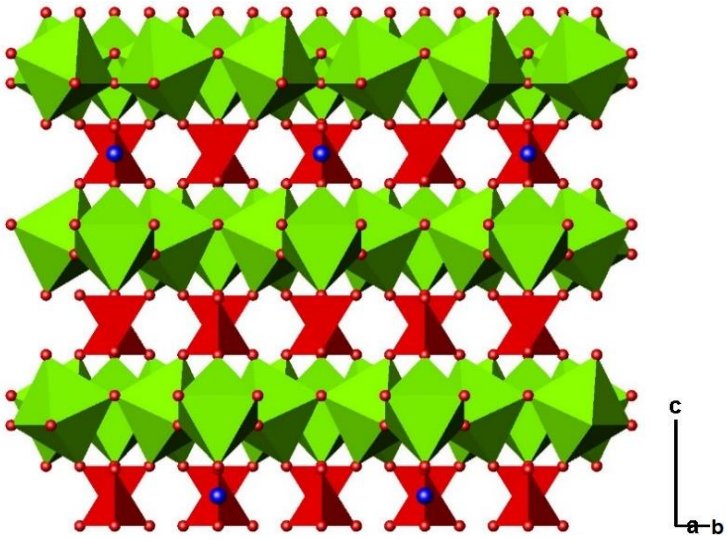

Figure 6.35 Structure of **(15),** viewed along [110]. Green polyhedra = $[GaO_6]^{3-}$, red polyhedra = $[SO_4]^{2-}$, blue = N. H-atoms omitted for clarity.

The layers in **(15)** are parallel with the [110] plane (Figure 6.34 and Figure 6.33), with ammonium cations residing between the layers. **(15)** resembles a material reported by Johansson,[259] stated to contain water in the pores rather than ammonium, with a formula of $((Ga_2O_3)_3(SO_3)_4(H_2O)_9)_{1.5}$. The material is described as relating to the mineral alunite; a potassium, aluminium sulphate with the formula $KAl_3(SO_4)_2(OH)_6$. Alunite is

isostructural with **(15)** and contains K^+ ions in the place of the ammonium species and Ga^{3+} instead of Al^{3+}. Alunite has also been reported with the countercations ammonium, oxonium, rubidium and sodium.[260, 261] It is therefore proposed that this structure is based on that of the ammonium alunite, with the Al^{3+} sites substituted with Ga^{3+}. This "galloalunite" material has previously been investigated by Rudolph *et al.*,[262] who carried out Rietveld refinements using PXRD. To date no single crystal structure solution of this phase has been reported.

6.3.4.4 *Powder X-Ray Diffraction*

Powder X-ray diffraction on **(15)** shows that the bulk is consistent with the structure from single-crystal data (Figure 6.36). It also shows similarities with the PXRD patterns of both the material reported by Johansson and alunite, although there are differences to both. Due to the differences in sizes of the ions contained in the alunite structure compared with **(15)**, there will be a difference between unit cell parameters. There will also be a difference between **(15)** and the structure by Johansson, due to the different charges of the materials reported and the absence of ammonium in the previously reported structure.

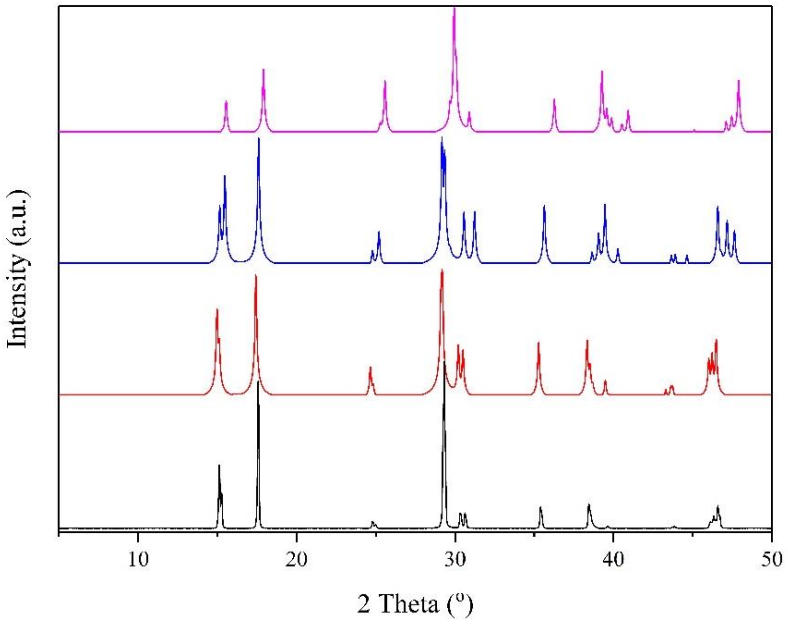

Figure 6.36 PXRD of sample containing **(15)** = black line, **(15)** simulated from SCXRD (red line), material reported by Johansson (blue line)[259] and alunite (magenta line).[263]

Table 6.12 Lattice parameters for **(15).** Parameters were refined against PXRD using DASH.[208]

SCXRD	**a/ Å**	**b/ Å**	**c/ Å**	**α/ º**	**β/ º**	**γ/ º**
	7.1659(7)	7.1659(7)	17.7397(19)	90	90	120
PXRD	**a/ Å**	**b/ Å**	**c/ Å**	**α/ º**	**β/ º**	**γ/ º**
	7.168(6)	7.168(6)	17.746(9)	90	90	120
Rudolph *et al.* PXRD	7.162(1)	7.162(1)	17.751(6)	90	90	120

Rudolph *et al* have not included a cif file with their published results, but unit-cell parameters are displayed in Table 6.12 and show good agreement with **(15)**.[262]

6.3.4.5 *Elemental Analysis*

The formula for **(15)** is $[NH_4][Ga_3(SO_4)_2(OH)_6]$. CHN results give the following experimental values: C = 1.56 %, H = 2.40%, N = 2.44 %, whilst calculated values are: C = 0 %, H = 1.93 %, N = 2.69 %. The inconsistency here comes from the presence of carbon. This value is too high to arise from experimental error, therefore it is suspected that there may be a small amount of organic solvent on the surface of the crystals; possibly residue from the 2,6-Lut. Values for hydrogen and nitrogen are higher and more consistent with the calculated formula, although may be slightly inaccurate due to the presence of solvent. These data therefore strongly suggest the presence of an ammonium cation.

6.3.4.6 *Infrared Spectroscopy*

FTIR of **(15)** (Figure 6.37) is consistent with the presence of ammonium and not water in the pores (Table 6.13). It also confirms the absence of 2,6-Lut from the material, due to the lack of C-H frequencies, as proposed from elemental analysis results. FTIR also confirms the presence of the sulphate species in the framework (Figure 6.37 and Table 6.13).

Table 6.13 Key FTIR frequencies for structure **(15).**[260, 264-266]

Wavenumber/ cm^{-1}	**Assignment**
3440, 2382	ν (O-H)
3260, 1424	Ammonium ν (N-H)
1424	Sulphate ν_a (S-O)
2183, 2013	ν (Ga-OH)
1039, 1010	Sulphate ν_s (S-O)
644	δ (S-O)

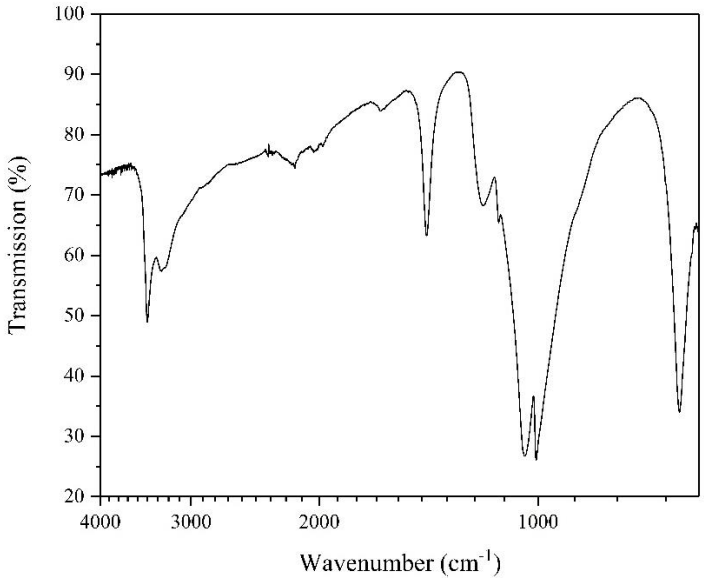

Figure 6.37 FTIR of **(15).**

6.3.4.7 *Thermogravimetric Analysis*

In the case of **(15)**, TGA measurements gave almost identical results in air (Figure 6.38) and under N_2 (Appendix 3). Rudolph *et al.* also carried out thermal analysis on this material and the results shown here are in agreement with those previously published.[262] The total loss of weight for this material is 46 %, where the decomposition temperature is *ca.* 614 K, compared to a literature value of 598 K.

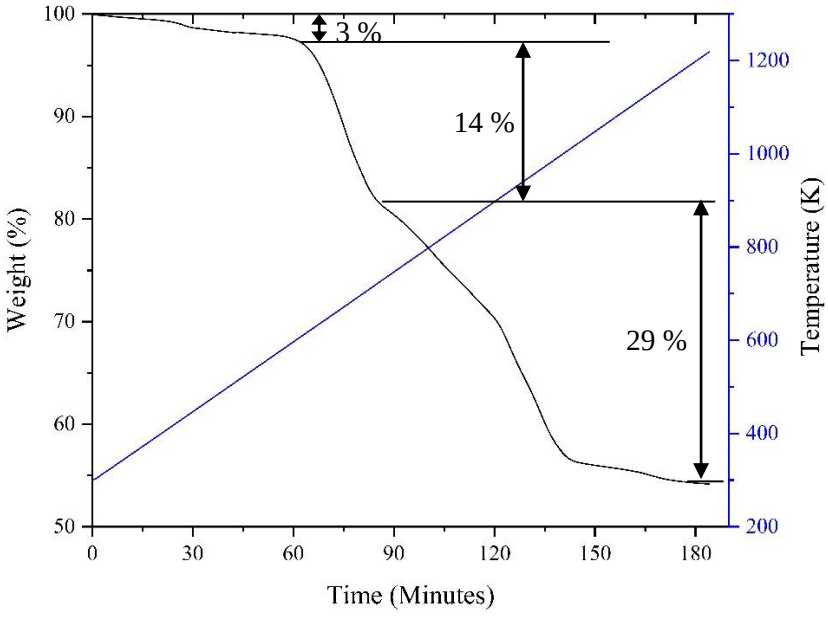

Figure 6.38 TGA for (15) in air.

The first 3 % shown in this measurement could correspond to the loss of surface solvent, such as ethanol or water from washing, as it is not reported by Rudolph *et al.* and is a small percentage to correspond to a decomposition step (Figure 6.38).[262] If this is the case then the following percentages should be calculated based on the material contributing 97 % of the total mass. The following weight-loss of 14 % is reported to be due to the loss of $3H_2O$ and NH_3. This has a calculated weight of 13.3 % and leaves Ga_2O_3 and $GaSO_4(HSO_4)$. The final weight-loss of 29 % is reported to include the loss of $0.5H_2O$ and $2SO_3$ to leave $1.5Ga_2O_3$, *via* an intermediate of $0.5Ga_2(SO_4)_3$. The final weight of the product is 54 %, compared to a calculated value of 52.4 %, this supports the proposal that the ammonium galloalunite material has been produced.

6.3.4.8 *Discussion*

Experimental results suggest the formation of the material previously-named ammonium galloalunite by Rudolph *et al.*.[262] Although this material has been synthesised previously, to the best of our knowledge, this is the first time that single crystals of this material have been prepared. Therefore, this is the first time the structure has been solved from SCXRD data. The synthetic method reported for **(15)** differs significantly to those previously reported.[259, 262] Both report the use of a sulphate as the starting material in the reactions, carried out *via* hydrothermal synthesis. However, **(15)** is suggested to be produced from the reaction of gallium(III) nitrate with sulphur, where water comes from the hydrated hygroscopic nitrate.

$$1/2\ S_8 + 3\ Ga_2(NO_3)_3{\cdot}xH_2O + (18\text{-}3x)\ H_2O \rightarrow 2\ [NH_4][Ga_3(SO_4)_2(OH)_6] + 2NO + 5HNO_3$$

Equation 6.1

This reaction is suggested to occur *via* a redox reaction between sulphur and $Ga_2(NO_3)_3$ (Equation 6.1). In this reaction, S_8 is the reducing agent and $Ga_2(NO_3)_3$ is the oxidising agent. It has not been proven whether 2,6-Lut is involved in this process and different nitrogen-species could be formed from the reduction of $[NO_3]^-$ other than $[NH_4]^+$ and NO, however there must be further nitrogen-species produced in order to facilitate the oxidation of S_8.

6.4 Solvothermal Synthesis Using Superbases

6.4.1 **Reactions Using Superbases as Solvents**

6.4.1.1 ***Summary of Reactions***

Reactions were carried out using superbases DBU and DBN as solvents, both with and without water. The conjugate acids of these amines have significantly higher pKa values than those of other amines used throughout this work, as described in Section 2.1.1 and 5.1. Reactions using superbases as templating agents are described in Section 6.4.2. Reactions took place with different reagents and parameters, as described in Table 6.14.

Table 6.14 Parameters changed throughout this investigation

Reaction Parameter	Variations Used
Metal Sources	Ga, Ga_2O_3 GeO_2
Sulphur Sources	S, Thioacetamide
Temperature/ ^oC	140, 170, 200
Solvent	DBU, DBN, H_2O
Auxiliary Amine	TMDPy, no amine
Time/ Days	5, 6, 10

6.4.1.2 ***Discussion***

Several attempts were made at using superbases as solvents throughout this work, from which a number of outcomes were obtained. In some cases amorphous phases were produced; where Ga and S were reacted in DBU at 200 ^oC. However when a low amount of sulphur was used no solid products were obtained, or when reactions were carried out at the lower temperature

Reactions were carried out with both Ga and GeO_2, either S or TAA in DBU, with either TMDPy or no auxiliary amine (Appendix 1.1 and Appendix 1.2). These reactions were carried out at 170 ^oC for 6 days with different stoichiometric-ratios and gave products that consisted of spheres made up of small crystallites; these phases could not be identified from PXRD (Figure 6.39). These varied in colour, with white spheres given in most cases, but also yellow or pink when TAA was used as the sulphur source. Yellow and pink spheres were given by larger and smaller amounts of TAA respectively.

When the amount of sulphur was reduced too far, in the absence of TMDPy, no product was obtained. When solid products were produced from these reactions carried out at 200 °C, the samples were amorphous. At other temperatures, no solid was produced.

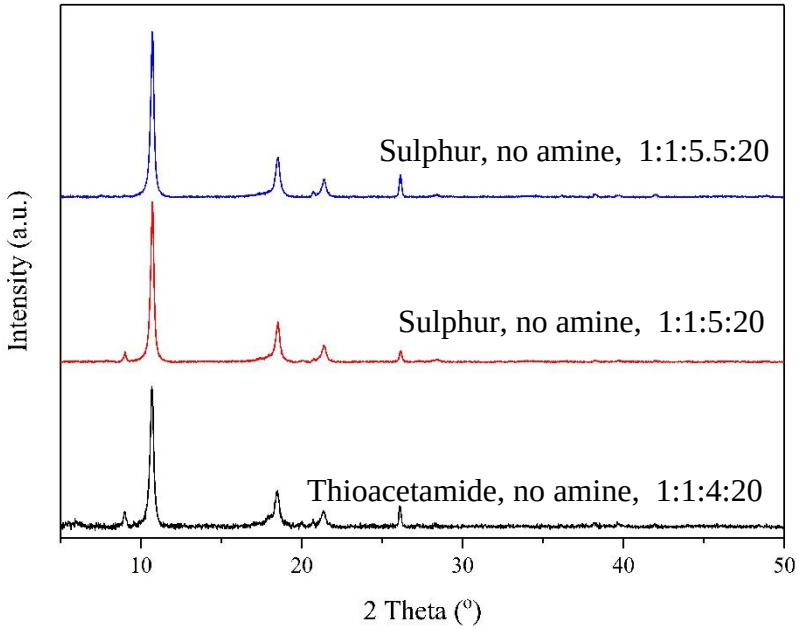

Figure 6.39 PXRD for selection of powders synthesised in DBU from Ga and GeO_2 at 170 °C for 6 days. Ga:GeO_2:Sulphur Source:Amine:DBU ratio shown on graph.

A successful reaction giving single-crystals of novel material **(13)**, synthesised in DBN, is described in Section 5.2.

6.4.2 Solvothermal Reactions Using Superbases as Templating Agents

6.4.2.1 *Summary of Reactions*

The superbases DBU, DBN, TBD and DABCO were also investigated for use as templating agents. DBU, DBN and DABCO are relatively well-known bicyclic amines, with DBU and DBN previously used in the synthesis of supertetrahedral clusters.[115, 116] As DABCO is a solid at room temperature, it was not investigated as a solvent and due to the fact that TBD is expensive, it was not investigated as a solvent as DBU and DBN did not product many new phases. All of the bicyclic amines used in this section have been previously investigated as templates by Ewing and produced novel materials.[267, 268] In this case, a number of different solvents were used, including both amine and non-amine based solvents (Table 6.15). Many of these reactions are based on reactions carried out by Ewing in the investigation of indium and gallium selenides;[249, 267] where indium has been substituted with gallium and selenium substituted with sulphur.

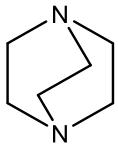

1,4-Diazabicyclo[2.2.2]octane
(DABCO)

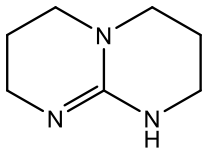

Triazabicyclodecene
(TBD)

Figure 6.40 Structures of different superbases used in this section.

Table 6.15 Parameters changed throughout this investigation

Reaction Parameter	Variations Used
Metal Sources	Ga, GeO_2
Sulphur Sources	S
Temperature/ ^oC	140, 150, 170, 200
Solvent	THF, DMF, ACN, 4-MPy, H_2O
Superbase	DBU, DBN, TBD, DABCO
Auxiliary Amine	Im, TMDPy, no amine
Time/ Days	5, 6, 10

6.4.2.2 *Discussion*

When using superbases as structure-directing agents in solvothermal reactions, a number of different phases were obtained. Details of these reactions carried out are described in Appendix 1.

A number of reactions were carried out at 140 ^oC for 5 days, using either DABCO or DBU as the base and water as the solvent. Only one of these reactions gave a solid product; when Ga, S and DABCO reacted in ACN (acetonitrile), which was gallium oxide. With an increased reaction temperature of 200 ^oC and DBN as the base, no product was formed. With DBU a white powder was formed, with very few peaks in the powder pattern that could not be identified.

When 4-MPy was used as the solvent, a number of products were formed; materials **(1)** and **(4)** (Chapter 3 and Figure 6.19) were produced from Ga and S with DABCO at 200 ^oC for 6 days. When GeO_2 was added, $GaGeS_3$ powder was formed.

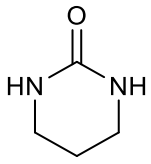

Figure 6.41 Structure of 3,4,5,6-tetrahydropyrimidin-2-one (THP).

In one case the organic material 3,4,5,6-tetrahydro pyrimidin-2-one (THP) (Figure 6.41) was produced from Ga (105 mg, 1.49 mmol) , S (101 mg, 3.16 mmol), TBD and THF. Single crystals of THP were produced,[269] of which the majority dissolved when the sample was washed with water. SCXRD was carried out on one of the remaining red/orange needles of THP to determine the structure. The cif for this material is included in the electronic appendices for this work.

Literature describes that TBD can react with CO_2 in THF to form the adduct displayed in Figure 6.42.[270, 271] If this adduct were to be formed under the autogenous pressures produced in the autoclave with CO_2 from the atmosphere, this could possibly go on to react further to produce 3,4,5,6-tetrahydropyrimidin-2-one.

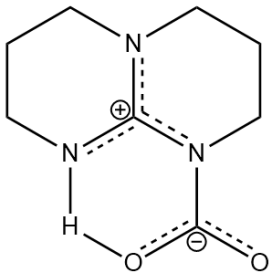

Figure 6.42 Carbamate adduct of TBD

6.5 Other Solvothermal Reactions

6.5.1 **Reactions with Gallium and Germanium Reagents**

6.5.1.1 ***Summary of Reactions***

Reactions were carried out with different gallium-sources and sulphur in different solvents, in attempts to obtain novel phases. These reactions were mainly based on the PhD thesis of Ewing,[268] substituting In and Se with Ga and S respectively.

Table 6.16 Parameters changed throughout this investigation

Reaction Parameter	Variations Used
Metal Sources	Ga, Ga_2O_3, Ga $(NO_3)_3$
Sulphur Sources	S
Temperature/ ^oC	170, 200
Solvent	DACH, DMM, DMF, THF, H_2O
Auxiliary Amine	Im, no amine
Time/ Days	5, 6, 10

6.5.1.2 *Discussion*

Ga and S reacted in water, both with and without GeO_2, with DACH as an auxiliary amine. The reactions were carried out at 170 ^oC for 5 days and both gave amorphous powders. When Ga and S reacted in DMM at 200 ^oC no product was formed and DMM was no longer used as a solvent in these reactions.

A number of reactions were carried out with S as the sulphur source in THF at 200 ^oC. Those containing superbases as auxiliary amines are described in Section 6.4.2. Other reactions were found to produce unidentified powders of different colours. Ga_2O_3 gave a brown powder after 10 days and a beige powder after 6 days, whereas $Ga(NO_3)_3$ produced a black powder after 10 days. Reactions with Ga in the presence of Im gave unidentified black powders.

6.6 Surfactant-Thermal Synthesis

6.6.1 **Introduction**

Surfactant-thermal synthesis has recently been explored as a potential route to producing new crystalline-chalcogenides (Sections 1.6 and 2.1.3).[151] Surfactant-thermal synthesis is a relatively new method of producing metal-chalcogenides (Section 1.6.1) and there are so far no reported T3 or larger supertetrahedral-clusters synthesised in surfactants. It was therefore investigated throughout this work as a possible way of creating new gallium-sulphide materials and supertetrahedral clusters. Different reagents and conditions that have been used throughout this investigation are shown in Table 6.17.

6.6.2 **Summary of Reactions**

The surfactants used in these reactions were polyethylene glycol (PEG-400), a polymer of ethylene oxide, with an average molecular weight of *ca.* 400 $gmol^{-1}$, which is a viscous liquid at room temperature (Figure 6.43). PEG-400 has been used to synthesise a number of novel crystalline-chalcogenides, as described in Section 1.6.1 and is a non-branched surfactant.[151, 176, 177, 180, 181] Polyvinylpyrrolidone (PVP) is a polymer of *N*-Vinylpyrrolidone and is a solid at room temperature with a melting point of between 150 and 180 ^oC (Figure 6.43), it has been investigated by Xiong *et al.* but there are a limited number of examples where it has been used.[176] One of the key properties that is has compared to PEG-400 is the bulky-group on its chain. Cetrimonium bromide (CTAB) is a quarternary ammonium surfactant (Figure 6.43) and is a solid at room

temperature; it was not discovered until a batch of reactions was carried out that the melting point is in fact too high for use as a solvent in these reactions, at between 237 and 243 °C. It was initially chosen as it is a common cationic-surfactant, previously used to form mesoporous chalcogenides by Kanatzidis *et al.*.[172]

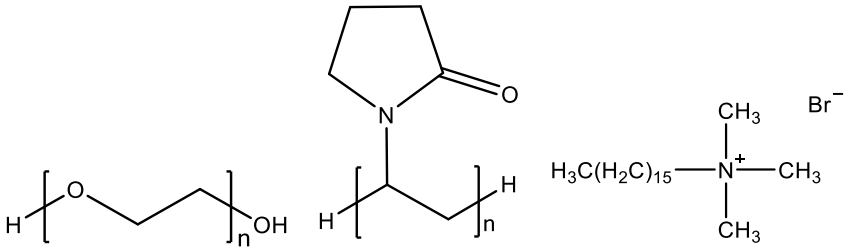

Polyethylene glycol PEG | Polyvinylpyrrolidone PVP | Cetrimonium Bromide (CTAB)

Figure 6.43 Structures of surfactants used in this section.

Table 6.17 Parameters changed throughout this investigation

Reaction Parameter	Variations Used
Metal Source	Ga, GeO_2
Sulphur Sources	S, TAA
Temperature/ °C	140, 160, 170, 190, 200
Solvent	PEG-400, PVP, CTAB, H_2O
Auxiliary Amine	DABCO, DBU, DBN, TBD, Im, 4-MPy, no amine
Time/ Days	5, 6, 8, 10

The auxiliary amines here were chosen based on both experience of forming new materials throughout this work (in the case of Im and 4-MPy) and due to the success of the superbases in reactions carried out by Ewing.[267]

6.6.2.1 *Reactions with CTAB and PVP*

As described, CTAB could not act as a solvent in the reactions in which it was used. In a reaction where CTAB was used with water, at 200 °C for 8 days, no product was formed (Appendix 1.9).

Reactions with PVP gave no product when water, 4-MPy or DBU were added. In the absence of auxiliary amines or solvents, many products consisted of yellow viscous liquids or gels, which did not appear to contain solid product. These reactions were carried out at 160 °C for 5, 6 or 10 days and 190 °C for 9 days.

On the only occurrence that a solid was formed, unidentified white powder was produced when Ga, TAA, DABCO and PVP reacted at 160 ^{o}C for 10 days, with a 2:1.8 ratio of Ga:DABCO, which contained the highest amount of both DABCO and PVP used. Due to the frequent formation of these gels or viscous liquids PVP was no longer investigated as a solvent. (Appendix 1.8).

6.6.2.2 *Reactions with PEG-400*

Reactions were carried out with Ga and S in PEG-400, both with and without water and with no auxiliary amine. Reactions gave either unidentified powders or Ga metal. When 4-MPy was added, unidentified powder was also formed. When GeO_2 was added to these reactions, reactions all gave no solid product, except for where 4-MPy was used as an auxiliary amine.

It was speculated that Ga metal may have been the only product in reactions where Ga^{3+} ions were not produced, due to the inability of PEG to facilitate redox reactions, as described in Sections 2.1.1 and 2.1.3. It would therefore be possible that adding a stronger base would help to produce these ions, therefore superbases DABCO, DBU, DBN and TBD were used as auxiliary amines in the subsequent reactions. To also promote the formation of S^{2-} ions *in situ* TAA was used as a sulphur source in many reactions.

Reactions including both Ga and GeO_2 gave no solid products when DBU was added; suggesting that the solubility may have been too high. From this point, Ga only was used in the surfactant-thermal reactions.

The majority of reactions using Ga with S gave unidentified powders, aside from when TBD was used as an auxiliary amine at 200 ^{o}C, which gave Ga metal only, suggesting that the solubility was too high in this case. Two of these reactions gave materials described in Chapter 5. **(12c)** was synthesised from Ga, S, DBU and PEG (Section 5.2) and **(13)** was produced from Ga, S, DBN and PEG (Section 5.3).

When TAA was used as the sulphur source, unidentified powders were also produced in most reactions. However, single crystals of **(12a)** were produced from Ga, TAA, DBU and PEG at 140 ^{o}C over 6 days (Section 5.2). Single crystals of **(12b)** were produced in two different reactions from the same reagents at 160 ^{o}C for 6 days and were formed with two different amounts of DBU (Section 5.2).

6.6.3 **Discussion**

Reactions were carried out based on the surfactant-thermal synthesis method. The most successful surfactant used was PEG-400, which gave single crystals of materials described in Chapter 5, along with a number of unidentified powders. Using superbases as auxiliary amines promoted the formation of single crystals and in most cases TAA was used as the sulphur source, although there was one exception to this rule.

PVP appeared to be too viscous when used as solvent, but when used in conjunction with a co-solvent or auxiliary amine caused the solubility of the reaction mixture to become too high and no products were formed.

6.7 Discussion of Chapter

This chapter describes the different types of reactions that have been carried out throughout this work. Initially, reactions were carried out in ionic liquids in attempts to obtain new phases *via* ionothermal synthesis (Section 6.2) and this case, reactions were unsuccessful. Reactions were therefore carried out using ionic liquids as templates in the amine 4-MPy, used numerous times throughout this work for its affinity to form hybrid T3 clusters (Section 6.2.4). These reactions gave both the novel phase **(2)** (Section 3.2.2), and isostructural compounds to known phases **(1)** and **(3)** (Section 3.2.1 and 3.3). A reaction was also carried out in water with the ionic liquid [THTDP]Cl and gave the novel doubly-interpenetrating framework material **(14)** (Section 6.2.6).

Solvothermal reactions were also carried out in 4-MPy. Reactions carried out with Ga metal gave materials **(4)** – **(7)**, which were isostructural with previously-synthesised materials. Synthesis of isostructural materials is described in Section 6.3.2. Single-crystals of the 2-dimensional-sulphate ammonium "galloalunite" were also synthesised for the first time, from $Ga_2(NO_3)_3$, S and 2,6-Lut (Section 6.3.4), allowing the full structure-determination of this material, which has been previously synthesised in powder form by Rudolph *et al.*[261]However, this is the first time single crystals of this material have been obtained.

GeO_2 was added into these reactions in an attempt to form mixed-metal hybrid clusters. Materials were formed of different dimensionalities, as described in Section 4. In this Chapter it has been discussed that the dimensionality appears to increase with temperature and different synthesis methods for producing materials isostructural to 1-

dimensional material **(9)** and 3-dimensional materials **(10)** and **(11)** are described in Section 6.3.3.

Reactions were also carried out using superbases as both templating agents and solvents (Section 6.4.1), due to the success of reactions carried out with these by Ewing.[267, 268] In most cases these reactions gave powder. However, the 1-dimensional chain-compound **(13)** was formed using DBN as an SDA, as described in Section 5.3. Successful reactions with DBU were carried out in the surfactant PEG (Section 5.2). In this case it was beneficial to use superbases as auxiliary amines, as PEG is a neutral solvent and does not facilitate the redox reactions required in these reactions (Sections 2.1.1, 2.1.3 and 6.6.2). The boiling point of the surfactant CTAB was found to be too high to be used in these reactions, whereas PVP was found to be too viscous (Section 6.6.2.1).

A number of reactions in different solvents, using both amine-based and non amine-based solvents were carried out. Mainly based on previous reactions by Ewing, but substituting In and Se with Ga and S respectively (Section 6.5) but did not successfully produce any new materials.

7 Conclusions

Throughout the course of this project, investigations have been carried out in the pursuit of novel materials, where a list of all reactions and products is contained in Appendix 1. The materials initially investigated were based on T3 gallium-sulphide supertetrahedra (Sections 3, 5.2 and 6.2.6), which have been previously explored by Vaqueiro and Feng (Sections 1.4.4 and 1.4.5). A number of materials based on hybrid gallium-sulphide T3 clusters with the formula $[Ga_{10}S_{16}(L)_4]^{2-}$ (L = pyridyl-based ligand) were synthesised in 4-MPy, where **(2)** $[C_{12}H_{13}N_2]_{0.5}[C_6H_8N]_{1.5}[Ga_{10}S_{16}(NC_6H_7)_4](C_6H_7N)_{0.5}$ was a novel material. **(1)** $[C_6H_8N]_2[C_{12}H_{14}N_2][Ga_{10}S_{16}(NC_6H_7)_4]_2(C_{12}H_{12}N_2)(C_6H_7N)_2$ and **(3)** $[C_3H_3N_2C_4H_9CH_3][C_6H_8N][Ga_{10}S_{16}(NC_6H_7)_2(NC_6H_6)_2](C_6H_7N)_{0.5}$ were synthesised using ionic liquids and **(4)** $[NC_6H_8]_{2.5}[N_2C_4H_6][C_3H_5N_2]_{0.5}[Ga_{20}S_{32}(N_2C_{12}H_{12})_2(NC_6H_7)_5]$, **(5)** $[C_6H_8N]_4[Ga_{10}S_{16}(NC_6H_7)_3(NC_6H_6)][Ga_{10}S_{16}(NC_6H_7)_4](C_6H_7N)_2$ and **(6)** $[C_6H_8N]_6[Ga_{20}S_{32}(NC_6H_7)_6(N_2C_{12}H_{12})][Ga_{10}S_{16}(NC_6H_7)_3(C_6H_6N)](C_6H_7N)_6$ were synthesised solvothermally; these five materials were isostructural to existing materials but synthesised in different ways and containing different countercations in the voids.

The semiconducting and photoluminescent properties of materials **(1)** to **(5)** were measured. All materials are wide-gap semiconductors and emit in the visible region when exposed to UV light. **(1)** showed the longest lifetime and highest quantum efficiency, whereas **(2)** had the benefit of emitting at the wavelength of white light. Photoluminescence is proposed to originate from the formation of ion-pair charge-transfer (IPCT) pairs between the clusters and the organic cations, where the clusters are electron-donors and the cations are the acceptors. This concept has previously been discussed by Zhang *et al.* in the context of supertetrahedral chalcogenide-clusters.[226] In the case of the hybrid T3 supertetrahedra, the intensity of the charge-transfer bands appears to be affected by the dimensionality of the materials. The intensity of the band appears to be the strongest for discrete clusters and becomes gradually weaker with the formation of dimers and then chains.

(7) $[C_6H_8N]_{14}[Ga_{10}S_{20}]_7(NC_2H_7)_4(NC_6H_7)_8(N_2C_{12}H_{12})_8$ was a previously-synthesised 2-dimensional material by Tong,[225] where the synthetic method was optimised throughout the course of this project and initial physical-property measurements were carried out. This material, which contained a tetrahedron of

supertetrahedra linked *via* EDPy ligands, was also found to be a wide-gap semiconductor, with no discernible charge-transfer band in the diffuse-reflectance spectrum (Section 3.6.1.7).

When germanium oxide was added into the reaction mixtures, T3 clusters were no longer formed and four different materials were produced (Chapter 4). **(9)** $[NC_6H_8]_2$-$[Ge_4S_9](C_6H_7N)_{0.5}$ and **(10)** $[C_6H_8N]_2[Ga_2Ge_2S_8]$ were isostructural to materials reported by Bedard and Feng respectively and both contained T2 supertetrahedral clusters based on the $[M_4S_{10}]^{n-}$,[104, 230] where M = Ga^{3+} or Ge^{4+}. **(8)** $[NC_6H_8]_8[Ge_{12}S_{28}]$ also contained these T2 supertetrahedral clusters and was a novel material consisting of trimers of clusters that unfortunately could not be reproduced (Section 4.2). **(8)** and **(9)** were both confirmed by EDX to contain no gallium in the composition and **(9)** could be formed in the absence of gallium (Sections 4.2.2.2 and 4.3.1.1). **(10)** $[NC_6H_8][GaGe_3S_8](NC_6H_7)(H_2O)_5$ was found to contain a 1:1 ratio of Ge:Ga (Section 4.4.2.1). **(11)** was a novel framework-material based on $[MS_4]^{n-}$, where M = Ga^{3+} or Ge^{4+} and the Ge:Ga ratio was determined using EDX analysis to be 3:1 (Section 4.5). Bond-valence sums for **(11)** indicated that there was no ordering of Ge and Ga between the metal sites and that these were likely to be disordered throughout the material (Section 4.5.2.4). The diameter of the pores appeared to be *ca.* 2.5 Å and CHN analysis indicated that these contain both protonated 4-MPy moieties and water (Section 4.5.2.6).

Compounds **(9)** – **(11)** were all found to be wide-gap semiconductors, which is consistent with the yellow-orange colours of the crystals. It is not trivial to compare the band-gaps of germanium-sulphides and gallium-sulphides to one another. As discussed in Section 4.5.2.9, it could be suggested that the band gap increases with increasing dimensionality and decreases with increasing Ga:Ge ratio, as this would also be consistent with the mixed germanium and gallium sulphide UCR-20 reported by Feng.[184] However, it is not clear whether the fact that **(11)** is not built from T2 clusters would have a great effect on the band gap.

T3 gallium-sulphide supertetrahedra were also synthesised in the absence of 4-MPy. In one case, a mixture of the ionic liquid [THTDP]Cl with water gave the doubly interpenetrating framework in **(14)** $[(CH_3(CH_2)_5)_3P(CH_2)_{13}CH_3]_{0.25}[NH_4]_{5.75}[Ga_{10}S_{18}]$-$(NH_3)$ (Section 6.2.6). To the best of our knowledge, this is the first time a material based on T3 supertetrahedra has been synthesised with an IL in the absence of an amine. During the course of this work, a number of reactions were carried out using ILs as solvents and

it was not found to be a good route for obtaining novel phases (Section 6.2), but instead led to materials synthesised by using ILs as templating agents (Section 6.2.4).

(12) contained the discrete T3 gallium-sulphide cluster $[Ga_{10}S_{16}(SH)_4]^{6-}$ (Section 5.2). The anionic charge of this cluster was balanced by six protonated DBU molecules, which could all be located in the crystal structure to give the formula $[C_9H_{18}N_2]_6$ - $[Ga_{10}S_{16}(SH)_4]$. In this case, the material was synthesised in PEG-400, a neutral surfactant, in the presence of DBU (a bicyclic amine), where the PEG appeared to act as a templating agent. This represents the first discrete inorganic T3 gallium-sulphide supertetrahedron formed, i.e. with no organic ligands coordinating to the corners. In this case, three different colours of crystal were formed, denoted **(12a), (12b)** and **(12c)** where the crystals are colourless, yellow and red respectively. From CHN analysis and PXRD it appears that there is no difference in the chemical composition of these materials, however diffuse-reflectance spectroscopy implies that the materials are different colours. It is possible that the different colours could stem from defects present in **(12b)** and **(12c)**, as described in Section 5.2.3.7.

Other reactions were carried out in both surfactants and bicyclic amines. When using the surfactant PVP, which is more viscous than PEG-400, as a solvent the products generally consisted of thick gels from which no suitable product could be obtained. When carrying out reactions in PEG, an auxiliary amine was required to facilitate the redox reactions that take place between gallium and sulphur.

Using the bicyclic amine DBN as a solvent, material **(13)** $[C_7H_{13}N_2][GaS_2]$, consisting of chains of $[GaS_2]^-$, was formed. These chains are analogous to those previously reported by Vaqueiro *et al.*[123, 129] however, in this material the chains are aligned parallel to one-another, which has not been displayed previously for these gallium-sulphide chains. This was the only material to successfully produce single crystals from the reactions carried out using bicyclic amines as solvents.

Single crystals of the gallium-sulphate material ammonium galloalunite, previously synthesised by Rudolph *et. al* were produced in a reaction between gallium nitrate and sulphur powder in 2,6-Lut. This was the first time the structure of this material has been determined from SCXRD rather than from PXRD data.

8 Future Work

In this work, reactions have been carried out using solvothermal, ionothermal and surfactant-thermal synthesis methods. Ionothermal synthesis has not proven to be successful in this work, although using ILs as templates could be pursued further. Regarding the series of hybrid T3 gallium-sulphide supertetrahedra, it is not possible to predict whether it will be possible to form new analogues of these materials, due to the recent unprecedented creation of materials **(2)** and **(7)**, however when varying the ratios and temperatures, these reactions regularly produced the same compounds, which on most occasions would be either **(1)** or **(4)**, as discussed in Section 6.3.2.

There could be room for development in the field of germanium-gallium sulphides, however, similarly to for the materials described above, the most stable of these materials **(9)** and **(10)** were regularly synthesised (Section 6.3.3). There is potential to optimise the reactions of the novel materials **(8)** and **(11)**, in order to reproduce and obtain a pure sample of the materials respectively. There may also be new phases of non-supertetrahedral frameworks in the family of **(11)** that have yet to be discovered, which could possibly be found using different solvents or SDAs. It is also possible that new phases could be accessible on the addition of transition metals into these reactions, although this has already been explored to a certain extent with gallium sulphides by a previous PhD student and attempts to incorporate copper into these reactions were unsuccessful in this work.[223]

Investigations could also be carried out into whether using different surfactants with an auxiliary solvent could produce novel phases, while ensuring that the relative amount of auxiliary solvent does not exceed the amount that would cause the formation of micelles. This is because the formation of micelles would promote the formation of mesoporous rather than microporous materials.

9 References

1. F. J. DiSalvo, *Science*, 1999, **285**, 703-706.
2. J. R. Sootsman, D. Y. Chung and M. G. Kanatzidis, *Angew. Chem. Int. Ed.*, 2009, **48**, 8616-8639.
3. N. L. Rosi, J. Eckert, M. Eddaoudi, D. T. Vodak, J. Kim, M. O'Keeffe and O. M. Yaghi, *Science*, 2003, **300**, 1127-1129.
4. O. M. Yaghi, M. O'Keeffe, N. W. Ockwig, H. K. Chae, M. Eddaoudi and J. Kim, *Nature*, 2003, **423**, 705-714.
5. B. Krebs and S. Pohl, *Z. Naturforsch., B: Anorg. Chem., Org. Chem., Biochem., Biophys., Biol.*, 1971, **B 26**, 853.
6. A. Hagfeldt, G. Boschloo, L. Sun, L. Kloo and H. Pettersson, *Chem. Rev.*, 2010, **110**, 6595-6663.
7. X. Chen and S. S. Mao, *Chem. Rev.*, 2007, **107**, 2891-2959.
8. A. Corma, *Chem. Rev.*, 1997, **97**, 2373-2419.
9. A. Taguchi and F. Schuth, *Microporous Mesoporous Mater.*, 2005, **77**, 1-45.
10. Q. H. Wang, K. Kalantar-Zadeh, A. Kis, J. N. Coleman and M. S. Strano, *Nat. Nanotechnol.*, 2012, **7**, 699-712.
11. I. Chung and M. G. Kanatzidis, *Chem. Mater.*, 2014, **26**, 849-869.
12. T. Trindade, P. O'Brien and N. L. Pickett, *Chem. Mater.*, 2001, **13**, 3843-3858.
13. A. Zakery and S. R. Elliott, *J. Non-Cryst. Solids*, 2003, **330**, 1-12.
14. J. L. Mohanan, I. U. Arachchige and S. L. Brock, *Science*, 2005, **307**, 397-400.
15. C. B. Murray, D. J. Norris and M. G. Bawendi, *J. Am. Chem. Soc.*, 1993, **115**, 8706-8715.
16. M. R. Hoffmann, S. T. Martin, W. Y. Choi and D. W. Bahnemann, *Chem. Rev.*, 1995, **95**, 69-96.
17. J. L. C. Rowsell and O. M. Yaghi, *Angew. Chem. Int. Ed.*, 2005, **44**, 4670-4679.
18. A. Corma, *J. Catal.*, 2003, **216**, 298-312.
19. J. S. Seo, D. Whang, H. Lee, S. I. Jun, J. Oh, Y. J. Jeon and K. Kim, *Nature*, 2000, **404**, 982-986.
20. M. E. Davis, *Acc. Chem. Res.*, 1993, **26**, 111-115.
21. J. R. Li, J. Sculley and H. C. Zhou, *Chem. Rev.*, 2012, **112**, 869-932.
22. A. Clearfield, *Chem. Rev.*, 1988, **88**, 125-148.
23. S. Kitagawa, R. Kitaura and S. Noro, *Angew. Chem. Int. Ed.*, 2004, **43**, 2334-2375.
24. P. Horcajada, C. Serre, M. Vallet-Regi, M. Sebban, F. Taulelle and G. Ferey, *Angew. Chem. Int. Ed.*, 2006, **45**, 5974-5978.
25. M. Vallet-Regi, F. Balas and D. Arcos, *Angew. Chem. Int. Ed.*, 2007, **46**, 7548-7558.
26. M. E. Davis and R. F. Lobo, *Chem. Mater.*, 1992, **4**, 756-768.
27. R. M. Barrer, *Zeolites*, 1981, **1**, 130-140.
28. C. S. Cundy and P. A. Cox, *Chem. Rev.*, 2003, **103**, 663-701.
29. E. Erdem, N. Karapinar and R. Donat, *J. Colloid Interf. Sci.*, 2004, **280**, 309-314.
30. G. E. Boyd, J. Schubert and A. W. Adamson, *J. Am. Chem. Soc.*, 1947, **69**, 2818-2829.
31. G. Blanchard, M. Maunaye and G. Martin, *Water Res.*, 1984, **18**, 1501-1507.
32. S. M. Kuznicki, V. A. Bell, S. Nair, H. W. Hillhouse, R. M. Jacubinas, C. M. Braunbarth, B. H. Toby and M. Tsapatsis, *Nature*, 2001, **412**, 720-724.

33. I. Hassan and H. D. Grundy, *Acta Crystallogr. C*, 1983, **39**, 3-5.
34. G. T. Kokotailo, S. L. Lawton, D. H. Olson and W. M. Meier, *Nature*, 1978, **272**, 437-438.
35. D. H. Olson, G. T. Kokotailo, S. L. Lawton and W. M. Meier, *J. Phys. Chem. U.S.*, 1981, **85**, 2238-2243.
36. S. T. Wilson, B. M. Lok, C. A. Messina, T. R. Cannan and E. M. Flanigen, *J. Am. Chem. Soc.*, 1982, **104**, 1146-1147.
37. J. B. Parise, *J. Chem. Soc. Chem. Comm.*, 1985, 606-607.
38. R. Fricke, H. Kosslick, G. Lischke and M. Richter, *Chem. Rev.*, 2000, **100**, 2303-2405.
39. R. Szostak and T. L. Thomas, *J. Chem. Soc. Chem. Comm.*, 1986, 113-114.
40. R. Szostak, V. Nair and T. L. Thomas, *J. Chem. Soc., Faraday Trans. 1*, 1987, **83**, 487-494.
41. D. M. Chapman and A. L. Roe, *Zeolites*, 1990, **10**, 730-737.
42. A. Corma, M. T. Navarro and J. P. Pariente, *J. Chem. Soc. Chem. Comm.*, 1994, 147-148.
43. B. Sulikowski and J. Klinowski, *Appl. Catal. A*, 1992, **84**, 141-153.
44. J. S. Chen, R. H. Jones, S. Natarajan, M. B. Hursthouse and J. M. Thomas, *Angew. Chem. Int. Ed.*, 1994, **33**, 639-640.
45. R. M. Barrer and E. F. Freund, *J. Chem. Soc., Dalton Trans.*, 1974, 1049-1053.
46. G. Coudurier, A. Auroux, J. C. Vedrine, R. D. Farlee, L. Abrams and R. D. Shannon, *J. Catal.*, 1987, **108**, 1-14.
47. B. Sulikowski, *Heterog. Chem. Rev.*, 1996, **3**, 203-268.
48. P. Y. Feng, X. H. Bu and G. D. Stucky, *Nature*, 1997, **388**, 735-741.
49. M. Iwamoto, H. Furukawa, Y. Mine, F. Uemura, S. I. Mikuriya and S. Kagawa, *J. Chem. Soc. Chem. Comm.*, 1986, 1272-1273.
50. S. Sato, Y. Yoshihiro, H. Yahiro, N. Mizuno and M. Iwamoto, *Appl. Catal.*, 1991, **70**, L1-L5.
51. C. R. Bayense and J. H. C. Vanhooff, *Appl. Catal.*, 1991, **79**, 127-140.
52. C. R. Bayense, A. Vanderpol and J. H. C. Vanhooff, *Appl. Catal.*, 1991, **72**, 81-98.
53. C. T. W. Chu and C. D. Chang, *J. Phys. Chem.*, 1985, **89**, 1569-1571.
54. M. S. Stave and J. B. Nicholas, *J. Phys. Chem.*, 1995, **99**, 15046-15061.
55. S. P. Yuan, J. G. Wang, Y. W. Li and H. J. Jiao, *J. Phys. Chem. A*, 2002, **106**, 8167-8172.
56. G. Ferey, *Chem. Soc. Rev.*, 2008, **37**, 191-214.
57. A. K. Cheetham, G. Ferey and T. Loiseau, *Angew. Chem. Int. Ed.*, 1999, **38**, 3268-3292.
58. M. O'Keeffe, M. Eddaoudi, H. L. Li, T. Reineke and O. M. Yaghi, *J. Solid State Chem.*, 2000, **152**, 3-20.
59. H. Li, M. Eddaoudi, M. O'Keeffe and O. M. Yaghi, *Nature*, 1999, **402**, 276-279.
60. X. C. Huang, Y. Y. Lin, J. P. Zhang and X. M. Chen, *Angew. Chem. Int. Ed.*, 2006, **45**, 1557-1559.
61. S. S. Y. Chui, S. M. F. Lo, J. P. H. Charmant, A. G. Orpen and I. D. Williams, *Science*, 1999, **283**, 1148-1150.
62. D. Maspoch, D. Ruiz-Molina and J. Veciana, *J. Mater. Chem.*, 2004, **14**, 2713-2723.
63. R. Vaidhyanathan, S. S. Iremonger, G. K. H. Shimizu, P. G. Boyd, S. Alavi and T. K. Woo, *Science*, 2010, **330**, 650-653.

64. A. Phan, C. J. Doonan, F. J. Uribe-Romo, C. B. Knobler, M. O'Keeffe and O. M. Yaghi, *Acc. Chem. Res.*, 2010, **43**, 58-67.
65. K. S. Park, Z. Ni, A. P. Cote, J. Y. Choi, R. Huang, F. J. Uribe-Romo, H. K. Chae, M. O'Keeffe and O. M. Yaghi, *P. Natl. Acad. Sci. U.S.A.*, 2006, **103**, 10186-10191.
66. R. Banerjee, A. Phan, B. Wang, C. Knobler, H. Furukawa, M. O'Keeffe and O. M. Yaghi, *Science*, 2008, **319**, 939-943.
67. D. Maspoch, D. Ruiz-Molina and J. Veciana, *Chem. Soc. Rev.*, 2007, **36**, 770-818.
68. I. Repins, M. A. Contreras, B. Egaas, C. DeHart, J. Scharf, C. L. Perkins, B. To and R. Noufi, *Prog. Photovoltaics*, 2008, **16**, 235-239.
69. B. J. Stanbery, *Crit. Rev. Solid State and Mater. Sci.*, 2002, **27**, 73-117.
70. S. Raoux, G. W. Burr, M. J. Breitwisch, C. T. Rettner, Y. C. Chen, R. M. Shelby, M. Salinga, D. Krebs, S. H. Chen, H. L. Lung and C. H. Lam, *IBM J. Res. Dev.*, 2008, **52**, 465-479.
71. S. Hudgens and B. Johnson, *MRS Bull.*, 2004, **29**, 829-832.
72. Y. Jung, S. H. Lee, D. K. Ko and R. Agarwal, *J. Am. Chem. Soc.*, 2006, **128**, 14026-14027.
73. M. R. Gao, Y. F. Xu, J. Jiang and S. H. Yu, *Chem. Soc. Rev.*, 2013, **42**, 2986-3017.
74. S. K. Mishra, S. Satpathy and O. Jepsen, *J. Phys.: Condens. Matter*, 1997, **9**, 461-470.
75. T. Zhu, Z. Wang, S. Ding, J. S. Chen and X. W. Lou, *RSC Adv.*, 2011, **1**, 397-400.
76. H. Zhong, G. Yang, H. Song, Q. Liao, H. Cui, P. Shen and C.-X. Wang, *J. Phys. Chem. C*, 2012, **116**, 9319-9326.
77. S. M. Kuo, Y. M. Chang, I. Chung, J. I. Jang, B. H. Her, S. H. Yang, J. B. Ketterson, M. G. Kanatzidis and K. F. Hsu, *Chem. Mater.*, 2013, **25**, 2427-2433.
78. P. Canarelli, Z. Benko, R. Curl and F. K. Tittel, *J. Opt. Soc. Am. B*, 1992, **9**, 197-202.
79. H. Lin, L. J. Zhou and L. Chen, *Chem. Mater.*, 2012, **24**, 3406-3414.
80. Y. Li, H. Wang, L. Xie, Y. Liang, G. Hong and H. Dai, *J. Am. Chem. Soc.*, 2011, **133**, 7296-7299.
81. M. Wang, A. M. Anghel, B. Marsan, N.-L. C. Ha, N. Pootrakulchote, S. M. Zakeeruddin and M. Graetzel, *J. Am. Chem. Soc.*, 2009, **131**, 15976-+.
82. H. L. Li, A. Laine, M. O'Keeffe and O. M. Yaghi, *Science*, 1999, **283**, 1145-1147.
83. A. Choy, D. Craig, I. Dance and M. Scudder, *J. Chem. Soc. Chem. Comm.*, 1982, 1246-1247.
84. I. G. Dance, A. Choy and M. L. Scudder, *J. Am. Chem. Soc.*, 1984, **106**, 6285-6295.
85. I. Dance and K. Fisher, *Prog. Inorg. Chemistry.*, 1994, **41**, 637-803.
86. P. Y. Feng, X. H. Bu and N. F. Zheng, *Acc. Chem. Res.*, 2005, **38**, 293-303.
87. X. H. Bu, N. F. Zheng, Y. Q. Li and P. Y. Feng, *J. Am. Chem. Soc.*, 2002, **124**, 12646-12647.
88. T. Vossmeyer, G. Reck, L. Katsikas, E. T. K. Haupt, B. Schulz and H. Weller, *Science*, 1995, **267**, 1476-1479.
89. C. Wang, Y. Q. Li, X. H. Bu, N. F. Zheng, O. Zivkovic, C. S. Yang and P. Y. Feng, *J. Am. Chem. Soc.*, 2001, **123**, 11506-11507.
90. A. Moller, P. Amann, V. Kataev and N. Schittner, *Z. Anorg. Allg. Chem.*, 2004, **630**, 890-894.

91. X. H. Bu, N. F. Zheng and P. Y. Feng, *Chem. Eur. J.*, 2004, **10**, 3356-3362.
92. N. F. Zheng, X. H. Bu and P. Y. Feng, *Angew. Chem. Int. Ed.*, 2004, **43**, 4753-4755.
93. Q. Zhang, X. Bu, L. Han and P. Feng, *Inorg. Chem.*, 2006, **45**, 6684-6687.
94. P. Vaqueiro, *Dalton Trans.*, 2010, **39**, 5965-5972.
95. S. Dehnen and M. K. Brandmayer, *J. Am. Chem. Soc.*, 2003, **125**, 6618-6619.
96. C. Zimmermann, M. Melullis and S. Dehnen, *Angew. Chem. Int. Ed.*, 2002, **41**, 4269-4272.
97. H. L. Li, J. Kim, M. O'Keeffe and O. M. Yaghi, *Angew. Chem. Int. Ed.*, 2003, **42**, 1819-1821.
98. G. S. H. Lee, D. C. Craig, I. Ma, M. L. Scudder, T. D. Bailey and I. G. Dance, *J. Am. Chem. Soc.*, 1988, **110**, 4863-4864.
99. B. Krebs, D. Voelker and K. O. Stiller, *Inorg. Chim. Acta*, 1982, **65**, L101-L102.
100. B. Eisenmann, M. Jakowski and H. Schafer, *Z. Naturforsch., B: J. Chem. Sci.*, 1983, **38**, 1581-1584.
101. M. J. MacLachlan, S. Petrov, R. L. Bedard, I. Manners and G. A. Ozin, *Angew. Chem. Int. Ed.*, 1998, **37**, 2076-2079.
102. C. L. Cahill and J. B. Parise, *Chem. Mater.*, 1997, **9**, 807-811.
103. J. B. Parise and K. M. Tan, *Chem. Commun.*, 1996, 1687-1688.
104. N. F. Zheng, X. G. Bu, B. Wang and P. Y. Feng, *Science*, 2002, **298**, 2366-2369.
105. N. F. Zheng, X. H. Bu and P. Y. Feng, *J. Am. Chem. Soc.*, 2003, **125**, 1138-1139.
106. S. Behrens, M. Bettenhausen, A. C. Deveson, A. Eichhofer, D. Fenske, A. Lohde and U. Woggon, *Angew. Chem. Int. Ed.*, 1996, **35**, 2215-2218.
107. S. Behrens, M. Bettenhausen, A. Eichhofer and D. Fenske, *Angew. Chem. Int. Ed.*, 1997, **36**, 2797-2799.
108. H. Pfistner and D. Fenske, *Z. Anorg. Allg. Chem.*, 2001, **627**, 575-582.
109. A. Eichhofer and P. Deglmann, *Eur. J. Inorg. Chem.*, 2004, 349-355.
110. A. Eichhofer and E. Troster, *Eur. J. Inorg. Chem.*, 2002, 2253-2256.
111. H. Pfistner and D. Fenske, *Z Anorg Allg Chem*, 2001, **627**, 575-582.
112. A. Eichhofer, A. Aharoni and U. Banin, *Z. Anorg. Allg. Chem.*, 2002, **628**, 2415-2421.
113. P. Vaqueiro and M. L. Romero, *Chem. Commun.*, 2007, 3282-3284.
114. P. Vaqueiro and M. L. Romero, *Inorg. Chem.*, 2009, **48**, 810-812.
115. T. Wu, X. Bu, P. Liao, L. Wang, S.-T. Zheng, R. Ma and P. Feng, *J. Am. Chem. Soc.*, 2012, **134**, 3619-3622.
116. T. Wu, R. Khazhakyan, L. Wang, X. H. Bu, S. T. Zheng, V. Chau and P. Y. Feng, *Angew. Chem. Int. Ed.*, 2011, **50**, 2536-2539.
117. N. F. Zheng, X. H. Bu, H. W. Lu, L. Chen and P. Y. Feng, *J. Am. Chem. Soc.*, 2005, **127**, 14990-14991.
118. J. L. Xie, X. H. Bu, N. F. Zheng and P. Y. Feng, *Chem. Commun.*, 2005, 4916-4918.
119. P. Vaqueiro and M. L. Romero, *J. Am. Chem. Soc.*, 2008, **130**, 9630-9631.
120. S. Heimann, G. Thiele and S. Dehnen, *J. Organomet. Chem.*, 2016, **813**, 36-40.
121. Z. H. Fard, R. Clerac and S. Dehnen, *Chem. Eur. J.*, 2010, **16**, 2050-2053.
122. J. Zhou, J. Dai, G. Q. Bian and C. Y. Li, *Coord. Chem. Rev.*, 2009, **253**, 1221-1247.
123. P. Vaqueiro, *Inorg. Chem.*, 2006, **45**, 4150-4156.
124. S. J. Ewing, D. I. Woodward, A. V. Powell and P. Vaqueiro, *J. Solid State Chem.*, 2013, **204**, 159-165.
125. P. Vaqueiro, *J. Solid State Chem.*, 2006, **179**, 302-307.

126. P. Vaqueiro and M. L. Romero, *Acta Crystallogr., Sect. E: Struct. Rep. Online*, 2007, **63**, m1700.
127. J. Zhou, C.-Y. Li, Y. Zhang and J. Dai, *J. Coord. Chem.*, 2009, **62**, 1112-1120.
128. C. Y. Li, J. Zhou, G. Q. Bian, M. H. Zhang and J. Dai, *Inorg. Chem. Commun.*, 2008, **11**, 1327-1329.
129. S. J. Ewing, M. L. Romero, J. Hutchinson, A. V. Powell and P. Vaqueiro, *Z. Anorg. Allg. Chem.*, 2012, **638**, 2526-2531.
130. D. X. Jia, J. Dai, Q. Y. Zhu, L. H. Cao and H. H. Lin, *J. Solid State Chem.*, 2005, **178**, 874-881.
131. G. N. Liu, G. C. Guo, M. S. Wang, L. Z. Cai and J. S. Huang, *J. Mol. Struct.*, 2010, **983**, 104-111.
132. J.-J. Liang, J. Zhao, W.-W. Tang, Y. Zhang and D.-X. Jia, *Inorg. Chem. Commun.*, 2011, **14**, 1023-1026.
133. X. Liu, F. Hu, J. Zhou, L. An, D. Liang and J. Lin, *Crystengcomm*, 2012, **14**, 3464-3468.
134. C. Y. Yue, Z. D. Yuan, L. G. Zhang, Y. B. Wang, G. D. Liu, L. K. Gong and X. W. Lei, *J. Solid State Chem.*, 2013, **206**, 129-133.
135. C. Y. Yue, X. W. Lei, L. Yin, X. R. Zhai, Z. R. Ba, Y. Q. Niu and Y. P. Li, *Crystengcomm*, 2015, **17**, 814-823.
136. C. S. Cundy and P. A. Cox, *Microporous Mesoporous Mater.*, 2005, **82**, 1-78.
137. R. E. Morris and S. J. Weigel, *Chem. Soc. Rev.*, 1997, **26**, 309-317.
138. G. Demazeau, *J. Mat. Chem.*, 1999, **9**, 15-18.
139. G. Demazeau, *J. Mater. Sci.*, 2008, **43**, 2104-2114.
140. E. R. Cooper, C. D. Andrews, P. S. Wheatley, P. B. Webb, P. Wormald and R. E. Morris, *Nature*, 2004, **430**, 1012-1016.
141. E. R. Parnham and R. E. Morris, *Accounts Chem. Res.*, 2007, **40**, 1005-1013.
142. Z. J. Lin, D. S. Wragg and R. E. Morris, *Chem. Comm.*, 2006, 2021-2023.
143. R. E. Morris, *Chem. Commun.*, 2009, 2990-2998.
144. K. Jin, X. Y. Huang, L. Pang, J. Li, A. Appel and S. Wherland, *Chem. Commun.*, 2002, 2872-2873.
145. E. R. Parnham, P. S. Wheatley and R. E. Morris, *Chem. Commun.*, 2006, 380-382.
146. E. R. Parnham and R. E. Morris, *J. Mat. Chem.*, 2006, **16**, 3682-3684.
147. E. R. Parnham and R. E. Morris, *J. Am. Chem. Soc.*, 2006, **128**, 2204-2205.
148. R. E. Morris, *Angew. Chem. Int. Ed.*, 2008, **47**, 442-444.
149. L. Xu, E. Y. Choi and Y. U. Kwon, *Inorg. Chem.*, 2008, **47**, 1907-1909.
150. Y. M. Lin, W. Massa and S. Dehnen, *Chem. Eur. J.*, 2012, **18**, 13427-13434.
151. W.-W. Xiong, G. Zhang and Q. Zhang, *Inorg. Chem. Front.*, 2014, **1**, 292-301.
152. Y. M. Lin and S. Dehnen, *Inorg. Chem.*, 2011, **50**, 7913-7915.
153. J. R. Li, Z. L. Xie, X. W. He, L. H. Li and X. Y. Huang, *Angew. Chem. Int. Ed.*, 2011, **50**, 11395-11399.
154. Y. M. Lin, W. Massa and S. Dehnen, *J. Am. Chem. Soc.*, 2012, **134**, 4497-4500.
155. W. W. Xiong, J. R. Li, B. Hu, B. Tan, R. F. Li and X. Y. Huang, *Chem. Sci.*, 2012, **3**, 1200-1204.
156. W. P. Su, X. Y. Huang, J. Li and H. X. Fu, *J. Am. Chem. Soc.*, 2002, **124**, 12944-12945.
157. L. Wang, T. Wu, F. Zuo, X. Zhao, X. H. Bu, J. Z. Wu and P. Y. Feng, *J. Am. Chem. Soc.*, 2010, **132**, 3283-3285.
158. N. N. Shen, B. Hu, C. C. Cheng, G. D. Zou, Q. Q. Hu, C. F. Du, J. R. Li and X. Y. Huang, *Cryst. Growth Des.*, 2018, **18**, 962-968.

159. J.-L. Lu, C.-Y. Tang, F. Wang, Y.-L. Shen, Y.-X. Yuan and D.-X. Jia, *Inorg. Chem. Comm.*, 2014, **47**, 148-151.
160. Q. Zhang, I. Chung, J. I. Jang, J. B. Ketterson and M. G. Kanatzidis, *J. Am. Chem. Soc.*, 2009, **131**, 9896-9897.
161. S. Santner, S. Yogendra, J. J. Weigand and S. Dehnen, *Chem. Eur. J.*, 2017, **23**, 1999-2004.
162. J.-R. Li, W.-W. Xiong, Z.-L. Xie, C.-F. Du, G.-D. Zou and X.-Y. Huang, *Chem. Comm.*, 2013, **49**, 181-183.
163. S. Santner, J. Heine and S. Dehnen, *Angew. Chem. Int. Ed.*, 2016, **55**, 876-893.
164. J. S. Beck, J. C. Vartuli, W. J. Roth, M. E. Leonowicz, C. T. Kresge, K. D. Schmitt, C. T. W. Chu, D. H. Olson, E. W. Sheppard, S. B. McCullen, J. B. Higgins and J. L. Schlenker, *J. Am. Chem. Soc.*, 1992, **114**, 10834-10843.
165. M. T. Anderson, J. E. Martin, J. G. Odinek and P. P. Newcomer, *Chem. Mater.*, 1998, **10**, 311-321.
166. M. Vallet-Regi, A. Ramila, R. P. del Real and J. Perez-Pariente, *Chem. Mater.*, 2001, **13**, 308-311.
167. S. A. Bagshaw, E. Prouzet and T. J. Pinnavaia, *Science*, 1995, **269**, 1242-1244.
168. C. J. Adams, A. E. Bradley and K. R. Seddon, *Aust. J. Chem.*, 2001, **54**, 679-681.
169. D. Baute, H. Zimmermann, S. Kababya, S. Vega and D. Goldfarb, *Chem. Mater.*, 2005, **17**, 3723-3727.
170. K. J. Fraser and D. R. MacFarlane, *Aust. J. Chem.*, 2009, **62**, 309-321.
171. J. S. Beck, J. C. Vartuli, G. J. Kennedy, C. T. Kresge, W. J. Roth and S. E. Schramm, *Chem. Mater.*, 1994, **6**, 1816-1821.
172. F. Bonhomme and M. G. Kanatzidis, *Chem. Mater.*, 1998, **10**, 1153-1159.
173. M. Wachhold, K. K. Rangan, M. Lei, M. F. Thorpe, S. J. L. Billinge, V. Petkov, J. Heising and M. G. Kanatzidis, *J. Solid State Chem.*, 2000, **152**, 21-36.
174. P. N. Trikalitis, K. K. Rangan and M. G. Kanatzidis, *J. Am. Chem. Soc.*, 2002, **124**, 2604-2613.
175. M. J. MacLachlan, N. Coombs and G. A. Ozin, *Nature*, 1999, **397**, 681-684.
176. W. W. Xiong, E. U. Athresh, Y. T. Ng, J. F. Ding, T. Wu and Q. C. Zhang, *J. Am. Chem. Soc.*, 2013, **135**, 1256-1259.
177. W.-W. Xiong, P.-Z. Li, T.-H. Zhou, A. L. Y. Tok, R. Xu, Y. Zhao and Q. Zhang, *Inorg. Chem.*, 2013, **52**, 4148-4150.
178. L. N. Nie, Y. Zhang, W. W. Xiong, T. T. Lim, R. Xu, Q. Y. Yan and Q. C. Zhang, *Inorg. Chem. Front.*, 2016, **3**, 111-116.
179. W. W. Xiong and Q. C. Zhang, *Angew. Chem. Int. Ed.*, 2015, **54**, 11616-11623.
180. G. Zhang, P. Li, J. Ding, Y. Liu, W.-W. Xiong, L. Nie, T. Wu, Y. Zhao, A. I. Y. Tok and Q. Zhang, *Inorg. Chem.*, 2014, **53**, 10248-10256.
181. L. N. Nie, W. W. Xiong, P. Z. Li, J. Y. Han, G. D. Zhang, S. M. Yin, Y. L. Zhao, R. Xu and Q. C. Zhang, *J. Solid State Chem.*, 2014, **220**, 118-123.
182. A. P. Alivisatos, *Science*, 1996, **271**, 933-937.
183. Y. Wang and N. Herron, *J. Phys. Chem. U.S.*, 1991, **95**, 525-532.
184. N. F. Zheng, X. H. Bu, H. W. Lu, Q. C. Zhang and P. Y. Feng, *J. Am. Chem. Soc.*, 2005, **127**, 11963-11965.
185. J. F. Corrigan, O. Fuhr and D. Fenske, *Adv. Mater.*, 2009, **21**, 1867-1871.
186. M. J. Manos, R. G. Iyer, E. Quarez, J. H. Liao and M. G. Kanatzidis, *Angew. Chem. Int. Ed.*, 2005, **44**, 3552-3555.
187. N. F. Zheng, X. H. Bu and P. Y. Feng, *Nature*, 2003, **426**, 428-432.
188. J. Lin, Q. Zhang, L. Wang, X. C. Liu, W. B. Yan, T. Wu, X. H. Bu and P. Y. Feng, *J. Am. Chem. Soc.*, 2014, **136**, 4769-4779.

189. T. Wu, Q. Zhang, Y. Hou, L. Wang, C. Mao, S.-T. Zheng, X. Bu and P. Feng, *J. Am. Chem. Soc.*, 2013, **135**, 10250-10253.
190. N. Zheng, X. H. Bu, H. Vu and P. Y. Feng, *Angew. Chem. Int. Ed.*, 2005, **44**, 5299-5303.
191. J. Li, Z. Chen, R. J. Wang and D. M. Proserpio, *Coord. Chem. Rev.*, 1999, **190**, 707-735.
192. P. K. Dorhout, N. B. Ford and C. C. Raymond, *Coord. Chem. Rev.*, 2017, **352**, 537-550.
193. A. V. Powell, *Int. J. Nanotechnol.*, 2011, **8**, 783-794.
194. M. Grun, K. K. Unger, A. Matsumoto and K. Tsutsumi, *Microporous Mesoporous Mater.*, 1999, **27**, 207-216.
195. Y.-N. Guo, Y. Li, B. Zhi, D. Zhang, Y. Liu and Q. Huo, *RSC Adv.*, 2012, **2**, 5424-5429.
196. J. Y. Ying, C. P. Mehnert and M. S. Wong, *Angew. Chem. Int. Ed.*, 1999, **38**, 56-77.
197. Y. Y. Shen, C. Liu, P. P. Hou, M. J. Zhi, C. M. Zhou, W. X. Chai, J. W. Cheng, Y. Liu and Q. C. Zhang, *Chem. - Asian J.*, 2015, **10**, 2603-2607.
198. W.-W. Xiong, J. Miao, K. Ye, Y. Wang, B. Liu and Q. Zhang, *Angew. Chem. Int. Ed.*, 2015, **54**, 546-550.
199. D. B. Mitzi, *Inorg. Chem.*, 2005, **44**, 3755-3761.
200. D. B. Mitzi, *Inorg. Chem.*, 2007, **46**, 926-931.
201. A. (2014), *CrysAlisPRO*, Oxford Diffraction Ltd, Abingdon, Oxfordshire, England.
202. A. Altomare, G. Cascarano, C. Giacovazzo and A. Guagliardi, *J. Appl. Crystallogr.*, 1993, **26**, 343-350.
203. L. Palatinus and G. Chapuis, *J. Appl. Crystallogr.*, 2007, **40**, 786-790.
204. S. J. Coles and P. A. Gale, *Chem. Sci.*, 2012, **3**, 683-689.
205. P. W. Betteridge, J. R. Carruthers, R. I. Cooper, K. Prout and D. J. Watkin, *J. App. Crystallogr.*, 2003, **36**, 1487.
206. A. L. Spek, *J. Appl. Crystallogr.*, 2003, **36**, 7-13.
207. C. F. Macrae, I. J. Bruno, J. A. Chisholm, P. R. Edgington, P. McCabe, E. Pidcock, L. Rodriguez-Monge, R. Taylor, J. van de Streek and P. A. Wood, *J. Appl. Crystallogr.*, 2008, **41**, 466-470.
208. W. I. F. David, K. Shankland, J. van de Streek, E. Pidcock, W. D. S. Motherwell and J. C. Cole, *J. Appl. Crystallogr.*, 2006, **39**, 910-915.
209. K. Nakamoto, *Infrared and Raman Spectra of Inorganic and Coordination Compounds. Part A, Theory and Applications in Inorganic Chemistry*, Wiley, Hoboken, N.J., 6th edn., 2009.
210. P. Vaqueiro and M. L. Romero, *J. Phys. Chem. Solids.*, 2007, **68**, 1239-1243.
211. P. Vaqueiro and M. L. Romero, *J. Am. Chem. Soc.*, 2008, **130**, 9630-+.
212. P. Vaqueiro, M. L. Romero, B. C. Rowan and B. S. Richards, *Chem. Eur. J.*, 2010, **16**, 4462-4465.
213. I. Dance, *New J. Chem.*, 2003, **27**, 22-27.
214. M. B. Power, J. W. Ziller, A. N. Tyler and A. R. Barron, *Organometallics*, 1992, **11**, 1055-1063.
215. N. J. Hardman, R. J. Wright, A. D. Phillips and P. P. Power, *J. Am. Chem. Soc.*, 2003, **125**, 2667-2679.
216. F. Kratz, B. Nuber, J. Weiss and B. K. Keppler, *Polyhedron*, 1992, **11**, 487-498.
217. G. H. Shang, M. J. HampdenSmith and E. N. Duesler, *Inorg. Chem.*, 1996, **35**, 2611-2615.

218. I. J. Bruno, J. C. Cole, P. R. Edgington, M. Kessler, C. F. Macrae, P. McCabe, J. Pearson and R. Taylor, *Acta Crystallogr. B*, 2002, **58**, 389-397.
219. I. L. Tocon, M. S. Woolley, J. C. Otero and J. I. Marcos, *J. Mol. Struct.*, 1998, **470**, 241-246.
220. Katcka, *B Acad. Pol. Sci.- Chim.*, 1967, **15**, 413-421.
221. D. Cook, *Can. J. Chem.*, 1961, **39**, 2009-2024.
222. D. A. Long, *Spectrochim. Acta*, 1963, **19**, 1777-1790.
223. M. L. Romero Perez, PhD Thesis, Heriot-Watt University, 2010.
224. Y. Tong, *MChem Project Report, Heriot-Watt University* 2013.
225. P. Vaqueiro, S. Makin, Y. Tong and S. J. Ewing, *Dalton Trans.*, 2017, **46**, 3816-3819.
226. Q. C. Zhang, T. Wu, X. H. Bu, T. Tran and P. Y. Feng, *Chem. Mater.*, 2008, **20**, 4170-4172.
227. T. H. Levchenko, Yining. and Corrigan, John F., in *Clusters – Contemporary Insight in Structure and Bonding*, Springer International Publishing, Switzerland, 2016, vol. 174, pp. 269-319.
228. X. H. Zeng, X. J. Yao, J. Y. Zhang, Q. Zhang, W. Q. Wu, A. H. Chai, J. L. Wang, Q. D. Zeng and J. L. Xie, *Inorg. Chem. Front.*, 2015, **2**, 164-169.
229. J. Lin, D. D. Hu, Q. Zhang, D. S. Li, T. Wu, X. H. Bu and P. Y. Feng, *J. Phys. Chem. C*, 2016, **120**, 29390-29396.
230. D. M. Nellis, Y. H. Ko, K. M. Tan, S. Koch and J. B. Parise, *J. Chem. Soc. Chem. Comm.*, 1995, 541-542.
231. Y. H. Ko, K. M. Tan, D. M. Nellis, S. Koch and J. B. Parise, *J. Solid State Chem.*, 1995, **114**, 506-511.
232. Q. Lin, X. Bu, C. Mao, X. Zhao, K. Sasan and P. Feng, *J. Am. Chem. Soc.*, 2015, **137**, 6184-6187.
233. J. Y. Pivan, O. Achak, M. Louer and D. Louer, *Chem. Mater.*, 1994, **6**, 827-830.
234. M. S. Wang, W. T. Chen, L. Z. Cai, G. W. Zhou, G. C. Guo and J. S. Huang, *J. Cluster Sci.*, 2003, **14**, 495-504.
235. J. Xu, L. J. Xue, J. L. Hou, Z. N. Yin, X. Zhang, Q. Y. Zhu and J. Da, *Inorg. Chem.*, 2017, **56**, 8036-8044.
236. C. L. Bowes, W. U. Huynh, S. J. Kirkby, A. Malek, G. A. Ozin, S. Petrov, M. Twardowski, D. Young, R. L. Bedard and R. Broach, *Chem. Mater.*, 1996, **8**, 2147-2152.
237. X. L. Sun, Q. Y. Zhu, W. Q. Mu, L. W. Qian, L. Yu, J. Wu, G. Q. Bian and J. Dai, *Dalton Trans.*, 2014, **43**, 12582-12589.
238. L. E. Maelia and S. A. Koch, *Inorg. Chem.*, 1986, **25**, 1896-1904.
239. K. Nakamoto, *Infrared and Raman Spectra of Inorganic and Coordination Compounds. Part B, Applications in Coordination, Organometallic, and Inorganic Chemistry*, Wiley, Hoboken, N.J., 6th edn., 2009.
240. I. D. Brown, *The Chemical Bond in Inorganic Chemistry: The Bond Valence Model*, Oxford University Press, Oxford, UK, 2006.
241. C. T. Prewitt and H. S. Young, *Science*, 1965, **149**, 535-537.
242. G. Thiele, S. Santner and S. Dehnen, *Z. Kristallogr. - Cryst. Mater.*, 2017, **232**, 47-54.
243. M. Bakavoli, M. Rahimizadeh, H. Eshghi, A. Shiri, Z. Ebrahimpour and R. Takjoo, *Bull. Korean Chem. Soc.*, 2010, **31**, 949-952.
244. N. Pathak, P. S. Ghosh, S. Saxena, D. Dutta, A. K. Yadav, D. Bhattacharyya, S. N. Jha and R. M. Kadam, *Inorg. Chem.*, 2018, **57**, 3963-3982.

245. Y. H. Wang, M. H. Zhang, Y. M. Yan, G. Q. Bian, Q. Y. Zhu and J. Dai, *Inorg. Chem.*, 2010, **49**, 9731-9733.
246. A. K. Pant and E. D. Stevens, *Phys. Rev. B*, 1988, **37**, 1109-1120.
247. J. W. Boon and C. H. Mac Gillavry, *Recl. Trav. Chim. Pays-Bas*, 1942, **60**, 910-920.
248. C. Wang, X. H. Bu, N. F. Zheng and P. Y. Feng, *Chem. Comm.*, 2002, 1344-1345.
249. S. J. Ewing and P. Vaqueiro, *Inorg. Chem.*, 2014, **53**, 8845-8847.
250. S. J. Ewing, A. V. Powell and P. Vaqueiro, *J. Solid State Chem.*, 2011, **184**, 1800-1804.
251. P. M. Forster, A. R. Burbank, C. Livage, G. Ferey and A. K. Cheetham, *Chem. Comm.*, 2004, 368-369.
252. Y. X. Sun and W. Y. Sun, *Chin. Chem. Lett.*, 2014, **25**, 823-828.
253. X. F. Xu, W. Wang, D. L. Liu, D. D. Hu, T. Wu, X. H. Bu and P. Y. Feng, *J. Am. Chem. Soc.*, 2018, **140**, 888-891.
254. L. Wang, T. Wu, F. Zuo, X. Zhao, X. H. Bu, J. Z. Wu and P. Y. Feng, *J. Am. Chem. Soc.*, 2010, **132**, 3283-+.
255. T. Wu, L. Wang, X. H. Bu, V. Chau and P. Y. Feng, *J. Am. Chem. Soc.*, 2010, **132**, 10823-10831.
256. M. Marezio and J. P. Remeika, *J. Chem. Phys.*, 1967, **46**, 1862.
257. S. J. Louisnathan, R. J. Hill and G. V. Gibbs, *Phys. Chem. Miner.*, 1977, **1**, 53-69.
258. F. C. Hawthorne, S. V. Krivovichev and P. C. Burns, *The Crystal Chemistry of Sulfate Minerals*, Mineralogical Society of America, Washington DC, 2000.
259. G. Johansson, *Arkiv. Kemi.*, 1963, **20**, 343-352.
260. S. P. Altaner, J. J. Fitzpatrick, M. D. Krohn, P. M. Bethke, D. O. Hayba, J. A. Goss and Z. A. Brown, *Am. Mineral.*, 1988, **73**, 145-152.
261. W. W. Rudolph, R. Mason and P. Schmidt, *Eur. J. Mineral.*, 2003, **15**, 913-924.
262. W. W. Rudolph and P. Schmidt, *Thermochim. Acta*, 2011, **521**, 112-120.
263. S. Hendricks, B, *Am. Mineral.*, 1937, **22**, 773-784.
264. J. L. Bishop and E. Murad, *Am. Miner.*, 2005, **90**, 1100-1107.
265. I. A. Oxton, O. Knop and M. Falk, *Can. J. Chem.*, 1975, **53**, 3394-3400.
266. I. A. Oxton, O. Knop and M. Falk, *Can. J. Chem.*, 1976, **54**, 892-899.
267. S. J. Ewing and P. Vaqueiro, *Dalton Trans.*, 2015, **44**, 1592-1600.
268. S. J. Ewing, PhD Thesis, Heriot-Watt University, 2014.
269. M. R. Rizal, I. Azizul and S. W. Ng, *Acta Crystallogr. Sect. E: Struct. Rep. Online*, 2008, **64**, o914.
270. A. Turockin, *Synlett*, 2014, **25**, 894-895.
271. N. von Wolff, C. Villiers, P. Thuery, G. Lefevre, M. Ephritikhine and T. Cantat, *Eur. J. Org. Chem.*, 2017, 676-686.

Appendix 1 Table of Syntheses

Tables containing all reactions carried out through the course of this project; in cases where reactions have been repeated, only one occurrence is included.

Appendix 1.1 Solvothermal Reactions of Gallium Reagents in 4-MPy

#	Reagents	Molar Ratio	Temp/ °C	Time/ Days	Product Appearance	Product
1	Ga, S, 4-MPy	1.5:5:30	200	6	Orange powder	**(1)**
2	Ga, S, 4-MPy	2:4:30	200	6	Red crystals + Ga	**(1) + Ga**
3	Ga, S, 4-MPy	2:4.5:30	200	6	Orange and red crystals + Ga	**(1) + (7) + Ga**
4	Ga, S, 4-MPy	2:5:24	200	6	Orange powder	**Low crystallinity**
5	Ga, S, 4-MPy	2:5:30	170	6	Red crystals + Ga	**(1) + Ga**
6	Ga, S, 4-MPy	2:5:30	200	6	Orange and red crystals + Ga	**(1) + (7) + Ga**
7	Ga, S, 4-MPy	2:5:30	200	10	Red crystals + Ga	**(1) + Ga**
8	Ga, S, 4-MPy: H_2O	2:5:30:26	200	6	Yellow crystals + Ga	**(3)**
9	Ga, S, 4-MPy: H_2O	2:5:30:28	170	6	Brown crystals + Ga	**(5) + Ga**
10	Ga, S, 4-MPy, H_2O	2:5:30:28	200	6	Orange crystals + Ga	**(7) + Ga**
11	Ga, S, 4-MPy	2:5:32	200	6	Red crystals + Ga	**(1) + Ga**
12	Ga, S, 4-MPy	2:5.2:30	200	6	Red crystals + Ga	**(1) + Ga**
13	Ga, S, 4-MPy	2:5.5:30	200	6	Red crystals + Ga	**(1) + Ga**
14	Ga, S, 4-MPy	2:6:30	200	6	Red and yellow crystals + Ga	**(4) + (1) + Ga**
15	Ga, S, 4-MPy	2:7:30	200	6	Red and yellow crystals + Ga	**(4) + (1) + Ga**
16	Ga_2O_3, S, 4-MPy	2:4.4:30	170	5	Orange crystals and powder	**(1) + (6)**
with 4,4′-Bipyridine (bipy)						
17	Ga, S, bipy, 4-MPy	2:5:1:30	200	6	Red crystals + Ga	**(1) + Ga**

18	Ga, S, bipy, 4-MPy	2:5.5:0.5:30	200	6	Red and yellow crystals + Ga	**(4) + (1) + Ga**
19	Ga, S, bipy, 4-MPy	2:6:1:30	200	6	Red crystals + Ga	**(1) + Ga**
20	Ga, S, bipy, 4-MPy	2:7:1:30	200	6	Red crystals + Ga	**(1) + Ga**
with 4,4'-Trimethylenedipyridine (TMDPy)						
21	Ga, S, TMDPy, 4-MPy	2:4:1:30	200	6	Red and yellow crystals + Ga	**(4) + (1) + Ga**
22	Ga, S, TMDPy, 4-MPy	2:4.5:1:30	200	6	Red and yellow crystals + Ga	**(1) + (4) + Ga**
23	Ga, S, TMDPy, 4-MPy	2:5:0.045:30	200	6	Yellow crystals + Ga	**(7) + Ga**
24	Ga, S, TMDPy, 4-MPy	2:5:1:30	200	6	Red and yellow crystals + Ga	**(1) + (6) + Ga**
25	Ga, S, TMDPy, 4-MPy	1:5:4:30	170	5	Orange powder	**(1)**
26	Ga, S, TMDPy, 4-MPy: H_2O	2:5:1:30:23	200	6	Yellow crystals + Ga	**(4) + Ga**
27	Ga, S, TMDPy, 4-MPy: H_2O	2:5:1:30:28	200	6	Red and orange crystals + Ga	**(1) + (6) + Ga**
28	Ga, S, TMDPy, 4-MPy	2:5.5:1:24	200	6	Yellow crystals	**(3)**
29	Ga, S, TMDPy, 4-MPy	2:5.5:1:30	200	6	Red and yellow crystals + Ga	**(4) + (1) + Ga**
30	Ga, S, TMDPy, 4-MPy	2:6:1:30	200	6	Red and yellow crystals + Ga	**(4) + (1) + Ga**
31	Ga, S, TMDPy, 4-MPy	2:6:1:30	200	10	Red and yellow crystals + Ga	**(4) + (1) + Ga**
32	Ga, S, TMDPy, 4-MPy	2:7:1:30	200	6	Red crystals + Ga	**(1) + Ga**
33	Ga, S, TMDPy, TBD, 4-MPy	2:5.5:1:1:30	200	6	Orange powder	Amorphous
34	Ga_2O_3, S, TMDPy, 4-MPy	2:5:1:30	170	5	Orange crystals and powder	**(1) + (6)**
with Imidazole (Im)						
35	Ga, S, Im, 4-MPy	2:4:1:30	200	6	Brown crystals + Ga	**(5) + Ga**
36	Ga, S, Im, 4-MPy	2:4.5:1:30	200	6	Brown powder + Ga	**(1) + Ga**

37	Ga, S, Im, 4-MPy	2:5:1:30	200	6	Red crystals + Ga	**(1) + Ga**
38	Ga, S, Im, 4-MPy	2:5.5:0.5:30	200	6	Yellow crystals + Ga	**(4) + Ga**
39	Ga, S, Im, 4-MPy	2:6:0.5:30	200	6	Red crystals + Ga	**(1) + Ga**
40	Ga, S, Im, 4-MPy	2:6:1:30	200	6	Yellow crystals	**(4)**
41	Ga, S, Im, 4-MPy	2:6:1:30	200	10	Red and yellow crystals + Ga	**(4) + (1) + Ga**
42	Ga, S, Im, 4-MPy	2:7:1:30	200	6	Red and yellow crystals	**(1) + (4)**
with Benzimidazole (BenzIm)						
43	Ga, S, BenzIm, 4-MPy	3:7.5:2:45	200	5	Red crystals + Ga	**(1) + Ga**
44	Ga, S, BenzIm, 4-MPy	3:7.5:2:45	200	6	Red crystals + Ga	**(1) + Ga**
with 1,4-Diazabicyclo[2.2.2]octane (DABCO)						
45	Ga, S, DABCO, 4-MPy	2:5.5:0.5:30	200	6	Yellow crystals + Ga	**(4) + Ga**
46	Ga, S, DABCO, 4-MPy	2:7:1:30	200	6	Red crystals + Ga	**(1) + Ga**
with 1-Butyl-2,3-dimethylimidazolium chloride [BMMIm]Cl						
47	Ga, S, [BMMIm]Cl, 4-MPy	2:6:1:30	200	6	Yellow crystals	**(3)**
48	Ga, S, [BMMIm]Cl, 4-MPy	2:7:1:30	200	6	Yellow crystals	**(3)**
with 1-Butyl-2,3-dimethylimidazolium tetrafluoroborate [BMMIm]BF_4						
49	Ga, S, [BMMIm]BF_4, 4-MPy	2:6:1:30	200	6	Yellow crystals	**(3)**
50	Ga, S, [BMMIm]BF_4, 4-MPy	2:7:1:30	200	6	Yellow crystals	**(3)**
with Trihexyltetradecylphosphonium chloride ([THTDP]Cl)						
51	Ga, S, [THTDP]Cl, 4-MPy, H_2O	2:5:1.75:30:28	200	6	Red crystals + orange powder	**(1)**
52	Ga, S, [THTDP]Cl, 4-MPy, H_2O	2:5:2.8:28:28	200	6	Red crystals	**(1)**

53	Ga, S, [THTDP]Cl, 4-MPy, H_2O	2:5:3.5:30:28	200	6	Orange crystals	**(2)**
54	Ga, S, [THTDP]Cl, 4-MPy, H_2O	2:5:3.5:30:17	200	6	Ga	**Ga**
55	Ga, S, [THTDP]Cl, 4-MPy, H_2O	2:5:3.6:30:28	170	6	Orange/brown powder	Amorphous
56	Ga, S, [THTDP]Cl, TMDPy, 4-MPy, H_2O	2:5:1.75:1:28:28	200	6	Brown powder	Amorphous
57	Ga, S, [THTDP]Cl, TMDPy, 4-MPy, H_2O	2:5:1.75:1:30:28	200	6	Red crystals + orange powder	**(1)** (Low crystallinity)
58	Ga, S, [THTDP]Cl, TMDPy, 4-MPy, H_2O	2:5:3.5:1:28:28	200	6	Brown powder	Amorphous
59	Ga, S, [THTDP]Cl, TMDPy, 4-MPy, H_2O	2:5:3.5:1:30:17	200	6	Ga	**Ga**
60	Ga, S, [THTDP]Cl, TMDPy, 4-MPy, H_2O	2:5:3.6:1:30:28	200	6	Orange/brown powder	Low crystallinity
61	Ga, S, [THTDP]Cl, bipy, 4-MPy, H_2O	2:5:1.75:1:30:28	200	6	Brown powder	Amorphous
62	Ga, S, [THTDP]Cl, bipy, 4-MPy, H_2O	2:5:3.5:1:30:28	200	6	Ga	**Ga**
63	Ga, S, [THTDP]Cl, 4-MPy, H_2O	2:5:4.4:30:28	200	6	Brown powder	Amorphous
64	Ga, S, [THTDP]Cl, 4-MPy	2:4.5:1:30	200	6	Orange/brown powder	Amorphous
65	Ga, S, [THTDP]Cl, 4-MPy	2:5:1:30	200	6	Orange/brown powder	**(1)**
66	Ga, S, [THTDP]Cl, 4-MPy	2:6:1:30	200	6	Orange/brown powder	Amorphous

with Gallium Nitrate $Ga(NO_3)_3$						
67	$Ga(NO_3)_3$, S, 4-MPy	1:2:28	200	10	Yellow flakes	Low crystallinity
68	$Ga(NO_3)_3$, S, 4-MPy	1:2:56	200	10	Yellow flakes	**(4)**
69	$Ga(NO_3)_3$, S, 4-MPy	2:7:31	200	10	Beige crystals	Organic
70	$Ga(NO_3)_3$, S, TMDPy, 4-MPy	2:6:1:30	200	10	Beige powder	Amorphous
71	$Ga(NO_3)_3$, S, 4-MPy	1.5:3:70	185	6	Yellow fibres	Amorphous
72	$Ga(NO_3)_3$, S, 4-MPy	2:3:70	185	6	Yellow fibres	Amorphous

Appendix 1.2 Solvothermal Reactions of Gallium and Germanium Reagents in 4-MPy

#	Reagents	Molar Ratio	Temp/ °C	Time/ Days	Product Appearance	Product
73	Ga, GeO_2, S, 4-MPy	1:1:4:25	200	6	Orange powder	Low crystallinity
74	Ga, GeO_2, S, 4-MPy	1:1:4:30	170	5	Orange crystals	**(9)**
75	Ga, GeO_2, S, 4-MPy	1:1:4:30	150	7	Orange powder	Amorphous
76	Ga:GeO_2:S:4-MPy	1:1:4:30	140	6	Pink powder	Unidentified powder
77	Ga, GeO_2, S, 4-MPy	1:1:4.4:30	170	5	Orange crystals	**(9)**
78	Ga, GeO_2, S, 4-MPy	1:1:4.4:30	150	7	Orange powder	Amorphous
79	Ga, GeO_2, S, 4-MPy:H_2O	1:1:4.4:30:28	170	5	Yellow crystals	**(10)**
80	Ga, GeO_2, S, 4-MPy	1:1:4.5:30	170	5	Orange crystals	**(9)**
81	Ga, GeO_2, S, 4-MPy	1:1:4.5:30	170	6	Orange crystals	**(9)**
82	Ga, GeO_2, S, 4-MPy	1:1:5:28	200	6	Yellow crystals + powder	**(11) +** Second phase
83	Ga, GeO_2, S, 4-MPy	1:1:5:30	170	5	Orange crystals	**(9)**
84	Ga, GeO_2, S, 4-MPy	1:1:5:30	200	6	Yellow crystals	**(10)**
85	Ga:GeO_2:S:4-MPy	1:1:5.4:30	200	8	Brown powder	**(10)**
86	Ga:GeO_2:S: 4-MPy:H_2O	1:1:5.4:30:30	200	8	Yellow crystals	**(10)**

87	Ga, GeO_2, S, 4-MPy	1:1:5.5:30	160	6	Orange powder	**(10) +** Ga_2S_3
88	Ga, GeO_2, S, 4-MPy	1:1:5.5:30	200	5	Yellow crystals + Ga	**(10) + Ga**
89	Ga, GeO_2, S, 4-MPy, H_2O	1:1:5.5:30:30	170	6	Yellow crystals	**(3)**
90	Ga, GeO_2, S, 4-MPy, H_2O	1:1:5.5:30:30	200	5	Yellow crystals	**(10) + (11)**
91	Ga, GeO_2, S, 4-MPy	1:1:6:43	170	5	Orange crystals	**(9)**
92	GeO_2, Ga, S, 4-MPy	2.5:1:4:30	170	5	Orange powder	**(9) +** Second phase
93	GeO_2, Ga, S, 4-MPy	2.5:1:4:60	170	5	Orange powder	**(9)**
94	Ga, GeO_2, S, 4-MPy, H_2O	2.5:1:1:60:55	170	6	Yellow crystals + Ga	**(10) + Ga**
95	Ga, GeO_2, S, 4-MPy	1.5:0.5:1.75:1:30	200	7	Yellow crystals	**(10)**
96	Ga:GeO_2:Thioacetamide: 4-MPy	1:1:5.5:30	140	6	White powder	Unidentified powder
with 4,4′-Bipyridine (bipy)						
97	Ga, GeO_2, S, bipy, 4-MPy	1:1:4:1:30	200	6	Yellow crystals	**(10)**
with 4,4'-Trimethylenedipyridine (TMDPy)						
98	Ga, GeO_2, S, TMDPy, 4-MPy	0.5:5:4:30	170	5	Yellow powder	Amorphous
99	Ga, GeO_2, S, TMDPy, 4-MPy	1:1:4:1:30	200	6	Yellow crystals	**(10)**
100	Ga, GeO_2, S, TMDPy, 4-MPy	1:1:4.4:0.5:30	200	6	Yellow crystals	**(10)**
101	Ga, GeO_2, S, TMDPy, 4-MPy	1:1:4.4:30	170	5	No solid	/
102	Ga, GeO_2, S. TMDPy, 4-MPy	1:1:4.7:1:30	200	6	Brown powder	Unidentified powder
103	Ga, GeO_2, S, TMDPy, 4-MPy	1:1:5:1:30	170	5	Orange crystals	**(9)**
104	Ga, GeO_2, S, TMDPy, 4-MPy	1:1:5:1:30	200	6	Red crystals + Ga	**(1) + Ga**
105	Ga, GeO_2, S, TMDPy, 4-MPy	1:1:5:1:30	200	7	Yellow crystals + powder	**(11) +** Second phase
106	Ga, GeO_2, S, TMDPy, 4-MPy	1:1:5:1:30	170	5	Orange crystals	**(9)**
107	Ga, GeO_2, S, TMDPy, 4-MPy, H_2O	1:1:5:1:30:30	170	5	Yellow crystals	**(10)**

108	Ga:GeO_2:S:TMDPy: 4-MPy	1:1:5.4:1:30	200	8	Yellow crystals	**(10)**
109	Ga:GeO_2:S:TMDPy: 4-MPy:H_2O	1:1:5.4:1:30:30	200	8	Yellow crystals + powder	**(11) +** Second phase
110	Ga, GeO_2, S, TMDPy, 4-MPy	1:1:5.5:0.5:30	170	6	Orange powder	Unidentified powder
111	Ga, GeO_2, S, TMDPy, 4-MPy, H_2O	1:1:5.5:0.5:30:30	170	6	Yellow crystals	**(11) + Powder**
112	Ga:GeO_2:S:TMDPy: 4-MPy	1:1:5.5:1:30	140	6	Orange powder	Unidentified Powder
113	Ga, GeO_2, S, TMDPy, 4-MPy	1:1:5.5:1:30	160	6 days	Orange powder	**(10) +** Ga_2S_3
114	Ga, GeO_2, S, TMDPy, 4-MPy	1:1:5.5:1:30	200	7	Orange crystals + Powder	**(8)**
115	Ga, GeO_2, S, TMDPy, 4-MPy	1:1:5.5:1:30	200	5	Orange powder	Unidentified powder
116	Ga, GeO_2, S, TMDPy, 4-MPy, H_2O	1:1:5.5:1:30:30	170	6	Orange crystals	**(9)**
117	Ga, GeO_2, S, TMDPy, 4-MPy, H_2O	1:1:5.5:1:30:30	200	5	Yellow crystals	**(10)+ (11)**
119	Ga, GeO_2, S, TMDPy, 4-MPy	1:1:6:0.5:30	200	6	Brown powder	Amorphous
120	Ga, GeO_2, S, TMDPy, 4-MPy	1:1:6:1:30	150	7	No solid	/
121	Ga, GeO_2, S, TMDPy, 4-MPy, H_2O	1:1:6:0.5:30:30	200	6	Yellow crystals	**(10)**
122	Ga, GeO_2, S, TMDPy, 4-MPy, H_2O	1:1:10:4:30:100	170	5	Brown powder	**(10)**
123	GeO_2, Ga, S, TMDPy, 4-MPy	2.5:1:4:1:30	170	5	Orange powder	GeO_2
124	GeO_2, Ga, S, TMDPy, 4-MPy	2.5:1:2:60	170	6	Red powder	Amorphous
125	Ga, GeO_2, S, TMDPy, 4-MPy	3:1:3.5:2:60	200	7	Yellow crystals + Powder	**(10) +** Second phase
126	Ga, GeO_2, Thioacetamide, TMDPy, 4-MPy	1:1:4:1:30	200	6	Orange powder	Unidentified powder
with Imidazole (Im)						
127	Ga, GeO_2, S, Im, 4-MPy	1:1:3.2:1:30	200	6	Yellow crystals	**(10)**
129	Ga, GeO_2, S, Im, 4-MPy	1:1:4:0.7:30	200	6	Brown powder	Amorphous
130	Ga, GeO_2, S, Im, 4-MPy	1:1:4:1:30	200	6	Yellow crystals	**(10)**
131	Ga, GeO_2, S, Im, 4-MPy	1:1:4:1:30	150	7	No solid	/

132	Ga, GeO_2, S, Im, 4-Mpy, H_2O	1:1:4:1:30:30	200	6	Yellow crystals	**(10)**
133	Ga, GeO2, S, Im, 4-MPy	1:1:5.5:0.5:30	200	6	Yellow crystals + powder	**(11) +** Second phase
134	Ga, GeO_2, S, Im, 4-MPy	1:3:8:2:60	200	6	Brown powder	GeO_2 and Ga_2S_3
with Benzimidazole (BenzIm)						
135	Ga, GeO_2, S, BenzIm, 4-MPy	2:0.6:7:1.3:38	200	6	Yellow crystals	**(10)**
136	Ga, GeO_2, S, BenzIm, 4-MPy	1:1:4:1:30	200	6	Yellow crystals	**(10)**
137	Ga, GeO_2, S, BenzIm, 4-MPy, H_2O	1:1:4:1:30	150	7s	Yellow crystals	**(10)**
138	Ga, GeO_2, S, BenzIm, 4-MPy	1:1:5.5:1:30	200	6	Brown powder	**(10)**
139	Ga, GeO_2, S, BenzIm, 4-MPy	1:1:5.5:1:30	170	5	Orange crystals	**(9)**
140	Ga, GeO_2, S, BenzIm, 4-MPy	3:1:3.5:2:60	170	5	Yellow crystals	**(10)**
with Phenanthroline (Phenan)						
141	Ga, GeO_2, S, Phenan, 4-MPy	1:1:4:1:30	200	6	Red powder	Amorphous
142	Ga, GeO2, S, Phenan, 4-MPy	1:1:4:1:30	150	7	No solid	/
with 1,4-Diazabicyclo[2.2.2]octane (DABCO)						
143	Ga, GeO_2, S, DABCO, 4-MPy	1:1:4:1:30	200	6	Yellow crystals	**(10) + (11)**
with Triazabicyclodecene (TBD)						
144	Ga, GeO_2, S, TBD, 4-MPy	1:1:5.5:1:30	170	5	Red powder	Low crystallinity
with 1-Butyl-2,3-dimethylimidazolium tetrafluoroborate [BMMIm]BF_4						
145	Ga, GeO_2, S, [BMMIm]BF_4, 4-MPy	1:1:5:1:30	200	7	Yellow crystals	**(10)**
146	Ga, GeO_2, S, [BMMIm]BF_4, 4-MPy	1:1:5.5:1:30	200	7	Orange powder	**(10)**
147	Ga, GeO_2, S, [BMMIm]BF_4, 4-MPy	3:1:3.5:2:60	200	7	Yellow crystals	**(10)**
with 1-Butyl-2,3-dimethylimidazolium chloride [BMMIm]Cl						
148	Ga, GeO_2, S, [BMMIm]Cl, 4-MPy	1:1:5:1:30	200	7	Yellow powder	Low crystallinity
149	Ga, GeO_2, S, [BMMIm]Cl, 4-MPy	1:1:5.5:1:30	200	7	Yellow powder	Amorphous

Appendix 1.3 Solvothermal Reactions of Germanium Reagents in 4-MPy

#	Reagents	Molar Ratio	Temp/ °C	Time/ Days	Product Appearance	Product
150	GeO_2, S, 4-MPy	2:4.4:30	150	7	Orange crystals + powder	**(9)** + Second phase
151	GeO_2, S, 4-MPy	2:4.4:30	170	5	Orange crystals	**(9)**
152	GeO_2, S, 4-MPy	2:5.5:30	200	5	Yellow powder	Sulphur
153	GeO_2, S, 4-MPy, H_2O	2:5.5:30:30	200	5	No solid	/
with 4,4'-Trimethylenedipyridine (TMDPy)						
154	GeO_2, S, TMDPy, 4-MPy	1:5:4:30	170	5	Yellow powder	Unidentified powder
155	GeO_2, S, TMDPy, 4-MPy	2:5:1:30	170	5	Orange crystals	**(9)**
156	GeO_2, S, TMDPy, 4-MPy	2:5.5:1:30	200	5	Orange crystals	**(9)**
157	GeO_2, Thioacetamide, TMDPy, 4-MPy	2:4:1:30	200	6	White powder	GeO_2
with Imidazole (Im)						
158	GeO_2, S, Im, 4-Mpy	1:4:1:30	200	6	Yellow powder	Amorphous
159	GeO_2, S, Im, 4-MPy	2:3.2:1:30	200	6	White powder	GeO_2
160	GeO_2, S, Im, 4-MPy	2:4:1:30	200	6	Yellow crystals	**(10)**

Appendix 1.4 Solvothermal Reactions in Superbases

#	Reagents	Molar Ratio	Temp/ °C	Time/ Days	Product Appearance	Product
	in 1,8-Diazabicyclo[5.4.0]undec-7-ene (DBU)					
161	Ga, S, DBU	1:3:16	200	6	No solid	/
162	Ga, S , DBU	1:2:18	200	10	Beige powder	Amorphous
163	Ga, S, DBU	2:4:37	140	5	Brown powder	Unidentified powder
164	Ga, S, DBU	2:5:20	140	5	No solid	/
165	Ga, S, TMDPy, DBU	2:5.5:1:20	200	6	Beige powder	Amorphous
166	Ga_2O_3, S, DBU	2:4:37	140	5	No solid	/
167	Ga, GeO_2, S, DBU	1:1:4:20	170	6	No solid	/
168	Ga, GeO_2, S, DBU	1:1:5:20	170	6	White spheres	Unidentified powder

169	Ga, GeO_2, S, DBU	1:1:5.5:20	170	6	White spheres	Unidentified powder
170	Ga, GeO_2, S, DBU	1.5:0.5:5.5:20	170	6	White spheres	Unidentified powder
171	Ga, GeO_2, Thioacetamide, DBU	1:1:4:20	170	6	White spheres	Unidentified powder
172	Ga, GeO_2, Thioacetamide, DBU	1:1:5.5:20	170	6	Yellow spheres	Unidentified powder
173	Ga, GeO_2, S, TMDPy, DBU	1:1:4:1:20	170	6	White powder	Unidentified powder
174	Ga, GeO_2, S, TMDPy, DBU	1:1:5:1:20	170	6	Yellow spheres	Unidentified powder
175	Ga, GeO_2, Thioacetamide, TMDPy, DBU	1:1:4:1:20	170	6	Pink spheres	Unidentified powder
176	GeO_2, S, TMDPy, DBU	2:5.5:1:20	200	6	No solid	/
in 1,5-Diazabicyclo[4.3.0]non-5-ene (DBN)						
177	Ga, S, DBN	1:3:19.2	200	6	No solid	**/**
178	Ga, GeO_2, S, TMDPy, DBN	1:1:5:1:24	200	6	Brown crystals + Ga	**(13) + Ga**

Appendix 1.5 Other Solvothermal Reactions

#	Reagents	Molar Ratio	Temp/ ^oC	Time/ Days	Product Appearance	Product
	in Ethylenediamine (en)					
179	Ga, GeO_2, S, en	1:1:4:30	150	6	White powder	Low crystallinity
180	Ga, GeO_2, S, en	1:1:4:45	150	6	Yellow powder	Unidentified Powder
181	Ga, GeO_2, S, en	1:1:4:60	150	6	Yellow powder	Unidentified Powder
182	Ga, GeO_2, S, Im, en	1:1:4:1:45	150	6	White powder	Low crystallinity
183	Ga, GeO_2, S, TMDPy, en	1:1:5:1:43	170	5	White powder	Amorphous
184	Ga, GeO_2, S, en	1:1:6:43	170	5	White powder	Unidentified powder
in 3,5-Lutidine (3,5-Lut)						
185	Ga, GeO_2, S, 3,5-Lut	1:1:4:30	170	5	Black powder	Unidentified powder
186	Ga, GeO_2, S, 3,5-Lut, H_2O	1:1:4:30:30	170	5	Colourless solid	Amorphous

in 2,6-Lutidine (2,6-Lut)						
187	Ga, GeO_2, S, Im, 2,6-Lut	1:1:4:1:30	170	5	Brown powder	Unidentified powder
188	Ga, GeO_2, S, Im, 2,6-Lut, H_2O	1:1:4:1:30:30	170	5	Grey powder	Unidentified powder
189	$Ga(NO_3)_3$, S, 2,6-Lut	1.5:3:60	185	6	Brown crystals	**(15)**
190	$Ga(NO_3)_3$, S, 2,6-Lut	2:3:60	185	6	Brown powder	**(15)**
in Water (Hydrothermal)						
191	Ga, S, DACH, H_2O	1:2:2:110	170	5	Brown powder	Amorphous
192	GeO_2, Ga, S, DACH, H_2O	2.5:1:5:5:300	170	5	Black solid	Low crystallinity
193	Ga, S, DABCO, H_2O	1:2:4:230	140	5	No solid	/
194	Ga, S , DABCO, H_2O	1:2:6:20	200	10	White powder	Gallium oxide
195	Ga, GeO_2, S, DABCO, H_2O	1:1:4:1:240	150	6	Yellow powder	Amorphous
196	Ga, S, DBU, H_2O	1:3:8:240	200	6	White powder	Ga_2O_3
197	Ga, S, DBU, H_2O	2:4:9:150	140	5	No solid	/
198	Ga, S, DBN, H_2O	1:3:9.6	200	6	No solid	/
199	Ga, S, TMDPy, TBD, H_2O	2:5.5:1:1:166	200	6	No solid	/
200	Ga, Thioacetamide, TBD, H_2O	2:5.5:3.3:222	170	5	Beige powder	Amorphous
201	Ga, S, [THTDP]Cl , TMDPy, H_2O	2:5:1.75:1:34	200	6	Colourless crystals	**(14)**
202	Ga, S, [THTDP]Cl , TMDPy, H_2O	2:5:3.5:1:28	200	6	Brown powder	Amorphous
in 2,6-Dimethylmorpholine (DMM)						
203	Ga, S, DMM	2:5:24	200	6	No solid	**/**
in Acetonitrile (ACN)						
204	Ga, S, DABCO, Acetonitrile	1:2:4:230	140	5	White powder	Ga_2O_3
205	Ga, S, DBU, Im, Acetonitrile	1.5:3:2:3:57	200	10	Brown powder	Unidentified powder
206	Ga, S, Im, DBU, Acetonitrile	1:2:2:1.5:40	140	5	No solid	/

in Dimethylformamide (DMF)						
207	Ga, S, DBU, DMF	1.5:3:3.3:65	200	10	Brown powder	Unidentified powder
208	Ga, S, DBU, DMF	1.5:3:3.3:77	200	10	Ga	Ga
209	Ga, S, TBD, H_2O, DMF	2:5.5:3.3:222:13	170	5	Beige powder	Amorphous
210	Ga_2O_3:S:DMF	1.8:3:65	200	10	White powder	Unidentified powder
in Tetrahydrofuran (THF)						
211	Ga, S, Im, THF	1.5:3:3:62	200	6	Brown powder	Unidentified powder
212	Ga, S, Im, THF	1.5:3:12:100	200	6	Brown powder	Unidentified powder
213	Ga, S, DBU, THF	1.5:3:6.6:62	200	10	Ga	Ga
214	Ga, S, DBU, THF	1.5:3:3.3:100	200	6	Brown powder	Unidentified powder
215	Ga, S, DBU, THF	1.5:3:6.6:100	200	6	Brown powder	Unidentified powder
216	Ga, S, DBN, THF	0.75:1.5:4:62	200	10	Brown powder	Unidentified powder
217	Ga, S, TBD, THF	1.5:3:3:62	200	6	Red crystals dissolved in H_2O	/
218	Ga, S, TBD, THF	1.5:3:12:100	200	10	Red crystals	3,4,5,6-tetrahydro-pyrimidin-2-one (THP)
219	Ga_2O_3, S, THF	1.8:3:62	200	6	Beige powder	Unidentified powder
220	Ga_2O_3, S, THF	1.9:3:62	200	10	Brown powder	Unidentified powder
221	$Ga(NO_3)_3$, S, THF	1.5:3:62	200	10	Black powder	Unidentified powder

Appendix 1.6 Ionothermal Synthesis

P1 = Precursor 1 $[C_6H_8N]_6[C_{12}H_{10}N_2]_2$ $[Ga_{10}S_{16}(NC_6H_7)_4]_4$ (Section 6.2.2.2)

P2 = Precursor 2 $[enH]_2[Ga_4S_7(en)_2]$ (Section 6.2.2.3).

DMA = dimethylamine, 40 % in H_2O

$Cu(NO_3)_2$ = $Cu(NO_3)_2.3H_2O$, $Ga(NO_3)_3$ = $Ga(NO_3)_3.3H_2O$

#	Reagents	Molar Ratio	Temp/ °C	Time/ Days	Product Appearance	Product
222	Ga, S, Im, 4-MPy, [BMMIm]Cl	1:3:0.5:4.7:5.2	200	6	No solid	/

223	Ga, S, Im, 4-MPy, [BMMIm]Cl	1:3:0.5:10:2.6	200	6	No solid	/
224	Ga, S, Im, 4-MPy, [BMMIm]Cl	1:3.5:0.5:5:5	200	6	No solid	/
225	Ga, S, Im, 4-MPy, [BMMIm]Cl	1:3.5:0.5:10:2.5	200	6	Yellow powder	Unidentified powder
226	Ga, S, Im, 4-MPy, $[BMMIm]BF_4$	1:3:0.5:4.7:8	200	6	Yellow powder	Unidentified powder
227	Ga, S, Im, 4-MPy, $[BMMIm]BF_4$	1:3.5:0.5:5:4	200	6	Orange powder	Unidentified powder
228	Ga, S, Im, 4-MPy, $[BMMIm]BF_4$	1:3.5:0.5:10:2	200	6	Yellow powder	Unidentified powder
229	Ga, S, Im, 4-MPy, [BMMIm]Cl	1:3:0.5:10:4	200	6	Orange powder	Unidentified powder
230	Ga, S, $Cu(NO_3)_2$, Thioacetamide, DMA, [BMMIm]Cl	10:18:1.2:17:40:40	200	6	Red powder + Ga	Unidentified powder +Ga
231	Ga, S, $Cu(NO_3)_2$, Thioacetamide, DMA, $[BMMIm]BF_4$	10:18:1.2:17:40:40	200	6	Orange powder	Unidentified powder
232	Ga, S, $Cu(NO_3)_2$, TMDPy, DMA, [BMMIm]Cl	10:16:7:100:70:94:240	160	6	Brown powder	Unidentified powder
233	Ga, S, Thioacetamide, $Cu(NO_3)_2$, TMDPy, DMA, [BMMIm]Cl	10:16:7:100:70:94:240	160	6	Yellow powder	Amorphous
234	Ga, S, $Cu(NO_3)_2$, Thioacetamide, TMDPy, DMA, [BMMIm]Cl	10:16:7:100:70:94:240	170	6	Red powder	Unidentified powder

235	Ga, S, $Cu(NO_3)_2$, Thioacetamide, TMDPy, DMA, [BMMIm]Cl	10:16:7:100:70:94:240	200	13	Red powder + Ga	Unidentified powder + Ga
236	Ga, S, $Cu(NO_3)_2$, Thioacetamide, TMDPy, DMA, [BMMIm]Cl	10:18:1.2:17:6:16:40	200	6	Red powder + Ga	Gallite, resembles **Figure 6.8**
237	Ga, S, $Cu(NO_3)_2$, Thioacetamide, TMDPy, DMA, [BMMIm]Cl	10:18:1.2:17:12:16:40	200	6	Red powder	Amorphous
238	Ga, S, $Cu(NO_3)_2$, Thioacetamide, TMDPy, DMA, [BMMIm]Cl	10:18:1.8:25:17.5:24:60	200	6	Red powder	Amorphous
239	Ga, S, $Cu(NO_3)_2$, Thioacetamide, TMDPy, DMA, [BMMIm]BF_4	10:16:7:100:70:94:240	160	6	Green powder	Amorphous
240	Ga, S, $Cu(NO_3)_2$, Thioacetamide, TMDPy, DMA, [BMMIm]BF_4	10:16:7:100:70:94:240	200	13	Red powder + Ga	Unidentified powder + Ga
241	Ga, S, $Cu(NO_3)_2$, Thioacetamide, TMDPy, DMA, [BMMIm]BF_4	10:18:1.2:17:6:16:40	200	6	Yellow powder	Unidentified powder
242	Ga, S, $Cu(NO_3)_2$, Thioacetamide, TMDPy, DMA, [BMMIm]BF_4	10:18:1.2:17:12:16:40	200	6	Yellow powder	Unidentified powder

243	Ga, S, $Cu(NO_3)_2$, Thioacetamide, TMDPy, DMA, $[BMMIm]BF_4$	40:64:7:100:70:94:240	160	6	Green powder	Unidentified powder
244	Ga, S, $Cu(NO_3)_2$, Thioacetamide, TMDPy, DMA, $[BMMIm]BF_4$	40:64:7:100:70:94:240	200	6	Red powder + yellow glass	Amorphous
245	Ga, S, $Cu(NO_3)_2$, TMDPy, en, [BMMIm]Cl	10:16:7:100:70:120:240	160	6	Brown powder	$Cu(NO_3)$ + Gallite
246	Ga, S, $Cu(NO_3)_2$, Thioacetamide, TMDPy, en, [BMMIm]Cl	10:16:7:100:70:120:240	200	13	Red powder	Unidentified powder
247	Ga, S, $Cu(NO_3)_2$, Thioacetamide, TMDPy, en, $[BMMIm]BF_4$	10:16:7:100:70:180:240	160	6	Red fragments	Amorphous
248	Ga, S, $Cu(NO_3)_2$, Thioacetamide, TMDPy, en, $[BMMIm]BF_4$	10:16:7:100:70:180:240	200	13	Red powder	Unidentified powder
249	Ga, S, $Cu(NO_3)_2$, Thioacetamide, TMDPy, 4-MPy, [BMMIm]Cl	10:16:7:100:70:120:240	170	6	Red powder	Low crystallinity
250	Ga, S, $Cu(NO_3)_2$, Thioacetamide, TMDPy, 4-MPy, [BMMIm]Cl	10:16:7:100:70:120:240	200	13	Black solid	Amorphous
251	Ga, S, $Cu(NO_3)_2$, Thioacetamide, TMDPy, 4-MPy, $[BMMIm]BF_4$	10:16:7:100:70:120:240	200	13 days	Red powder	Unidentified powder

252	Ga, S, Thioacetamide, TMDPy, DMM, [BMMIm]Cl	10:16:100:70:97:240	170	6	No solid	/
253	Ga, S, $Cu(NO_3)_2$, Thioacetamide, TMDPy, DMM, [BMMIm]Cl	10:16:7:100:70:97:240	200	13	Brown powder	Gallite and Digenite (Cu_9S_5)
254	Ga, S, $Cu(NO_3)_2$, Thioacetamide, TMDPy, DMM, [BMMIm]BF_4	10:16:7:100:70:97:240	200	13	Green powder	Unidentified powder
255	$Ga(NO_3)_3$,.S, Thioacetamide, TMDPy, DMA, [BMMIm]Cl	10:4:100:70:94:240	170	6	No solid	/
256	$Ga(NO_3)_3$,.S, Thioacetamide, TMDPy, en, [BMMIm]Cl	10:16:7:100:70:45:240	170	6	Orange fragments	Not enough product to characterise
257	$Ga(NO_3)_3$. Thioacetamide, TMDPy, DMM, [BMMIm]Cl	10:4:100:70:97:240	170	6	No solid	/
with $[C_6H_8N]_6[C_{12}H_{10}N_2]_2$ $[Ga_{10}S_{16}(NC_6H_7)_4]_4$ (P1)						
258	P1, S, TMDPy, DMA, [BMMIm]Cl	1:35:70:94:240	170	6	No solid	/
259	P1, Thioacetamide, TMDPy, DMA, [BMMIm]Cl	1:100:70:94:240	170	6	No solid	/
260	P1, Thioacetamide, TMDPy, DMA, [BMMIm]Cl	1:100:70:94:240	200	6	No solid	/
261	P1, Thioacetamide, Im, DMA, [BMMIm]Cl	1:100:70:94:240	170	6	No solid	/

262	P1, $Cu(NO_3)_2$, Thioacetamide, TMDPy, DMA, [BMMIm]Cl	1:7:100:70:94:240	160	6	Red powder and yellow glass	Amorphous
263	P1, $Cu(NO_3)_2$, Thioacetamide, TMDPy, DMA, [BMMIm]Cl	1:7:100:70:94:240	170	6	Orange powder	Figure 6.3
264	P1, $Cu(NO_3)_2$, Thioacetamide, TMDPy, DMA, [BMMIm]Cl	1:7:100:70:94:240	200	6	Yellow powder	Figure 6.3
266	P1, $Cu(NO_3)_2$, Thioacetamide, Im, DMA, [BMMIm]Cl	1:7:100:70:94:240	170	6	Orange powder	Figure 6.4
267	P1, $Cu(NO_3)_2$, Thioacetamide, Im, DMA, [BMMIm]Cl	1:7:100:70:94:240	200	6	Orange powder	Figure 6.4
268	P1, $Cu(NO_3)_2$, Thioacetamide, TMDPy, en, [BMMIm]Cl	1:7:100:70:180:240	170	6	Red powder	Figure 6.3
265	P1, $Cu(NO_3)_2$, Thioacetamide, Im, DMM, [BMMIm]Cl	1:7:100:70:94:240	160	6	Brown powder	Figure 6.4
269	P1, $Cu(NO_3)_2$, Thioacetamide, TMDPy, DMM, [BMMIm]Cl	1:7:100:70:97:240	170	6	Brown powder	Figure 6.3
with $[enH]_2[Ga_4S_7(en)_2]$ (P2)						
270	P2, Thioacetamide, TMDPy, DMA, [BMMIm]Cl	10:100:70:94:240	160	6	No solid	/
271	P2, $Cu(NO_3)_2$, S, TMDPy, DMA, [BMMIm]Cl	10:7:100:70:94:240	200	6	Orange powder	Amorphous

272	P2, $Cu(NO_3)_2$, Thioacetamide, TMDPy, DMA, [BMMIm]Cl	10:7:100:70:94:240	160	6	Red powder and yellow glass	Amorphous
273	P2, $Cu(NO_3)_2$, Thioacetamide, TMDPy, DMA, [BMMIm]Cl	10:7:100:70:94:240	200	6	Yellow powder	**Figure 6.6**
274	P2, $Cu(NO_3)_2$, Thioacetamide, TMDPy, DMA, $[BMMIm]BF_4$	10:7:100:70:94:240	160	6	Green powder	Figure 6.7
275	P2, $Cu(NO_3)_2$, Thioacetamide, TMDPy, DMA, $[BMMIm]BF_4$	10:7:100:70:94:240	200	13	Yellow powder	Amorphous
276	P2, $Cu(NO_3)_2$, Thioacetamide, TMDPy, DMA, [BMMIm]Cl, H_2O	10:7:100:70:94:240:1110	160	6	White solid	Amorphous
277	P2, $Cu(NO_3)_2$, Thioacetamide, Im, DMA, [BMMIm]Cl	10:7:10:70:94:240	160	6	Orange powder	**Figure 6.6**
278	P2, $Cu(NO_3)_2$, Thioacetamide, TMDPy, en, [BMMIm]Cl	10:7:100:70:180:240	160	6	Yellow powder	Amorphous
279	P2, $Cu(NO_3)_2$, Thioacetamide, TMDPy, en, [BMMIm]Cl	10:7:100:70:180:240	170	6	Orange powder	Amorphous
280	P2, $Cu(NO_3)_2$, Thioacetamide, TMDPy, 4-MPy, [BMMIm]Cl	10:7:100:70:120:240	170	6	Green powder	Low crystallinity
281	P2, $Cu(NO_3)_2$, Thioacetamide, TMDPy, 4-MPy, [BMMIm]Cl	10:7:100:70:120:240	200	13	Brown powder	**Figure 6.6**

282	P2, $Cu(NO_3)_2$, Thioacetamide, TMDPy, 4-MPy, $[BMMIm]BF_4$	10:7:100:70:120:240	160	6	Green powder	Figure 6.7
283	P2, $Cu(NO_3)_2$, Thioacetamide, TMDPy, 4-MPy, $[BMMIm]BF_4$	10:7:100:70:120:240	200	6	Yellow powder	Figure 6.7
284	P2, $Cu(NO_3)_2$, Thioacetamide, TMDPy, DMM, [BMMIm]Cl	10:7:100:70:97:240	170	6	Brown powder	Amorphous
285	P2, $Cu(NO_3)_2$, Thioacetamide, TMDPy, DMM, $[BMMIm]BF_4$	10:7:100:70:97:240	160	6	Green powder	Figure 6.7
286	P2, $Cu(NO_3)_2$, Thioacetamide, TMDPy, DMM, $[BMMIm]BF_4$	10:7:100:70:97:240	200	13	Yellow powder	Figure 6.7

Appendix 1.7 Surfactant-Thermal Reactions in PEG-400

#	Reagents	Molar Ratio	Temp/ °C	Time/ Days	Product Appearance	Product
287	Ga, S, PEG, H_2O	2:5.5:2ml:30	190	5	Pink powder	Unidentified powder
288	Ga, Thioacetamide, PEG	2:4:3ml	200	8	Ga	Ga
289	Ga, Thioacetamide, PEG	2:5.4:3ml	200	8	Beige powder	Amorphous
with 1,4-Diazabicyclo[2.2.2]octane (DABCO)						
290	Ga, Thioacetamide, DABCO, PEG	2:5.4:0.5:3ml	140	6	Ga	Ga
291	Ga, Thioacetamide, DABCO, PEG	2:5.5:0.4:4ml	160	10	Yellow Powder + Ga	Unidentified powder
292	Ga, Thioacetamide, DABCO, PEG	2:5.5:1.8:4ml	160	10	Yellow Powder + Ga	Unidentified powder

with 1,8-Diazabicyclo[5.4.0]undec-7-ene (DBU)						
293	Ga, S, DBU, PEG	1:3:8:4ml	200	6	Brown powder	Unidentified powder
294	Ga, S, DBU, PEG	2:5.5:3.3:4ml	160	6	Brown powder	Unidentified powder
295	Ga, S, DBU, PEG	2:5.5:6.6:4ml	160	6	Red crystals + Ga	**(12c) + Ga**
296	Ga, S, DBU, PEG	2:5.5:6.6:4ml	200	6	Brown powder	Unidentified powder
297	Ga, S, DBU, PEG	2:5.5:6.6:6ml	200	6	Red crystals + Ga	**(12c) + Ga**
298	Ga, S, DBU, PEG, H_2O	2:5.5:6.7:2ml:30	190	5	White powder	Unidentified powder
299	Ga, S, DBU, Im, PEG	2:5.5:3.3:1:4ml	160	6	Brown powder	Unidentified powder
300	Ga, S, DBU, Im, PEG	2:5.5:6.6:1:4ml	160	6	Brown powder	Unidentified powder
301	Ga, Thioacetamide, DBU, PEG	2:5.4:3.3:4ml	140	6	Colourless crystals	**(12a)**
302	Ga, Thioacetamide, DBU, PEG	2:5.5:3.3:4ml	160	6	Yellow crystals	**(12b)**
303	Ga, Thioacetamide, DBU, PEG	2:4:3.3:4ml	160	10	No solid	**/**
304	Ga, Thioacetamide, DBU, PEG	2:5.5:6.6:4ml	160	6	Yellow crystals	**(12b)**
305	Ga, Thioacetamide, DBU, Im, PEG	2:5.5:3.3:1:4ml	160	6	Yellow powder	Unidentified powder
306	Ga, Thioacetamide, DBU, Im, PEG	2:5.5:6.6:1:4ml	160	6	Yellow powder	Unidentified powder
307	Ga, GeO_2, S, DBU, PEG, H_2O	1:1:5.5:6.7:2ml:30	190	5	No solid	/
with 1,5-Diazabicyclo[4.3.0]non-5-ene (DBN)						
308	Ga, S, DBN, PEG	1:3:8:4ml	200	6	Brown powder	**(12)**
with Triazabicyclodecene (TBD)						
309	Ga, S, TBD, PEG	1:3:0.3:4ml	170	5	Black powder + Ga	Unidentified powder + **Ga**
310	Ga, S, TBD, PEG	1:3:0.6:4ml	170	5	Brown powder + Ga	Unidentified powder + **Ga**
311	Ga, S, TMDPy, TBD, PEG	2:5.5:1:1:3ml	200	6	Ga	Ga

312	Ga, Thioacetamide, TBD, PEG	2:5.5:3.3:4ml	170	5	White powder	Unidentified powder
313	Ga, S, TBD, PEG, DMF	2:5.5:3.3:4ml:13	170	5	No solid	/

Appendix 1.8 Surfactant-Thermal Reactions in PVP

#	Reagents	Molar Ratio	Temp/ ^{o}C	Time/ Days	Product Appearance	Product
314	Ga, S, PVP, H_2O	2:5.5:1g:180	190	5	No solid	/
315	Ga, GeO_2, S, PVP, H_2O	1:1:5.5:1g:180	190	5	No solid	/
with 1,4-Diazabicyclo[2.2.2]octane (DABCO)						
316	Ga, Thioacetamide, DABCO, PVP	2:5.5:0.4:3.3g	160	10	See section 6.6.2.1	/
317	Ga, Thioacetamide, DABCO, PVP	2:5.5:1.8:1.15g	160	10	See section 6.6.2.1	/
318	Ga, Thioacetamide, DABCO, PVP	2:4:1.7:3.3g	160	10	White powder	Unidentified powder
319	Ga, Thioacetamide, DABCO, PVP	2:5.5:1.8:1.15g	160	10	See section 6.6.2.1	/
with 1,8-Diazabicyclo[5.4.0]undec-7-ene (DBU)						
320	Ga, S, DBU, PVP, H_2O	2:5.5:6.7:1g:30	190	5	No solid	/
321	Ga, Thioacetamide, DBU, PVP	2:4:3.3:3.3g	160	10	White powder	Unidentified powder
322	Ga, Thioacetamide, DBU, PVP	2:5.5:3.3:1.15g	160	10	See section 6.6.2.1	/
323	Ga, Thioacetamide, DBU, PVP	2:5.5:3.3:3.3g	160	10	See section 6.6.2.1	/
324	Ga, GeO_2, S, DBU, PVP, H_2O	1:1:5.5:6.7:1g:30	190	5	No solid	/

Appendix 1.9 Surfactant-Thermal Reactions in CTAB

#	Reagents	Molar Ratio	Temp/ ^{o}C	Time/ Days	Product Appearance	Product
325	Ga, S, CTAB	2:5.4:4	200	8	Orange solid	See section 6.6.2.1
326	Ga, S, CTAB, H_2O	2:5.4:4:30	200	8	No solid	/

Appendix 2 EDX Data for (10)

EDX Data for (10) showing weight % by element.

Element	Weight %	Weight %	Weight %	Weight %	Average Weight %
N			10.51		2.62
O	3.69	7.49	2.8	1.46	3.86
S	38.15	48.27	45.51	43.53	43.865
Ga	32.76	20.19	18.19	23.81	23.7375
Ge	25.4	24.06	22.99	31.19	25.91
Sum	100	100.01	100	99.99	99.9925

Appendix 3 TGA Data for (15) Under N_2

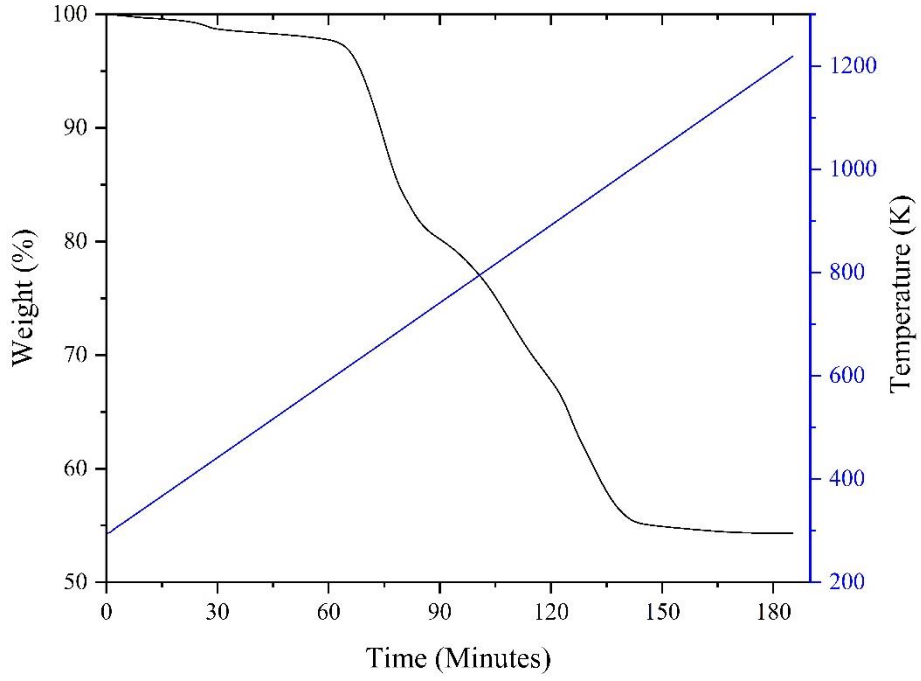

TGA for (15) under N_2.